



METAL CARBONYL FLUORIDE  
COMPLEXES

by  
Ernst Horn, B.Sc. (Hons.)

A Thesis presented for the degree of  
Doctor of Philosophy

Department of Physical and Inorganic Chemistry  
The University of Adelaide

August 1983

To My Mother  
and  
In Memory of My Father

# TABLE OF CONTENTS

	Page
SUMMARY	vi
STATEMENT	ix
ACKNOWLEDGEMENTS	x
ABBREVIATIONS	xi
<u>CHAPTER 1 - INTRODUCTION</u>	1
1.1 Manganese and Rhenium Carbonyl Fluorides	2
1.1.1 Manganese Fluorides	2
1.1.2 Rhenium Fluorides	4
1.2 Coordinated Fluoro- and Oxy-ligands	5
1.3 Characterization of Metal Carbonyls	7
<u>CHAPTER 2 - METAL CARBONYL CLUSTERS</u>	11
2.1 Introduction	11
2.2 Preparation and Properties of the Clusters	12
2.2.1 $[\text{Mn}(\text{CO})_3\{\text{F}_x(\text{OH})_{1-x}\}]_4$ and $[\text{Re}(\text{CO})_3\text{F}]_4 \cdot 4(\text{H}_2\text{O})$	12
2.2.2 $[\text{M}(\text{CO})_3\text{F}]_4$	14
2.2.3 $[\text{Rh}(\text{PPh}_3)\text{X}]_4$	15
2.3 Structure Determination of $[\text{Mn}(\text{CO})_3\{\text{F}_x, (\text{OH})_{1-x}\}]_4 \cdot 2(\text{C}_6\text{H}_6)$	17
2.3.1 Crystal Data	17
2.3.2 Structure Solution and Refinement	18
2.3.3 Description of the Structure	19
2.3.4 Discussion	25
2.4 Structure Determination of $[\text{Re}(\text{CO})_3\text{F}]_4 \cdot 4(\text{H}_2\text{O})$	26
2.4.1 Crystal Data	26
2.4.2 Structure Solution and Refinement	27
2.4.3 Description of the Structure	33
2.5 Structure Determination of $[\text{Rh}(\text{PPh}_3)\text{Cl}]_4$	34
2.5.1 Crystal Data	34
2.5.2 Structure Solution and Refinement	34
2.5.3 Description of the Structure	40

	Page
2.6 Discussion	42
2.7 Experimental	47
<u>CHAPTER 3 - COORDINATED FLUORIDE IN RHENIUM(I) COMPLEXES</u>	50
3.1 Introduction	50
3.2 Preparation and Properties of $[\text{Re}(\text{CO})_3(\text{L}_2)\text{F}]_2\text{H}\cdot\text{HOBf}_3$	52
3.2.1 Preparation	52
3.2.2 Properties	52
3.3 Preparation and Properties of $[\text{Re}(\text{CO})_3(\text{L}_2)\text{F}]$	54
3.3.1 Preparation	54
3.3.2 Properties	54
3.4 Structure Determination of $[\text{Re}(\text{CO})_3(\text{tmen})\text{F}]\text{H}\cdot\text{HOBf}_3$	57
3.4.1 Crystal Data	57
3.4.2 Structural Solution and Refinement	57
3.4.3 Description of the Structure	59
3.5 Structure Determination of $[\text{Re}(\text{CO})_3(\text{tmen})\text{F}]$	66
3.5.1 Crystal Data	66
3.5.2 Structural Solution and Refinement	67
3.5.3 Description of the Structure	72
3.6 Discussion	73
3.7 Experimental	77
<u>CHAPTER 4 - MANGANESE CARBONYL COMPLEXES</u>	81
4.1 Introduction	81
4.2 Preparations	83
4.2.1 $[\text{Mn}(\text{CO})_3\{\text{P}(\text{OPh})_3\}_2\text{OC10}_3]$	83
4.2.2 $[\text{Mn}(\text{CO})_3(\text{diphos})(\text{BF}_3\text{OH})]\cdot\frac{1}{2}(\text{dpeo})$	83
4.2.3 Preparation of <i>fac</i> - $\text{Mn}(\text{CO})_3(\text{L}_2)\text{F}$	85
4.3 Structure Determination of $[\text{Mn}(\text{CO})_3\{\text{P}(\text{OPh})_3\}_2\text{OC10}_3]$	87
4.3.1 Crystal Data	87
4.3.2 Structure Solution and Refinement	89
4.3.3 Description of the Structure	89

	Page	
4.4	Structure Determination of $[\text{Mn}(\text{CO})_3(\text{diphos})(\text{BF}_3\text{OH})] \cdot \frac{1}{2}(\text{dpeo})$	94
4.4.1	Crystal Data	94
4.4.2	Structure Solution and Refinement	96
4.4.3	Description of the Structure	97
4.5	Discussion	104
4.5.1	Metal Carbonyl Perchlorates	104
4.5.2	Metal Carbonyl Trifluorohydroxy borates	106
4.5.3	Manganese Carbonyl Fluorides	108
4.6	Experimental	109
 <u>CHAPTER 5 - METAL CARBONYL AQUA COMPLEXES</u>		 112
5.1	Introduction	112
5.2	Preparations and Properties	113
5.2.1	$[\text{M}(\text{CO})_3(\text{L}_2)(\text{H}_2\text{O})]^+ \cdot \text{Y}^-$	113
5.2.2	$\text{Re}(\text{CO})_3(\text{L}_2)\text{Y} \cdot \text{H}_2\text{O}$	114
5.2.3	Characterization by Infrared Spectroscopy	115
5.2.4	Reactions of $[\text{M}(\text{CO})_3(\text{L}_2)(\text{H}_2\text{O})]^+ \cdot \text{Y}^-$ and $\text{Re}(\text{CO})_3(\text{L}_2)\text{Y} \cdot (\text{H}_2\text{O})$	121
5.3	Structure Determination of $[\text{Re}(\text{CO})_5(\text{H}_2\text{O})]^+ \cdot \text{AsF}_6^-$	122
5.3.1	Crystal Data	122
5.3.2	Structure Solution and Refinement	128
5.3.3	Description of the Structure	128
5.4	Structure Determination of $[\text{Re}(\text{CO})_3(\text{tmen})(\text{H}_2\text{O})]^+ \cdot \text{AsF}_6^-$	131
5.4.1	Crystal Data	131
5.4.2	Structure Solution and Refinement	133
5.4.3	Description of the Structure	138
5.5	Structure Determination of $[\text{Re}(\text{CO})_3(\text{tmen})(\text{H}_2\text{O})]^+ \cdot \text{BF}_4^-$	139
5.5.1	Crystal Data	139
5.5.2	Structural Solution and Refinement	140
5.5.3	Description of the Structure	142
5.6	A $^{19}\text{F}$ N.M.R. Study	147
5.6.1	$^{19}\text{F}$ N.M.R. Spectra	147
5.6.2	Variable Temperature $^{19}\text{F}$ N.M.R.	150

	Page
5.7 Discussion	153
5.8 Experimental	155
<u>CHAPTER 6 - CONCLUSION</u>	157
6.1 Rhenium-Fluoride and -Oxygen Bond Lengths	157
6.2 Suggestions for Further Research	160
<u>CHAPTER 7 - CRYSTALLOGRAPHY AND EXPERIMENTAL</u>	161
7.1 Crystallography	161
7.1.1 Instrumental	161
7.1.2 Computing	164
7.2 Experimental	167
7.2.1 General	167
7.2.2 Physical Measurements and Instrumentation	167
7.2.3 Gas, Ligands, Reagents and Solvents	169
7.2.4 Preparation of the Precursors	171
<u>APPENDIX 1 - SELECTED SOLID STATE INFRARED SPECTRA</u>	173
<u>APPENDIX 2 - OTHER POSSIBLE METAL CARBONYL FLUORIDE COMPLEXES</u>	176
<u>LIST OF PUBLICATIONS</u>	179
<u>REFERENCES</u>	180

MICROFICHE

The microfiche containing the hydrogen atomic parameters and the tabulated structure factors are given at the end of the thesis.

## SUMMARY

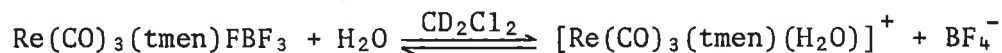
Halogen abstraction reactions were investigated using manganese(I) and rhenium(I) carbonyl halide (where, halide = Cl, Br) complexes as substrates during attempts to coordinate fluoride or fluoro- and oxy-anion ligands. The preparative methods developed were then applied to a selected number of other transition metal carbonyl halide complexes.

The complexes  $\text{Mn}(\text{CO})_5\text{X}$  (where, X = Cl, Br) react with thallium fluoride and silver fluoride in dichloromethane solutions to give a mixture of the cluster species,  $[\text{Mn}(\text{CO})_3\{\text{F}_x, (\text{OH})_{1-x}\}]_4$ . Similarly, rhenium pentacarbonyl bromide reacts with silver fluoride in dichloromethane and hexafluorobenzene to form the cubane-type cluster,  $[\text{Re}(\text{CO})_3\text{F}]_4$ . These compounds have been characterized by infrared, mass spectroscopy and crystal structure determinations. The crystal structures of the two complexes show that the fluoro or hydroxy groups are involved in  $\mu_3$ -type bridging with the respective metals. When the manganese and rhenium pentacarbonyl complexes were reacted with silver bifluoride ( $\text{AgF}_2\text{H}$ ) in fluorinated solvents ( $\text{C}_6\text{H}_5$ ,  $\text{C}_6\text{F}_6$ ) using plastic reaction vessels the products formed were the anhydrous clusters,  $[\text{M}(\text{CO})_3\text{F}]_4$  (where, M = Mn, Re). The rhodium cluster,  $[\text{Rh}(\text{PPh}_3)\text{Cl}]_4$  crystallizes from solution when the product of the reaction between  $\text{Rh}(\text{CO})(\text{PPh}_3)_2\text{Cl}$  and  $\text{AgF}_2\text{H}$  is left in dichloromethane. However, with the use of dry hexafluorobenzene and plastic reaction vessels only the fluoride cluster,  $[\text{Rh}(\text{PPh}_3)\text{F}]_4$  was isolated.

The reactions of the substituted rhenium carbonyl bromides,  $\text{Re}(\text{CO})_3(\text{L}_2)\text{Br}$  (where,  $\text{L}_2$  = bpy, diphos,  $2\text{PPh}_3$ , tmen), with  $\text{AgF}_2\text{H}$  in dichloromethane in plastic vessels yielded the anhydrous fluoride

analogues. The complexes,  $\text{Re}(\text{CO})_3(\text{L}_2)\text{Br}$  (where,  $\text{L}_2 = \text{bpy}, \text{tmen}$ ), react with  $\text{AgF}_2\text{H}$  in dichloromethane or hexafluorobenzene in pyrex glass vessels to form the species,  $[\text{Re}(\text{CO})_3(\text{L}_2)\text{F}]_2\text{H}\cdot\text{HOBF}_3$ .  $\text{Mn}(\text{CO})_3(\text{diphos})\text{Cl}$  reacts with the  $[\text{Ph}_4\text{As}]^+[\text{HOBF}_3]^-$  impurity in  $\text{Ph}_4\text{AsF}$  to form  $[\text{Mn}(\text{CO})_3(\text{diphos})(\text{HOBF}_3)]$ . The trifluorohydroxy borate anion,  $[\text{HOBF}_3]^-$ , results from a reaction involving  $\text{AgF}_2\text{H}$  and the glass surfaces. All substituted rhenium fluoride complexes have been characterized by infrared and mass spectroscopy. While the species  $\text{Re}(\text{CO})_3(\text{tmen})\text{F}$ ,  $[\text{Mn}(\text{CO})_3(\text{diphos})(\text{HOBF}_3)]\cdot\frac{1}{2}(\text{dpeo})$  and  $[\text{Re}(\text{CO})_3(\text{tmen})\text{F}]_2\text{H}\cdot\text{HOBF}_3$  have also been characterized by their crystal structures. When  $\text{Fe}(\text{CO})_2\text{CpI}$  is treated with  $\text{AgF}_2\text{H}$  decarboxylation products result which have not been characterized.

Pentacarbonyl and substituted rhenium bromide complexes react with  $\text{AgAsF}_6$  or  $\text{AgBF}_4$  in dichloromethane to form the respective aquo species,  $[\text{Re}(\text{CO})_5(\text{OH}_2)]^+\text{Y}^-$  (where,  $\text{Y} = \text{AsF}_6^-, \text{BF}_4^-$ ) and  $[\text{Re}(\text{CO})_3(\text{L}_2)(\text{OH}_2)]^+\text{BF}_4^-$  ( $\text{L}_2 = \text{bpy}, \text{diphos}, \text{PPh}_3$ ). These aquo complexes have been characterized by infrared and mass spectroscopy. In addition, the species,  $[\text{Re}(\text{CO})_3(\text{L}_2)(\text{OH}_2)]^+\text{Y}^-$  (where, 1.  $\text{L}_2 = 2(\text{CO})$ ,  $\text{Y} = \text{AsF}_6^-$ , 2.  $\text{L}_2 = \text{tmen}$ ,  $\text{Y} = \text{AsF}_6^-, \text{BF}_4^-$ ), were also characterized by their crystal structures. A  $^{19}\text{F}$  nuclear magnetic resonance study of the  $[\text{Re}(\text{CO})_3(\text{tmen})(\text{H}_2\text{O})]^+\cdot\text{BF}_4^-$  system has established that in solution ( $\text{CD}_2\text{Cl}_2$ ) an equilibrium exists between the coordinated and "free" tetrafluoroborate anion, according to the following equation:



Variable temperature  $^{19}\text{N.M.R.}$  spectroscopy has shown that this equilibrium is temperature dependant. The rhenium complexes  $\text{Re}(\text{CO})_3(\text{bpy})\text{FAsF}_5$  and  $\text{Re}(\text{CO})_3(\text{tmen})\text{FBF}_3$  formed when solutions ( $\text{C}_6\text{H}_5\text{F}, \text{C}_6\text{F}_6$ ) containing the corresponding aquo-species were allowed to evaporate at *ca.*  $-10^\circ\text{C}$  in a



dry nitrogen atmosphere over phosphorus pentoxide.

The investigation presented in this thesis led to the facile pathway for the preparation of the respective fluoride complexes. The complexes were obtained by employing relatively mild reagents compared to fluorine gas, hydrogen fluoride and xenon hexafluoride. This was achieved when using (a) the right solvents, which were not susceptible to halide substitution reactions; (b) dry solvents, reaction atmosphere and fluorinating reagents; and (c) when using plastic reaction vessels.

## STATEMENT

This thesis contains no material previously submitted for a degree or diploma in any University, and, to the best of the candidate's knowledge, contains no material previously published or written by another person, except where due reference is made in the text of this thesis.

The author accepts full responsibility for any errors present in the treatise, regardless of their nature.

---

Ernst Horn

## ACKNOWLEDGEMENTS

I am sincerely grateful to my supervisor, Dr. M.R. Snow, for his encouragement, guidance and help throughout the course of this research.

My thanks are due to Professors D.O. Jordan and M.I. Bruce for making available to me the facilities of the department. I thank Doctors S.F. Lincoln, T. Spotswood and E. Williams for their assistance in obtaining N.M.R. spectra. I also extend my thanks to Dr. J.R. Rodgers and to my colleagues for their help and friendship.

I am greatly indebted to my parents whose devotion, patience, sacrifices and support during these years made this work possible. Finally, my thanks are due to Mrs. E. Curran for typing the manuscript.

## ABBREVIATIONS

### CHEMICAL SYMBOLS

bpy	2,2'bipyridyl
Cp	$\eta$ -cyclopentadienyl
diphos	1,2-bis(diphenylphosphino)ethane
dpeo	1,2-bis(diphenylphosphino oxide)ethane
Ph	phenyl
phen	1,10-phenanthroline
tmen	NNN'N'-tetramethylethane-1,2-diamine

### CRYSTALLOGRAPHIC SYMBOLS

C	C face-centred unit cell
$D_c$	calculated density
$D_m$	measured density
F	function in Fourier space structure factor
$h, k, l$	Miller indices reciprocal lattice point indices
M.W.	molecular weight
P	primitive unit cell
$U_{mn}$	thermal parameters ( $m = 1 - 3, n = 1 - 3$ )
$x, y, z$	fractional coordinates within the unit cell
Z	number of molecules or asymmetric units per cell
$\alpha, \beta, \gamma$	crystallographic angles
$\theta$	Bragg angle scattering angle
$\mu$	linear absorption coefficient
$\lambda$	wavelength (X-rays)

## MISCELLANEOUS SYMBOLS

$\delta$	small amount of . . . (e.g. $\delta(\text{H}_2\text{O})$ , $\delta = 0 - 2.5$ mole)
FT	Fourier transform
N.M.R.	nuclear magnetic resonance
R.temp.	room temperature (15 - 30°C)

### Abbreviations used for Infrared spectra:

br	broad	sh	shoulder
m	medium	ssh	strong shoulder
ms	medium strong	sp	sharp
mw	medium weak	w	weak
s	strong	vw	very weak
vs	very strong		



## CHAPTER 1

### INTRODUCTION

The discovery of the formation of nickel tetracarbonyl<sup>1,2</sup> in the late nineteenth century initiated the great interest in the preparation and properties of metal carbonyls. The development in this field has been so enormous that, today, metal carbonyl complexes are known for most transition metals. The majority of these can now be routinely prepared from the respective metals or metal ions in the presence of carbon monoxide.<sup>3-5</sup>

The increased interest in inorganometallic chemistry lead to the preparation of metal carbonyl halide (Cl, Br, I) complexes of virtually every transition metal.<sup>6</sup> In contrast, however, the number of metal carbonyl fluoride complexes reported to date is limited. Thus, the preparation and characterization of manganese and rhenium fluorides has become the main aim of the research presented in this thesis. Manganese(I) and rhenium(I) carbonyl halide complexes were chosen because they are readily obtained by halogen (Cl, Br, I) oxidation of the respective dimeric metal carbonyls,  $M_2(CO)_{10}$ . Furthermore, the pentacarbonyl halide complexes thus formed are stable crystalline solids and are easily converted to the substituted metal carbonyl halides which are also resistant to further oxidation. The next three sections are summaries limited to the chemical background of manganese and rhenium complexes relevant to this report.

## 1.1 MANGANESE AND RHENIUM CARBONYL FLUORIDES

The pentacarbonyl and substituted tricarbonyl halide (Cl, Br, I) complexes of manganese(I) and rhenium(I) have been known for over twenty years.<sup>7,8,9</sup> However, successful synthetic routes to a limited number of carbonyl fluorides of these group VIIa metals have been reported only in the last ten years. In this section a brief account of the reported carbonyl fluorides of relevance is given.

### 1.1.1 Manganese Carbonyl Fluorides

The attempts to prepare manganese pentacarbonyl fluoride by reacting silver fluoride with the corresponding pentacarbonyl bromide at room temperature were unsuccessful. The products isolated when the manganese bromide dissolved in dichloromethane reacted with a two- and seven-fold molar excess of silver fluoride were formulated as the species  $[\text{Mn}(\text{CO})_4\text{F}]_2$  and  $\text{Mn}(\text{CO})_3\text{F}_3$ , respectively.<sup>10</sup> It is now believed that the latter is one of the cluster species,  $[\text{Mn}(\text{CO})_3\{\text{F}_x, (\text{OH})_{1-x}\}]_4$  (where,  $x = 0 - 1$ ).<sup>11</sup> The manganese pentacarbonyl fluoride is presumably the unstable intermediate giving rise to both the dimer and tetramer complexes.

Another attempt to prepare the manganese fluoride involved the use of silver hexafluorophosphate as a fluorinating agent. The hexafluorophosphate ion is potentially a source of fluoride as shown by the following equation:



Some molybdenum carbonyl complexes have been successfully fluorinated when using nitrosonium-<sup>12</sup> and silver-hexafluorophosphate.<sup>13</sup> However, when the silver salt was added to dichloromethane solutions containing the manganese and rhenium pentacarbonyl bromides at room temperature

hydrolysis of the hexafluorophosphate ion occurred resulting in the difluorophosphate complexes,  $M(\text{CO})_5(\text{PO}_2\text{F}_2)$  (where,  $M = \text{Mn},^{14} \text{Re}^{15}$ ). When the manganese bromide was reacted with silver hexafluoroarsenate no hydrolysis occurred and the product was formulated as  $\text{Mn}(\text{CO})_5\text{F}\cdot\text{AsF}_5$ .<sup>16</sup>

Manganese pentacarbonyl perchlorate was reacted with tetraethylammonium fluoride in another attempt to prepare the manganese fluoride,  $\text{Mn}(\text{CO})_5\text{F}$ .<sup>14</sup> On addition of the fluoride salt dissolved in methanol to a dichloromethane solution of the manganese perchlorate, carbon monoxide was evolved and the yellow product was assigned by its carbonyl absorption bands to  $\text{Mn}(\text{CO})_3\text{F}_3$ . When left in solution an uncharacterized yellow precipitate formed. The above reaction occurred more slowly when the solid tetraethylammonium fluoride was added to the manganese perchlorate dissolved in dichloromethane. The unstable intermediate  $\text{Mn}(\text{CO})_5\text{F}$  was identified in the reaction mixture by solution infrared spectroscopy. However, as in the above case decomposition occurred and a number of uncharacterized compounds formed. The first aim of the work presented in this thesis was to characterize the main decomposition product of the silver- and tetraethylammonium-fluoride reactions by x-ray crystal structure determination.

The complex  $[\text{Mn}_2(\text{CO})_9\text{F}]^- \cdot [\text{Dibenzo-18-crown-6}] \cdot \text{K}^+$  has been prepared photochemically from  $\text{Mn}_2(\text{CO})_{10}$ .<sup>17</sup> The crown ether in this compound has a stabilizing effect on the  $[\text{Mn}_2(\text{CO})_9\text{F}]^-$  anion and attempts to replace the crown- $\text{K}^+$  with  $\text{Et}_4\text{N}^+$  resulted in decomposition. Abel and Towle reported<sup>18</sup> that the reaction between  $[\text{Mn}_3(\text{CO})_9(\mu_3\text{-OEt})_2(\mu_2\text{-OEt})]$  and boron trifluoride produced another one of the few metal carbonyl fluorides namely,  $[\text{Mn}_3(\text{CO})_9(\text{OEt})_2\text{F}]$ . When hydrogen fluoride was used instead of boron trifluoride no reaction occurred.

To date no manganese tricarbonyl fluoride complexes of the type,



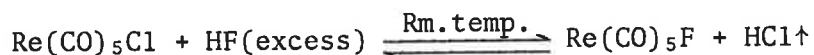
$Mn(CO)_3(L_2)F$  (where,  $L_2$  = two mono- or a bi-dentate ligand) have been reported in the literature. This report investigates the effect of different ligands on the stability of the manganese fluoride.

### 1.1.2 Rhenium Carbonyl Fluorides

Rhenium carbonyl fluoride compounds are more abundant in the literature than the manganese fluorides. This is believed to be due to the greater stability of the corresponding rhenium complexes. For this reason systematic studies of the preparation of rhenium fluorides have been more successful.

The rhenium carbonyl halides,  $Re(CO)_5X$  (where,  $X = Cl, Br, I$ ) are stable and can easily be prepared by reacting  $Re_2(CO)_{10}$  with the respective halogens.<sup>19,20</sup> However, attempts to prepare the rhenium fluoride by adding fluorine to the rhenium carbonyl were unsuccessful. At room temperature no reaction was observed. While, at elevated temperatures rhenium pentafluoride and a number of uncharacterized species were produced.<sup>21</sup>

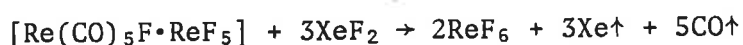
O'Donnel, Phillips and Waugh<sup>22</sup> have prepared rhenium pentacarbonyl fluoride by a halogen exchange reaction at room temperature between rhenium(I) chloride ( $Re(CO)_5Cl$ ) and anhydrous hydrogen fluoride. During the course of the reaction hydrogen chloride was given off and a light brown solid,  $Re(CO)_5F$ , formed. The overall stoichiometry of the reaction is given in the following equation:



The rhenium fluoride was also obtained when  $Re_2(CO)_{10}$  was oxidized by a molar equivalent of xenon difluoride dissolved in anhydrous hydrogen fluoride.<sup>22</sup> Further oxidation of the rhenium fluoride using xenon

difluoride in anhydrous hydrogen fluoride produced an insoluble brown solid which was formulated as  $\text{Re}(\text{CO})_3\text{F}_3$ .<sup>23</sup> When excess xenon difluoride was added to  $\text{Re}(\text{CO})_5\text{F}$  or  $\text{Re}(\text{CO})_3\text{F}_3$  the green product that formed was identified as rhenium pentafluoride. An attempt to prepare the rhenium monofluoride complex by reacting  $\text{Re}_2(\text{CO})_{10}$  with rhenium hexafluoride resulted in the formation of the mixture of products  $\text{Re}(\text{CO})_5\text{F}$ ,  $\text{Re}(\text{CO})_3\text{F}_3$  and  $\text{ReF}_5$ .<sup>22,23</sup>

Bruce and co-workers, however, reported<sup>24,25</sup> that the reaction of  $\text{Re}_2(\text{CO})_{10}$  with rhenium hexafluoride in anhydrous hydrogen fluoride yielded a mixture of an orange and a green product characterized as  $[\text{Re}(\text{CO})_5\text{F}\cdot\text{ReF}_5]$  and  $[\text{Re}(\text{CO})_6]^+[\text{Re}_2\text{F}_{11}]^-$ , respectively. A systematic study<sup>26</sup> of reactions of  $\text{Re}_2(\text{CO})_{10}$  with varying amounts of xenon difluoride in 1,1,2-trichlorotrifluoroethane at room temperature led to the preparation of pure  $[\text{Re}(\text{CO})_5\text{F}\cdot\text{ReF}_5]$ . The crystal structure of the latter shows that the two rhenium atoms are linked by a fluoride bridge.<sup>25</sup> When  $[\text{Re}(\text{CO})_5\text{F}\cdot\text{ReF}_5]$  was reacted with excess xenon difluoride rhenium hexafluoride was produced according to the following stoichiometric equation:



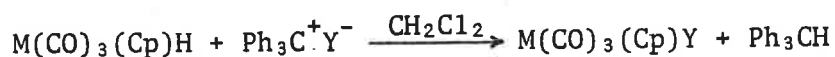
Other compounds of the type  $[\text{Re}(\text{CO})_5\text{F}\cdot\text{YF}_5]$  (where, Y = As, I, Ta) and  $[\text{Re}(\text{CO})_6]^+[\text{MnF}_{5n+1}]^-$  (where, M = Re, Sb) have been tabulated by Bruce and Holloway.<sup>27</sup>

## 1.2 COORDINATED FLUORO- AND OXY-LIGANDS

Some transition metal carbonyl complexes containing poor coordinating ligands such as  $(\text{AsF}_6^-)^{16}$ ,  $(\text{BF}_4^-)^{28,29}$ ,  $(\text{ClO}_4^-)^{14,30,31}$  and  $(\text{PO}_2\text{F}_2^-)^{14,30}$  have been prepared by halide abstraction reactions. The corresponding silver salt (e.g.  $\text{AgAsF}_6$ , etc.) is simply added to a solution (e.g.  $\text{CH}_2\text{Cl}_2$ )

containing the metal halide (i.e. Cl, Br, I). The method involves the removal of the halide from the metal by the silver ion producing a "16-electron" intermediate. When the reactions are carried out in chloroform, dichloromethane, sulphur dioxide or tetrahydrofuran a solvent molecule coordinates initially and is subsequently replaced by the respective anion.

The molybdenum and tungsten complexes  $M(\text{CO})_3(\text{Cp})\text{Y}$  (where, 1.  $M = \text{Mo}$ ,  $\text{Y} = \text{BF}_4^-$ ,  $\text{PF}_6^-$ ; 2.  $M = \text{W}$ ,  $\text{Y} = \text{BF}_4^-$ )<sup>32</sup> were prepared by hydride abstraction. The corresponding metal hydrides were reacted with triphenylmethyl carbonium salts ( $\text{Ph}_3\text{C}^+\text{Y}^-$ ) in the dichloromethane according to the following equation:



The reactions are carried out in the temperature ranges  $-40^\circ\text{C}$  to  $-30^\circ\text{C}$  and  $-5^\circ\text{C}$  to  $+10^\circ\text{C}$  when preparing the metal-tetrafluoroborates and -hexafluorophosphate, respectively. The complexes were characterized by the nature of the carbonyl stretching bands and  $\nu(\text{X}-\text{F})$ , ( $\text{X} = \text{B}, \text{P}$ ) bands in their infrared spectra. The coordinated fluoro- and oxy-anion ligands in these and the above complexes are labile and are easily substituted by halide ions ( $\text{Cl}^-$ ,  $\text{Br}^-$ ,  $\text{I}^-$ ), some organic ligands and by water.

Aquo-complexes have been prepared by a number of methods including performing the halide and hydride abstraction reactions in the presence of water.<sup>28, 32, 33, 34</sup> The  $[\text{Mn}(\text{CO})_5(\text{H}_2\text{O})]^+$  species was identified as a by-product of the acidic hydrolysis of the 3- and 4-pyridiomethyl-manganesepentacarbonyl ions in aqueous solution.<sup>35</sup> The rhenium complexes,  $\text{Re}(\text{CO})_3(\text{H}_2\text{O})_2\text{X}$  (where,  $\text{X} = \text{Cl}, \text{Br}$ ) were prepared by refluxing the respective pentacarbonyl halides in a formic acid-hydrochloric acid mixture.<sup>36</sup>

Transition metal (Cr, Ir, Mo, Rh, W) carbonyl hydroxo complexes are relatively common and have been prepared by several methods<sup>37, 38, 39, 40, 41, 42, 43, 44</sup>. Many of these exist as hydroxy-bridged dimers. Of the few manganese(I) and rhenium(I) hydroxo complexes prepared to date the following tetrameric species are of interest. The manganese cluster,  $[\text{Mn}(\text{CO})_3\text{OH}]_4$  was prepared by refluxing the complexes  $[\text{fac-Mn}(\text{CO})_3\text{L}_3]^+[\text{Mn}(\text{CO})_5]^-$  (where,  $\text{L} = \text{NH}_3, \text{CH}_3\text{CN}$ )<sup>45</sup> in wet tetrahydrofuran for 12 to 15 hours. It has been shown that the cation,  $[\text{Mn}(\text{CO})_3\text{L}_3]^+$  is responsible for the formation of the hydroxo cluster. Reacting the complex  $[\text{fac-Mn}(\text{CO})_3(\text{CH}_3\text{CN})_3]\text{PF}_6$ <sup>46</sup> with water under reflux conditions also produced the manganese cluster according to the following equation:



The rhenium cluster,  $[\text{Re}(\text{CO})_3\text{OH}]_4$  was prepared by reacting either  $\text{Re}_2(\text{CO})_{10}$  or  $\text{Re}(\text{CO})_5\text{Cl}$  with water in a diethylether-diazoethane-water mixture under photolytic conditions at 200°C.<sup>47, 48</sup> In both the manganese and rhenium clusters the  $\text{M}(\text{CO})_3$  groups are linked by triply-bridging hydroxo ligands.<sup>49</sup>

### 1.3 CHARACTERIZATION OF METAL CARBONYLS

The bonding between the metal and the carbonyl group in transition metal carbonyl complexes can be understood in terms of two components. First, the "forward"  $\sigma$ -bond, which results from the overlap of a filled carbon  $\sigma$  orbital ( $5\sigma$ ) with an empty  $\sigma$ -type orbital ( $d$ ) on the metal atom. Second, the "back"  $\pi$ -bond, which results from the overlap of a filled  $d\pi$  metal orbital with the empty  $2p\pi^*$  antibonding orbital of carbon monoxide. The two components of the metal-carbonyl bonding are synergic. The  $\pi$  "back-bonding" makes the metal a better  $\sigma$ -acceptor and thus enhances

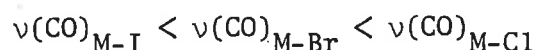
the  $\sigma$ -bond strength.<sup>50, 51, 52</sup> This characteristic has become very useful to the synthetic chemist, since the back-donation from the metal to the carbonyl group determines the value of the carbonyl stretching frequency. This section discusses how the complexes presented in this thesis have been characterized on the basis of their carbonyl stretching modes.

Most of the thousands of metal carbonyl complexes synthesized exhibit strong and sharp carbonyl stretching bands in the region 2200 - 1650  $\text{cm}^{-1}$  of the infrared spectrum. The spectra and structures of these complexes have been studied extensively and the results are well documented in the literature.<sup>4, 53, 54, 56, 57, 58</sup> The  $\nu(\text{CO})$  stretching motions are sensitive to the electronic environment. Hence, the  $\nu(\text{CO})$  frequencies give information about the electron availability within the molecule. While, the number of bands and their relative intensity provides information about the symmetry of the arrangement of the carbonyl groups in the molecule.

It is often possible to infer the type of non-carbonyl ligand that is also coordinated from a comparison of the  $\nu(\text{CO})$  stretching frequencies of similar compounds. A study of the infrared spectra of the series of compounds,  $\text{M}(\text{CO})_5\text{X}$ , and  $\text{M}(\text{CO})_3(\text{PPh}_3)_2\text{X}$  (where,  $\text{M} = \text{Mn}, \text{Re}$ ;  $\text{X} = \text{Cl}, \text{Br}, \text{I}$ )<sup>53, 58</sup> shows that the electronegativities of the coordinated halides is reflected in the carbonyl frequencies. The increasing electronegativity of the halide in the following sequence:



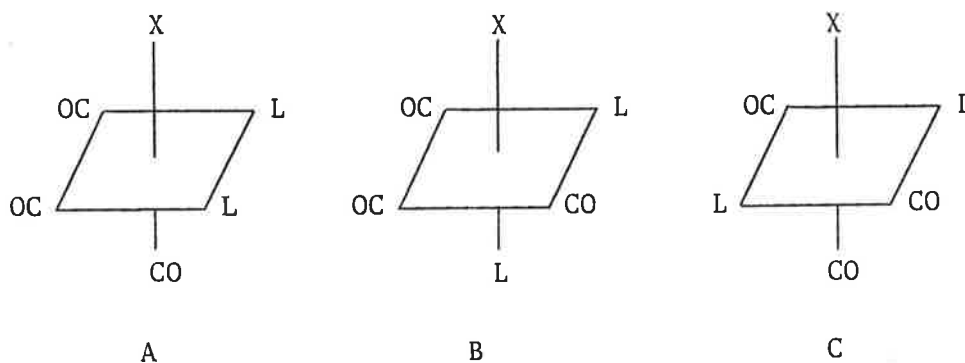
results in an increase in the  $\nu(\text{CO})$  stretching frequencies for the respective compounds in the order:



From such trends one can deduce that substituting the bromide atom in a

molecule with a fluorine (Chapter 3), for example, will result in an increase in the  $\nu(\text{CO})$  stretching frequencies. Hence, the synthetic chemist can monitor the progress of a reaction by following the change in the carbonyl absorption bands.

The arrangement of ligands about the metal centre of the complexes present in this thesis has been deduced from the number and the relative intensities of the  $\nu(\text{CO})$  stretching bands. A few examples of the type of compounds encountered are given here, but for more comprehensive information the literature<sup>53, 57, 58, 59, 60</sup> should be consulted. Most metal pentacarbonyl complexes,  $\text{M}(\text{CO})_5\text{X}$  (where,  $\text{M} = \text{Mn}, \text{Re}$ ;  $\text{X} = \text{halogen}$ ) exhibit three infrared-active carbonyl modes ( $2\text{A}_1 + \text{E}$ ) in their spectra. The intensity of the  $\text{A}_1^{(2)}$  mode at the high frequency ranges from medium to extremely weak. While, the low frequency  $\text{A}_1^{(1)}$  mode is usually medium to weak in intensity. The absorption due to the E mode is always intense. The relative order of occurrence of the bands from high to low frequency is:  $\text{A}_1^{(2)} > \text{E} > \text{A}_1^{(1)}$ . The compounds of the type *cis*- $[\text{M}(\text{CO})_3\text{X}_3]$  or *cis*- $[\text{M}(\text{CO})_3\text{X}]_4$  (e.g.  $[\text{Re}(\text{CO})_3\text{F}]_4$ , Chapter 2) exhibit two infrared-active  $\nu(\text{CO})$  modes ( $\text{A}_1 + \text{E}$ ). The intensity of the  $\text{A}_1$  mode at the higher frequency is usually about one half of the E mode absorption. Complexes with the general formula  $\text{M}(\text{CO})_3(\text{L}_2)\text{X}$  (where,  $\text{L}_2 =$  two mono- or one bi-dentate ligand) can exist as three isomeric forms: *fac*, *mer-cis*- $\text{L}_2$  and *mer-trans*- $\text{L}_2$  (Diagrams A, B and C, respectively). In the *fac* form



(e.g.  $\text{Mn}(\text{CO})_3(\text{diphos})\text{X}$ , Chapter 4) the carbonyl groups are in a mutually *cis* arrangement and three strong absorption bands ( $2\text{A}' + \text{A}''$ ) are expected. The *mer-cis*- $\text{L}_2$  isomer has one of the ligands (L) *trans* to X and a spectrum with a weak absorption band is expected. However, this isomer is not expected to form, since carbonyl substitution normally occurs in a position *cis* to the halide group. The *mer-trans* isomer has the ligands (L) *trans* with respect to each other and the spectra of such compounds exhibit a weak ( $\text{A}_1^{1\text{b}}$ , at high freq.) and two strong ( $\text{A}_1^{1\text{a}} + \text{B}_1$ ) absorption bands. Hence, the three isomers can be distinguished by the relative band intensities.

Where X in the above formulae is a coordinated fluoro- or oxy-ligand (e.g.  $\text{AsF}_6^-$ ,  $\text{BF}_4^-$ ) a consideration of the  $\nu(\text{As}, \text{B-F})$  stretching modes also assists in the characterization of the carbonyl complexes. More details on these type of stretching modes are given in Chapter 5.

## CHAPTER 2

### METAL CARBONYL CLUSTERS

#### 2.1 INTRODUCTION

The chemistry of the manganese carbonyl halide species  $\text{Mn}(\text{CO})_5\text{X}$  and  $[\text{Mn}(\text{CO})_4\text{X}]_2$  (where,  $\text{X} = \text{Cl}, \text{Br}, \text{I}$ ) has been well established<sup>7,61,62,63,64,65,66</sup> since the initial preparation of  $\text{Mn}(\text{CO})_5\text{I}$ , reported<sup>9</sup> in 1954. However, till recently<sup>67</sup> fluorocarbonyls of manganese have been unknown. Prior to the commencement of the work reported in this chapter only three manganese carbonyl fluorides had been reported, namely  $[\text{Mn}(\text{CO})_5\text{F}] \cdot \text{AsF}_5$ ,<sup>16</sup>  $\text{Mn}(\text{CO})_3\text{F}_3$ <sup>10</sup> and  $[\text{Mn}(\text{CO})_4\text{F}]_2$ .<sup>10</sup> This lack of manganese fluoride complexes initiated the search for facile reaction pathways to fluoro-organometallic complexes. An investigation<sup>11</sup> into the preparation of  $\text{Mn}(\text{CO})_5\text{F}$  and  $\text{Mn}(\text{CO})_3\text{F}_3$  from  $\text{Mn}(\text{CO})_5\text{Cl}$  using silver and thallium fluoride lead to the characterisation of the cluster species  $[\text{Mn}(\text{CO})_3\{\text{F}_x, (\text{OH})_{1-x}\}]_4$  (where,  $x = 0 - 1$ ) and  $[\text{Mn}(\text{CO})_3\text{F}]_4$ , as is reported in this chapter.

Rhenium carbonyl chlorides, bromides and iodides, as for the manganese analogues, have been known<sup>68,69,70</sup> for decades. But, the few rhenium fluoride complexes have only recently been reported.<sup>16,22,23,24,47,48</sup> The attempts to isolate the  $\text{Re}(\text{CO})_5\text{F}$  complex have given rise to the establishment of a method for obtaining the pure  $[\text{Re}(\text{CO})_3\text{F}]_4$  cluster. As described in this chapter, the generality of the method was subsequently tested with the preparation of the rhodium cluster,  $[\text{Rh}(\text{PPh}_3)\text{F}]_4$ .



## 2.2 PREPARATION AND PROPERTIES OF THE CLUSTERS

### 2.2.1 $[\text{Mn}(\text{CO})_3\{\text{F}_x(\text{OH})_{1-x}\}]_4$ and $[\text{Re}(\text{CO})_3\text{F}]_4 \cdot 4(\text{H}_2\text{O})$

The manganese(I) cluster series has been prepared by Zeleny<sup>11</sup> from  $\text{Mn}(\text{CO})_5\text{Cl}$  using both silver and thallium fluoride. These preparations yielded clusters where  $x$  varied from 0 to 1 depending on the amount of water present during the reaction. The highest percentage fluoride content was achieved using silver fluoride. Mass spectra showed that the isolated products contained a mixture of clusters, where  $x = .5$ ,  $.75$  and  $1$ . However, because of a small amount of water ( $\delta$ ) present in the silver fluoride the pure  $[\text{Mn}(\text{CO})_3\text{F}]_4$  cluster could not be isolated. The cluster series was further characterized by infrared spectra (Table 2.2.1), microanalysis and x-ray structure analysis (§ 2.3).

The reaction of bromopentacarbonylrhenium(I) with excess silver fluoride in fluorobenzene ( $\text{C}_6\text{H}_5\text{F}$ ) at room temperature yields an unstable fluoropentacarbonyl rhenium(I) intermediate and silver bromide, by bromide-abstraction:



The reaction also occurs in dichloromethane, but due to the formation of the solvated complex  $[\text{Re}(\text{CO})_5(\text{CH}_2\text{Cl}_2)]^+$  and  $[\text{Re}(\text{CO})_5\text{Cl}]$ , which have since been reported<sup>15, 21</sup> for the preparation of  $[\text{M}(\text{CO})_3\text{L}_2\text{Y}]$  compounds (where,  $\text{M} = \text{Mo}, \text{W}$ ,  $\text{L}_2 = \text{C}_5\text{H}_5$  and  $\text{Y} = \text{PF}_6^-$ ;  $\text{M} = \text{Re}$ ,  $\text{L}_2 = 2(\text{CO})$ , bpy and  $\text{Y} = \text{ClO}_4^-$ ), fluorobenzene was used. To date compound (1) has not been isolated due to the partial conversion to the tetramer at and above room temperature. The carbonyl  $\nu(\text{CO})$  absorption pattern of the former in fluorobenzene is consistent with the stretching modes for  $\text{M}(\text{CO})_5\text{X}$  type molecules (where,  $\text{M} =$  transition metal and  $\text{X} =$  halide). The difference between the CO

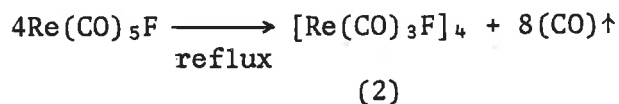
TABLE 2.2.1  
Infrared Stretching Frequencies ( $\text{cm}^{-1}$ )

Compound	$\nu(\text{CO})$	$\nu(\text{OH})$	Medium
Compound (1)	2152w, 2057s, 1981s		fluorobenzene
$\text{Re}(\text{CO})_5\text{F}^a$	2160w, 2050s, 1970s, 1955ssh		nujol
$\text{Re}(\text{CO})_5\text{Br}$	2161w, 2051s, 1985s		fluorobenzene
$[\text{Re}(\text{CO})_3\text{F}]_4 \cdot 4\text{H}_2\text{O}$	2043ms, 1932s		fluorobenzene
	2092m, 2041s, 1932ssh, 1901s	3570wsh, 3530w(sharp)	nujol
$[\text{Re}(\text{CO})_3\text{Cl}]_4^{b,c}$	2060s, 1943s		in KBr disc
$[\text{Re}(\text{CO})_3\text{Br}]_4$	2059s, 1941s <sup>b,c</sup>		in KBr disc
	2032s, 1913s		fluorobenzene
$[\text{Re}(\text{CO})_3\text{I}]_4^c$	2050br, 1950br		in KBr disc
$[\text{Re}(\text{CO})_3(\text{OH})]_4^d$	2021s, 1919vs	3550 (sharp doublet)	THF

$a$  = Ref. 11;  $b$  = Ref. 57;  $c$  = Ref. 71;  $d$  = Ref. 24

stretching frequencies (Table 2.2.1) of compound (1) and of the reported  $\text{Re}(\text{CO})_5\text{F}$ <sup>22</sup> complex can be attributed to solvent effects.

After separating the silver bromide precipitate and the excess silver fluoride ( $\text{AgF}\cdot\delta(\text{H}_2\text{O})$ ) from the solution, the rhenium fluoride intermediate (1) is completely converted to the cluster complex (2) under reflux conditions (90 - 100°C):



The product (2) crystallizes as yellow crystals of  $[\text{Re}(\text{CO})_3\text{F}]_4\cdot 4(\text{H}_2\text{O})$  from fluorobenzene after concentration and cooling (*ca* 0°C) the solution. The fluorine atoms were initially identified as coordinating ligands by a comparison of the carbonyl stretching frequencies of the analogous hydroxo-cluster (Table 2.2.1) and a consideration of the fragmentation series in the mass spectra. The infrared spectra in the carbonyl stretching region shows strong  $A_1$  and E modes at respectively higher and lower frequencies, which are typical of a *fac*-tricarbonyl geometry.<sup>11, 57, 72</sup> In the (OH)-stretching region the infrared spectra exhibits relatively sharp  $\nu(\text{OH})$  absorption signals due to both ( $-\text{F}\cdots\text{H}-\text{O}-$ ) and ( $\text{HO}-\text{H}\cdots\text{OH}_2$ ) type hydrogen bonding (Figure 2.4.2). The above physical properties are consistent with the structure of  $[\text{Re}(\text{CO})_3\text{F}]_4\cdot 4(\text{H}_2\text{O})$  (§ 2.4).

### 2.2.2 $[\text{M}(\text{CO})_3\text{F}]_4$ (where, M = Mn, Re)

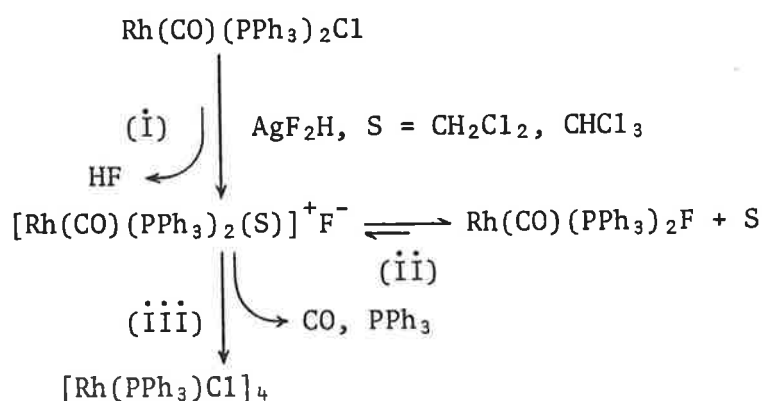
The manganese and rhenium pentacarbonyl halides ( $\text{Mn}(\text{CO})_5\text{Cl}$  and  $\text{Re}(\text{CO})_5\text{Br}$ ) react with dry silver bifluoride in dry fluorobenzene and a dry nitrogen atmosphere at 25°C to form the respective unstable metal pentacarbonyl fluoride complexes. These, subsequently disproportionate

and form the less soluble metal carbonyl clusters  $[M(CO)_3F]_4$  (where,  $M = Mn, Re$ ). The only difference in the preparation of these two clusters is that, due to the greater stability of the rhenium carbonyl fluoride, reflux conditions ( $90 - 100^\circ C$ ) were required for the formation of the rhenium cluster. Both clusters have been characterized by infrared (Table 2.2.1 and § 2.6) and microanalysis (§ 2.7) results. However, due to the formation of only multi-twinned crystals during crystallization, no structural evidence is available to date.

Both clusters are stable in solution to both solvent and halide (e.g.  $Cl^-$ ,  $Br^-$ ) substitution. But, the metal pentacarbonyl fluoride intermediates will undergo halide substitution within seconds. Thus, it is essential to use calcium fluoride solution cells and not sodium chloride cells when monitoring the reaction progress by infrared measurements.

### 2.2.3 $[Rh(PPh_3)X]$ (where, $X = Cl, F$ )

Attempts to prepare  $Rh(CO)(PPh_3)_2F$  by chloride abstraction from  $Rh(CO)(PPh_3)_2Cl$  using silver bifluoride in dichloromethane and chloroform solutions resulted in the formation of the  $[Rh(PPh_3)Cl]_4$  cluster. The proposed reaction pathway is shown in Scheme 2.2.1.



SCHEME 2.2.1 The Formation of  $[Rh(PPh_3)Cl]_4$

Step (i) in the reaction scheme is complete within minutes after the addition of silver bifluoride to a solution of  $\text{Rh}(\text{CO})(\text{PPh}_3)_2\text{Cl}$ . The solvato complex  $[\text{Rh}(\text{CO})(\text{PPh}_3)_2(\text{S})]^+$  (where,  $\text{S} = \text{CH}_2\text{Cl}_2, \text{CHCl}_3$ ) is in equilibrium with the rhodium fluoride species (step (ii)). The final step (iii) as monitored by infrared shows the loss of the carbonyl group within 90 min at  $25^\circ\text{C}$ . Structure analysis results (§ 2.5) further indicate that the disproportionation of the solvato complex also involves the loss of a triphenyl phosphate ligand and the chloride substitution from the coordinated solvent molecule, resulting in the formation of the cluster,  $[\text{Rh}(\text{PPh}_3)\text{Cl}]_4$ .

When fluorobenzene ( $\text{C}_6\text{H}_5\text{F}$ ) is used as the solvent in the above scheme the halide abstraction results in the formation of the rhodium carbonyl fluoride complex. This intermediate slowly disproportionates forming the rhodium fluoride cluster and a black non-carbonyl containing precipitate over a period of *ca* 5 hr at  $25^\circ\text{C}$ . The formation of the black product is minimised by stirring the filtered rhodium(I) carbonyl fluoride solution in the dark. As has been reported (§ 2.2) for the manganese and rhenium clusters, the rhodium halide clusters are stable to further halide (i.e.  $\text{Cl}^-$ ,  $\text{Br}^-$ ) substitution. But, the solvent or rhodium carbonyl fluoride intermediates will react with halides (e.g.  $\text{Cl}^-$ ,  $\text{Br}^-$ ) in seconds. To date no structural evidence is available due to both the slow decomposition of the cluster in crystallizing solutions and due to the formation of unsuitable crystals for x-ray studies.

2.3 STRUCTURE DETERMINATION OF  $[\text{Mn}(\text{CO})_3\{\text{F}_x, (\text{OH})_{1-x}\}]_4 \cdot 2(\text{C}_6\text{H}_6)$   
(where,  $x = 0.35$ )

2.3.1 Crystal Data

Crystals of the title compound crystallize as regular dodecahedra and precession photography determined them to be of the cubic space group,  $\text{Pn}\bar{3}\text{m}$ . Dr. O. Geiss kindly confirmed the space group using a silicon calibrated (NBS-SRM 640,  $a = 5.403088 \text{ \AA}$ ) powder photograph and calculated the cell constants by best fit of 40 reflections with the least-squares program LSUCRE.<sup>73</sup> The density was measured by floatation in a mixture of 1,2-dibromoethane and carbon tetrachloride. The crystals slowly dissolve in this mixture, hence the unusually large uncertainty in the measured density. The value of  $x$  in the formula was calculated from the microanalysis results of a sample of crystals taken from the same batch from which samples were used for structure analysis and all the other physical measurements. The crystal data is:

$\text{C}_{24}\text{H}_{14.6}\text{F}_{1.4}\text{Mn}_4\text{O}_{14.6}$ ; M.W. = 782.67; Cubic, space group  $\text{Pn}\bar{3}\text{m}$ ,  
 $a = 11.2771(5) \text{ \AA}$ ;  $U = 1434.13(21) \text{ \AA}^3$ ;  $Z = 2$ ;  $D_c = 1.814 \text{ g.cm}^{-3}$ ,  
 $D_m = 1.89(9) \text{ g.cm}^{-3}$ ;  $\lambda_{\text{MoK}\alpha} = 0.7107 \text{ \AA}$ ;  $F(000) = 776$  electrons;  
 $\mu_{\text{MoK}\alpha} = 17.0 \text{ cm}^{-1}$ .

A dodecahedral crystal of dimensions  $0.21 \times 0.21 \times 0.21 \text{ mm}^3$  was coated with epoxy-resin and mounted about a cubic axis (c) on the STOE (Chapter 7.1). The reflection intensities were collected in the range  $2.5 < 2\theta < 70^\circ$  by the  $\omega$  scan technique for the levels  $hk0$  to  $hk10$ . A basic step counting time of 0.07 seconds at each  $0.01^\circ$  of the scan range ( $\Delta\omega$ ) was used with 5.0 seconds for each background counting time.  $\Delta\omega$  for the upper level reflections was varied according to the formula:

$$\Delta\omega = 1.3 + 0.95(\sin\mu/\tan(\psi/2))$$

where,  $\mu$  is the equi-inclination angle and  $\psi$  is the detector angle. Lorentz and polarisation corrections were applied on a total of 2652 reflections by the data reduction program AUPTP.<sup>74</sup> Absorption corrections and symmetry averaging with program SHELX<sup>75</sup> gave 600 unique reflections with  $I > 2.5\sigma(I)$ .

### 2.3.2 Structure Solution and Refinement

The density, unit-cell volume and the space group (Pn3m) require that the 8 manganese atoms per cell occupy the special positions  $3(8,3m)$  along the body diagonal. The unique manganese coordinates of the type (x,x,x) were determined from the largest peaks of the Patterson map. A difference map based on the manganese position revealed the cubane nature of the cluster with the fluorine-hydroxy atoms also located on e sites and with the carbonyl groups on  $k(24,m)$  sites. Following a least-square refinement for all the cluster atoms, the associated Fourier difference map revealed a benzene molecule centred on each of the  $c(4,\bar{3}m)$  sites. A full-matrix least-squares refinement, with all non-hydrogen atoms modelled anisotropically and the benzene hydrogen isotropically, converged with an R value of 0.050<sub>3</sub> using unit-weights. In the final calculation the weighting scheme (Chapter 7.1) was employed and R converged at 0.042<sub>8</sub> and  $R_w$  at 0.042<sub>2</sub>, with  $k = 7.86$  and  $g = 5.4 \times 10^{-5}$ . The  $\mu_3$ -hydroxy oxygen and fluoro sites were refined as oxygen atoms (0(2)). The hydroxide hydrogen atom could not be located in the final difference map. In this map the largest peak was 0.7 eÅ<sup>-3</sup>. In the first structure determination based on the previous data collection two problems were encountered. Firstly, the refinement using the program FUORFLS,<sup>76</sup> in which the necessary constraints had to be applied after each least-squares cycle, lead to a false minimum with a much higher R-factor (0.18). When using the program SHELX<sup>75</sup> the

calculation converged smoothly giving an R value of 0.12. Secondly, this value high value was a result of disorder in the benzene groups.

In all refinements the scattering factors<sup>77</sup> for the corresponding neutral atoms were used. The final atomic parameters, bond lengths and bond angles are given in Tables 2.3.1, 2.3.2 and 2.3.3 respectively. The tabulated observed and calculated structure factors are given on the microfiche enclosed in this thesis.

### 2.3.3 Description of the Structure

ORTEP<sup>78</sup> plots of the cluster and of a packing diagram of the structure are given in Figures 2.3.1 and 2.3.2. The structure consists of a body-centred cubic array of cubane-type clusters  $Mn_4(CO)_{12}\{F,OH\}_4$ , with benzene of solvation on the cube diagonals between adjacent pairs of (F/OH) sites. The very high symmetry of the crystals appears to result from the benzene of solvation. The cluster itself has the very high crystallographic symmetry  $\bar{4}3m$ , which is so far unique for clusters of this type. It is, however, achieved by disorder of hydroxide and fluoride. Many clusters of the type  $[MRX]_4$  have been described with lower crystallographic symmetry, e.g.  $[Os(CO)_3O]_4$  ( $\bar{4}2m$ )<sup>79</sup> and  $[Mo(NO)(CO)_2(OH)]_4$  (23).<sup>80</sup> Other species where R contains carbonyl groups or X is hydroxide include  $[W(CO)_3(OH)]_4$ ,<sup>81</sup>  $[Pt(CH_3)_3(OH)]_4$ ,<sup>82</sup>  $[Re(CO)_3SCH_3]_4$ <sup>83</sup> and  $[Re(CO)_3X]_4$  (where, X = F, I).<sup>84,85</sup> The geometry of the clusters are all similar and as here do not involve metal-metal bonding.<sup>81</sup> The angles within the cluster cube tend to remain constant for the carbonyl/hydroxy clusters since the M-O and M-M distances increase congruently from the manganese to the molybdenum and tungsten examples. All have O-M-O angles near  $76^\circ$  and M-O-M angles near  $102^\circ$ . The cube geometry is determined by the limiting non-bonding contacts on



TABLE 2.3.1

Atomic positional, thermal and occupancy (k) parameters for  $\text{Mn}_4(\text{CO})_{12}(\text{F}_x(\text{OH})_{4-x}) \cdot (\text{C}_6\text{H}_6)_2$ 

Atom <sup>a</sup>	x	y	z	k	U <sub>11</sub>	U <sub>22</sub>	U <sub>33</sub>	U <sub>23</sub>	U <sub>13</sub>	U <sub>12</sub>
Mn	14971 (3)	14971 (3)	14971 (3)	16667	2875(22)	2875(22)	2875(22)	-284(11)	-284(11)	-284(11)
O(1)	1445 (1)	1445 (1)	-1116 (2)	5000	735(10)	735(10)	362(10)	-76 (7)	-76 (7)	-36(11)
O(2) <sup>b</sup>	3293 (1)	3293 (1)	3293 (1)	1667	255 (5)	255 (5)	255 (5)	-10 (5)	-10 (5)	-10 (5)
C(1)	1476 (1)	1476 (1)	-100 (2)	5000	419 (8)	419 (8)	371(11)	-49 (6)	-49 (6)	-36(10)
C(2)	4515 (2)	4515 (2)	5980 (3)	5000	981(17)	981(17)	472(16)	-48 (9)	-48 (9)	-529(20)
H	4181(30)	4181(30)	6612(36)	5000	1279(162)					

<sup>a</sup> Mn parameters  $\times 10^5$  and the others  $\times 10^4$ .<sup>b</sup> O(2) represents the disordered atomic average of F<sup>-</sup> and OH<sup>-</sup> (F, OH).

TABLE 2.3.2

Atomic Distances (Å) for  $[\text{Mn}(\text{CO})_3(\text{F}_x, \{\text{OH}\}_{1-x})]_4^a$ 

(a) Bond lengths			
O(2)-Mn	2.052(3)	C(1)-O(1)	1.146(3)
C(1)-Mn	1.802(3)	C(2) <sup>I</sup> -C(2)	1.349(3)
H(2)-C(2)	0.90 (4)		
(b) Hydrogen bonding distance			
O(2)··· $\pi(\text{C}_6\text{H}_6)$ centre	3.334(2)		
(c) Non-bonding distances			
Mn <sup>II</sup> ···Mn	3.199(1)	O(2) <sup>II</sup> ···O(2)	2.529(3)

TABLE 2.3.3

Bond Angles (°) for  $[\text{Mn}(\text{CO})_3(\text{F}_x, \{\text{OH}\}_{1-x})]_4^a$ 

O(2) <sup>II</sup> -Mn-O(2)	76.1(1)	C(1) <sup>III</sup> -Mn-C(1)	88.5(1)
C(1)-Mn-O(1)	178.7(2)	Mn <sup>II</sup> -O(2)-Mn	102.4(1)
C(1)-Mn-O(2)	97.5(1)		

<sup>a</sup>Superscripts in Roman refer to the following equivalent positions, with respect to the unique asymmetric unit at x, y, z:

$$\begin{aligned} \text{I} &= 1-z, 1-x, 1-y & \text{III} &= z, x, y \\ \text{II} &= x, \frac{1}{2}-y, \frac{1}{2}-z \end{aligned}$$

the diagonals of the cube faces (Fig. 2.3.1) which are both less than van der Waal distances (O-O, 3.3 Å). The Mn(I)(CO)<sub>3</sub> moiety has normal geometry with a Mn-C distance at the lower end of the range of values reported<sup>64-66</sup> for Mn(I)(CO)<sub>5</sub>X species (1.76 - 1.88 Å). A lower value is expected with the electronegative substituents OH and F.

The most notable feature of the structure is that it establishes  $\mu_3$  bridging by fluoride in discrete organometallic species. An example involving CO(II), tetrakis(fluoro, tris(N-ethylimidazole)CO(II))(BF<sub>4</sub>)<sub>4</sub>, has also been reported for a discrete species.<sup>86</sup> Many examples of  $\mu_2$  fluoride bridges are known,<sup>87</sup> but these appear to be the only  $\mu_3$  ones. A recently reported complex, Mn<sub>3</sub>(CO)<sub>9</sub>(OEt)<sub>2</sub>F, has a metal-metal bonded Mn<sub>3</sub> triangle and  $\mu_2$  fluoride and ethoxy groups.<sup>18</sup> The Mn-F distances were 1.97(2) and 1.93(2) Å, about 0.1 Å shorter than the disordered average Mn-(OH,F) of 2.052(3) Å of the tetranuclear cluster in which Mn-Mn bonding is absent.

Figure 2.3.2 shows that the benzene lies directly perpendicular to the cube diagonal of the complex over the (OH,F) groups. The benzene solvate has a single OH stretch at 3543 cm<sup>-1</sup>.<sup>84</sup> No OH...F hydrogen bonding is possible in either compound as it is precluded by benzene interference in the solvate and adjacent clusters cannot have OH...F separations much closer than 3.5 Å. The latter conclusion was arrived at by plotting the non-bonded energy as two clusters were brought together and their orientations adjusted by energy minimisation.<sup>88</sup> Effective OH...F hydrogen bonding normally occurs in the region below 2.8 Å. Hydrogen bonding to aromatics is well known and characterised by a red shift of 60 - 90 cm<sup>-1</sup> of the  $\nu(\text{OH})$  in the infrared and denoted O-H... $\pi$ .<sup>89, 90, 91</sup> Interactions between water and the phenyl rings of tetraphenylborate have been observed crystallographically in

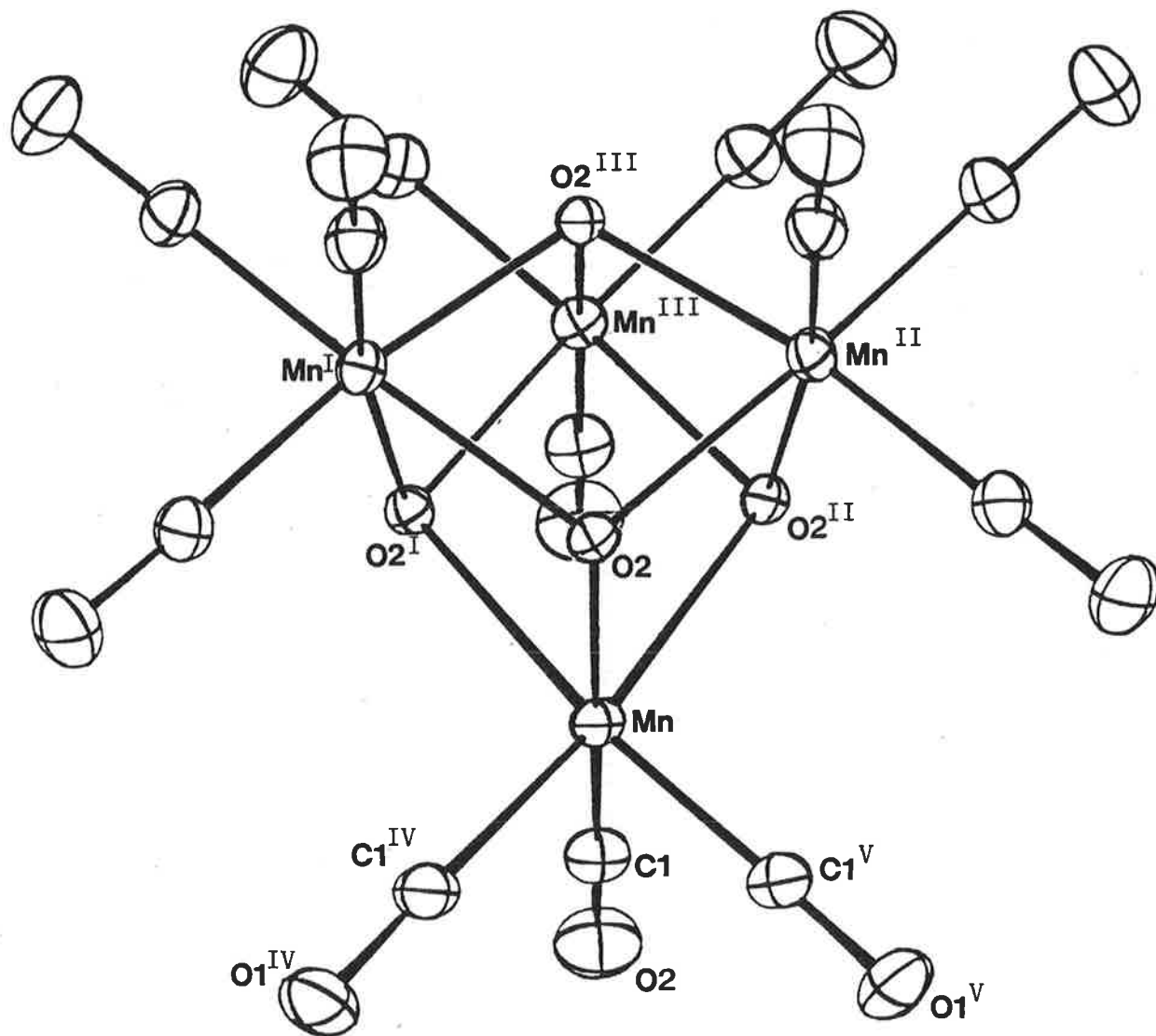


FIGURE 2.3.1. The molecular structure of  $[\text{Mn}(\text{CO})_3\{\text{F}_x, (\text{OH})_{1-x}\}]_4$  (50% probability ellipsoids). Superscripts in Roman refer to the following equivalent positions, with respect to the unique asymmetric unit at

x, y, z:	I	$x, \frac{1}{2}-y, \frac{1}{2}-z$	IV	$z, x, y$
	II	$\frac{1}{2}-x, y, \frac{1}{2}-z$	V	$y, z, x$

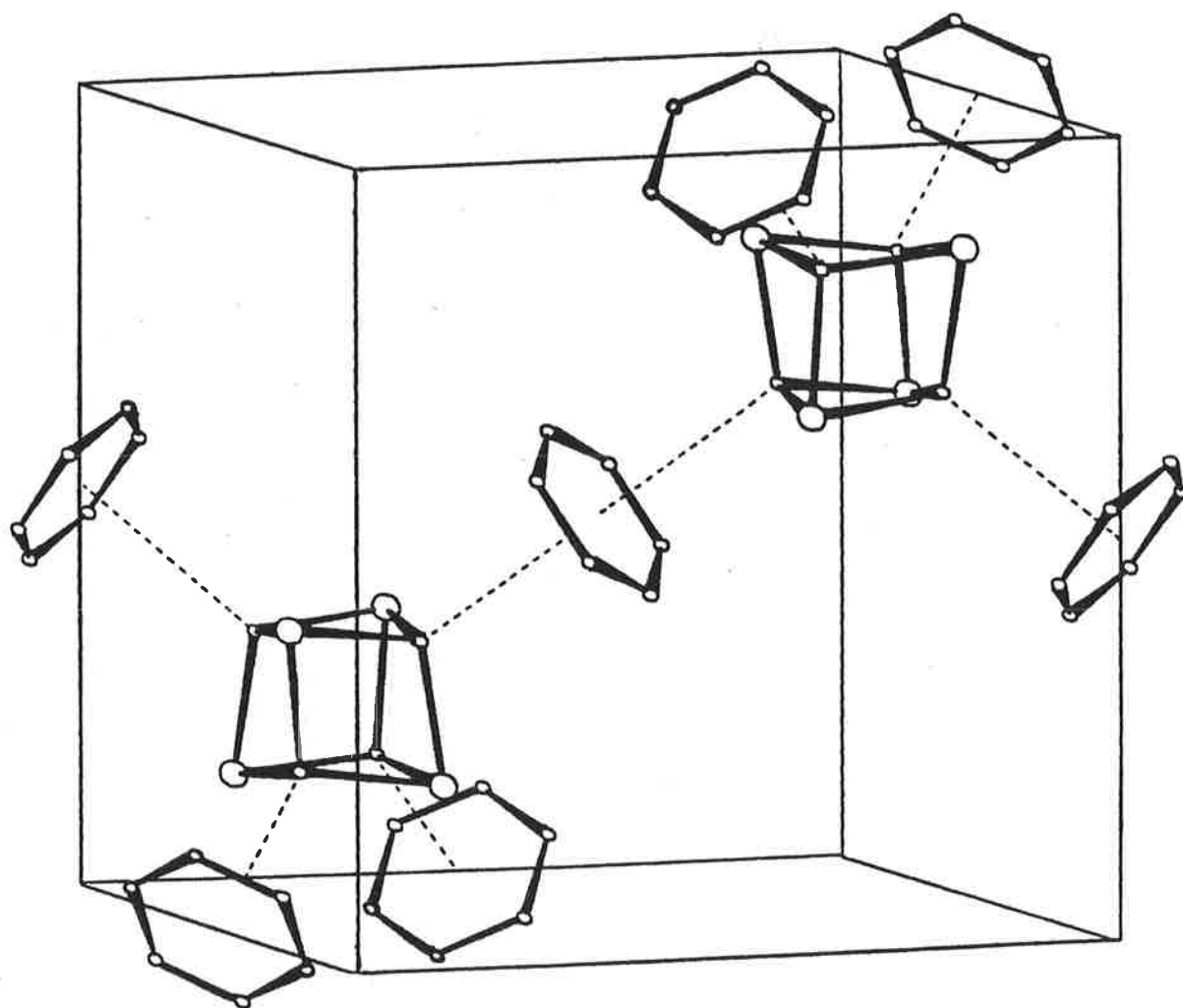
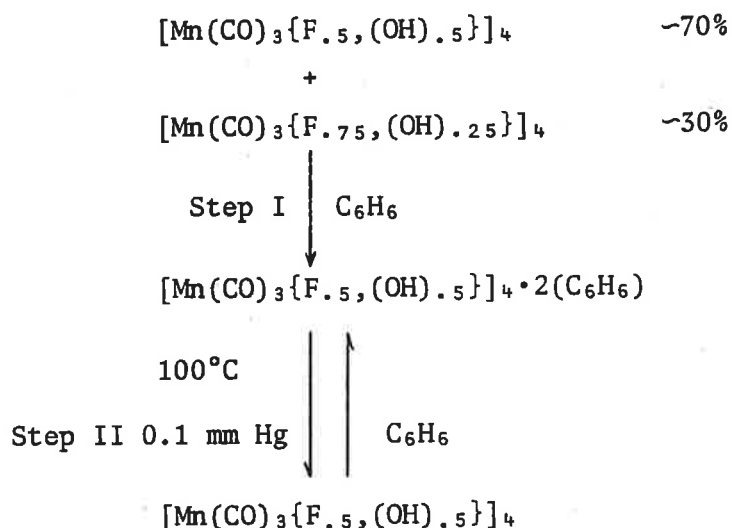


FIGURE 2.3.2. A unit cell plot showing the packing arrangement for  $[\text{Mn}(\text{CO})_3\{\text{F}_x, (\text{OH})_{1-x}\}]_4 \cdot 2(\text{C}_6\text{H}_6)$ . The large spheres represent the manganese tricarbonyl corners of the clusters and the  $(\text{OH} \cdots \pi)$  hydrogen bonding is represented by the broken lines.

tributylammonium tetrphenylborate monohydrate,<sup>92</sup> but there the OH group vector is aligned near to, but not exactly colinear with the perpendicular to the aromatic ring through its centre as is the case here. The distances of the water to the centre of the phenyl group of the tetrphenylborate are 3.12 and 3.17 Å. The distances of the OH,F site of the cluster to the benzene centroid is 3.334(2) Å.

#### 2.3.4 Discussion

The fluorine content ( $x = 0.35$ ) of the above structure was determined from microanalysis results. Since both density measurements and structural refinement methods are insensitive to the difference between a fluorine and a hydroxy group. Snow<sup>11</sup> and co-workers have characterised the four isomers ( $x = 0.25, 0.5, 0.75, 1.0$ ) by mass spectrometry. Furthermore, it was observed that only the mono-fluoride and di-fluoride clusters ( $x = 0.25$  and  $0.5$ , respectively) crystallized with benzene of crystallization from an acetone-benzene mixture. This lead to the development of a purification method (shown below) for the cluster  $[\text{Mn}(\text{CO})_3\{\text{F}_{.5},(\text{OH})_{.5}\}]_4$ . The major products of the silver fluoride reaction are the di-fluoride and tri-fluoride clusters and due to the crystallization properties the former can be isolated (Step I) as the di-fluoride solvate tetramer  $[\text{Mn}(\text{CO})_3\{\text{F}_{.5},(\text{OH})_{.5}\}]_4 \cdot 2(\text{C}_6\text{H}_6)$ . At  $100^\circ\text{C}$  and  $0.1$  mmHg the benzene is removed (Step II, reversible) leaving the pure  $[\text{Mn}(\text{CO})_3\{\text{F}_{.5},(\text{OH})_{.5}\}]_4$  species and resulting in the characteristic infrared shift (§ 2.3.3) of the  $\nu(\text{OH})$  stretching bond from  $3543\text{ cm}^{-1}$  to  $3620\text{ cm}^{-1}$ .



## 2.4 STRUCTURE DETERMINATION OF $[\text{Re}(\text{CO})_3\text{F}]_4 \cdot 4(\text{H}_2\text{O})$

### 2.4.1 Crystal Data

Crystals of the complex were obtained directly from the reaction mixture as needle-like prisms elongated along  $c$  with 110 and 001 faces. The tetragonal space group  $I\bar{4}$ , was determined from systematic absences and confirmed by structure determination. The initial unit-cell parameters from the precession photographs were refined on the Stoe diffractometer as previously described. For the data collection a crystal with dimensions  $0.05 \times 0.05 \times 0.29 \text{ mm}^3$  was coated with epoxy resin and mounted above the  $c$ -axis on a Stoe automated Weissenberg diffractometer equipped with a graphite monochromator. A total of 1531 reflections in the range  $2.5 < 2\theta < 70^\circ$  were obtained by the  $\omega$ -scan technique for the levels  $hk0$  to  $hk11$ . On the upper levels  $\omega$  was varied according to the formula

$$\Delta\omega^\circ = 1.2 + 0.9(\sin \mu / \tan \frac{1}{2}\psi)$$

where,  $\mu$  is the equi-inclination angle and  $\psi$  is the detector angle.

Lorentz and polarization corrections were applied with program AUPTP.<sup>74</sup> Absorption corrections were applied and symmetry averaging with program

SHELX<sup>75</sup> yielded 1380 unique reflections with  $I > 2.5\sigma(I)$ .

Crystal data:  $C_{12}H_8F_4O_{16}Re_4$ , MW = 1229, tetragonal, space group  $I\bar{4}$ ,  $a = 11.716(5)$ ,  $c = 8.988(3)$  Å,  $U = 1233.7(13)$  Å<sup>3</sup>,  $Z = 2$ ,  $D_c = 3.308$  g cm<sup>-3</sup>,  $\lambda(\text{MoK}\alpha) = 0.7107$  Å,  $F(000) = 1056$ ,  $\mu(\text{MoK}\alpha) = 198.89$  cm<sup>-1</sup>.

#### 2.4.2 Structure Solution and Refinement

The position of the unique rhenium atom was determined from a Patterson map. A full-matrix least-squares refinement for isotropic rhenium atoms reduced  $R$  to 0.172; a difference map then revealed all the other atoms in the cluster. A further difference map based on all the cluster atoms revealed the oxygen atom of the water molecules. The subsequent least-squares refinement with anisotropic cluster atoms and isotropic oxygen atoms for the water molecules reduced  $R$  to 0.0332, using the weighting scheme (Chapter 7.1). The calculation was repeated with the sign of all coordinates of the atoms inverted, and  $R$  was reduced to 0.0288; hence the absolute configuration was determined (Chapter 7.1). In the final least-squares calculations all the located atoms were refined anisotropically and the inter-layer scale factors were refined alternatively.  $R$  converged at 0.0268 and  $R_w$  at 0.0277 (Chapter 7.1) with  $k = 1.0$  and  $g = 2.35 \times 10^{-4}$ . The largest peak ( $.8 \text{ e}\text{\AA}^{-3}$ ) remaining in the final difference map was located near the rhenium atom.

In the refinement the scattering factors of the neutral atoms were used from International Tables Vol. IV. The observed and calculated structure factors are given on microfiche. The final atomic parameters, bond lengths and bond angles with the estimated standard deviations are given in Tables 2.4.1, 2.4.2 and 2.4.3, respectively. The structure of  $[\text{Re}(\text{CO})_3\text{F}]_4$  was drawn using the program ORTEP<sup>78</sup> and is shown in Figure 2.4.1. The hydrogen bonding interactions between water molecules and fluorine atoms of two clusters in the same unit cell are shown in Figure 2.4.2.



TABLE 2.4.1

Atomic positional and thermal parameters for  $[\text{Re}(\text{CO})_3\text{F}]_4 \cdot (\text{H}_2\text{O})_4$ 

Atom <sup>a</sup>	x	y	z	U <sub>11</sub>	U <sub>22</sub>	U <sub>33</sub>	U <sub>23</sub>	U <sub>13</sub>	U <sub>12</sub>
Re	-14575(2)	-3458(2)	-13240 (3)	1780(12)	1780(12)	2218(18)	95(10)	-358(10)	-111 (9)
F	-1085(4)	-263(4)	1073 (6)	278(21)	257(21)	360(28)	14(24)	-39(21)	37(18)
O1	-2757(7)	-2593(7)	-1381(17)	515(50)	306(32)	1070(81)	179(55)	-308(60)	-217(33)
O2	-3776(6)	798(8)	-1098(13)	281(31)	634(48)	752(69)	-36(56)	-53(43)	137(33)
O3	-1796(7)	-238(7)	-4696 (8)	523(43)	561(48)	272(32)	-31(34)	-129(30)	00(35)
O4	-3205(7)	-152(8)	-7401(10)	479(43)	571(47)	411(43)	108(37)	-45(35)	-08(37)
C1	-2276(7)	-1752(7)	-1348(17)	301(33)	222(29)	510(52)	41(42)	-135(45)	-121(27)
C2	-2903(6)	373(6)	-1209(13)	207(27)	269(31)	331(44)	11(37)	-27(32)	37(23)
C3	-1642(7)	-302(6)	-3423 (9)	213(29)	187(29)	315(37)	-12(29)	-30(26)	-34(24)

<sup>a</sup> Re parameters  $\times 10^5$  and the others  $\times 10^4$ .

TABLE 2.4.2  
Atomic distances for  $[\text{Re}(\text{CO})_3\text{F}]_4 \cdot (\text{H}_2\text{O})_4$

Atoms <sup>a</sup>	Distance(Å)	Atoms	Distance(Å)
(a) Bond lengths (and standard deviations)			
Re-F	2.200 (5)	Re-C(3)	1.899 (8)
Re-F <sup>II</sup>	2.196 (5)	Re-C	ave. 1.893 (3)
Re-F <sup>III</sup>	2.205 (5)	C(1)-O(1)	1.155 (9)
Re-F	ave. 2.200 (5)	C(2)-O(2)	1.142(11)
Re-C(1)	1.886 (7)	C(3)-O(3)	1.161(12)
Re-C(2)	1.894 (7)	C-O	ave. 1.153(10)
(b) Hydrogen bonds			
F ...O(4) <sup>I</sup>	2.840(11)	O(4) <sup>I</sup> ...O(4) <sup>IV</sup>	2.991(12)
(c) Selected non-bonding distances			
Re...Re <sup>I</sup>	3.510 (3)	F...F <sup>I</sup>	2.616(10)
Re...Re <sup>II</sup>	3.439 (3)	F...F <sup>II</sup>	2.672(10)
Re...Re <sup>III</sup>	3.439 (3)	F...F <sup>III</sup>	2.672(10)

<sup>a</sup> Superscripts in Roman refer to the following equivalent positions, with respect to the unique asymmetric unit at x, y, z:

I = -x, -y, -z

III = -y, x, -z

II = y, -x, -z

IV =  $\frac{1}{2} - y, \frac{1}{2} + x, \frac{1}{2} - z$

TABLE 2.4.3

Bond angles ( $^{\circ}$ )<sup>a</sup> and their standard deviations for  $[\text{Re}(\text{CO})_3\text{F}]_4 \cdot (\text{H}_2\text{O})_4$ 

F-Re-F <sup>II</sup>	74.9(2)	C(1)-Re-C(2)	85.9(4)
F-Re-F <sup>III</sup>	74.7(2)	C(1)-Re-C(3)	87.4(5)
F <sup>II</sup> -Re-F <sup>III</sup>	73.0(2)	C(2)-Re-C(3)	86.6(4)
Re-F-Re <sup>II</sup>	102.6(3)	C-Re-C	ave. 86.6(8)
Re-F-Re <sup>III</sup>	102.9(4)	C(1)-Re-F	98.6(5)
Re-F-Re <sup>III</sup>	105.8(4)	C(2)-Re-F	96.0(4)
		C(3)-Re-F	173.6(3)

<sup>a</sup> Superscripts in Roman refer to the following equivalent positions, with respect to the unique asymmetric unit at x, y, z:

II = y, -x, -z

III = -y, x, -z

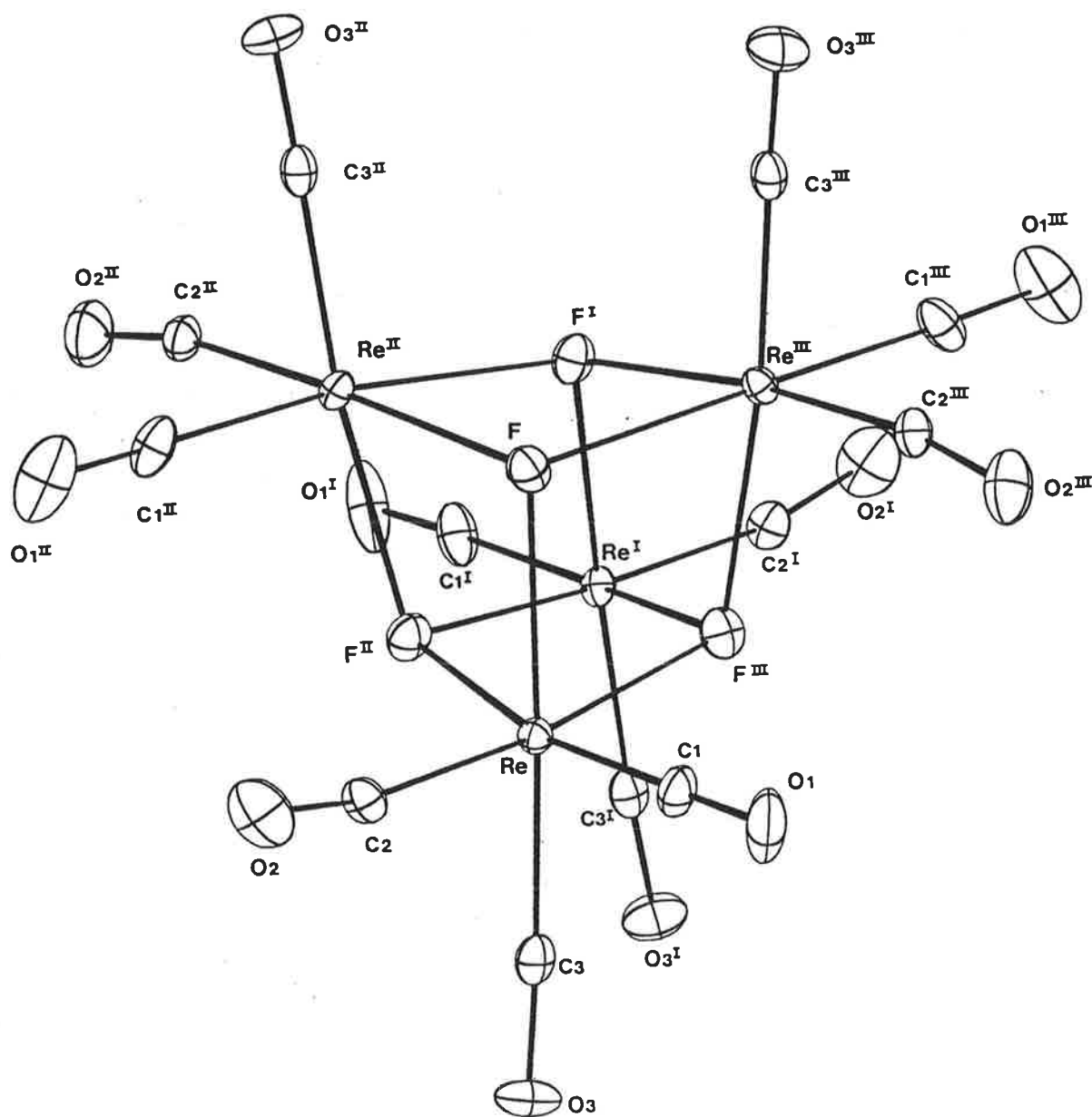


FIGURE 2.4.1. The molecular structure of  $[\text{Re}(\text{CO})_3\text{F}]_4$ . (ORTEP diagram with 25% probability ellipsoids.) Superscripts in Roman refer to the following equivalent positions, with respect to the unique asymmetric unit of the cluster at  $x, y, z$ : I  $-x, -y, z$ ; II  $y, -x, -z$ ; III  $-y, x, -z$ .

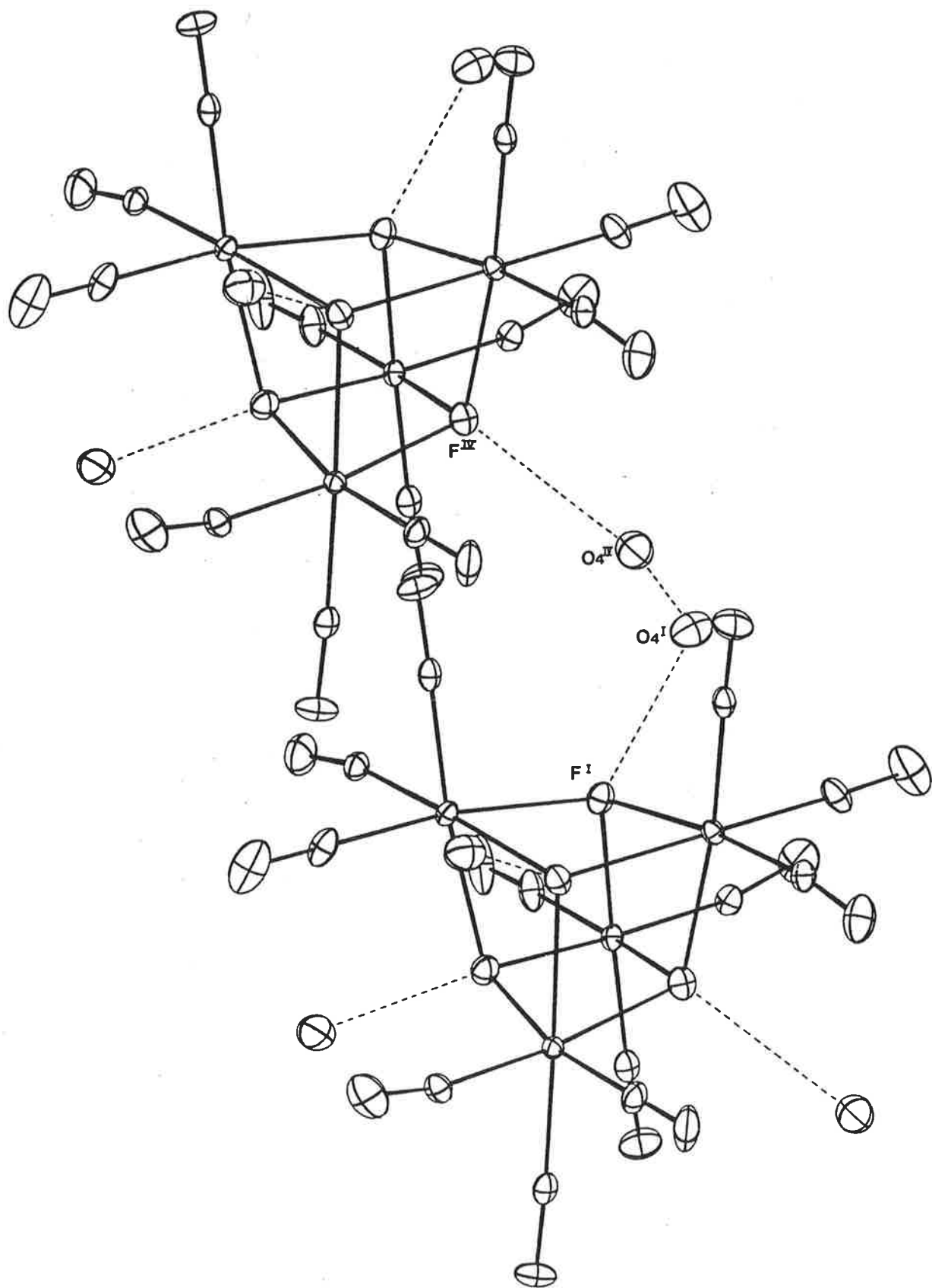


FIGURE 2.4.2. Packing arrangement for  $[\text{Re}(\text{CO})_3\text{F}]_4 \cdot (\text{H}_2\text{O})_4$ , showing  $\text{F} \cdots \text{H}-\text{O}$  and  $\text{HOH} \cdots \text{OH}_2$  hydrogen bonding interactions.

### 2.4.3 Description of the Structure

The compound has a pseudocubane structure, whose corners are alternatively occupied by rhenium and fluorine atoms. The four Re(CO) groups are held together by four triply bridged ( $\mu_3$ ) fluorine ligands exhibiting the non-crystallographic  $\bar{4}3m$  symmetry. The rhenium tetramer belongs to the well established family of compounds with the general formula  $[ML_3X]_4$  (e.g.  $[Co(CO)_3Sb]_4$ ,<sup>93</sup>  $[CoL_3F]_4$ ,  $4(BF_4)$  (where, L = *N*-ethylimidazole or *N*-propylimidazole),<sup>86</sup>  $[Mo(NO)(CO)_2(OH)]_4$ ,<sup>81</sup>  $[Os(CO)_3O]_4$ ,<sup>79</sup>  $[Re(CO)_3I]_4$ ,<sup>85</sup>  $[Re(CO)_3OH]_4$ ,<sup>47</sup> and  $[Re(CO)_3(SCH_3)]_4$ <sup>94</sup>). Unlike the hydride clusters the metal atoms in the above clusters are not involved in metal-metal bonding.<sup>80</sup> The Re-F bonds of the rhenium cluster are longer than Re-F (1.97(2) Å) *trans* to a carbonyl group in  $(CO)_5Re-FReF_5$ .<sup>25</sup> The slight shortening of the *trans* Re-C bonds is consistent with the observed trend for  $[Re(CO)_3L_2X]$  compounds (where, (i) L = 2(CO), X = halide,<sup>50, 51, 52, 53</sup> (ii) L = bipyridyl, X =  $PF_2O_2$ <sup>15</sup>), where the carbonyl group is *trans* to X. This is believed to be due to a relatively greater  $\pi$ -back-donation from the metal to the carbonyl *trans* to a weaker  $\pi$ -acceptor.

The structure of the fluoro cluster closely resembles that of the anhydrous iodide,  $[Re(CO)_3I]_4$ .<sup>85</sup> In the fluoro cluster the X-Re-X and Re-X-Re angles are 74° and 104°, while in the iodo cluster they are 85° and 95°, respectively (Re-F 2.200(5), Re-I 2.838(7) Å).

## 2.5 STRUCTURE DETERMINATION OF [Rh(PPh<sub>3</sub>)Cl]<sub>4</sub>

### 2.5.1 Crystal Data

Crystals were grown by cooling a dichloromethane solution containing the rhodium cluster species, [Rh(PPh<sub>3</sub>)Cl]<sub>4</sub>. The yellow crystals are needle-like in morphology elongated along the b axis. The cell parameters were refined by the least-squares routine on the CAD4 using 25 high angle reflections. While the space group, Pcnb, was determined from the systematic absences in the reflection data. The density was measured using a floatation solution of petroleum spirit (30 - 40°) and carbon tetrachloride.

Crystal data: C<sub>72</sub>H<sub>60</sub>Cl<sub>4</sub>P<sub>4</sub>Rh<sub>4</sub>; M.W. = 1602.6; Orthorhombic space group, Pcnb, a = 17.876(5), b = 18.23(2), c = 20.749(6) Å; U = 6751(9); Z = 4; D<sub>c</sub> = 1.577 g.cm<sup>-3</sup>, D<sub>m</sub> = 1.58(2) g.cm<sup>-3</sup>; λMoK<sub>α</sub> = 0.7107 Å; F(000) = 3200 electrons; μMoK<sub>α</sub> = 12.50 cm<sup>-1</sup>.

For the data collection a crystal with dimensions 0.08 × 0.11 × 0.50 mm<sup>3</sup> was coated and mounted using epoxy resin. 3542 unique reflections in the range 1.5 < θ < 20.0° and with intensities I > 2.5σ(I) were collected using a ω-n/3θ scan mode (Chapter 7.1) (where, n = 1). The intensity of three standard reflections was measured at 67 minute intervals and no crystal decomposition was observed. The data was corrected for Lorentz, polarization<sup>98</sup> and for crystal absorption<sup>99</sup> effects. Further experimental details are given in Table 2.5.1.

### 2.5.2 Structure Solution and Refinement

The structure was solved by the heavy atom method.<sup>100,101</sup> The coordinates of the two unique rhodium atoms were determined from a Patterson synthesis. The difference Fourier synthesis that followed was

TABLE 2.5.1

Crystallographic details for  $[\text{Rh}(\text{PPh}_3)\text{Cl}]_4$ 

Temperature	298°K	Crystal dimension	$0.08 \times 0.11 \times 0.50 \text{ mm}^3$
$(\text{Sin } \theta_{\text{max}})/\lambda$	$0.48 \text{ \AA}^{-1}$	Crystal faces	[100], [-100], [010], [0-10], [001], [00-1]
Radiation	$\text{MoK}\alpha$	Aperture width	$2.40 + 0.50 * \tan(\theta)$
Scan method	$\omega/2\theta$	Sig(I)/I(pre-scan)	0.4
Scan range (°)		Sig(I)/I(final scan)	0.08
	$\theta_{\text{min}} = 1.50, \theta_{\text{max}} = 20.0$	Speed (pre-scan)	6.7 deg/min
	$\Delta\omega = 1.20 + 0.35 * \tan(\theta)$	Scan time (max)	200 sec
Slit width	3 mm		
Total number of independent reflections collected is 3542.			



TABLE 2.5.2  
Atomic positional and thermal parameters for  $[\text{Rh}(\text{PPh}_3)\text{Cl}]_4$

Atom <sup>a</sup>	x	y	z	U <sub>11</sub>	U <sub>22</sub>	U <sub>33</sub>	U <sub>23</sub>	U <sub>13</sub>	U <sub>12</sub>
Rh(1)	9416 (5)	20749 (6)	5341 (5)	385 (5)	870 (8)	636 (7)	-54 (6)	97 (5)	145 (6)
Rh(2)	6063 (6)	33044 (5)	17335 (5)	632 (7)	471 (6)	662 (7)	-100 (6)	-73 (5)	-121 (5)
C1(1)	904 (2)	1958 (1)	1842 (1)	46 (2)	54 (2)	58 (2)	3 (1)	-9 (1)	4 (1)
C1(2)	391 (2)	3418 (2)	459 (1)	56 (2)	58 (2)	62 (2)	10 (2)	5 (2)	-4 (2)
P(1)	2143 (2)	1812 (2)	115 (1)	42 (2)	53 (2)	51 (2)	0 (2)	5 (2)	8 (2)
P(2)	927 (2)	4400 (2)	2290 (1)	49 (2)	44 (2)	54 (2)	1 (1)	-6 (2)	-3 (2)
C(1)	2318 (4)	2108 (4)	-705 (3)	49 (8)	54 (7)	49 (8)	-1 (7)	8 (6)	-13 (6)
C(2)	2791 (4)	1723 (4)	-1119 (3)	76(10)	79 (9)	57 (9)	11 (8)	21 (7)	20 (8)
C(3)	2963 (4)	2010 (4)	-1725 (3)	116(13)	113(13)	49(10)	-1 (9)	17 (9)	17(10)
C(4)	2661 (4)	2682 (4)	-1917 (3)	68(11)	103(13)	64(10)	27 (9)	-10 (8)	-14 (8)
C(5)	2188 (4)	3068 (4)	-1503 (3)	87(11)	63 (9)	74(10)	24 (8)	6 (8)	6 (8)
C(6)	2016 (4)	2780 (4)	-897 (3)	73(15)	28 (7)	74 (9)	11 (6)	-3 (8)	9 (6)
C(7)	2914 (4)	2198 (4)	576 (4)	57 (8)	59 (8)	59 (9)	-8 (7)	11 (7)	2 (7)
C(8)	2862 (4)	2162 (4)	1246 (4)	60 (9)	100(11)	69(11)	-17 (9)	-16 (8)	-16 (8)
C(9)	3425 (4)	2464 (4)	1628 (4)	70(11)	183(17)	83(11)	-45(13)	12(10)	-7(12)
C(10)	4041 (4)	2802 (4)	1340 (4)	97(13)	108(13)	99(13)	-36(11)	-9(12)	-5(11)
C(11)	4092 (4)	2838 (4)	670 (4)	77(11)	87(11)	126(15)	4(10)	-20(11)	-14 (9)
C(12)	3529 (4)	2536 (4)	288 (4)	54(15)	64 (9)	93(11)	23 (9)	2 (8)	-3 (7)
C(13)	2339 (5)	842 (3)	96 (4)	54 (8)	45 (7)	49 (8)	12 (6)	9 (6)	-4 (7)
C(14)	3022 (5)	542 (3)	287 (4)	61 (9)	47 (9)	78 (9)	-1 (7)	12 (7)	11 (6)
C(15)	3149 (5)	-211 (3)	224 (4)	75(11)	65(11)	95(11)	17 (8)	20 (9)	20 (9)
C(16)	2593 (5)	-664 (3)	-30 (4)	119(13)	59(10)	96(12)	7(10)	20(11)	-9(12)

TABLE 2.5.2 (Continued)

Atom	x	y	z	U <sub>11</sub>	U <sub>22</sub>	U <sub>33</sub>	U <sub>23</sub>	U <sub>13</sub>	U <sub>12</sub>
C(17)	1910 (5)	-364 (3)	-222 (4)	120(14)	60(11)	85(11)	-7 (9)	1(10)	-29(10)
C(18)	1784 (5)	389 (3)	-159 (4)	64(15)	57 (9)	92(11)	-15 (8)	-4 (8)	-16 (8)
C(19)	494 (4)	4408 (5)	3079 (3)	31 (7)	73 (8)	45 (7)	-3 (7)	3 (6)	-13 (7)
C(20)	395 (4)	3727 (5)	3376 (3)	82(11)	95(11)	67(10)	18 (8)	38 (8)	-34 (8)
C(21)	40 (4)	3684 (5)	3973 (3)	123(15)	124(15)	83(13)	9(11)	20(11)	-48(12)
C(22)	-217 (4)	4322 (5)	4274 (3)	46 (9)	207(20)	66(11)	-23(15)	15 (8)	-7(12)
C(23)	-118 (4)	5003 (5)	3977 (3)	89(12)	155(17)	73(13)	-12(11)	16(10)	46(12)
C(24)	237 (4)	5046 (5)	3379 (3)	69(15)	90(11)	63(10)	-10 (8)	1 (8)	30 (8)
C(25)	587 (5)	5215 (3)	1891 (4)	53 (8)	49 (8)	63 (9)	-9 (6)	-1 (7)	0 (7)
C(26)	886 (5)	5913 (3)	1996 (4)	69 (9)	53 (8)	87(10)	13 (8)	-36 (8)	-6 (7)
C(27)	602 (5)	6518 (3)	1662 (4)	132(14)	44 (9)	116(13)	4 (9)	-33(11)	-10 (9)
C(28)	18 (5)	6424 (3)	1224 (4)	105(12)	66(11)	71(10)	-9 (7)	-4 (9)	14 (9)
C(29)	-281 (5)	5727 (3)	1119 (4)	62 (9)	61 (9)	97(11)	10 (9)	-29 (8)	3 (8)
C(30)	3 (5)	5122 (3)	1452 (4)	51(15)	62 (8)	64 (8)	-1 (7)	-11 (7)	10 (7)
C(31)	1896 (4)	4605 (4)	2437 (4)	35 (7)	42 (7)	57 (8)	2 (6)	3 (7)	-3 (6)
C(32)	2158 (4)	4967 (4)	2985 (4)	56(10)	75 (9)	70(10)	-7 (8)	-17 (8)	-16 (7)
C(33)	2908 (4)	5173 (4)	3026 (4)	46(10)	39(10)	97(12)	-21 (9)	-15 (9)	-3 (8)
C(34)	3395 (4)	5016 (4)	2520 (4)	51 (9)	84(10)	149(16)	21(10)	-3(12)	-4 (8)
C(35)	3133 (4)	4653 (4)	1972 (4)	55(11)	133(14)	97(12)	-31(11)	20 (9)	2(10)
C(36)	2383 (4)	4447 (4)	1931 (4)	67(15)	112(11)	78(11)	0 (9)	-1 (9)	-8 (9)

<sup>a</sup> Rh coordinates  $\times 10^5$  and the thermal parameters  $\times 10^4$ ;  
 All other coordinates  $\times 10^4$  and the thermal parameters  $\times 10^3$ .

TABLE 2.5.3  
Atomic distances for  $[\text{Rh}(\text{PPh}_3)\text{Cl}]_4$

Atoms <sup>a</sup>	Distance(Å)	Atoms	Distance(Å)
(a) Bond lengths (and standard deviations)			
Cl(1)-Rh(1)	2.723 (3)	Cl(2)-Rh(1)	2.639 (3)
Cl(2) <sup>I</sup> -Rh(1)	2.552 (3)	Cl(1)-Rh(2)	2.517 (3)
P(1)-Rh(1)	2.368 (3)	Cl(1) <sup>I</sup> -Rh(2)	2.753 (8)
Cl(2)-Rh(2)	2.679 (3)	P(2)-Rh(2)	2.375 (3)
C(1)-P(1)	1.812 (7)	C(7)-P(1)	1.818 (9)
C(13)-P(1)	1.799 (7)	C(19)-P(2)	1.811 (7)
C(25)-P(2)	1.804 (7)	C(31)-P(2)	1.798 (7)
(b) Intra-molecular distances			
Rh(1)...Rh(1) <sup>I</sup>	3.707 (5)	Cl(2) <sup>I</sup> ...Rh(2)	4.471 (6)
Rh(2)...Rh(1) <sup>I</sup>	3.786 (5)	Cl(1)...Cl(1) <sup>I</sup>	3.789 (5)
Rh(1)...Rh(2)	3.399 (4)	Cl(2)...Cl(1) <sup>I</sup>	3.750 (5)
Rh(2)...Rh(2) <sup>I</sup>	3.643 (5)	Cl(1)...Cl(2)	4.016 (6)
Cl(1) <sup>I</sup> ...Rh(1)	4.622 (6)	Cl(2)...Cl(2) <sup>I</sup>	3.621 (5)

<sup>a</sup> Superscripts in Roman refer to the following equivalent position, with respect to the unique asymmetric unit at x, y, z:

$$I = -x, .5 - y, z$$

TABLE 2.5.4  
Bond<sup>α</sup> angles (°) for [Rh(PPh<sub>3</sub>)Cl]<sub>4</sub>

C1(2)-Rh(1)-C1(1)	97.0(1)	C1(2)-Rh(1)-C1(1)	90.6(1)
C1(2)-Rh(1)-C1(2) <sup>I</sup>	88.4(1)	P(1)-Rh(1)-C1(1)	111.9(1)
P(1)-Rh(1)-C1(2)	120.3(1)	C1(1)-Rh(2)-C1(1) <sup>I</sup>	91.8(1)
P(2)-Rh(2)-C1(1)	136.3(1)	C1(2)-Rh(2)-C1(1)	101.2(1)
Rh(2)-C1(1)-Rh(1)	80.8(1)	C1(2)-Rh(2)-C1(1) <sup>I</sup>	87.3(1)
Rh(2)-C1(1)-Rh(1)	87.5(1)	P(2)-Rh(2)-C1(2)	116.7(1)
Rh(2)-C1(1)-Rh(2)	87.3(1)	Rh(2)-C1(2)-Rh(1)	79.5(1)
Rh(1)-C1(2)-Rh(1)	91.1(1)	Rh(2)-C1(2)-Rh(1) <sup>I</sup>	92.7(1)
C(1)-P(1)-Rh(1)	116.2(3)	C(7)-P(1)-Rh(1)	114.6(3)
C(7)-P(1)-C(1)	104.4(4)	C(13)-P(1)-Rh(1)	112.5(3)
C(13)-P(1)-C(1)	103.7(4)	C(13)-P(1)-C(7)	104.0(4)
C(19)-P(2)-Rh(2)	110.0(3)	C(25)-P(2)-Rh(2)	112.7(3)
C(25)-P(2)-C(19)	105.3(4)	C(31)-P(2)-Rh(2)	119.3(3)
C(31)-P(2)-C(19)	104.9(4)	C(31)-P(2)-C(25)	103.5(4)
C(2)-C(1)-P(1)	122.2(6)	C(6)-C(1)-P(1)	117.5(5)
C(8)-C(7)-P(1)	117.1(6)	C(12)-C(7)-P(1)	122.9(7)
C(14)-C(13)-P(1)	123.2(6)	C(18)-C(13)-P(1)	116.7(6)
C(20)-C(19)-P(2)	116.5(6)	C(24)-C(19)-P(2)	123.4(6)
C(26)-C(25)-P(2)	123.1(6)	C(30)-C(25)-P(2)	116.9(5)
C(32)-C(31)-P(2)	124.0(6)	C(36)-C(31)-P(2)	115.6(6)

<sup>α</sup>Superscripts in Roman refer to the following equivalent position, with respect to the unique asymmetric unit at x, y, z:

$$I = -x, .5 - y, z$$

based on the two rhodium atoms and gave a difference map which revealed all phosphorus, chloride atoms and some phenyl carbons. At this stage the R value was 0.42. A subsequent calculation, which accounted for the rhodium, chloride, phosphorus and the six phenyl carbon atoms directly bonded to the phosphorus atoms, refined to an R value of 0.24 and the associated difference map revealed all remaining non-hydrogen atoms of the cluster. In subsequent full-matrix least-squares calculations the phenyls were refined as rigid groups (C-C = 1.395 and C-H = 0.97 Å) with all hydrogen atoms refined with a common thermal parameter. In the final full-matrix refinement the weighting scheme (Chapter 7.1) was employed and all the non-hydrogen atoms were modelled anisotropically. The calculation converged with  $R = 0.034$ ,  $R_w = 0.036$ ,  $k = 1.13$  and  $g = 6.1 \times 10^{-4}$ . The largest peak remaining in the last difference map was of the order of  $0.3 \text{ e}\text{\AA}^{-3}$ . The final heavier atom coordinates, bond lengths and bond angles are given in Tables 2.5.2, 2.5.3 and 2.5.4, respectively. The hydrogen atom parameters and the tabulated structure factors are given on microfiche.

### 2.5.3 Description of the Structure

Figure 2.5.1 shows the structure of  $[\text{Rh}(\text{PPh}_3)\text{Cl}]_4$  giving the atomic numbering scheme employed. The tetranuclear complex assumes the pseudocubane structure type,  $[\text{MRX}]_4$  (§ 2.3 and § 2.4). The cluster exhibits  $\bar{4}m$  crystallographic symmetry with the corners alternatively occupied by the rhodium and chloride atoms. The four rhodium triphenylphosphine groups are thus held together by triply bridging ( $\mu_3$ ) chloride atoms. The rhodium-chloride bond distance varies from 2.517(3) to 2.753(8) Å (Table 2.5.3). The rhodium-rhodium distances (ave. 3.63 Å) suggests that no metal-metal bonding exists. The bonding about each rhodium atom consists of a distorted tetrahedral geometry, with an

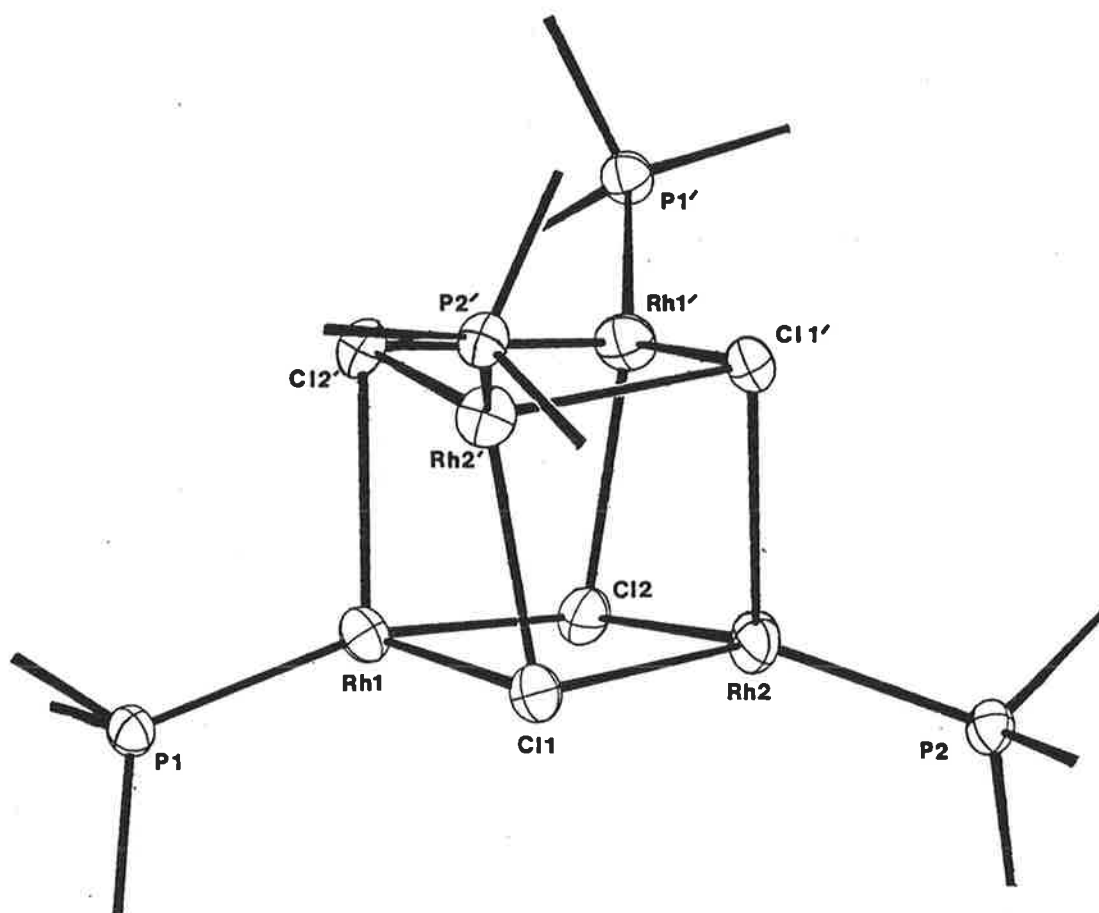


FIGURE 2.5.1. Molecular structure of [Rh(PPh<sub>3</sub>)Cl]<sub>4</sub>. (30% probability ellipsoids). The PPh<sub>3</sub> groups have been omitted for simplicity. The primed labels refer to the following equivalent position with respect to the unique asymmetric unit of the cluster at  $x, y, z$ :

$$I = -x, .5 - y, z$$

average (P-Rh-Cl) bond angle of  $121.3^\circ$  and an average (Cl-Rh-Cl) angle of  $92.6^\circ$  (Table 2.5.4). The average (Rh-Cl-Rh) angle ( $86.5^\circ$ ) is found to be smaller than the average (Re-F-Re) angle ( $103.8^\circ$ ) of  $[\text{Re}(\text{CO}_3)\text{F}]_4$  (§ 2.4). This can be understood on the basis of the difference in the metal : halide atomic radii ratio (§ 2.6).

## 2.6 DISCUSSION

The work presented in this chapter establishes an efficient synthetic route for metal fluoride clusters without the need for hazardous reagents such as fluorine gas, anhydrous hydrogen fluoride and xenon hexafluoride or for high pressure equipment. Thus with the employment of a suitable solvent (e.g. fluoro-benzene) the halide abstraction method will produce the cluster complexes with good yields. It has been found that in these preparations the type of reaction vessels used has not been critical and the use of "plastic" containers (Chapter 3) instead of pyrex glass containers has not been essential for the reaction scales employed.

The reaction progress can conveniently be followed by periodic monitoring of the infrared spectrum of the reaction mixtures because of the characteristic  $\nu(\text{CO})$  stretching frequencies and band intensities associated with the precursors, intermediates and the products. Furthermore, the infrared spectra also give an insight into the mechanism of cluster formation. The complexes  $\text{M}(\text{CO})_5\text{X}$  (where,  $\text{M} = \text{Mn}, \text{Re}$  and  $\text{X} = \text{Cl}, \text{Br}$ , respectively) have the characteristic  $(2\text{A}_1 + \text{E})$  carbonyl stretching bands (Chapter 1). The manganese and rhenium clusters, in contrast, exhibit the  $(\text{A}_1 + \text{E})$  type bands, which define a mutually *cis*-geometry for the carbonyl groups. Figure 2.6.1 shows the  $\nu(\text{CO})$  solution spectra of  $\text{Re}(\text{CO})_5\text{Br}$ , reaction intermediates (i.e.  $[\text{Re}(\text{CO})_5(\text{S},\text{F})]$

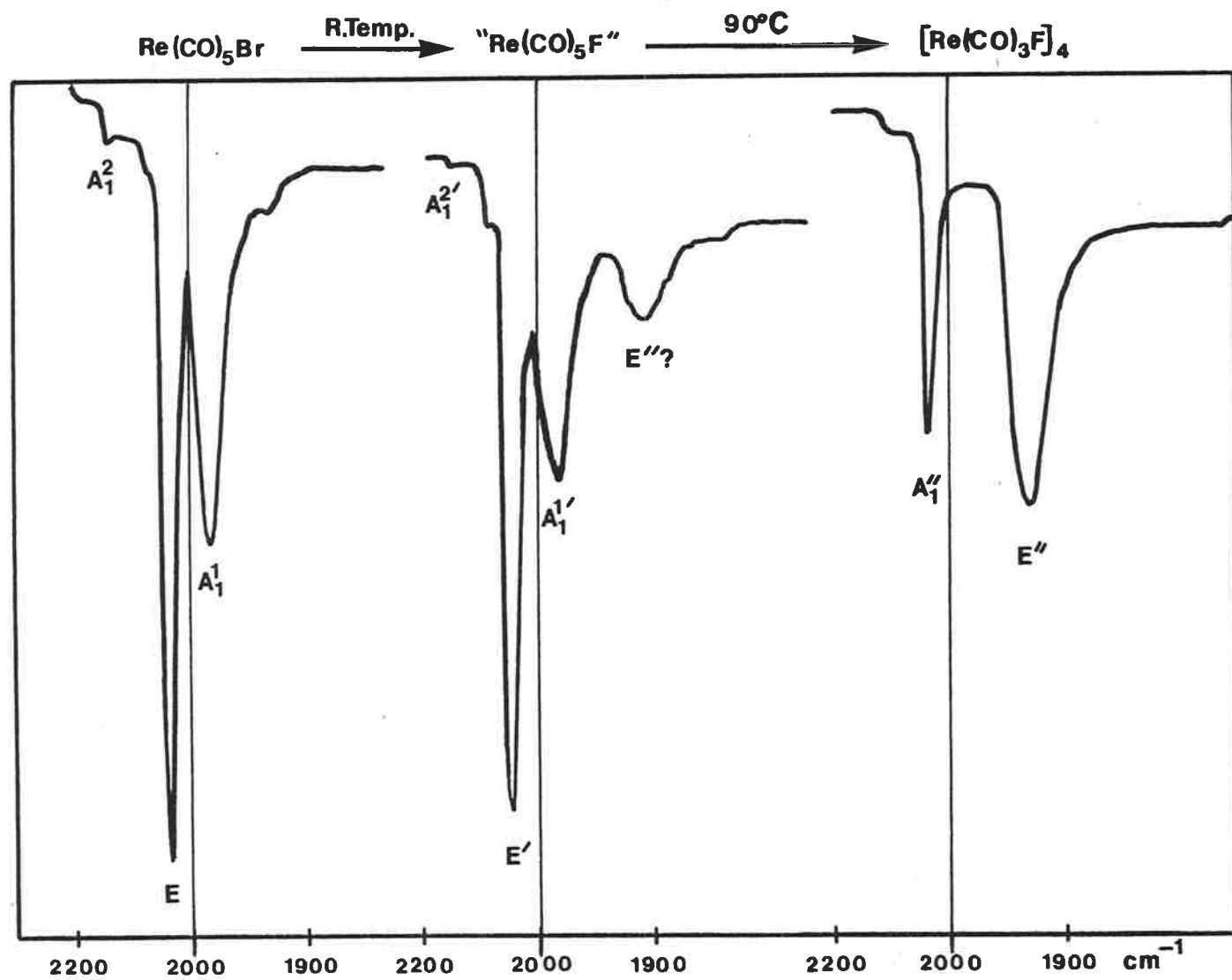


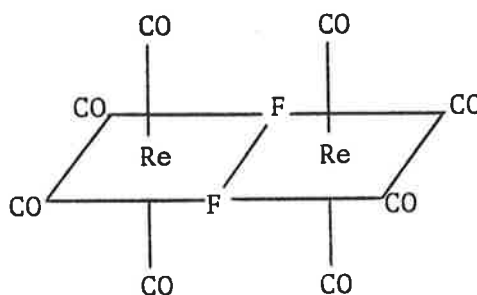
FIGURE 2.6.1. The  $\nu(\text{CO})$  stretching patterns of the compounds  $\text{Re}(\text{CO})_5\text{Br}$ , "Re(CO)<sub>5</sub>F" and  $[\text{Re}(\text{CO})_3\text{F}]_4$  in dichloromethane.



and decarboxylated species) and of  $[\text{Re}(\text{CO})_3\text{F}]_4$ , respectively. From a comparison of the ( $2A_1 + E$ ) carbonyl bands of (a) and (b) one can conclude that a  $\text{M}(\text{CO})_5\text{X}$  (where,  $\text{X} = \text{solvent or fluorine}$ ) intermediate forms before decarboxylation begins:



Figure 2.6.1(b) also shows a carbonyl band for a decarboxylation intermediate at  $1908\text{cm}^{-1}$ . An intermediate consistent with a single  $\nu(\text{CO})$  band would be of the type *trans*- $[\text{M}(\text{CO})_4\text{L}_2]$  or more likely the dimer  $[\text{Re}(\text{CO})_4\text{F}]_2$  shown below:



The rate of decarboxylation of the manganese and rhenium pentacarbonyl fluoride complexes is faster than the reported<sup>7,102</sup> rates for the corresponding chloride, bromide and iodide complexes. For example, in the rhenium system the formation of  $[\text{Re}(\text{CO})_4\text{X}]_2$  under reflux condition takes 1 - 2, 4 and 36 hr for  $\text{X} = \text{F}, \text{Cl}, \text{and Br}$ , respectively. While refluxing  $\text{Re}(\text{CO})_5\text{I}$  for 7 days yields no trace of the dimer species. This trend in reactivity can not be explained by steric consideration of the halogen-carbonyl interaction, since one would expect the opposite trend. However, the observed trend may be explained in terms of metal to ligand  $\pi$ -bonding. The back bonding effect is seen to decrease from fluorine to iodine for the interactions between halogens and the heavier transition metals.<sup>20</sup>

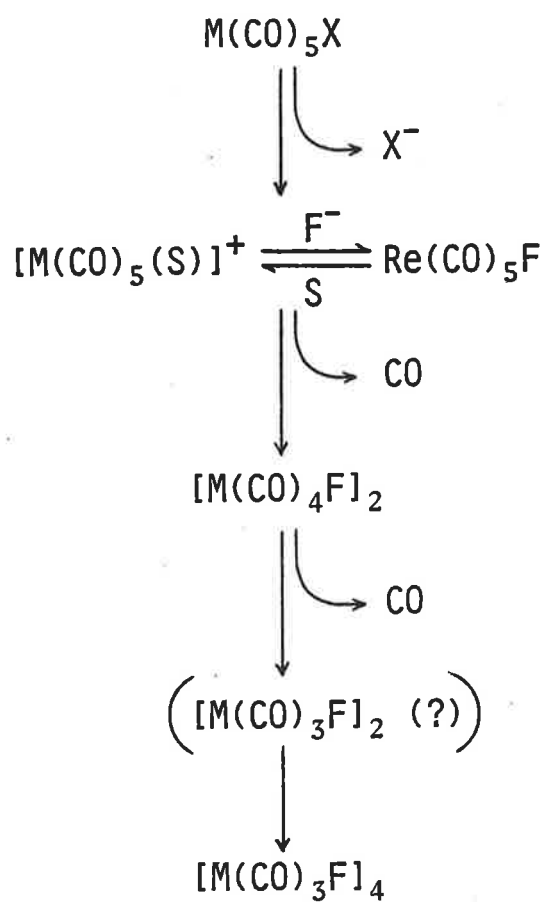
A close study of infrared spectra during the course of a reaction

shows the presence of no other carbonyl intermediate species when assuming that its  $\nu(\text{CO})$  band are not hidden by the bands of the main species. Thus the rate determining step (Scheme 2.6.1) involves a further decarboxylation of the species,  $[\text{M}(\text{CO})_4\text{F}]_2$ . The reactive and unobserved intermediate  $[\text{M}(\text{CO})_3\text{F}]_2$  is then predicted to form and to immediately condense with another such species to give the final product,  $[\text{M}(\text{CO})_3\text{F}]_4$ . The generalised reaction pathway for the formation of the metal carbonyl clusters is shown in Scheme 2.6.1. In the rhodium system  $\nu(\text{CO})$  monitoring only provides insight about the mechanism till the end of decarboxylation (§ 2.2.3).

Whereas, the  $\nu(\text{CO})$  bands give an insight into the geometry of the molecular species, microanalysis and mass spectra of the products unambiguously characterise the triply bridging atom. With the manganese clusters the species,  $[\text{Mn}(\text{CO})_3\{\text{F}_x, (\text{OH})_{1-x}\}]_4^{11,103}$  were identified by the molecular ions  $[\text{Mn}(\text{CO})_3(\text{OH})]_4^+$ ,  $[\text{Mn}(\text{CO})_3\{\text{F}_{0.25}, (\text{OH})_{0.75}\}]_4^+$ ,  $[\text{Mn}(\text{CO})_3\{\text{F}_{0.5}, (\text{OH})_{0.5}\}]_4^+$ ,  $[\text{Mn}(\text{CO})_3\{\text{F}_{0.75}, (\text{OH})_{0.25}\}]_4^+$ , and  $[\text{Mn}(\text{CO})_3\text{F}]_4^+$  and their respective fragmentation series. Similarly, for the rhenium cluster, the triply bridging atom was identified as a fluorine atom by the molecular ion fragments found in the mass spectra (§ 2.7), although the parent ion was not observed. The structural results for each cluster (§ 2.3, 2.4, 2.5) are consistent with the other physical properties of the complexes and with the general formula,  $[\text{MLX}]_4$ , where (1)  $\text{M} = \text{Mn}$ ,  $\text{L} = 3(\text{CO})$ ,  $\text{X} = \text{F}, (\text{OH})$ ; (2)  $\text{M} = \text{Re}$ ,  $\text{L} = 3(\text{CO})$ ,  $\text{X} = \text{F}$ ; and, (3)  $\text{M} = \text{Rh}$ ,  $\text{L} = (\text{PPh}_3)$  and  $\text{X} = \text{Cl}$ .

Scheme 2.6.1

A generalised pathway to the formation of the  $[M(CO)_3F]$  clusters.

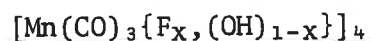


where, (1)  $M = Mn$ ,  $X = Cl$ ,

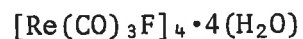
(2)  $M = Re$ ,  $X = Br$ , and  $S = \text{solvent}$  (e.g.  $CH_2Cl_2$ ,  $C_6H_5F$ ).

## 2.7 EXPERIMENTAL

All reactions were carried out in a high-purity dry nitrogen atmosphere. The preparations of the starting materials are described in Chapter 8.2. The solvents used were dried using Linde 4A molecular sieves. All compounds prepared below were stored in the dark in a desiccator containing dry nitrogen at *ca* 25°C. The infrared carbonyl stretching frequencies of the compounds in solution were recorded using calcium fluoride solution cells. Subsequently, the complete infrared spectra of the isolated compounds was recorded as nujol mulls using calcium fluoride plates.



This compound was prepared from  $\text{Mn}(\text{CO})_5\text{Cl}$  by the literature method<sup>11</sup> using silver fluoride and thallium fluoride.



To  $\text{Re}(\text{CO})_5\text{Br}$  (50 mg, 0.12 mmol) dissolved in *ca* 8 ml of fluorobenzene ( $\text{C}_6\text{H}_5\text{F}$ ) finely divided silver fluoride (30 mg, 0.24 mmol, 2 fold excess) was added and the resulting mixture was stirred at room temperature for 2 hr. The silver bromide precipitate and the excess silver fluoride were removed from the solution by filtration. The remaining solution was then refluxed at 90 - 100°C for 5 hr, cooled to room temperature and the solvent removed by vacuum leaving behind the yellow product (44 mg, 0.036 mmol, 75% yield). The product recrystallizes from ether over fluorobenzene as needle-like to prismatic crystals.

(Found: C, 12.5; H, 0.5; F, 6.2

$[\text{Re}(\text{CO})_3\text{F}]_4 \cdot 4(\text{H}_2\text{O})$  requires: C, 11.7; H, 0.7; F, 6.2%)

The mass spectrum showed only the following fragmentation series (m/e, assignment, (intensity)\*): 845\*\*  $[\text{Re}_4(\text{CO})\text{F}_3\text{C}]^+$  (27), 714  $[\text{Re}_3(\text{CO})_3\text{F}_3\text{C}]^+$  (44), 686  $[\text{Re}_3(\text{CO})_2\text{F}_3\text{C}]^+$  (88), 658  $[\text{Re}_3(\text{CO})\text{F}_3\text{C}]^+$  (109),  $[\text{Re}_3\text{F}_3\text{C}]^+$  (49), 187  $[\text{Re}]^+$  (1000).

$[\text{Re}(\text{CO})_3\text{F}]_4$

Finely divided silver bifluoride (35 mg, 0.24 mmol, 70% excess) was added to  $\text{Re}(\text{CO})_5\text{Br}$  (60 mg, 0.14 mmol) dissolved in fluorobenzene (12 ml) and the mixture was stirred for 1 hr. The silver bromide and excess silver bifluoride were removed by filtration. The solution was then refluxed at 90 - 100°C for *ca* 5 hr, cooled to room temperature and dried *in vacuo*. The yellow product (52 mg, 0.043 mmol, 76% yield) was recrystallized from ether-fluorobenzene.

(Found: C, 12.1; H, 0.2; F, 6.9  
 $[\text{Re}(\text{CO})_3\text{F}]_4$  requires: C, 12.5; H, 0.0; F, 6.6%)

$[\text{Mn}(\text{CO})_3\text{F}]_4$

The method is identical to that for  $[\text{Re}(\text{CO})_3\text{F}]_4$ , except that no reflux conditions were required during the 5 hr stirring period after filtration; yield *ca* 70%.

(Found: C, 22.5; H, 0.3; F, 12.3  
 $[\text{Mn}(\text{CO})_3\text{F}]_4$  requires: C, 22.8; H, 0.0; F, 12.0%)

---

\*Intensity relative to the  $\text{Re}^+$  ion.

\*\*Showing only the molecular ions with the isotope  $\text{Re}^{187}$ .

[Rh(PPh<sub>3</sub>)F]<sub>4</sub>

To a solution of fluorobenzene (10 ml) containing Rh(CO)(PPh<sub>3</sub>)<sub>2</sub>Cl (40 mg, 0.058 mmol) finely divided silver bifluoride (17 mg, 0.12 mmol, 1 fold excess) was added and the mixture was stirred for 30 min. The silver bromide and excess silver bifluoride were removed by filtration. The solution was then stirred for a further 2 hr and dried *in vacuo*. The product was washed with minimum benzene to remove the uncoordinated triphenylphosphate and recrystallized from acetone-benzene (yield, *ca* 50%).

(Found: C, 55.8; H, 4.2; F, 5.3

[Rh(PPh<sub>3</sub>)F]<sub>4</sub> requires: C, 56.3; H, 3.9; F, 4.9%)

## CHAPTER 3

### COORDINATED FLUORIDE IN RHENIUM(I) COMPLEXES

#### 3.1 INTRODUCTION

The preparation and properties of  $\pi$ -ligand derivatives of manganese(I) and rhenium(I) halocarbonyls have been researched and reported extensively for complexes where the halide is chlorine, bromide and iodine.<sup>7,104,105,106,107,108-110</sup> By the correct choice of solvent and reaction conditions tricarbonyl complexes are easily prepared by a simple quantitative method from the respective metal pentacarbonyl halides. However, to date no metal tricarbonyl fluoride complexes of the type  $M(\text{CO})_3(\text{L}_2)\text{F}$  (where, M = transition metal,  $\text{L}_2$  = one or two bi-dentate or mono-dentate  $\pi$ -donor ligands, respectively) have been reported.

Halide abstraction from metal carbonyl halide complexes has become an efficient method for the coordination of such poor coordinating anions as  $(\text{BF}_4^-)$ ,<sup>29</sup>  $(\text{ClO}_4^-)$ ,<sup>14,15</sup> and  $(\text{PO}_2\text{F}_2^-)$ .<sup>14,15</sup> The method involves the removal of the halide (i.e. Cl, Br, I) from the metal by the silver ion producing a solvated intermediate. When the reaction is carried out in  $\text{CHCl}_3$ ,  $\text{CH}_2\text{Cl}_2$ <sup>15,32</sup> or  $\text{THF}$ <sup>112</sup> the solvent coordinates initially and is subsequently replaced by the respective anion. More recently abstraction reactions were investigated with complexes of the type  $M(\text{CO})_5\text{X}$  (where, M = Mn, Re and X = Cl, Br) using  $\text{AgF}$  with the aim of preparing and isolating the corresponding fluoro species,  $M(\text{CO})_5\text{F}$ . However, these compounds are unstable intermediates which polymerize to form the respective tetrameric clusters  $[\text{Mn}(\text{CO})_3\{\text{F}_X, (\text{OH})_{1-X}\}]_4$ <sup>11</sup> and

$[\text{Re}(\text{CO})_3\text{F}]_4 \cdot 4\text{H}_2\text{O}$ .<sup>84</sup> The abstraction studies with AgF involving manganese(I)<sup>113</sup> and rhenium(I)<sup>114</sup> were greatly hampered due to the formation of the by-products such as  $\text{M}(\text{CO})_3(\text{L}_2)\text{X}$  (where,  $\text{X} = \text{Cl}^-$ ,  $\text{OH}^-$ ). Thus, analysis by the conventional methods such as infrared, N.M.R. and microanalysis was difficult. Furthermore, because of the formation of oils and "gums" during attempted crystallisations, X-ray molecular structure determination was impossible. This chapter describes how, by careful selection of solvents and reaction conditions, the abstraction technique can be utilised to form the stable fluoro complexes  $\text{Re}(\text{CO})_3(\text{L}_2)\text{F}$  from the corresponding substituted rhenium carbonyl bromide precursors.

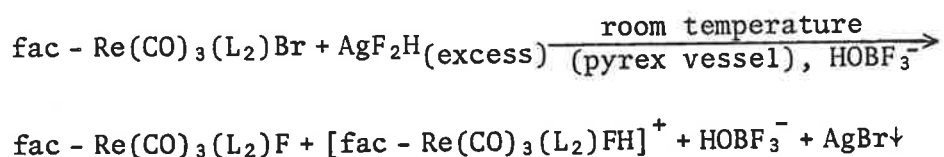


### 3.2 PREPARATION AND PROPERTIES OF $[\text{Re}(\text{CO})_3(\text{L}_2)\text{F}]_2\text{H}\cdot\text{HOBf}_3$

(where,  $\text{L}_2 = \text{bpy}, \text{tmen}$ )

#### 3.2.1 Preparation

The title compounds were prepared from their bromide analogs by halide-abstraction under a dry nitrogen atmosphere and in dry dichloromethane according to the following scheme:



When these reactions are carried out at room temperature in pyrex glass reaction vessels the fluorine from the silver bifluoride attacks the glass surface covered with the reaction mixture turning it visibly opaque. As a result of this etching the unusual trifluoroborate anion ( $\text{HOBf}_3^-$ ) is introduced into the system. On the removal of the silver bromide and any excess insoluble silver bifluoride by filtration the less soluble products crystallize as  $[\text{fac} - \text{Re}(\text{CO})_3(\text{L}_2)\text{F}]_2\text{H}\cdot\text{HOBf}_3$ . ((1)  $\text{L}_2 = \text{bpy}$ , (2)  $\text{L}_2 = \text{tmen}$ ). If the amount of  $\text{AgF}_2\text{H}$  used is decreased the products crystallize as two crystal types. One type contains  $[\text{Re}(\text{CO})_3(\text{L}_2)\text{F}]_2\text{H}\cdot\text{HOBf}_3$ , while the second crystal type consists only of  $\text{Re}(\text{CO})_3(\text{L}_2)\text{F}$  molecules. Compounds (1) and (2) were characterised by their  $\nu(\text{CO})$ -stretches (Table 3.3.1), mass spectra (Chapter 3.7) and in the case of compound (2) also by structure analysis (§ 3.5).

#### 3.2.2 Properties

The number and relative band intensities (Table 3.3.1) in the carbonyl stretching region of infrared spectra of compounds (1) and (2) are consistent with the formulation of the co-existence of two species,

namely [fac - Re(CO)<sub>3</sub>(L<sub>2</sub>)F] and [fac - Re(CO)<sub>3</sub>(L<sub>2</sub>)FH]<sup>+</sup>. The ν(O-H) and ν(B-F) stretching bands also verify the presence of the trifluoroborate anion (HOBf<sub>3</sub><sup>-</sup>).<sup>114</sup>

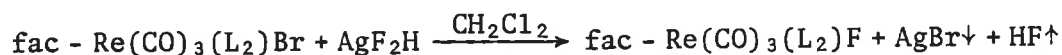
In the mass spectra of compounds (1) and (2) no peak corresponding to molecular ions [[Re(CO)<sub>3</sub>(L<sub>2</sub>)F]<sub>2</sub>H•HOBf<sub>3</sub>]<sup>+</sup> was observed. The largest molecular ions seen are [Re(CO)<sub>3</sub>(L<sub>2</sub>)F]<sup>+</sup>, which undergo a fragmentation process by successive loss of carbon monoxide, fluoride and, finally, by loss of the bidentate ligand (L<sub>2</sub>).

The solids of compounds (1) and (2) are not hygroscopic and can be stored for months without decomposition. However, when dissolved in dichloromethane for several weeks the by-product Re(CO)<sub>3</sub>(L<sub>2</sub>)Cl is formed. In chloroform this decomposition<sup>is</sup> enhanced further and Re(CO)<sub>3</sub>(L<sub>2</sub>)Cl forms in a matter of days. If suitable crystals need to be grown for x-ray structure analysis, then this chloride substitution is reduced when the dichloromethane solution is kept at ca. 5°C. The decomposition is stopped if fluorinated solvents such as monofluorobenzene and hexafluorobenzene are used.

### 3.3 PREPARATION AND PROPERTIES OF [Re(CO)<sub>3</sub>(L<sub>2</sub>)F] (where, L<sub>2</sub> = bpy, dpe, 2SbPh<sub>3</sub>, tmen)

#### 3.3.1 Preparation

The problem of the formation of the trifluoroborate anion (Chapter 3.2) was overcome by using "plastic" reaction vessels made of polyethylene. As a result, the reaction of the rhenium tricarbonyl bromide complexes Re(CO)<sub>3</sub>(L<sub>2</sub>)Br with silver bifluoride in dry dichloromethane and under a dry nitrogen atmosphere produces good yields of the respective rhenium fluoride complexes according to the general reaction:



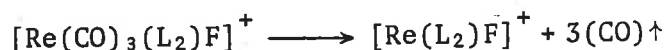
((1) L<sub>2</sub> = bpy, (2) L<sub>2</sub> = dpe, (3) L<sub>2</sub> = 2SbPh<sub>3</sub>, (4) L<sub>2</sub> = tmen)

Precipitation of silver bromide occurs within minutes after adding the silver bifluoride to the respective solutions of substrate. However, the reaction mixtures should be stirred for ca. 30 min. to ensure a complete conversion of the solvento intermediates (Chapter 3.6) to the respective rhenium fluoride complexes. The halogen abstraction reaction can also be carried out using the chloride and iodide precursors. Furthermore, the reaction scales reported in the experimental section (§ 3.7), can easily be increased in proportion as desired, but the synthesis should be performed in a well ventilated area because of the potent hydrogen fluoride fumes given off.

#### 3.3.2 Properties

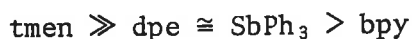
As with the preparations reported in Section 3.2 the course of the above reactions were followed by periodically recording the carbonyl stretching bands of samples of the reaction mixture. On isolation of

the compounds (1) to (2) their full infrared spectrum was recorded (Appendix 1). The  $\nu(\text{CO})$  stretching frequencies are given in Table 3.3.1. The number and relative intensities of the carbonyl stretching bands ( $2A' + A''$ ) are consistent with the *fac*-geometry as observed for the bromide precursors. This has been verified by the molecular structure of  $[\text{Re}(\text{CO})_3(\text{tmen})\text{F}]$  (§ 3.5). Compounds (1) and (4) have also been characterised by their mass spectrum, which can be understood as the fragmentation of the parent molecular ion  $[\text{Re}(\text{CO})_3(\text{L}_2)\text{F}]^+$  by successive loss of carbon monoxide:



The  $[\text{Re}(\text{L}_2)\text{F}]^+$  molecular ion then further fragments by two possible modes. One mode involves the loss of the ligand ( $\text{L}_2$ ) followed by the loss of the fluorine. While, in the second mode the order is reversed.

The complexes (1) to (4) are less soluble in halogenate solvents (e.g.  $\text{CHCl}_3$ ,  $\text{CH}_2\text{Cl}_2$ ,  $\text{C}_6\text{H}_5\text{Cl}$ ,  $\text{C}_6\text{H}_5\text{F}$  and  $\text{C}_6\text{F}_6$ ) than the respective bromides. Their solubility is dependent on the ligand ( $\text{L}_2$ ) and decreases in the following order:



The compounds are mildly hygroscopic in solid form and thus should be stored in a dry atmosphere, in which they can be stored for months at room temperature without decomposition. In solution the fluoro complexes are stable towards halide ( $\text{X}^-$ ) substitution as observed over a period of 24 hr. However, in chloroform and dichloromethane solvents slow decomposition to the chloro-complex occurs.

TABLE 3.3.1

Infrared stretching frequencies ( $\text{cm}^{-1}$ )

Compound	$\nu(\text{CO})$	$\nu(\text{FH}), \nu(\text{OH})$	$\nu(\text{BF})$	Medium
$\text{Re}(\text{CO})_3(\text{bpy})\text{F}$	2040s, 1926s 2032sm, 1902s			$\text{CH}_2\text{Cl}_2$ nujol
$[\text{Re}(\text{CO})_3(\text{bpy})\text{F}]_2\text{H}\cdot\text{HOBf}_3$	2039s, 2031s, 1928s, 1914ssh 2011s, 1890sh, 1878sh, 1865s	3442wsh, 3328m	1083s, 1001m, 980m	$\text{CH}_2\text{Cl}_2$ nujol
$\text{Re}(\text{CO})_3(\text{dpe})\text{F}$	2046s, 1966s, 1928s 2034s, 1954s, 1905s			$\text{CH}_2\text{Cl}_2$ nujol
$\text{Re}(\text{CO})_3(\text{SbPh}_3)_2\text{F}$	2031s, 2027msh, 1916s 2042msh, 2020s, 1900s			$\text{CH}_2\text{Cl}_2$ nujol
$\text{Re}(\text{CO})_3(\text{tmen})\text{F}$	2039s, 1933s, 1908s 2008s, 1878sh, 1863s			$\text{CH}_2\text{Cl}_2$ nujol
$[\text{Re}(\text{CO})_3(\text{tmen})\text{F}]_2\text{H}\cdot\text{HOBf}_3$	2037s, 2026s, 1930s, 1900s 2005s, 1892sh, 1881sh, 1867s	3440wsh, 3325m	1080s, 1002m, 982m	$\text{CH}_2\text{Cl}_2$ nujol

### 3.4 STRUCTURE DETERMINATION OF [Re(CO)<sub>3</sub>(tmen)F]H·HOBf<sub>3</sub>

#### 3.4.1 Crystal Data

A crystal of [Re(CO)<sub>3</sub>(tmen)F]<sub>2</sub>H·HOBf<sub>3</sub> with dimensions 0.08 × 0.15 × 0.16 mm<sup>3</sup> was mounted on the CAD4 and the unit-cell parameters were obtained by least-squares refinement using 25 reflections in the range 5 < θ < 15. The cell constants found are: C<sub>18</sub>H<sub>34</sub>BF<sub>5</sub>N<sub>4</sub>O<sub>7</sub>Re<sub>2</sub>; M.W. = 896.7; Monoclinic space group P2<sub>1</sub>/c, a = 17.495(2), b = 10.772(2), c = 15.447(1) Å, β = 101.409(8)°; U = 2854(1) Å<sup>3</sup>; Z = 4; D<sub>c</sub> = 2.087 gm.cm<sup>-3</sup>, D<sub>m</sub> = 2.08(2) gm.cm<sup>-3</sup>; λ<sub>Cu</sub> = 1.5418 Å; F(000) = 1704; μ<sub>Cu</sub> = 163.3 cm<sup>-1</sup>.

During the data collection the intensity of three reference reflections was checked at 1.9 hr intervals. The profiles were corrected for changes in intensity before analysis. Further crystallographic detail is given in Table 3.4.1. The intensities were corrected for Lorentz, polarization<sup>98</sup> and absorption effects.<sup>99</sup>

#### 3.4.2 Structural Solution and Refinement

The approximate positions of the two rhenium atoms (i.e. Re1, Re2) were calculated from a conventional Patterson map. A least-squares refinement with these atoms gave an R value of 0.203. The difference map revealed the locations of all the non-hydrogen atoms, with the exception of one carbonyl group in each of the [M(CO)<sub>3</sub>(tmen)F] molecules (where, M = Re1, Re2). In subsequent blocked-matrix least-squares calculations, which included all the located atoms and with only the rhenium atoms modelled anisotropically, the value of R reduced to 0.109. With the addition of the last two carbonyl group atoms and when using the weighting scheme, R converged at 0.081 and R<sub>w</sub> at 0.095 with

TABLE 3.4.1

Crystallographic details for  $[\text{Re}(\text{CO})_3(\text{tmen})\text{F}]_2\text{H}\cdot\text{HOBf}_3$ 

Temperature	298°K	Crystal dimensions	.08 × .15 × .16 mm <sup>3</sup>
$(\text{Sin } \theta_{\text{max}})/\lambda$	0.59 Å <sup>-1</sup>	Crystal faces	[100], [-100], [010],
Radiation	Cu		[0-10], [001], [00-1]
Scan method	$\omega/2\theta$	Aperture width	1.25 + 0.5 * tan( $\theta$ )
Scan range (°)		Sig(I)/I (pre scan)	0.4
	$\theta_{\text{min}} = 2, \theta_{\text{max}} = 25$	Sig(I)/I (final scan)	0.03
	$\Delta\omega = 0.9 + 0.15 * \tan(\theta)$	Speed (pre scan)	6.7 deg/min
Slit width	3 mm	Scan time (max)	100 sec
		Number of unique reflections collected	2904

$g = 7.9 \times 10^{-3}$ . In the subsequent four blocked calculations the rhenium, boron-oxygen, fluorine, carbonyl-carbons and -oxygens atoms were modelled anisotropically, resulting in an R value of 0.061 and an  $R_w$  value of 0.066.

In the final blocked-matrix least-squares refinement the tmen hydrogen atom positions were calculated assuming a tetrahedral geometry about the carbon atoms and a (C-H) bond length of 0.97 Å. The methyl groups were refined as rigid groups and the temperature factor of all the hydrogen atoms was refined as a common group factor. In addition, the final calculation included an isotropic extinction correction (Chapter 8.1). The final R converged at 0.057 and  $R_w$  at 0.061, with  $k = 1.2$  and  $g = 5.4 \times 10^{-5}$ . The two largest peaks ( $2 \text{ eÅ}^{-3}$ ) in the final difference map were located near the rhenium centres.

The scattering factors for the corresponding neutral atoms were obtained from the International Tables Volume IV. The tabulated observed and calculated structure factors and hydrogen atomic parameters are stored on the microfiche supplied with the thesis. The final non-hydrogen atomic parameters, bond lengths and bond angles are given in Tables 3.4.2, 3.4.3 and 3.4.4, respectively.

### 3.4.3 Description of the Structure

Figure 3.4.1 shows an ORTEP plot of  $[\text{Re}(\text{CO})_3(\text{tmen})\text{F}]_2\text{H}\cdot\text{HOBf}_3$  giving the atomic numbering scheme. The compound crystallizes with two  $\text{Re}(\text{CO})_3(\text{tmen})\text{F}$  molecules joined by a bifluoride bridge ( $-\text{F}\cdots\text{H}-\text{F}-$ ) while, the trifluoroborate anion is hydrogen bonded to the second fluoride atom (F(2)) via the hydroxy group. The hydrogen atom can not directly be allocated to either fluorine atom F(1) or F(2) because of the spread of electron density between them. However, by a careful consideration of



TABLE 3.4.2

Atomic positional and thermal parameters for  $[\text{Re}(\text{CO})_3(\text{tmen})\text{F}]_2\text{H}\cdot\text{HOBFB}_3$ 

Atom <sup>a</sup>	x	y	z	U <sub>11</sub>	U <sub>22</sub>	U <sub>33</sub>	U <sub>23</sub>	U <sub>13</sub>	U <sub>12</sub>
Re(1)	38554 (5)	-10613 (6)	16061 (4)	319(11)	263 (6)	355 (6)	5 (3)	-77 (5)	-5 (3)
Re(2)	17626 (5)	15357 (6)	14746 (4)	342(11)	230 (6)	377 (6)	-1 (3)	-42 (5)	11 (3)
F(1)	3058 (6)	-880 (8)	424 (6)	34 (8)	48 (6)	39 (5)	10 (4)	-5 (5)	6 (5)
F(2)	1841 (7)	-39 (9)	-518 (7)	79(10)	49 (7)	71 (7)	16 (5)	0 (6)	-6 (6)
F(3)	869(17)	-3974(16)	-1572(12)	301(30)	90(13)	128(15)	-8(11)	-84(17)	-68(16)
F(4)	1922(16)	-3311(25)	-746(14)	168(27)	248(29)	117(16)	24(15)	10(18)	4(20)
F(5)	1043(19)	-3298(28)	-201(15)	249(32)	271(32)	120(17)	-34(18)	78(19)	-53(25)
O(1)	5029 (8)	-1421(13)	3306 (8)	32(12)	93(11)	46 (8)	9 (7)	-18 (7)	-10 (7)
O(2)	5057(10)	616(15)	1037(10)	64(15)	86(11)	102(11)	8 (9)	31(10)	-27(10)
O(3)	3330(10)	1145(13)	2553(11)	42(14)	76(10)	117(13)	-55 (9)	-1 (9)	18 (8)
O(4)	1534(10)	3603(13)	-2820 (8)	74(14)	71 (9)	56 (8)	28 (7)	26 (8)	-5 (8)
O(5)	3351(14)	1093(13)	-1894(13)	80(18)	54 (9)	136(15)	-3 (9)	26(13)	1 (9)
O(6)	1114 (9)	-30(14)	-3075 (9)	58(13)	79(10)	81(10)	-23 (8)	11 (8)	-16 (9)
O(7)	1105(15)	-2015(13)	-1331(14)	233(27)	20 (8)	172(18)	6(10)	-115(17)	-6(11)
C(1)	4629(12)	-1291(14)	2659(11)	31 (4)					
C(2)	4591(14)	-36(18)	1233(11)	47 (5)					
C(3)	3510(12)	333(18)	2174(11)	47 (5)					
C(4)	3910(14)	-2907(21)	22(13)	66 (6)					
C(5)	5032(15)	-3088(21)	1186(14)	69 (6)					

<sup>a</sup>Re coordinates  $\times 10^5$  and the others  $\times 10^4$ ,  
 Re thermal parameters  $\times 10^4$  and the others  $\times 10^3$ .

TABLE 3.4.2 (Continued)

Atom	x	y	z	U <sub>11</sub>	U <sub>22</sub>	U <sub>33</sub>	U <sub>23</sub>	U <sub>13</sub>	U <sub>12</sub>
C(6)	3742(15)	-3894(19)	1386(13)	63 (6)					
C(7)	2954(14)	-3480(16)	1414(11)	46 (5)					
C(8)	2110(13)	-1835(18)	1669(12)	55 (5)					
C(9)	3090(14)	-2706(20)	2864(14)	67 (6)					
C(10)	1629(12)	2842(18)	-2307(12)	47 (5)					
C(11)	2729(17)	1252(16)	-1736(12)	41 (5)					
C(12)	1314(11)	531(15)	-2431(11)	34 (4)					
C(13)	2646(16)	3840(20)	-532(15)	82 (7)					
C(14)	2650(16)	2068(24)	479(15)	73 (7)					
C(15)	1408(14)	3253(21)	-21(13)	67 (6)					
C(16)	901(16)	2282(23)	-108(16)	80 (7)					
C(17)	96(18)	766(26)	-1093(18)	64 (6)					
C(18)	92(13)	2829(20)	-1590(13)	94 (8)					
N(1)	4169(10)	-2831(12)	977 (8)	41 (4)					
N(2)	2960 (9)	-2351(12)	1950 (8)	40 (4)					
N(3)	2185(10)	2723(13)	-294 (9)	46 (4)					
N(4)	652(10)	1872(14)	-1049(10)	51 (4)					
B	1158(20)	-3194(22)	1001(15)	54(27)	62(16)	34(13)	7(11)	-34(13)	-1(14)

TABLE 3.4.3

Atomic Distances for  $[\text{Re}(\text{CO})_3(\text{tmen})\text{F}]_2\text{H}\cdot\text{BF}_3\text{OH}$ 

Atoms	Distance(Å)	Atoms	Distance(Å)
(a) Bond lengths (and standard deviations)			
Re(1)-F(1)	2.076 (9)	Re(2)-F(2)	2.236(10)
Re(1)-C(1)	1.915(19)	Re(2)-C(10)	1.890(20)
Re(1)-C(2)	1.872(23)	Re(2)-C(11)	1.841(30)
Re(1)-C(3)	1.898(20)	Re(2)-C(12)	1.874(18)
Re(1)-C	ave. 1.895(21)	Re(2)-C	ave. 1.868(23)
Re(1)-N(1)	2.257(14)	Re(2)-N(3)	2.231(14)
Re(1)-N(2)	2.236(14)	Re(2)-N(4)	2.200(17)
Re(1)-N	ave. 2.247(14)	Re(2)-N	ave. 2.216(16)
C(1)-O(1)	1.109(20)	C(10)-O(4)	1.129(21)
C(2)-O(2)	1.161(22)	C(11)-O(5)	1.175(24)
C(3)-O(3)	1.131(21)	C(12)-O(6)	1.157(19)
C-O	ave. 1.127(21)	C-O	ave. 1.154(21)
C(6)-C(7)	1.459(31)	C(15)-C(16)	1.360(32)
N(1)-C(4)	1.456(24)	N(3)-C(13)	1.534(27)
N(1)-C(5)	1.506(27)	N(3)-C(14)	1.484(29)
N(1)-C(6)	1.567(26)	N(3)-C(15)	1.607(26)
N(2)-C(7)	1.471(21)	N(4)-C(16)	1.499(28)
N(2)-C(8)	1.568(26)	N(4)-C(17)	1.532(31)
N(2)-C(9)	1.436(24)	N(4)-C(18)	1.548(25)
B-F(3)	1.250(27)	B-F(4)	1.323(33)
B-F(5)	1.295(31)	B-F	ave. 1.289(30)
B-O(7)	1.366(28)		
(b) Hydrogen bond lengths (and standard deviations)			
F(1)...H-F(2)	2.50 (2)	F(2)...H-O(7)	2.67 (2)
(c) Some non-bonding distances			
F(1)...C(13)	3.25 (3)	O(2)...O(6)	3.09 (3)
O(2)...O(4)	3.09 (3)	C(2)...O(13)	3.32 (4)

TABLE 3.4.4

Bond Angles ( $^{\circ}$ ) For  $[\text{Re}(\text{CO})_3(\text{tmen})\text{F}]_2\text{H}\cdot\text{BF}_3\text{OH}$ 

F(1)-Re(1)-C(1)	176.5 (5)	F(2)-Re(2)-C(10)	176.4 (7)
F(1)-Re(1)-C(2)	93.3 (6)	F(2)-Re(2)-C(11)	94.6 (6)
F(1)-Re(1)-C(3)	96.4 (6)	F(2)-Re(2)-C(12)	92.5 (5)
F(1)-Re(1)-N(1)	83.1 (5)	F(2)-Re(2)-N(3)	85.9 (4)
F(1)-Re(1)-N(2)	83.5 (4)	F(2)-Re(2)-N(4)	82.5 (5)
C(1)-Re(1)-C(2)	85.7 (8)	C(10)-Re(2)-C(11)	88.3 (8)
C(1)-Re(1)-C(3)	86.9 (7)	C(10)-Re(2)-C(12)	85.3 (7)
C(2)-Re(1)-C(3)	88.7 (8)	C(11)-Re(2)-C(12)	89.5 (8)
N(1)-Re(1)-C(1)	93.8 (6)	N(3)-Re(2)-C(10)	96.0 (6)
N(1)-Re(1)-C(2)	97.2 (7)	N(3)-Re(2)-C(11)	96.0 (7)
N(1)-Re(1)-C(3)	174.1 (7)	N(3)-Re(2)-C(12)	174.4 (7)
N(2)-Re(1)-C(1)	97.4 (6)	N(4)-Re(2)-C(10)	94.7 (7)
N(2)-Re(1)-C(2)	175.7 (6)	N(4)-Re(2)-C(11)	175.4 (7)
N(2)-Re(1)-C(3)	94.6 (7)	N(4)-Re(2)-C(12)	94.2 (7)
N(1)-Re(1)-N(2)	79.5 (5)	N(3)-Re(2)-N(4)	80.3 (6)
Re(1)-C(1)-O(1)	174.4(16)	Re(2)-C(10)-O(4)	178.1(17)
Re(1)-C(2)-O(2)	177.1(16)	Re(2)-C(11)-O(5)	178.7(17)
Re(1)-C(3)-O(3)	176.4(17)	Re(2)-C(12)-O(6)	170.9(16)
N(1)-C(6)-C(7)	108.5(16)	N(3)-C(15)-C(16)	105.6(16)
N(2)-C(7)-C(6)	111.6(17)	N(4)-C(16)-C(15)	112.4(20)
Re(1)-N(1)-C(4)	115.5(12)	Re(2)-N(3)-C(13)	111.1(11)
Re(1)-N(1)-C(5)	112.4(12)	Re(2)-N(3)-C(14)	115.1(13)
Re(1)-N(1)-C(6)	105.6(11)	Re(2)-N(3)-C(15)	104.9(10)
C(4)-N(1)-C(5)	107.8(15)	C(13)-N(3)-C(14)	109.6(17)
C(4)-N(1)-C(6)	106.9(15)	C(13)-N(3)-C(15)	107.3(15)
C(5)-N(1)-C(6)	108.4(15)	C(14)-N(3)-C(15)	108.4(14)
Re(1)-N(2)-C(7)	107.9(11)	Re(2)-N(4)-C(16)	103.5(14)
Re(1)-N(2)-C(8)	112.6(10)	Re(2)-N(4)-C(17)	116.7(14)
Re(1)-N(2)-C(9)	114.7(13)	Re(2)-N(4)-C(18)	116.8(11)
C(7)-N(2)-C(8)	103.7(14)	C(16)-N(4)-C(17)	109.4(17)
C(7)-N(2)-C(9)	108.4(13)	C(16)-N(4)-C(18)	111.0(16)
C(8)-N(2)-C(9)	108.9(15)	C(17)-N(4)-C(18)	99.5(16)
F(3)-B-F(4)	113.0(30)	F(3)-B-F(5)	119.9(28)
F(4)-B-F(5)	92.6(23)	F(3)-B-O(7)	112.0(19)
F(4)-B-O(7)	100.9(27)	F(5)-B-O(7)	115.1(27)

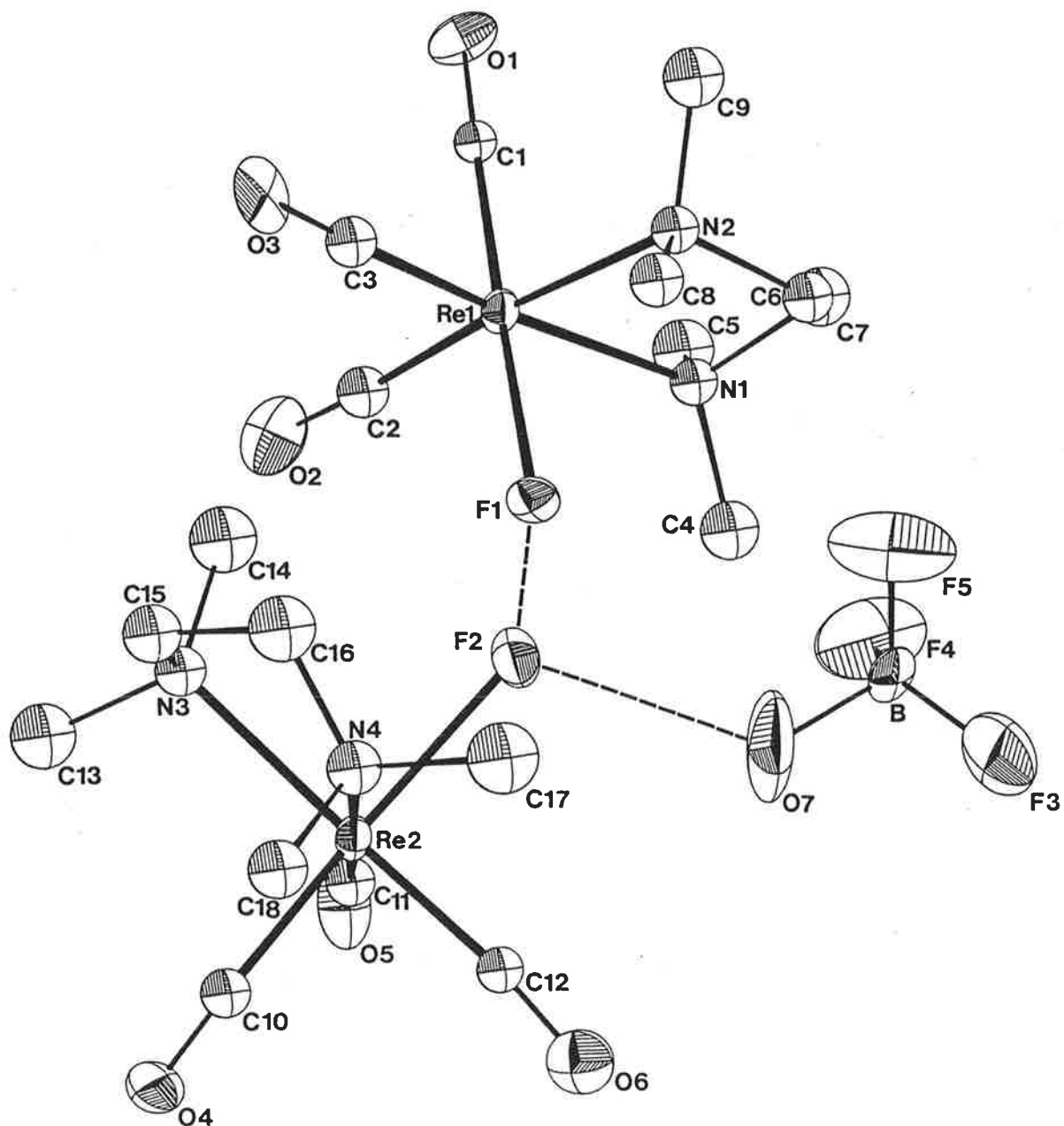


FIGURE 3.4.1. Molecular structure of  $[\text{Re}(\text{CO})_3(\text{tmen})\text{F}]_2\text{H}\cdot\text{HOBf}_3$  (25% probability ellipsoids) showing the hydrogen bonding interactions (----).

the metal-fluoride bond lengths reported ( § 3.6 ),<sup>11,84,115</sup> the hydrogen has formally been assigned to F(2). The geometry at about the two rhenium atoms is essentially octahedral with the carbonyls in a *fac*-configuration consistent with the infrared data. The two rhenium molecules significantly differ only in the rhenium-fluoride bonding distances of 2.076(9) and 2.236(10) Å for Re(1)-F(1) and Re(2)-F(2), respectively. Further discussions are given in Section 3.6.

### 3.5 STRUCTURE DETERMINATION OF [Re(CO)<sub>3</sub>(tmen)F]

#### 3.5.1 Crystal Data

Suitable crystals of Re(CO)<sub>3</sub>(tmen)F were obtained from a dichloromethane solution of the compound by the vapour diffusion crystallization technique using dry petroleum spirit (30 - 40°C) in a nitrogen filled desiccator at room temperature. The crystals have a blade and plate-like morphology. Precession photographs were used to determine the space group and the initial cell constants, which were later refined from 25 reflections by the least-squares routine of the CAD4. The crystal density was measured by flotation in a solution mixture of carbon tetrachloride and 1,2-dibromoethane.

Crystal data: C<sub>9</sub>H<sub>16</sub>FN<sub>2</sub>O<sub>3</sub>Re; M.W. = 405.4, Monoclinic space group P2<sub>1</sub>/c, a = 8.202(2), b = 13.115(9), c = 12.048(4) Å, β = 102.24(3)°. The reduced cell constants<sup>116</sup> are: a = 8.202, b = 12.04, c = 13.115 Å, γ = 102.24 °; U = 1267 Å<sup>3</sup>; Z = 4; D<sub>c</sub> = 2.126 gm.cm<sup>-1</sup>, D<sub>m</sub> = 2.12(1) gm.cm<sup>-1</sup>, λMoK<sub>α</sub> = 0.7107 Å; F(000) = 768 electrons; μMoK<sub>α</sub> = 97.3 cm<sup>-1</sup>.

A crystal of dimensions 0.25 × 0.46 × 0.65 mm<sup>3</sup> was coated with epoxy resin and mounted about a on the STOE (Chapter 7). The intensities were collected in the range 2.5 < 2θ < 65° by the ω scan technique for the levels 0 Kl to 8 Kl. A step counting time of 0.09 s at each 0.01° of the scan range (Δω) was used with 4 s for each background counting time. Δω for the upper level reflections was varied according to the formula below:

$$\Delta\omega = 1.3 + 0.95(\sin\mu/\tan(\psi/2))$$

where, μ is the equi-inclination angle and ψ is the detector angle. Lorentz and Polarisation corrections were applied by the data reduction program AUPTP.<sup>74</sup> Absorption corrections and symmetry averaging using

the program SHELX<sup>75</sup> gave 2876 unique reflections with  $I > 2.5\sigma(I)$ .

### 3.5.2 Structural Solution and Refinement

The rhenium atomic position was determined from a Patterson map. A least-square refinement based on the rhenium atom gave a conventional R value of 0.123 and a difference map revealed the position of all the non-hydrogen atoms. A subsequent full-matrix least-squares refinement with the rhenium atom anisotropic and with all the other located atoms isotropic gave an R value of 0.054. In the third calculation the inter-layer scale factors were refined, while the temperature factors of all the located atoms remained fixed. In the next calculation all the located atoms were refined anisotropically reducing R to 0.049. In the final full-matrix least-squares refinement the two hydrogen atom positions were calculated assuming a tetrahedral geometry about the carbon atoms at a fixed (C-H) bond length of 0.97 Å. The methyl groups were refined as rigid groups and group temperature factors were employed for all hydrogen atoms. The final calculation also included an isotropic extinction correction (Chapter 8.1). The refinement converged with an R value of 0.037,  $R_w = 0.042$ ,  $k = 1.0$ ,  $g = 1.5 \times 10^{-3}$ . The largest peak ( $1.8 \text{ e}\text{\AA}^{-3}$ ) in the final difference map was associated with the rhenium atom.

In the above refinements the scattering factors for the corresponding neutral atoms were used and these were obtained from the International Tables Volume IV. The tabulated observed and calculated structure factors and hydrogen atomic parameters are given on the microfiche. The final non-hydrogen atomic parameters, bond lengths and bond angles are given in Tables 3.5.1, 3.5.2 and 3.5.3, respectively.



TABLE 3. 5.1

Atomic parameters for  $\text{Re}(\text{CO})_3(\text{tmen})\text{F}$ 

Atom <sup>a</sup>	x	y	z	U <sub>11</sub> <sup>b</sup>	U <sub>22</sub>	U <sub>33</sub>	U <sub>23</sub>	U <sub>13</sub>	U <sub>12</sub>
Re	22580 (3)	69951(2)	26650(2)	284(2)	340(2)	298(2)	-15(1)	68(1)	-13(1)
F	3319 (5)	7701(3)	1489(3)	47(2)	56(2)	33(2)	-1(2)	17(2)	-5(2)
O(1)	664 (9)	6055(5)	4497(5)	91(5)	95(4)	52(3)	9(3)	21(3)	-49(4)
O(2)	-1253 (9)	6936(5)	1188(7)	35(4)	105(5)	70(5)	1(3)	-8(3)	-4(3)
O(3)	2676 (7)	4801(4)	1906(8)	58(4)	48(3)	152(7)	-35(4)	27(4)	0(2)
C(1)	1308 (9)	6405(5)	3833(5)	50(4)	48(3)	35(3)	3(2)	6(3)	-15(3)
C(2)	88(11)	6968(5)	1737(6)	39(4)	57(4)	33(3)	-8(2)	2(3)	-3(2)
C(3)	2534 (9)	5634(6)	2189(7)	53(4)	43(3)	67(5)	-9(3)	18(4)	3(3)
N(1)	2160 (6)	8614(4)	3246(4)	39(3)	33(2)	36(2)	-1(2)	5(2)	4(2)
N(2)	4871 (8)	7151(4)	3746(5)	29(3)	42(2)	44(3)	5(2)	5(2)	1(2)
C(4)	1247(10)	8727(6)	4173(6)	55(5)	59(4)	46(4)	-4(3)	17(3)	16(3)
C(5)	1358(11)	9298(5)	2290(7)	68(5)	48(3)	51(4)	7(3)	7(4)	1(3)
C(6)	3909(10)	8936(4)	3611(6)	56(4)	34(3)	53(4)	-1(2)	4(3)	-4(3)
C(7)	4890(11)	8134(4)	4373(7)	49(5)	48(3)	47(4)	-1(3)	-4(3)	-7(3)
C(8)	6152(12)	7160(7)	3069(9)	43(5)	72(5)	70(6)	0(4)	24(4)	3(4)
C(9)	5288(10)	6317(5)	4600(6)	50(4)	54(3)	47(3)	17(3)	1(3)	7(3)

<sup>a</sup> Re positional parameters  $\times 10^5$  and the others  $\times 10^4$ .

<sup>b</sup> Re temperature factors  $\times 10^4$  and the others  $\times 10^3$ .

TABLE 3.5.2  
Interatomic Distances<sup>a</sup> for Re(CO)<sub>3</sub>(tmen)F

(a) Bonding distances (Å) and their standard deviations			
Re-F	2.039 (4)	C(3)-O(3)	1.162 (9)
Re-N(1)	2.250 (5)	N(1)-C(4)	1.480 (9)
Re-N(2)	2.273 (6)	N(1)-C(5)	1.502 (9)
Re-C(1)	1.913 (6)	N(1)-C(6)	1.472 (9)
Re-C(2)	1.894 (8)	N(2)-C(7)	1.498 (9)
Re-C(3)	1.910 (8)	N(2)-C(8)	1.461(11)
C(1)-O(1)	1.146 (9)	N(2)-C(9)	1.495 (8)
C(2)-O(2)	1.160(11)	C(6)-C(7)	1.516 (9)
(b) Some non-bonding distances			
O1 ... F(1) <sup>II</sup>	3.334	O(1) ... O(1) <sup>I</sup>	3.303
C7 ... F(1) <sup>II</sup>	3.273	C(6) ... O(3) <sup>III</sup>	3.196

<sup>a</sup>Superscripts in Roman refer to the following equivalent positions, with respect to the unique asymmetric unit at x, y, z:

$$\text{I} = -x, -y, -z$$

$$\text{III} = -x, .5 + y, .5 - z$$

$$\text{II} = x, .5 - y, .5 + z$$

TABLE 3.5.3

Bond Angles ( $^{\circ}$ ) for  $\text{Re}(\text{CO})_3(\text{tmen})\text{F}$ 

F-Re-N(1)	80.4(2)	Re-N(1)-C(5)	111.5(4)
F-Re-N(2)	82.5(2)	Re-N(1)-C(6)	105.6(4)
F-Re-C(1)	176.3(2)	C(4)-N(1)-C(5)	108.1(6)
F-Re-C(2)	94.7(3)	C(4)-N(1)-C(6)	111.2(6)
F-Re-C(3)	97.1(3)	C(5)-N(1)-C(6)	107.4(5)
N(1)-Re-N(2)	80.0(2)	Re-N(2)-C(7)	106.1(4)
N(1)-Re-C(1)	96.2(2)	Re-N(2)-C(8)	112.4(6)
N(1)-Re-C(2)	96.4(2)	Re-N(2)-C(9)	112.4(4)
N(1)-Re-C(3)	175.3(3)	C(7)-N(2)-C(8)	110.0(7)
N(2)-Re-C(1)	95.4(3)	C(7)-N(2)-C(9)	108.0(6)
N(2)-Re-C(2)	175.8(2)	C(8)-N(2)-C(9)	107.8(6)
N(2)-Re-C(3)	95.7(3)	Re-C(1)-O(1)	176.7(6)
C(1)-Re-C(2)	87.2(3)	Re-C(2)-O(2)	178.3(8)
C(1)-Re-C(3)	86.2(3)	Re-C(3)-O(3)	178.7(7)
C(2)-Re-C(3)	87.7(3)	N(1)-C(6)-C(7)	109.9(5)
Re-N(1)-C(4)	112.8(4)	N(2)-C(7)-C(6)	110.3(6)

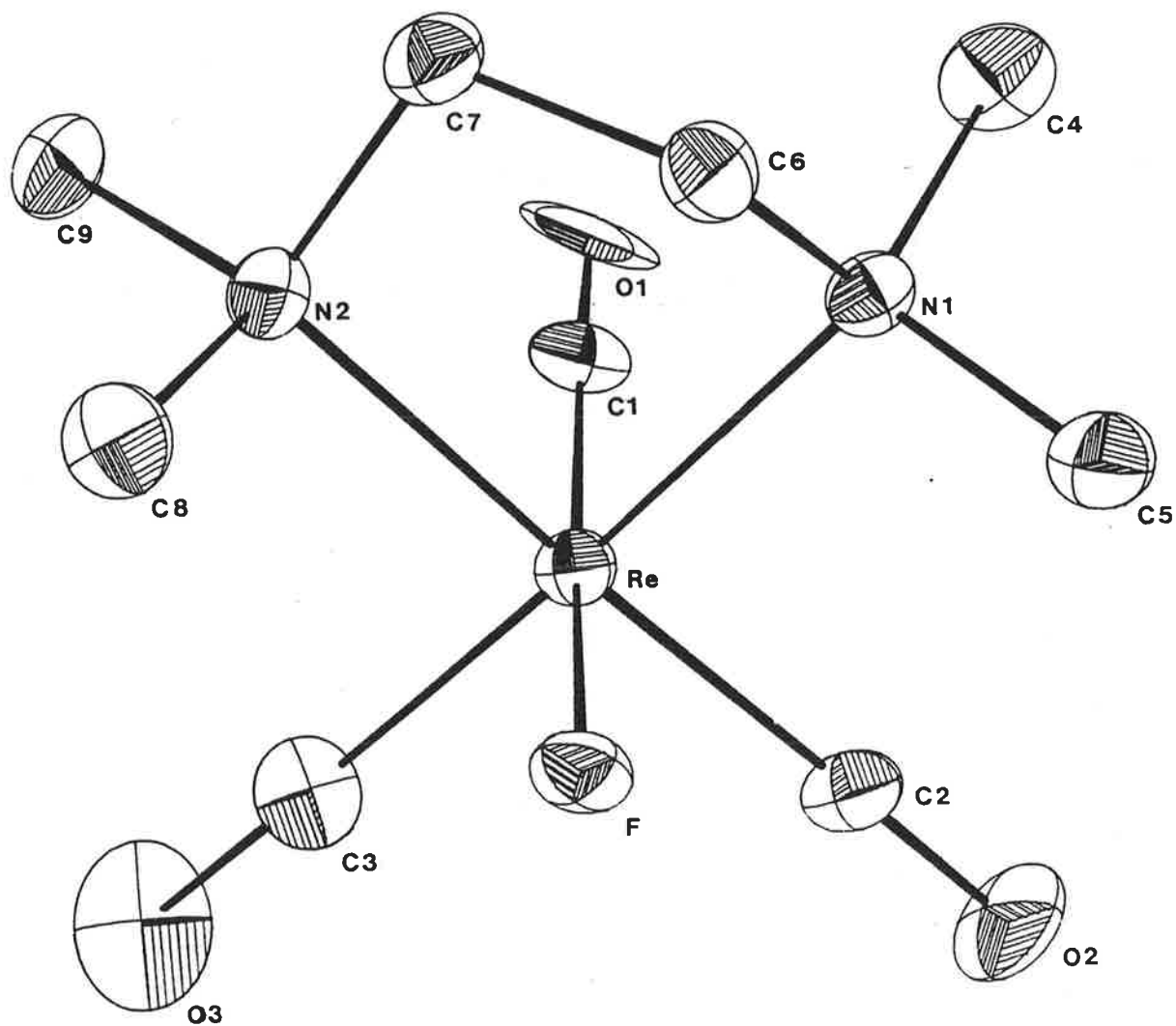


FIGURE 3.5.1. The molecular structure of  $\text{Re}(\text{CO})_3(\text{tmen})\text{F}$  (ORTEP diagram with 25% probability ellipsoids).

The molecular structure of  $\text{Re}(\text{CO})_3(\text{tmen})\text{F}$  was drawn using the programme ORTEP<sup>78</sup> and is shown in Figure 3.5.1.

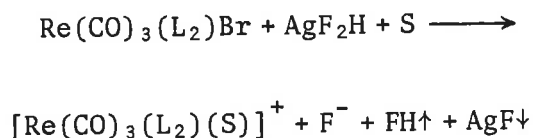
### 3.5.3 Description of the Structure

Crystals of  $\text{Re}(\text{CO})_3(\text{tmen})\text{F}$  consist of discrete molecules separated by a minimum distance of 3.196 Å. Figure 3.5.1 shows the atomic numbering scheme employed for all non-hydrogen atoms of the molecule. The rhenium atom assumes an approximate octahedral geometry with the carbonyl groups in a *fac*-configuration and with the fluorine atom *cis* to the nitrogen atoms of the tmen ligand. This stereochemistry is consistent with the three strong carbonyl bands ( $2A' + A''$ ) observed in the infrared spectra (Table 3.3.1). The fluorine atom resides at a distance of 2.040(4)Å from the rhenium which is essentially the same (i.e. within three standard deviations) as observed for the  $\text{Re}(1) - \text{F}(1)$  bond in  $[\text{Re}(\text{CO})_3(\text{tmen})\text{F}]_2\text{H}\cdot\text{HOBf}_3$ , 2.076(9)Å (Table 3.5.3).

### 3.6 DISCUSSION

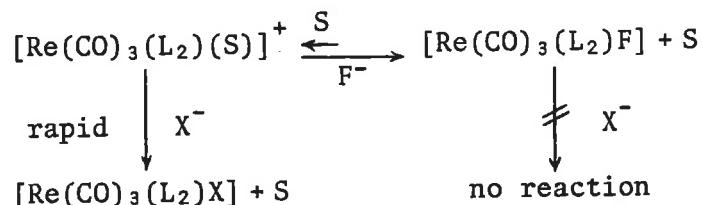
This chapter has shown that, by using "plastic" reaction vessels, fluorinated solvents, anhydrous silver bifluoride and a dry nitrogen atmosphere, the halide abstraction reactions will produce rhenium tricarbonyl fluoride complexes in good yields and free of any by-products. The use of the "plastic" vessels eliminates the introduction of the trifluoroborate anion into the system, while the use of fluorinated solvents and dry silver bifluoride prevents the formation of by-products such as  $\text{Re}(\text{CO})_3(\text{L}_2)\text{Cl}$ ,  $[\text{Re}(\text{CO})_3(\text{L}_2)(\text{H}_2\text{O})]^+$  and  $\text{Re}(\text{CO})_3(\text{L}_2)\text{OH}$ . The abstraction technique is easily extended to the preparation of metal fluoride complexes using the respective metal carbonyl chlorides, bromides and iodide as precursors.

When the rhenium halide precursors are dissolved in the minimum volume of solvent and the excess silver bifluoride is added three general observations can be made. Firstly, as described in Chapter 3.2 and 3.3, precipitation of silver bromide commences and is complete within minutes. Secondly, crystallization of the less soluble rhenium fluoride does not occur till 15 to 20 min. later. And, thirdly, on introduction of a foreign halide (i.e.  $\text{Cl}^-$ ,  $\text{Br}^-$ ,  $\text{I}^-$ ) into the system during this period leads to the formation of the respective rhenium halide by-products. These observations are consistent with the formation of a labile solvento intermediate immediately after the abstraction of the halide from the parent complex:



(where, S = solvent molecule e.g.  $\text{CH}_2\text{Cl}_2$ )

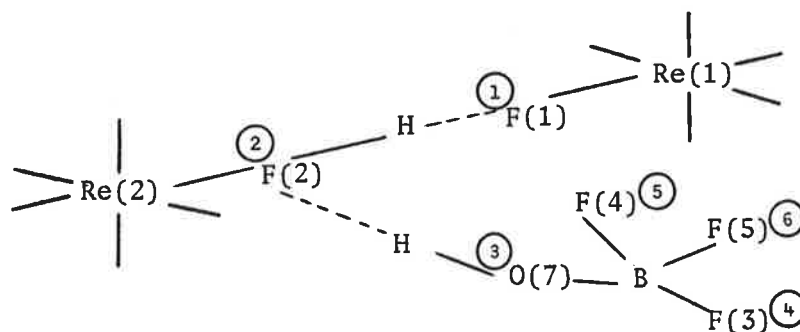
Thus, the final and rate determining step is the replacement of the solvent molecule by a fluoride or other halide anion:



(where, X = Cl<sup>-</sup>, Br<sup>-</sup>, I<sup>-</sup>)

This scheme, therefore, offers an explanation for the relative lability of the solvento intermediate as compared to the rhenium fluoride, which undergoes no observable halide (X) substitution within 24 hr. It is essential, therefore, to use calcium fluoride solution cells as opposed to sodium chloride cells when recording infrared spectra to avoid the rapid chloride substitution in the solution cells. The scheme also points to the source of the chloride in the  $\text{Re}(\text{CO})_3(\text{L}_2)\text{Cl}$  by-product, namely chloroform and dichloromethane when used; and, suggests that an equilibrium exists between the solvento intermediate and the rhenium fluoride, even if it lies far towards the latter.

In the  $[\text{Re}(\text{CO})_3(\text{tmen})\text{F}]_2\text{H}\cdot\text{HOBf}_3$  structure the assignment of atoms F(2) and O(7) requires further explanation. The presence of the molecular ion  $[\text{Re}(\text{CO})_3(\text{tmen})\text{F}]^+$  and the absence of  $[\text{Re}(\text{CO})_3(\text{tmen})(\text{OH}_2)]^+$  in the mass spectrum is not strong enough evidence to assign both F(1) and F(2) as fluorine atoms (i.e. only one, at least). The microanalysis results (Chapter 3.7) requires the structure to have five fluorine atoms. Consider the following diagram, where the atoms of interest are additionally numbered from ① to ⑥;



From the microanalysis requirement one of the six atoms (i.e. ① to ⑥) must be an oxygen atom. Of these, atom ① can be identified as a fluorine by a comparison of the (Re-F) bond length in  $[\text{Re}(\text{CO})_3(\text{tmen})\text{F}]$  and the (Re-O) bond in  $[\text{Re}(\text{CO})_3(\text{tmen})(\text{OH}_2)]^+ \cdot \text{BF}_4^-$  (Table 3.6.1). Since, the molecular ions  $[\text{OBF}_3]^+$ ,  $[\text{OBF}_2]^+$  and  $[\text{BF}_2]^+$  can be identified in the mass spectra, and since the infrared spectrum shows  $\nu(\text{B-F,OH})$  and  $\nu(\text{O-H})$  stretching bands, the trifluoroborate anion  $[\text{HOBF}_3]^-$  is thus characterized. Hence, atom ② is required to be a fluorine atom. Now, by elimination any of the atoms ③, ④, ⑤ and ⑥ could possibly be an oxygen atom. But, because the atom pairs ① - ② and ② - ③ are both at hydrogen bonding distance then the  $[\text{HOBF}_3]^-$  anion must provide its hydrogen. Hence, atom ③ can be assigned as the unique oxygen atom. One would have expected that the oxygen atom could be identified by comparing the (B-F,OH) bond lengths in this structure with those in  $[\text{Mn}(\text{CO})_3(\text{diphos})(\text{HOBF}_3)] \cdot \frac{1}{2}(\text{dpeo})$ ,  $[\text{Re}(\text{CO})_3(\text{tmen})(\text{H}_2\text{O})]^+ \cdot \text{BF}_4^-$  and literature values. However, due to the generally large standard deviations in the (B-F,OH) bond lengths no atom characterisation can be made on this basis.

The coordination geometry around the rhenium atom in the  $\text{Re}(\text{CO})_3(\text{tmen})\text{F}$  molecules of both structures studied in this chapter is the same and is consistent with the carbonyl groups in a *fac* configuration as predicted from the infrared spectra. However, the rhenium-fluoride bond length increases from  $2.039(4)\text{\AA}$  to  $2.24(1)\text{\AA}$  as the bond order of



TABLE 3.6.1

A comparison of rhenium fluoride and oxygen bond lengths (Å)

Compound	Bond length
(tmen) (CO) <sub>3</sub> Re-F	2.039(4)
(tmen) (CO) <sub>3</sub> Re-F···H	2.076(9)
(tmen) (CO) <sub>3</sub> Re-FH···HOBF <sub>3</sub>	2.24 (1)
(tmen) (CO) <sub>3</sub> Re-OH <sub>2</sub> ···FAsF <sub>5</sub>	2.268(8)
(tmen) (CO) <sub>3</sub> Re-OH <sub>2</sub> ···BF <sub>4</sub>	2.24 (1)
(CO) <sub>5</sub> Re-OH <sub>2</sub> ···FAsF <sub>5</sub>	2.206(8)

the fluorine atom is increased (Table 3.6.1). In fact, the bonding properties of fluorine are seen to approach those of an oxygen atom, which makes an average bonding distance of 2.246(5)Å with rhenium(I) (Chapter 5). In Chapter 6 a detailed comparison of metal-fluoride and -oxygen bond lengths is presented showing how the value of the bond length identifies the atom type.

### 3.7 EXPERIMENTAL

#### General

All preparations, reactions and reagent transfers were carried out in a dry box containing a high-purity dry nitrogen atmosphere. The preparations of the starting materials are described in Chapter 7.2. Only solvents of analytical grade purity which had been dried over Linde 4A molecular sieves were used. The compounds prepared below were stored in a desiccator containing dry nitrogen at ca. 5°C. The description of the instruments used for recording the physical measurements is given in Chapter 7. The reactions were monitored by the periodic measurement of the carbonyl stretching frequencies of samples of the respective mixtures using calcium fluoride solution cells. On isolation of the compounds their complete infrared spectra were recorded as nujol mulls using calcium fluoride plates.

#### [Re(CO)<sub>3</sub>(bpy)F]<sub>2</sub>H·HOBf<sub>3</sub>

To a glass flask containing 90 mg (0.18 mmol) of Re(CO)<sub>3</sub>(bpy)Br dissolved in dichloromethane (18 ml) 160 mg of silver bifluoride (1.09 mmol, 5 fold excess) was added and stirred at room temperature for 40 minutes. The silver bromide, which precipitated within minutes, and the excess silver bifluoride were removed by filtration. The solution

was then concentrated to ca. 5 ml; light petroleum (40°C) added to precipitate very fine yellow crystals of the product (yield, 60 - 70%) which were washed with petroleum (ca. 5°C); and then dried in a vacuum.

(Found: C, 32.08; H, 1.94; F, 9.5; N, 5.79  
 $C_{26}H_{18}BF_5N_4O_7Re_2$  requires: C, 31.96; H, 1.86; F, 9.7; N, 5.74%).  
 Mass spectrum [m/e,\* assignment (intensity)]: 446,  $[Re(CO)_3(bpy)F]^+(100)$ ;  
 418,  $[Re(CO)_2(bpy)F]^+(29)$ ; 390,  $[Re(CO)(bpy)F]^+(133)$ ; 362,  
 $[Re(bpy)F]^+(205)$ ; 343,  $[Re(bpy)]^+(29)$ ; 206,  $[ReF]^+(5)$ ; 187,  $[Re]^+(57)$ ;  
 156,  $(bpy)^+(1095)$ ; 85,  $[HOBF_3]^+(1752)$ ; 49,  $[BF_2]^+(1750)$ .

$[Re(CO)_3(tmen)F]_2H \cdot HOBF_3$

Finely divided silver bifluoride (188 mg, 1.28 mmol, 5 fold excess) was added to a glass flask containing a dichloromethane (12 ml) solution with  $Re(CO)_3(tmen)Br$  (100 mg, 0.21 mmol) at room temperature and the mixture was stirred for 30 minutes. The  $AgBr$  precipitate and the excess unreacted  $AgF_2H$  were removed by filtration. The solution was concentrated to ca. 4 ml and the white product (65%) was precipitated and washed with light petroleum spirit.

(Found: C, 24.10; H, 4.04; F, 10.8; N, 6.38  
 $C_{18}H_{34}BF_5N_4O_7Re_2$  requires: C, 24.11; H, 3.82; F, 10.6; N, 6.25%).  
 Mass spectrum [m/e, assignment (intensity)]: 406,  $[Re(CO)_3(tmen)F]^+(100)$ ;  
 378,  $[Re(CO)_2(tmen)F]^+(265)$ ; 350,  $[Re(CO)(tmen)F]^+(632)$ ; 322,  
 $[Re(tmen)F]^+(85)$ ; 303,  $[Re(tmen)]^+(35)$ ; 206,  $[ReF]^+(10)$ ; 187,  $[Re]^+$   
 (170); 116,  $(tmen)^+(955)$ ; 84,  $[OBF_3]^+(250)$ ; 65,  $[OBF_2]^+(176)$ ;  
 36,  $[BF_2]^+(983)$ .

---

\* All m/e values are based on  $^{187}Re$  and  $^{11}B$ , and the intensities are relative to the parent ion.

Re(CO)<sub>3</sub>(bpy)F

A mixture of dichloromethane (20 ml), Re(CO)<sub>3</sub>(bpy)Br (90 mg, 0.18 mmol) and AgF<sub>2</sub>H (31 mg, 0.21 mmol, 17% excess) was stirred for 30 min. in a plastic vessel at room temperature. The solution was then filtered, concentrated to ca. 5 ml and the yellow product (yield, 70%) precipitated and washed with light petroleum.

(Found: C, 34.95; H, 1.87; F, 4.18; N, 6.32  
 C<sub>13</sub>H<sub>8</sub>FN<sub>2</sub>O<sub>3</sub>Re requires: C, 35.06; H, 1.81; F, 4.26; N, 6.29%).  
 Mass spectrum [m/e, assignment (intensity)]: 446, [Re(CO)<sub>3</sub>(bpy)F]<sup>+</sup>(100);  
 418, [Re(CO)<sub>2</sub>(bpy)F]<sup>+</sup>(230); 390, [Re(CO)(bpy)F]<sup>+</sup>(163); 362,  
 [Re(bpy)F]<sup>+</sup>(232); 343, [Re(bpy)]<sup>+</sup>(35); 206, [ReF]<sup>+</sup>(9); 187, [Re]<sup>+</sup>(63);  
 156, (bpy)<sup>+</sup>(1340).

Re(CO)<sub>3</sub>(dpe)F

This compound (yield, 65%; white) was prepared from Re(CO)<sub>3</sub>(dpe)Br (40 mg, 0.058 mmol) and AgF<sub>2</sub>H (10 mg, 0.068 mmol, 17% excess) in dichloromethane (6 ml) similar to Re(CO)<sub>3</sub>(bpy)F.

(Found: C, 50.72; H, 3.45; F, 2.69; P, 9.08  
 C<sub>29</sub>H<sub>24</sub>FO<sub>3</sub>P<sub>2</sub>Re requires: C, 50.65; H, 3.52; F, 2.76; P, 9.1%).

Re(CO)<sub>3</sub>(SbPh<sub>3</sub>)<sub>2</sub>F

The title compound (yield, 75%; white) was prepared from Re(CO)<sub>3</sub>(SbPh<sub>3</sub>)<sub>2</sub>Br (90 mg, 0.11 mmol) and AgF<sub>2</sub>H (19 mg, 0.13 mmol, 18% excess) in dichloromethane (8 ml), in a plastic vessel, similar to preparation of Re(CO)<sub>3</sub>(bpy)F.

(Found: C, 56.81; H, 3.57; F, 2.3  
 C<sub>39</sub>H<sub>30</sub>FReSb requires: C, 56.73; H, 3.66; F, 2.30%).

Re(CO)<sub>3</sub>(tmen)F

This compound (yield, 60%; white) was prepared using the method as described for [Re(CO)<sub>3</sub>(tmen)F]<sub>2</sub>H·HOBf<sub>3</sub> with the exception that here plastic reaction vessels were used.

(Found: C, 26.75; H, 4.10; F, 5.2; N, 6.98  
C<sub>9</sub>H<sub>16</sub>FN<sub>2</sub>O<sub>3</sub>Re requires: C, 26.66; H, 3.98; F, 4.68; N, 6.91%).

Mass spectrum [m/e, assignment (intensity)]: 406, [Re(CO)<sub>3</sub>(tmen)F]<sup>+</sup>(100);  
378, [Re(CO)<sub>2</sub>(tmen)F]<sup>+</sup>(375); 350, [Re(CO)(tmen)F]<sup>+</sup>(750); 322,  
[Re(tmen)F]<sup>+</sup>(100); 303, [Re(tmen)]<sup>+</sup>(50); 187, [Re]<sup>+</sup>(150);  
116, (tmen)<sup>+</sup>(800).

## CHAPTER 4

### MANGANESE CARBONYL COMPLEXES

#### 4.1 INTRODUCTION

The perchlorate ion is a poor coordinating ligand. It has been successfully coordinated to a limited number of transition metal ions.<sup>31, 117, 118 - 120</sup> Until the work reported by Snow and co-workers<sup>14, 15</sup> the only known metal carbonyl complexes containing coordinated perchlorate were  $\text{Co}(\text{CO})_2(\text{PPh}_3)_2\text{OClO}_3$  and  $\text{M}(\text{CO})(\text{PPh}_3)_2\text{OClO}_3$  (where,  $\text{M} = \text{Rh}, \text{Ir}$ ). The investigations resulted in the development of an efficient method for the coordination of the perchlorate anion to metal carbonyl complexes. One of the aims in preparing these complexes was to use them as precursors of metal fluoride complexes and this is discussed in this chapter. The knowledge of the preparative conditions gained from the metal perchlorate preparations led to the modification of techniques and apparatus for the preparation of the fluoride complexes (Chapters 2, 3 and 5). The crystal structure of  $[\text{Mn}(\text{CO})_3(\text{P}(\text{OPh})_3)_2(\text{OClO}_3)]$  presented in this chapter serves to provide direct evidence for the coordination of the perchlorate anion and thus to verify the infrared and mass spectra results.<sup>14, 15</sup>

Following the successful preparation of the metal perchlorate and difluorophosphato complexes it was proposed to investigate the preparation of the analogous fluoride complexes. These compounds are produced by reacting both the pentacarbonyl (Chapter 2) and substituted (Chapter 3) precursors with the reagents  $\text{AgF} \cdot \delta(\text{H}_2\text{O})$  (where,  $\delta = 0.4 - 1.0$ ),  $\text{AgF}_2\text{H}$  and  $\text{Ph}_4\text{AsF}$ . During the initial reactions using the last two reagents and pyrex glass vessels the trifluorohydroxy borate anion,

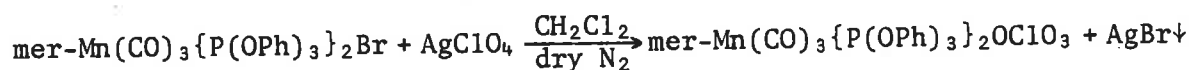
$[\text{HOBf}_3]^-$ , was formed in an unexpected side reaction on the glass surface. In the previous chapter this anion has been identified as a non-coordinating group in the crystal structure of  $[\text{Re}(\text{CO})_3(\text{tmen})\text{F}]_2\text{H}\cdot\text{HOBf}_3$ . This chapter includes the details of the preparation and structural characterization of the complex  $[\text{Mn}(\text{CO})_3(\text{diphos})(\text{HOBf}_3)]\cdot\frac{1}{2}(\text{dpeo})$ , in which the anion is found to coordinate to the metal centre.

The halide abstraction method developed in Chapter 3 is applied to the substituted manganese carbonyl system. Thus, the subject of a minor part of this chapter is the preparation and characterization of the manganese carbonyl fluoride complexes.

## 4.2 PREPARATIONS

### 4.2.1 $[\text{Mn}(\text{CO})_3\{\text{P}(\text{OPh})_3\}_2\text{OC1O}_3]$

This compound was prepared by the general method as developed by Snow and co-workers<sup>14,15</sup> for the preparation of metal carbonyl perchlorates,  $\text{M}(\text{CO})_3(\text{L}_2)(\text{OC1O}_3)$  (where,  $\text{M} = \text{Mn}, \text{Re}$ ;  $\text{L} = \text{PPh}_3, \text{P}(\text{OPh})_3$ ;  $\text{L}_2 = \text{bpy}$ ). The reaction of  $\text{AgClO}_4$  (30% molar excess) with  $\text{Mn}(\text{CO})_3\{\text{P}(\text{OPh})_3\}_2\text{Br}$  in a dry dichloromethane methane solution and under an atmosphere of dry nitrogen is complete after *ca.* 30 min. of stirring at room temperature.



The reaction progress was monitored by periodic infrared measurements in the carbonyl region of the sample of the solution. The excess  $\text{AgClO}_4$  and the  $\text{AgBr}$  precipitate was removed by filtration. Suitable crystals for x-ray analysis were grown from the remaining solution by concentration and the addition of light petroleum (30-40°). A sample of the product (*ca.* 70% yield) was subsequently used to prepare a nujol mull for a full infrared spectrum and the coordinated perchlorate was characterized by the (Cl-O) stretching bands (§ 4.5).

### 4.2.2 $[\text{Mn}(\text{CO})_3(\text{diphos})(\text{BF}_3\text{OH})] \cdot \frac{1}{2}(\text{dpeo})$

The title compound was prepared<sup>103</sup> by reacting  $[\text{Mn}(\text{CO})_3(\text{diphos})\text{Cl}]$  with tetraphenyl arsonium fluoride ( $\text{Ph}_4\text{AsF}$ ) under dry conditions using dichloromethane as the solvent. The source of the trifluorohydroxy borate anion  $(\text{BF}_3\text{OH})^-$  was traced back to the  $\text{Ph}_4\text{AsF}$  sample, which contained the impurity  $(\text{Ph}_4\text{As})^+(\text{BF}_3\text{OH})^-$ . The presence of the  $(\text{BF}_3\text{OH})^-$  ion was identified by the author as a quartet in the  $\text{F}^{19}$  N.M.R. spectra at a chemical shift of 1934 Hz from the  $\text{F}^-$  signal of  $\text{Ph}_4\text{AsF}$  (Diagram 4.2.1). The tetraphenyl arsonium salts were prepared<sup>121</sup> from a reaction



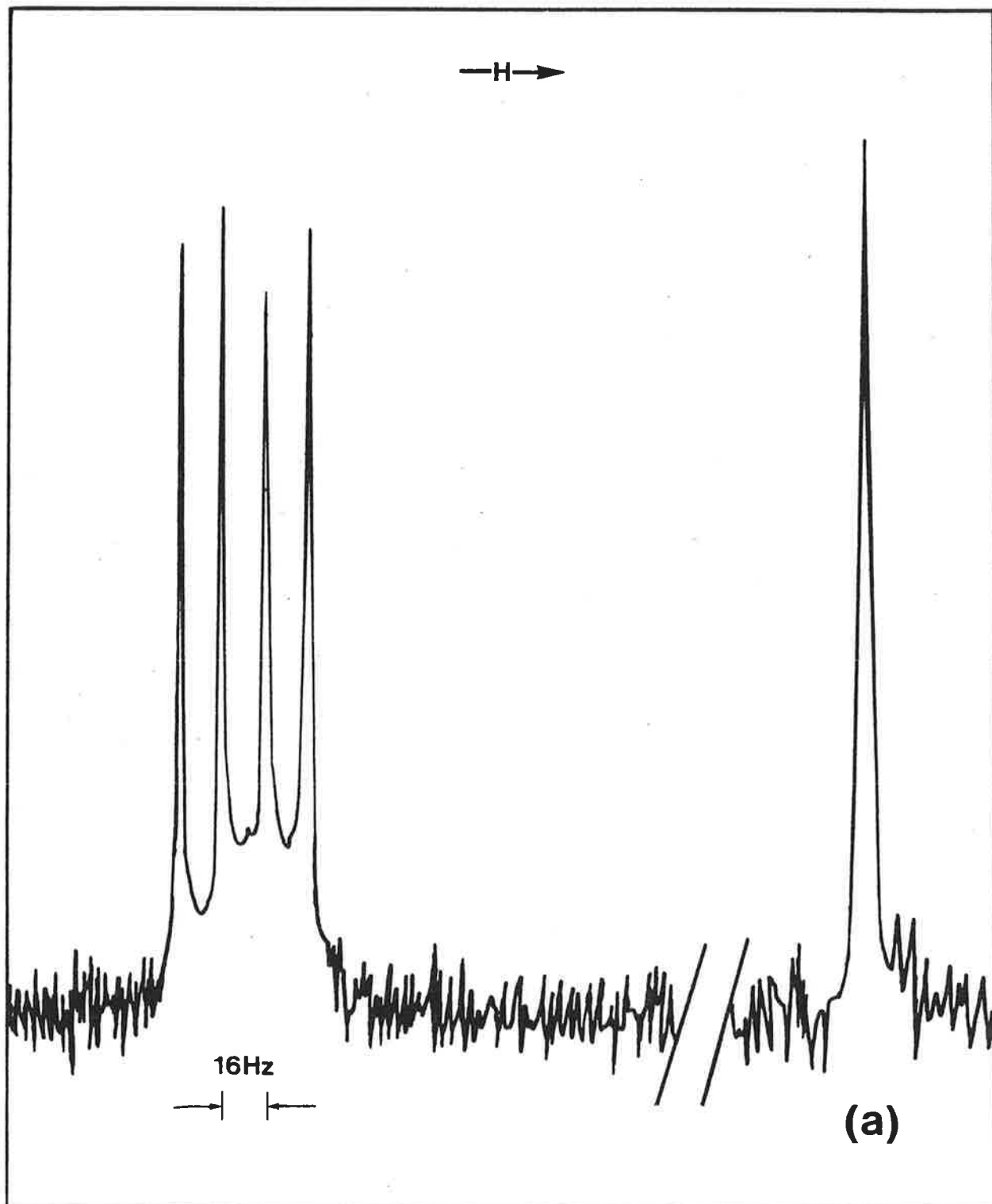
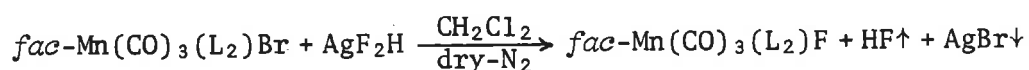


FIGURE 4.2.1. A proton decoupled  $^{19}\text{F}$  N.M.R. (84.67 MHz) spectrum of a dry  $\text{CD}_2\text{Cl}_2$  solution (298°K) saturated with the tetraphenyl arsonium salts  $[\text{Ph}_4\text{As}]^+[\text{HOBf}_3]^-$  and  $[\text{Ph}_4\text{As}]^+\text{F}^-$ . The coupling constant  $J(^{11}\text{B}-^{19}\text{F})$  of 16 Hz identifies the quartet (chemical shift w.r.t.  $\text{C}_6\text{F}_6$ , -627 Hz) as resulting from the  $\text{HOBf}_3^-$  anion.<sup>121</sup> The upfield singlet (a) arises from the fluorine anion (chemical shift w.r.t.  $\text{C}_6\text{F}_6$ , -2561 Hz).

between AgF and Ph<sub>4</sub>AsClO<sub>4</sub>. (Ph<sub>4</sub>As)<sup>+</sup>(BF<sub>3</sub>OH)<sup>-</sup> was formed as a by-product resulting from a surface reaction involving AgF and the pyrex glass reaction vessel (§ 4.5). The dpeo in the above formula is believed to have originated from uncoordinated diphos which was oxidized during the chloride abstraction reaction.

#### 4.2.3 Preparation of *fac*-Mn(CO)<sub>3</sub>(L<sub>2</sub>)F (where, L<sub>2</sub> = diphos, Phen, tmen)

These complexes were prepared from the respective manganese(I) carbonyl bromides using the halide abstraction method developed for the rhenium fluorides (Chapter 3). When finely divided silver bifluoride is added to dry dichloromethane solutions containing the manganese bromides good yields of the respective fluoride complexes are obtained according to the following equation:



After stirring the reaction mixture for *ca.* 30 min. in a dry nitrogen atmosphere the silver bromide precipitate is easily filtered off leaving behind a clear yellow solution in each case. The compounds are then isolated by removing the solvent and recrystallized from dichloromethane-petroleum spirit (100 - 120°C).

All compounds were initially characterized <sup>by</sup> solution infrared spectra in the carbonyl absorption region. The  $\nu(CO)$  stretching modes of the manganese fluorides occur at higher frequencies than for the bromide precursors (Table 4.2.1). A comparison of number and relative intensities of the  $\nu(CO)$  absorption bands indicates that the fluoride compounds have an octahedral geometry with the carbonyl groups in a *fac*-configuration.<sup>57</sup> The full nujol infrared spectrum of the isolated compounds is given in Appendix 1.

TABLE 4.2.1

Compound	Colour	$\nu(\text{CO})$	Medium
<i>fac</i> -Mn(CO) <sub>3</sub> (diphos)Br	yellow	2022s, 1960s, 1919s	CH <sub>2</sub> Cl <sub>2</sub>
<i>fac</i> -Mn(CO) <sub>3</sub> (diphos)F	yellow	2085msp, 2010s, 1042s, 1910s, 1860w	CH <sub>2</sub> Cl <sub>2</sub> nujol
<i>fac</i> -Mn(CO) <sub>3</sub> (Phen)Br	yellow	2028s, 1939s, 1923s 2020s, 1945s, 1920s, 1890wsh	CH <sub>2</sub> Cl <sub>2</sub> nujol
<i>fac</i> -Mn(CO) <sub>3</sub> (Phen)F	yellow	2043s, 1949s, 1935s	CH <sub>2</sub> Cl <sub>2</sub>
<i>fac</i> -Mn(CO) <sub>3</sub> (tmen)Br	yellow	2017s, 1937s, 1900s 2018s, 1930s, 1898s	CH <sub>2</sub> Cl <sub>2</sub> nujol
<i>fac</i> -Mn(CO) <sub>3</sub> (tmen)F	yellow	2090w, 2019s, 1944s, 1905s 2090w, 2020s, 1950s, 1912s	CH <sub>2</sub> Cl <sub>2</sub> nujol

The manganese fluoride complexes absorb water when exposed to the atmosphere. They can be stored for months in a desiccator at room temperature without decomposition. Slow halide substitution will occur if the compounds are left dissolved in chloroform or dichloromethane. The by-products formed are the respective chloride complexes,  $\text{Mn}(\text{CO})_3(\text{L}_2)\text{Cl}$  (Chapter 3). Hence for crystallization experiments which extend over a number of days monofluoro- or hexafluoro-benzene solvents should be used.

#### 4.3 STRUCTURE DETERMINATION OF $[\text{Mn}(\text{CO})_3\{\text{P}(\text{OPh})_3\}_2\text{OCIO}_3]$

##### 4.3.1 Crystal Data

The yellow needle-like crystal prepared (§ 4.2.1) are elongated along the a axis. The cell constants were refined using 25 high angle reflections and from the absences in the data collection the space group was unambiguously determined to be monoclinic  $P2_1/c$ . The density was measured using a flotation mixture of petroleum spirit (40-60°) and carbontetrachloride.

Crystal Data:  $\text{C}_{39}\text{H}_{30}\text{ClMnO}_{13}\text{P}_2$ ; M.W. = 859.0; Monoclinic space group  $P2_1/c$ ,  $a = 8.963(2)$ ,  $b = 22.516(4)$ ,  $c = 19.943(3)$ ,  $\beta = 93.85(1)^\circ$ ;  
 $U = 4016(2) \text{ \AA}^3$ ;  $Z = 4$ ;  $D_c = 1.421 \text{ g.cm}^{-3}$ ,  $D_m = 1.41(2) \text{ g.cm}^{-3}$ ;  
 $\lambda_{\text{MoK}\alpha} = 0.7107 \text{ \AA}$ ,  $F(000) = 1760$  electrons;  $\mu = 5.21 \text{ cm}^{-1}$ .

A crystal of dimensions  $0.24 \times 0.30 \times .64 \text{ mm}^3$  was mounted on the CAD4. 3505 unique reflections in the range  $1.2 < \theta < 20^\circ$  with intensities  $I > 2.5\sigma(I)$  were collected using a  $\omega$ - $n/3\theta$  scan mode (where,  $n = 3$ ) (Chapter 7). A comparison of the intensities of three standard reflections measured every 50 minutes showed that the crystal had not decomposed. The intensities were corrected for Lorentz, polarization<sup>98</sup> and crystal absorption<sup>99</sup> effects. The maximum and minimum transmission

TABLE 4.3.1

Crystallographic details for  $[\text{Mn}(\text{CO})_3\{\text{P}(\text{OPh})_3\}_2\text{OCIO}_3]$ 

Temperature	298°K	Crystal dimension	.12 × .14 × .29 mm <sup>3</sup>
(Sin $\theta_{\text{max}}$ )/ $\lambda$	0.48 Å <sup>-1</sup>	Crystal faces:	[100], [-100], [021], [0-2-1], [02-1], [0-21]
Radiation	MoK $\alpha$		
Scan method	$\omega/2\theta$	Aperture width	2.4 + 0.5 * tan( $\theta$ )
Scan range (°)		Sig(I)/I (pre-scan)	0.4
$\theta_{\text{min}} = 1.2$ , $\theta_{\text{max}} = 20$		Sig(I)/I (final scan)	0.08
$\Delta\omega = 1.0 + 0.35 * \tan(\theta)$		Speed (pre-scan)	6.7 deg/min
Slit width	3 mm	Scan time (max)	350 sec
Total number of independent reflections collected 3505			

factors were estimated to be 0.61 and 0.45, respectively. Further experimental details are given in Table 4.3.1.

#### 4.3.2 Structure Solution and Refinement

The structure was solved by the Direct Methods routine in SHELX.<sup>75</sup> The associated EEES map gave the location of the manganese, chlorine, phosphorus and some of the oxygen atoms. A difference Fourier synthesis based on the manganese, chlorine and phosphorus contributions gave a difference map which revealed three phenol rings and all the perchlorate oxygen atoms. A full matrix least-squares calculation at this stage gave an R value of 0.41. The difference map, based on all previously located atoms, revealed all the non-hydrogen atoms. In the next cycle of refinement the phenyl groups were modelled as rigid groups with the hydrogen positions calculated at a carbon-hydrogen distance of 1.08 Å from the respective carbon atoms. In addition, only the manganese atom was modelled anisotropically and a common group temperature factor was used and refined for the hydrogen atoms. The final weighted (Chapter 7) Block-matrix least-squares refinement converged with  $R = 0.064$ ,  $R_w = 0.069$ ,  $k = 12$  and  $g = 4.5 \times 10^{-5}$ . The largest peak in the final difference map was  $0.7 \text{ e}\text{\AA}^{-3}$ . The tabulated observed and calculated structure factors and the hydrogen atomic parameters are given on microfiche. The final non-hydrogen atomic parameters, bond lengths and bond angles are tabulated in Tables 4.3.2, 4.3.3 and 4.3.4, respectively.

#### 4.3.3 Description of the Structure

The geometry of *trans*- $\text{Mn}(\text{CO})_3\{\text{P}(\text{OPh})_3\}_2\text{OCIO}_3$  and the atom numbering scheme are given in Figure 4.3.1. The coordination geometry about the manganese consists of a distorted octahedra. However, only the three

TABLE 4.3.2

Atomic positional and thermal parameters for  $[\text{Mn}(\text{CO})_3\{\text{P}(\text{OPh})_3\}_2\text{OCIO}_3]$ 

Atom <sup>a</sup>	x	y	z	U <sub>11</sub> <sup>b</sup>	U <sub>22</sub>	U <sub>33</sub>	U <sub>23</sub>	U <sub>13</sub>	U <sub>12</sub>
Mn	20583(12)	11450(5)	22289(5)	428(7)	354(8)	396(7)	7(6)	-62(6)	-2(6)
Cl	4272(3)	2230(1)	2117(1)	67(2)	52(2)	98(2)	11(1)	-7(1)	-14(1)
P(1)	722(2)	1390(1)	1275(1)	48(1)	42(1)	40(1)	0(1)	-6(1)	1(1)
P(2)	3224(2)	926(1)	3238(1)	48(1)	43(1)	42(1)	-1(1)	-8(1)	4(1)
O(1)	862(7)	-60(3)	2103(3)	87(5)	44(4)	108(5)	14(4)	-31(4)	-14(4)
O(2)	-533(7)	1474(3)	3018(3)	70(5)	117(6)	68(5)	3(4)	16(4)	22(4)
O(3)	4436(7)	705(3)	1361(3)	69(5)	91(5)	62(4)	-9(4)	5(3)	22(4)
O(4)	2824(5)	2007(2)	2333(3)	54(3)	34(3)	71(4)	-3(3)	-7(3)	-10(3)
O(5)	5437(6)	1826(3)	2320(3)	53(4)	78(5)	118(6)	8(4)	-15(4)	3(4)
O(6)	4154(8)	2260(4)	1403(4)	110(6)	166(8)	103(6)	72(6)	25(5)	-4(5)
O(7)	4474(8)	2787(3)	2403(5)	98(6)	59(5)	314(12)	-57(7)	22(7)	-39(4)
O(8)	429(5)	2061(2)	1064(2)	68(4)	31(3)	52(3)	1(3)	5(3)	13(3)
O(9)	-897(5)	1091(2)	1287(2)	50(3)	60(4)	43(3)	-3(3)	-15(3)	-10(3)
O(10)	1373(5)	1156(2)	610(2)	71(4)	53(4)	28(3)	6(3)	1(3)	8(3)
O(11)	4806(5)	594(2)	3342(2)	53(3)	47(3)	57(3)	-11(3)	-14(3)	12(3)
O(12)	2086(5)	510(2)	3607(2)	66(4)	65(4)	38(3)	4(3)	-3(3)	-1(3)
O(13)	3551(5)	1466(2)	3727(2)	63(4)	54(4)	48(3)	-12(3)	-24(3)	11(3)
C(1)	1354(9)	416(4)	2161(4)	64(6)	42(6)	55(6)	11(5)	-10(5)	1(5)
C(2)	469(10)	1376(4)	2708(4)	61(6)	52(6)	43(6)	-2(5)	-12(5)	3(5)
C(3)	3606(9)	894(4)	1700(4)	51(6)	46(6)	59(6)	2(5)	-5(5)	1(5)

<sup>a</sup> Mn coordinates  $\times 10^5$ , and the others  $\times 10^4$ .<sup>b</sup> Mn thermal parameters  $\times 10^4$  and the others  $\times 10^3$ .

TABLE 4.3.3  
Atomic Distances for  $[\text{Mn}(\text{CO})_3\{\text{P}(\text{OPh})_3\}_2\text{OCIO}_3]$

Atoms <sup>a</sup>	Distance(Å)	Atoms	Distance(Å)
(a) Bond lengths (and standard deviations)			
P(1)-Mn(1)	2.248 (2)	P(2)-Mn(1)	2.259 (2)
O(4)-Mn(1)	2.066 (5)	C(1)-Mn(1)	1.761 (9)
C(2)-Mn(1)	1.843 (9)	C(3)-Mn(1)	1.885 (9)
O(4)-Cl(1)	1.483 (6)	O(5)-Cl(1)	1.423 (6)
O(6)-Cl(1)	1.421 (9)	O(7)-Cl(1)	1.384 (8)
O(8)-P(1)	1.585 (5)	O(9)-P(1)	1.601 (5)
O(10)-P(1)	1.575 (5)	O(11)-P(2)	1.604 (5)
O(12)-P(2)	1.599 (6)	O(13)-P(2)	1.574 (5)
C(1)-O(1)	1.162(11)	C(2)-O(2)	1.144(11)
C(3)-O(3)	1.123(11)	C(9)-O(8)	1.371 (7)
C(15)-O(9)	1.371 (7)	C(21)-O(10)	1.372 (8)
C(27)-O(11)	1.361 (7)	C(33)-O(12)	1.384 (7)
C(39)-O(13)	1.383 (7)		
(b) Some non-bonding distances			
O(7)...C(25) <sup>II</sup>	2.15 (2)	C(28)...C(30) <sup>I</sup>	3.44 (2)
H(19)...O(7) <sup>II</sup>	2.42 (2)	H(12)...H(3) <sup>III</sup>	2.15 (2)

<sup>a</sup> Superscripts in Roman refer to the following equivalent positions, with respect to the unique asymmetric unit at x, y, z:

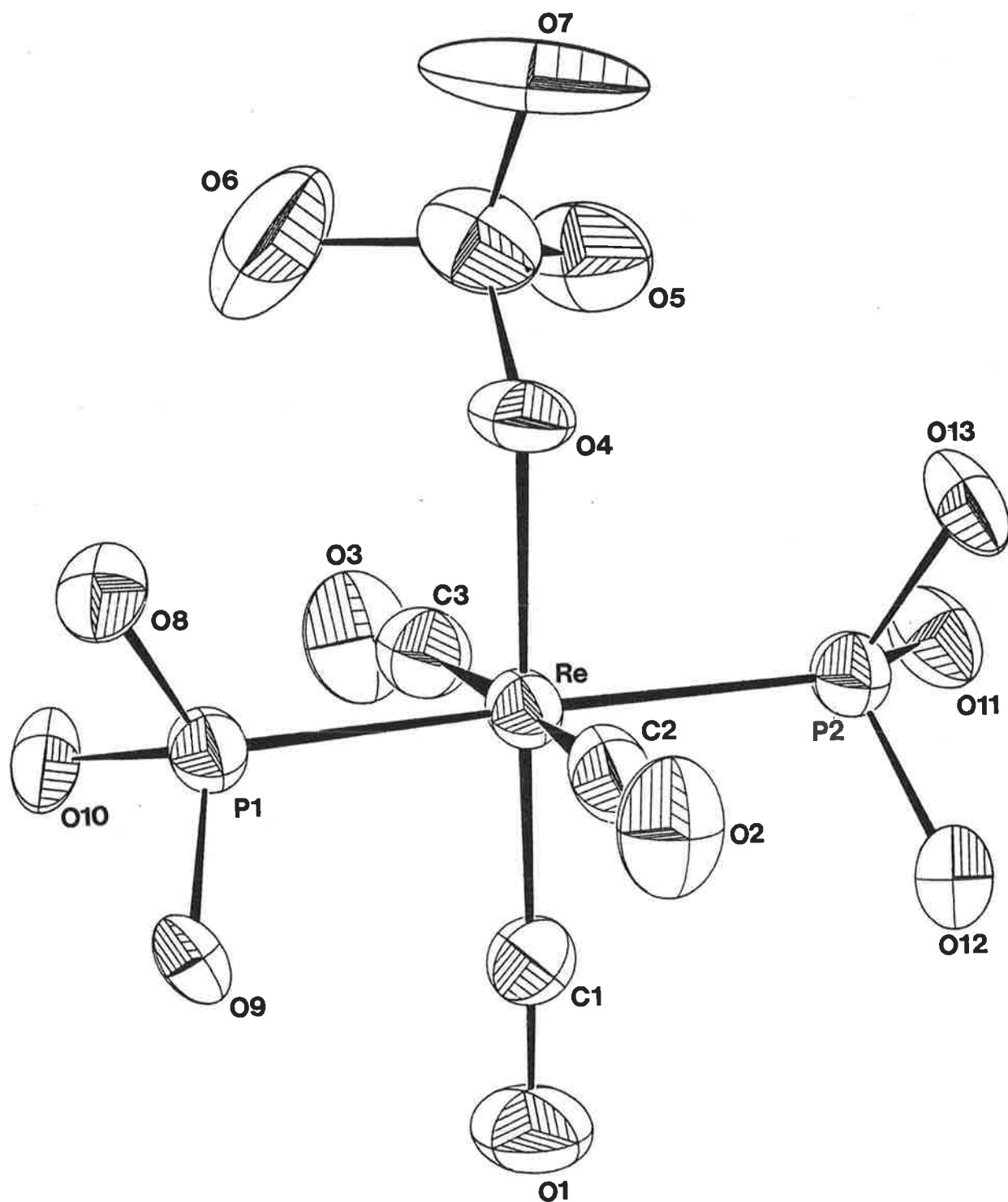
$$\text{I} = -x, -y, z; \quad \text{II} = -x, .5 + y, .5 - y; \quad \text{III} = x, .5 - y, .5 + z$$



TABLE 4.3.4

Bond angles ( $^{\circ}$ ) and their standard deviations for  $[\text{Mn}(\text{CO})_3\{\text{P}(\text{OPh})_3\}_2\text{OC}_{10}\text{H}_{18}]$ 

P(2)-Mn(1)-P(1)	174.8(1)	O(4)-Mn(1)-P(1)	90.5(2)
O(4)-Mn(1)-P(2)	89.1(2)	C(1)-Mn(1)-P(1)	89.8(3)
C(1)-Mn(1)-P(2)	90.4(3)	C(1)-Mn(1)-O(4)	177.8(3)
C(2)-Mn(1)-P(1)	89.0(3)	C(2)-Mn(1)-P(2)	85.8(3)
C(2)-Mn(1)-O(4)	86.9(3)	C(2)-Mn(1)-C(1)	91.0(4)
C(3)-Mn(1)-P(1)	88.3(3)	C(3)-Mn(1)-P(2)	96.9(3)
C(3)-Mn(1)-O(4)	95.0(3)	C(3)-Mn(1)-C(1)	87.2(4)
C(3)-Mn(1)-C(2)	176.8(4)	O(5)-C1(1)-O(4)	109.9(3)
O(6)-C1(1)-O(4)	107.5(4)	O(6)-C1(1)-O(5)	108.6(4)
O(7)-C1(1)-O(4)	106.2(4)	O(7)-C1(1)-O(5)	112.8(4)
O(7)-C1(1)-O(6)	111.7(6)	O(8)-P(1)-Mn(1)	121.8(2)
O(9)-P(1)-Mn(1)	108.4(2)	O(9)-P(1)-O(8)	105.7(3)
O(10)-P(1)-Mn(1)	115.1(2)	O(10)-P(1)-O(8)	99.2(3)
O(10)-P(1)-O(9)	105.1(3)	O(11)-P(2)-Mn(1)	124.6(2)
O(12)-P(2)-Mn(1)	105.4(2)	O(12)-P(2)-O(11)	104.7(3)
O(13)-P(2)-Mn(1)	116.1(2)	O(13)-P(2)-O(11)	98.9(3)
O(13)-P(2)-O(12)	105.4(3)	C1(1)-O(4)-Mn(1)	125.5(3)
C(9)-O(8)-P(1)	127.5(4)	C(15)-O(9)-P(1)	125.6(4)
C(21)-O(10)-P(1)	129.9(4)	C(27)-O(11)-P(2)	124.2(4)
C(33)-O(12)-P(2)	126.5(4)	C(39)-O(13)-P(2)	129.7(4)
O(1)-C(1)-Mn(1)	178.2(7)	O(2)-C(2)-Mn(1)	174.6(8)
O(3)-C(3)-Mn(1)	173.5(7)	C(4)-C(9)-O(8)	122.3(4)
C(8)-C(9)-O(8)	117.6(5)	C(10)-C(15)-O(9)	122.2(5)
C(14)-C(15)-O(9)	117.8(5)	C(16)-C(21)-O(10)	118.0(5)
C(20)-C(21)-O(10)	122.0(5)	C(22)-C(27)-O(11)	119.6(4)
C(26)-C(27)-O(11)	120.4(5)	C(28)-C(33)-O(12)	118.3(5)
C(32)-C(33)-O(12)	121.7(5)	C(34)-C(39)-O(13)	119.3(5)
C(38)-C(39)-O(13)	120.6(5)		



**FIGURE 4.3.1.** The molecular structure of  $\text{Mn}(\text{CO})_3(\text{P}(\text{OPh})_3)_2\text{OC}_{10}\text{H}_{16}$  (30% probability ellipsoids). For simplicity the phenyl groups on the oxygen atoms O8 - O13 have been omitted.

angles C(2)-Mn(1)-P(2), C(3)-Mn(1)-P(2) and C(2)-Mn(1)-O(4) deviate (ave.  $5.4^\circ$ ) notably from  $90^\circ$ . This distortion is due to the steric repulsion effects of the two *trans* P(OPh)<sub>3</sub> ligands and the coordinated perchlorate on the carbonyl groups. The carbon atoms of the carbonyl groups and the phosphorus atoms are at the expected bond distances of 1.830 and 2.254 Å, respectively, from the manganese atom. The perchlorate coordinates with a manganese-oxygen distance of 2.066(5) Å and with an Cl(1)-O(4)-Mn(1) angle of  $125.5(3)^\circ$ . A list of the closest intermolecular contacts is given in Table 4.3.2(b).

#### 4.4 STRUCTURE DETERMINATION OF [Mn(CO)<sub>3</sub>(diphos)(BF<sub>3</sub>OH)] · $\frac{1}{2}$ (dpeo)

##### 4.4.1 Crystal Data

Needle-like to prismatic crystals of this dichloromethane soluble yellow compound were grown by vapour diffusion using petroleum spirit ( $80-100^\circ$ ). The cell constants and the space group (P2<sub>1</sub>/n) were determined from reflections collected on the CAD4. The crystal density was measured by the floatation technique using a solution mixture of petroleum spirit ( $40-60^\circ$ ) and carbontetrachloride.

Crystal data: C<sub>42</sub>H<sub>37</sub>BF<sub>3</sub>MnO<sub>4</sub>P<sub>2</sub>, M.W. = 790.5, Monoclinic space group P2<sub>1</sub>/n, a = 15.125(2), b = 20.503(2), c = 13.199(2) Å, β = 101.35(1)<sup>o</sup> U = 4013(2) Å<sup>3</sup>, Z = 4, D<sub>C</sub> = 1.308 g.cm<sup>-3</sup>, D<sub>m</sub> = 1.32(2) g.cm<sup>-3</sup>, λMoK<sub>α</sub> = 0.7107 Å, F(000) = 1670 electrons, μ = 42.1 cm<sup>-1</sup>.

A crystal with dimensions 0.03 × 0.03 × 0.11 mm<sup>3</sup> was coated and mounted using epoxy resin. 2932 reflections with intensities  $I > 2.5\sigma(I)$  were collected using a ω-n/3θ scan mode (where, n = 3). The intensity of three reference reflections was checked at 1.4 hour intervals and the data was corrected for 18% decomposition. The intensities were corrected

TABLE 4.4.1

Crystallographic details for  $[\text{Mn}(\text{CO})_3(\text{diphos})(\text{BF}_3\text{OH})] \cdot \frac{1}{2}(\text{dpeo})$ 

Temperature	295°K	Crystal dimensions	.03 × .03 × .11 mm <sup>3</sup>
$(\text{Sin } \theta_{\text{max}})/\lambda$	0.27 Å <sup>-1</sup>	Crystal faces	[100], [-100], [010]
Radiation	Cu		[0-10], [001], [00-1]
Scan method	$\omega/2\theta$	Aperture width	1.25 + 0.5 * tan( $\theta$ )
Scan range (°)		Sig(I)/I (pre scan)	2.0
$\theta_{\text{min}} = 2.0, \theta_{\text{max}} = 25.0$		Sig(I)/I (final scan)	0.03
$\Delta\omega = 0.53 + 0.15 * \tan(\theta)$		Speed (pre scan)	6.67 deg/min
Slit width	3 mm	Scan time (max)	120 sec
		Total unique reflections collected	2932

for Lorentz and polarization effects and for crystal absorption.<sup>99</sup>

The maximum and minimum transmission factors were estimated to be 0.75 and 0.53, respectively. The experimental crystallographic details are given in Table 4.4.1.

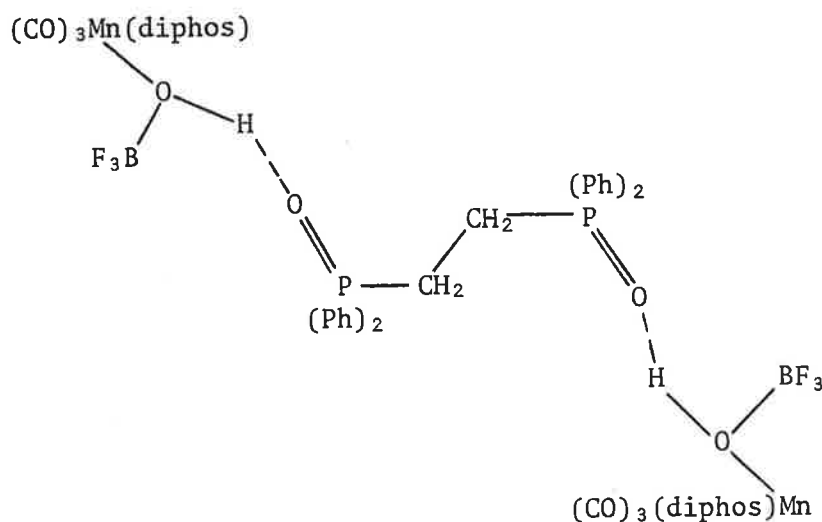
#### 4.4.2 Structure Solution and Refinement

The manganese coordinates as deduced from a Patterson map were refined in a least-squares calculation, which converged with an R value of 0.59. A difference Fourier synthesis based on the manganese atom gave a difference map which revealed the phosphorus atoms, one carbonyl group and the oxygen atom of the coordinated borate anion,  $[\text{BF}_3\text{OH}]^-$ . A full matrix least-squares refinement based on the above atoms reduced R to 0.49 and the associated difference map revealed all non-hydrogen atoms with a dpeo group located on a centre of symmetry. The R value reduced to 0.11 in a full matrix refinement with manganese, phosphorus and oxygen atoms anisotropic and all other non-hydrogen atoms modelled isotropically. The phenyl groups were refined as rigid groups with their hydrogen atoms at a calculated carbon-hydrogen distance of 1.08 Å. The remaining hydrogen atom sites for dpeo and diphos were calculated for the respective carbon atoms assuming tetrahedral geometry (i.e. C-H, 0.97 Å) with the hydrogens modelled with a different group temperature factor. When employing the weighting scheme the refinement converged at 0.097. In the subsequent least-square refinements all the borate, carbonyl, dpeo and diphos atoms were refined anisotropically the respective difference map revealed the hydrogen atom of the  $[\text{BF}_3\text{OH}]^-$  anion. In the final blocked least-squares calculation all non-hydrogen atoms were refined anisotropically and the refinement converged with  $R = 0.084$ ,  $R_w = 0.087$ ,  $k = 2.5$  and  $g = 2.2 \times 10^{-3}$ . The observed and calculated structure factors and the hydrogen atomic parameters are given on

microfiche. While, the final non-hydrogen atomic parameters, bond lengths and bond angles are tabulated in Tables 4.4.2, 4.4.3 and 4.4.4, respectively.

#### 4.4.3 Description of the Structure

Figure 4.4.1 shows the molecular structure of *cis*-Mn(CO)<sub>3</sub>(diphos)(HOBf<sub>3</sub>) and the atom numbering scheme employed. A distorted octahedral coordination geometry exists about the manganese atom with the bite angle of the bidentate ligand being 83.9(1)°. The carbonyl carbon atoms and the two *cis* phosphorus atoms are at the average distances of 1.79 and 2.34 Å, respectively, from the manganese. While, the trifluorohydroxy borate group coordinates via the oxygen (i.e. O(5)) at a distance of 2.094(9) Å from the manganese atom. The B-O(5)-Mn angle is 125(1)°. The notable feature of the structure of [*cis*-Mn(CO)<sub>3</sub>(diphos)(HOBf<sub>3</sub>)]·½(dpeo) is that the dpeo group is located on the centre of symmetry (0,½,0) and is involved in hydrogen bonding with two Mn(CO)<sub>3</sub>(diphos)(HOBf<sub>3</sub>) molecules (see below). The oxygen atoms



of dpeo hydrogen bond to the hydroxy group of the coordinated trifluorohydroxy borate at a distance of 2.77(2) Å. The hydrogen atom was

TABLE 4.4.2

Atomic positional and thermal parameters for  $[\text{Mn}(\text{CO})_3(\text{diphos})(\text{BF}_3\text{OH})] \cdot \frac{1}{2}(\text{dpeo})$ 

Atom <sup>a</sup>	x	y	z	U <sub>11</sub> <sup>b</sup>	U <sub>22</sub>	U <sub>33</sub>	U <sub>23</sub>	U <sub>13</sub>	U <sub>12</sub>
Mn	-574 (1)	2126(1)	2169 (2)	44 (1)	53 (1)	60 (2)	-8 (1)	11(1)	2 (1)
P1	-2059 (2)	2143(2)	1234 (3)	40 (1)	45 (2)	66 (3)	-7 (2)	14(2)	4 (2)
P2	-209 (2)	1981(2)	542 (3)	44 (2)	51 (2)	65 (3)	-9 (2)	16(2)	-3 (2)
P3	-967 (2)	4255(2)	-733 (3)	47 (2)	47 (2)	71 (3)	-4 (2)	7(2)	-7 (2)
F1	-367 (7)	3463(5)	3691 (7)	164 (9)	124 (9)	76 (7)	-35 (6)	41(7)	-59 (7)
F2	-474 (8)	4213(5)	2476 (8)	231(12)	68 (8)	132(10)	-32 (8)	51(9)	-18 (8)
F3	765 (7)	3627(6)	2895 (9)	94 (8)	243(14)	177(11)	-141(10)	38(7)	-63 (8)
O1	-1217 (7)	2153(6)	4151 (9)	88 (8)	113 (9)	65 (8)	-8 (8)	13(7)	-2 (7)
O2	1296 (7)	2015(6)	3301 (9)	67 (7)	149(11)	87 (9)	-21 (8)	-16(6)	-1 (7)
O3	-531 (7)	717(6)	2578 (9)	91 (8)	63 (7)	108(10)	-13 (7)	19(7)	-2 (7)
O4	-834 (5)	3748(4)	64 (6)	80 (6)	62 (6)	53 (6)	8 (5)	21(5)	-1 (5)
O5	-554 (5)	3139(4)	1975 (7)	59 (7)	48 (6)	70 (7)	-32 (6)	11(5)	-10 (5)
C1	-959(10)	2191(7)	3379(12)	71(10)	76(11)	53(11)	9(10)	-2(9)	-8 (9)
C2	561(10)	2099(6)	2823(10)	87(11)	35 (8)	43 (9)	-16 (7)	-14(8)	-7 (8)
C3	-570 (9)	1265(9)	2366(11)	59(10)	96(14)	62(11)	-22(11)	-7(8)	-10(10)
C4	-2656 (5)	1363(4)	1108 (9)	32 (8)	49 (9)	61(10)	-3 (9)	2(8)	15 (7)
C5	-3129 (5)	1148(4)	152 (9)	40 (8)	52(10)	93(13)	7 (9)	7(9)	-13 (7)
C6	-3599 (5)	559(4)	78 (9)	61(10)	71(12)	63(12)	2 (9)	7(8)	-1 (9)
C7	-3595 (5)	185(4)	96 (9)	38 (8)	89(13)	87(13)	-18(12)	2(9)	-1 (8)

TABLE 4.4.2 (Continued)

Atom	x	y	z	U <sub>11</sub>	U <sub>22</sub>	U <sub>33</sub>	U <sub>23</sub>	U <sub>13</sub>	U <sub>12</sub>
C28	1697 (6)	3388 (4)	507(10)	72(12)	47(11)	166(21)	2(12)	38(13)	-20 (9)
C29	1101 (6)	2948 (4)	822(10)	50 (9)	61(10)	102(13)	-1(11)	11(10)	3 (8)
C30	-1021 (7)	3951 (5)	-2026 (7)	49 (8)	55 (8)	62(10)	0 (8)	2 (7)	-5 (7)
C31	-1599 (7)	3421 (5)	-2291 (7)	58 (9)	98(13)	54(11)	-12 (9)	8 (8)	-1 (9)
C32	-1687 (7)	3135 (5)	-3264 (7)	80(11)	70(11)	110(15)	6(12)	33(11)	-16 (9)
C33	-1196 (7)	3378 (5)	-3973 (7)	96(13)	86(14)	99(15)	-8(11)	14(12)	-8(10)
C34	-618 (7)	3908 (5)	-3708 (7)	93(13)	114(16)	95(15)	-14(12)	50(11)	-14(11)
C35	-530 (7)	4194 (5)	-2734 (7)	78(11)	82(12)	76(12)	15(11)	27(10)	-23 (9)
C36	-2024 (6)	4657 (5)	-743(11)	51 (9)	75(11)	92(13)	5(10)	-14(10)	15 (8)
C37	-2462 (6)	5019 (5)	-1586(11)	91(13)	119(15)	97(15)	-1(12)	7(11)	37(12)
C38	-3301 (6)	5298 (5)	-1577(11)	89(15)	158(20)	150(20)	-14(15)	-7(13)	51(14)
C39	-3701 (6)	5215 (5)	-719(11)	68(13)	139(21)	242(29)	-12(20)	6(17)	32(13)
C40	-3263 (6)	4853 (5)	127(11)	106(17)	148(21)	222(27)	16(18)	78(18)	34(15)
C41	-2424 (6)	4574 (5)	115(11)	91(14)	108(15)	136(18)	4(13)	51(12)	26(11)
C42	-109(12)	4862 (8)	-610(11)	88(12)	69(11)	76(12)	-18 (9)	26(10)	-24 (9)
B	-182(15)	3578(11)	2718(22)	87(17)	71(18)	133(25)	-6(18)	22(16)	-16(14)

<sup>a</sup> All atomic positional parameters  $\times 10^4$ .

<sup>b</sup> All thermal parameters  $\times 10^3$ .



TABLE 4.4.2 (Continued)

Atom	x	y	z	U <sub>11</sub>	U <sub>22</sub>	U <sub>33</sub>	U <sub>23</sub>	U <sub>13</sub>	U <sub>12</sub>
C8	-3121(5)	400(4)	1919 (9)	49 (9)	59(11)	92(14)	10 (9)	36 (9)	-4 (8)
C9	-2652(5)	989(4)	1992 (9)	46 (9)	61(11)	89(13)	-4(10)	11 (7)	14 (8)
C10	-2874(6)	2709(4)	1551 (8)	55(10)	53(10)	35 (9)	-8 (7)	3 (7)	1 (7)
C11	-2623(6)	3196(4)	2289 (8)	63(10)	99(13)	72(12)	-25(10)	32 (9)	5(10)
C12	-3267(6)	3633(4)	2510 (8)	105(14)	59(11)	101(14)	-26(10)	59(12)	5(10)
C13	-4162(6)	3582(4)	1992 (8)	57(11)	90(13)	102(14)	3(12)	8(10)	5(10)
C14	-4413(6)	3094(4)	1254 (8)	70(11)	98(14)	95(14)	2(12)	7(10)	9(11)
C15	-3770(6)	2658(4)	1034 (8)	68(10)	64(10)	84(12)	-30 (9)	23(10)	22 (9)
C16	-1983(8)	2370(6)	-87 (9)	46 (8)	52 (9)	57 (9)	-1 (7)	12 (7)	-4 (7)
C17	-1270(8)	1949(6)	-423(10)	75(10)	58(10)	45 (9)	-10 (8)	25 (8)	4 (8)
C18	368(6)	1244(4)	287 (8)	38 (8)	65(10)	57(10)	-9 (8)	2 (7)	-10 (7)
C19	63(6)	890(4)	-617 (8)	69(11)	39 (9)	120(16)	-11(10)	25(11)	5 (8)
C20	570(6)	369(4)	-871 (8)	80(12)	83(14)	94(13)	5(11)	28(11)	-3(10)
C21	1381(6)	200(4)	-222 (8)	101(15)	60(12)	117(16)	2(12)	76(12)	1(11)
C22	1686(6)	554(4)	682 (8)	61(11)	86(14)	172(20)	-10(13)	23(12)	25(11)
C23	1179(6)	1076(4)	937 (8)	54(10)	63(11)	107(14)	-30(10)	-7(10)	24 (9)
C24	525(6)	2576(4)	89(10)	60(10)	38 (9)	74(12)	-3 (9)	26 (9)	9 (7)
C25	544(6)	2643(4)	-958(10)	59(10)	72(11)	77(14)	-3 (9)	28 (9)	11 (9)
C26	1140(6)	3083(4)	-1272(10)	85(12)	97(15)	121(16)	19(13)	71(13)	3(10)
C27	1717(6)	3455(4)	-540(10)	84(13)	71(14)	155(20)	26(14)	51(16)	-6(10)

TABLE 4.4.3

Atomic distances for  $[\text{Mn}(\text{CO})_3(\text{diphos})(\text{BF}_3\text{OH})] \cdot \frac{1}{2}(\text{dpeo})$ 

Atoms <sup><math>\alpha</math></sup>	Distance(Å)	Atoms	Distance(Å)
(a) Bond length (and standard deviations)			
P(1)-Mn	2.340 (3)	O(4)-P(3)	1.465 (8)
P(2)-Mn	2.339 (4)	C(30)-P(3)	1.803(10)
O(5)-Mn	2.094 (9)	C(36)-P(3)	1.795(10)
C(1)-Mn	1.809(17)	C(42)-P(3)	1.781(17)
C(2)-Mn	1.765(15)	B-F(1)	1.387(32)
C(3)-Mn	1.786(19)	B-F(2)	1.391(26)
C-Mn	ave. 1.787(17)	B-F(3)	1.409(25)
C(4)-P(1)	1.826 (8)	B-F	ave. 1.396(28)
C(10)-P(1)	1.802(10)	O(5)-B	1.369(26)
C(16)-P(1)	1.831(13)	C(1)-O(1)	1.164(21)
C(17)-P(2)	1.843(12)	C(2)-O(2)	1.178(18)
C(18)-P(2)	1.809 (9)	C(3)-O(3)	1.156(22)
C(24)-P(2)	1.827(10)	C-O	ave. 1.166(20)
		C(42)-C(42) <sup>I</sup>	1.677(29)
(b) Hydrogen bonding distances			
H(37)-O(4)	1.47 (20)	H(37)-O(5)	1.41 (18)
		O(4)...O(5)	2.770(23)
(c) Shortest non-bonding distances			
B...H(37)	2.37 (3)	C(41)...O(4) <sup>I</sup>	3.21 (4)
F(2)...H(37)	2.57 (3)	F(3)...F(2)	2.20 (3)
O(3)...P(1)	3.07 (3)	C(6)...C(4)	2.41 (3)
F(1)...O(1)	3.08 (3)	C(1)...P(1)	2.99 (3)
F(3)...C(6) <sup>II</sup>	3.31 (4)	H(29)...C(41)	2.63 (4)
F(2)...H(35)	2.46 (3)	F(3) <sup>II</sup> ...H(1)	2.48 (3)
		H(5)...H(22) <sup>II</sup>	2.43 (3)

<sup>$\alpha$</sup>  Superscripts in Roman refer to the following equivalent positions, with respect to the unique asymmetric unit at x, y, z: I = -x, -y, -z; II = .5 + x, .5 - y, .5 + z

TABLE 4.4.4

Bond angles ( $^{\circ}$ ) for  $[\text{Mn}(\text{CO})_3(\text{diphos})(\text{BF}_3\text{OH})] \cdot \frac{1}{2}(\text{dpeo})$ 

P(2)-Mn-P(1)	83.9(1)	C(36)-P(3)-O(4)	109.1(6)
O(5)-Mn-P(1)	87.5(2)	C(36)-P(3)-C(30)	106.1(1)
O(5)-Mn-P(2)	90.1(3)	C(42)-P(3)-O(4)	115.8(6)
C(1)-Mn-P(1)	91.3(4)	C(42)-P(3)-C(30)	103.0(6)
C(1)-Mn-P(2)	174.2(5)	C(42)-P(3)-C(36)	108.2(7)
C(1)-Mn-O(5)	92.9(6)	F(2)-B-F(1)	105.1(1.9)
C(2)-Mn-P(1)	177.4(5)	F(3)-B-F(1)	104.0(1.7)
C(2)-Mn-P(2)	93.6(5)	F(3)-B-F(2)	103.8(1.7)
C(2)-Mn-O(5)	93.2(4)	O(5)-B-F(1)	114.9(1.8)
C(2)-Mn-C(1)	91.2(6)	O(5)-B-F(2)	112.5(1.8)
C(3)-Mn-P(1)	93.8(4)	O(5)-B-F(3)	115.3(2.0)
C(3)-Mn-P(2)	90.8(5)	B-O(5)-Mn	125.4(1.2)
C(3)-Mn-O(5)	178.5(5)	O(1)-C(1)-Mn	171.9(1.4)
C(3)-Mn-C(1)	86.3(7)	O(2)-C(2)-Mn	172.7(1.2)
C(3)-Mn-C(2)	85.5(6)	O(3)-C(3)-Mn	174.2(1.3)
C(4)-P(1)-Mn	116.2(3)	C(5)-C(4)-P(1)	121.0(8)
C(10)-P(1)-Mn	103.7(4)	C(9)-C(4)-P(1)	119.0(7)
C(16)-P(1)-Mn	105.6(4)	C(11)-C(10)-P(1)	121.3(7)
C(16)-P(1)-C(4)	105.0(6)	C(15)-C(10)-P(1)	118.7(7)
C(16)-P(1)-C(10)	103.4(5)	C(17)-C(16)-P(1)	108.4(8)
C(17)-P(2)-Mn	108.0(5)	C(16)-C(17)-P(2)	110.5(8)
C(18)-P(2)-Mn	119.1(4)	C(23)-C(18)-P(2)	119.3(7)
C(18)-P(2)-C(17)	103.1(5)	C(25)-C(24)-P(2)	121.6(7)
C(24)-P(2)-Mn	118.9(4)	C(29)-C(24)-P(2)	118.4(1.0)
C(24)-P(2)-C(17)	107.5(6)	C(31)-C(30)-P(3)	114.6(8)
C(24)-P(2)-C(18)	98.6(5)	C(35)-C(30)-P(3)	125.4(8)
C(30)-P(3)-O(4)	114.1(5)	C(37)-C(36)-P(3)	122.1(1.0)
		C(41)-C(36)-P(3)	117.8(8)

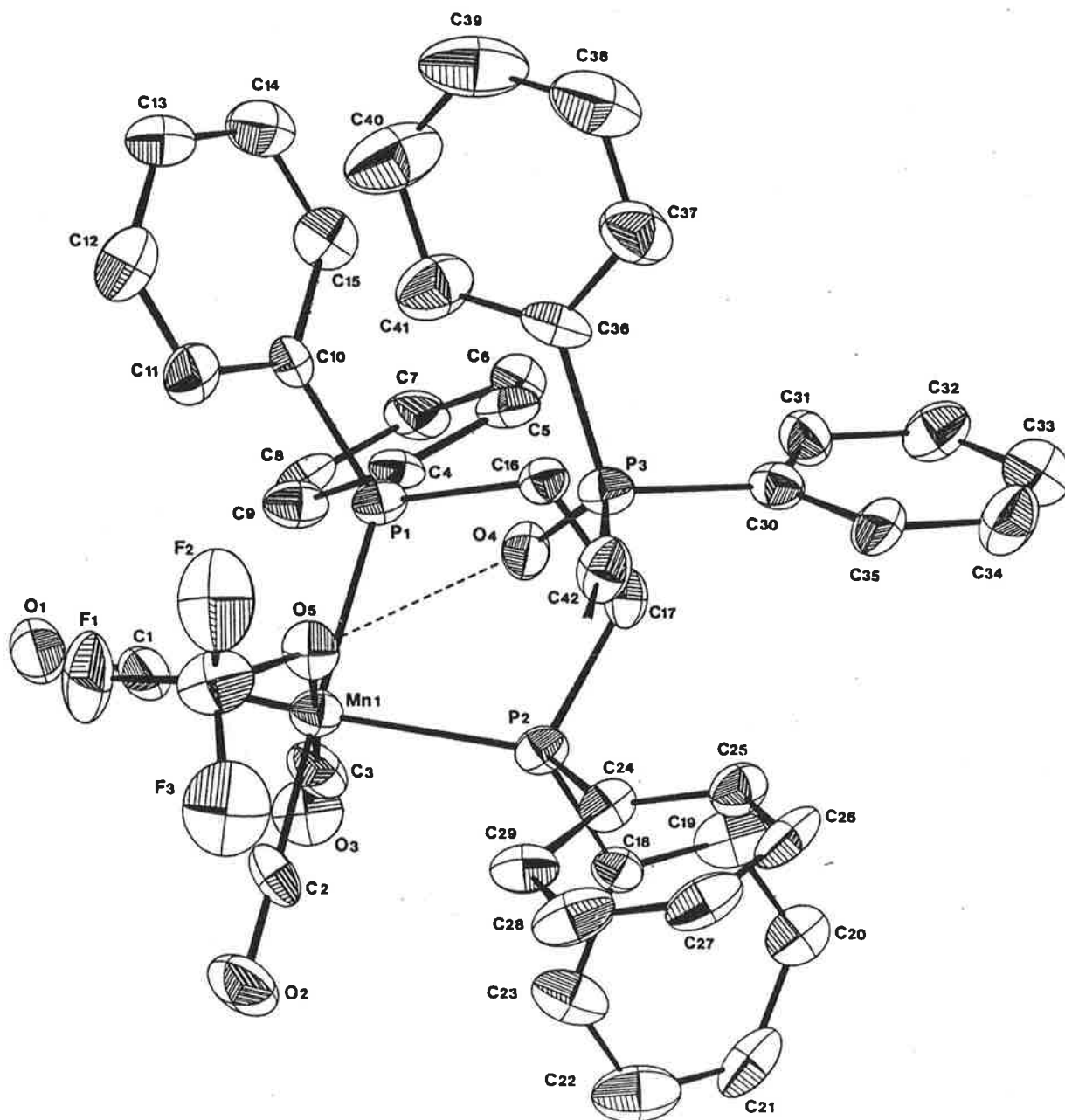


FIGURE 4.4.1. The molecular structure of *cis*-Mn(CO)<sub>3</sub>(diphos)(BF<sub>3</sub>OH)· $\frac{1}{2}$ (dpeo) (ORTEP plot with 50% probability ellipsoids) showing the hydrogen bonding interaction (----) between the manganese complex and dpeo. For simplicity only one half of the dpeo is shown.

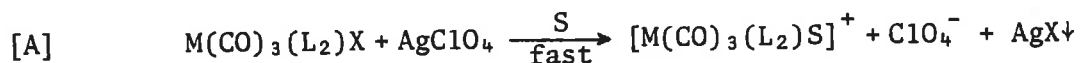
located at an average distance of 1.44 Å between O(4) and O(5). Some of the shortest non-bonding distances are given in Table 4.4.3(c).

## 4.5 DISCUSSION

### 4.5.1 Metal Carbonyl Perchlorates

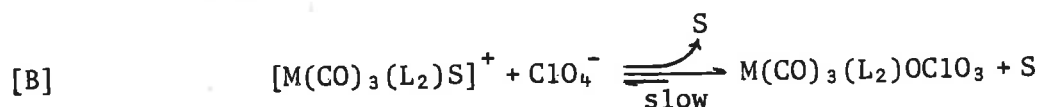
An initial characterization of  $[\text{Mn}(\text{CO})_3(\text{diphos})(\text{OClO}_3)] \cdot \frac{1}{2}(\text{dpeo})$  based on an infrared spectrum<sup>um</sup> of a sample in nujol was shown to be in complete agreement with the molecular structure presented in this chapter. Firstly, the evidence for the monodentate coordination of the  $[\text{ClO}_4]^-$  anion is exhibited by the splitting of both the asymmetric bending and stretching bands into two bands ( $A_1 + E$ ), as a result of the lowering of the point group symmetry of the tetrahedral perchlorate ion from  $T_d$  to  $C_{3v}$ .<sup>122, 123, 124</sup> Secondly, the weak ( $A_1^{1b}$ ) and the two strong ( $A_1^{1a} + B_1$ ) carbonyl absorption bands characterize the coordination geometry as *mer-trans* (Chapter 1).<sup>125, 126</sup>

The study<sup>14, 15</sup> of the reactivity and stability of the metal carbonyl perchlorates initiated two precautions for the preparations of metal fluoride complexes. Firstly, the instability of the former complexes in a moist atmosphere lead to the strict precaution of drying all reaction reagents and solvents, as well as, the reaction atmosphere (Chapter 7). Secondly, due to the high reactivity towards halide exchange, the presence of free halide ions was avoided. In particular, during the initial characterization of the compounds using infrared solution cells, the sodium chloride cells were abandoned in favour of calcium fluoride cells. This can be understood when considering the reaction steps (A and B) involved in the formation of the metal perchlorates.



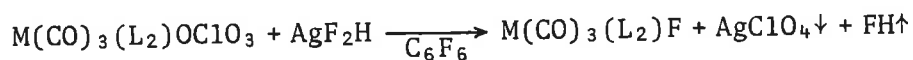
(where,  $\text{L}_2 = 2(\text{PPh}_3)$ , bpy, etc.,  $\text{S} = \text{solvent}$ )

In step A halide ( $\text{X} = \text{Cl}, \text{Br}$ ) is removed by halide abstraction and the "free" coordination site at the metal ( $\text{M} = \text{Mn}, \text{Re}$ ) centre is filled by a solvent molecule ( $\text{S} = \text{CH}_2\text{Cl}_2, \text{CHCl}_3$ ) resulting in the solvato intermediate,  $[\text{M}(\text{CO})_3(\text{L}_2)\text{S}]^+$ .



In the second step (B), the perchlorate anion competes with the solvent for the "free" coordination site. The equilibrium is forced to the right by removing the solvent by evaporation. However, any water or halides present during the reaction will also compete for the sixth coordination site and form the more stable hydroxy or halide complexes,  $[\text{M}(\text{CO})_3(\text{L}_2)\text{OH}]$  or  $[\text{M}(\text{CO})_3(\text{L}_2)\text{X}]$ , respectively.

Their susceptibility towards halide attack makes the metal carbonyl perchlorates possible precursors for the respective fluoride analogues. The conversion is best achieved when reacting the corresponding metal perchlorate with  $\text{AgF}_2\text{H}$  in plastic vessels containing hexafluoro benzene (Appendix 2).



where, 1.  $\text{M} = \text{Mn}$ ,  $\text{L}_2 = 2(\text{P}(\text{OPh})_3)$ ,

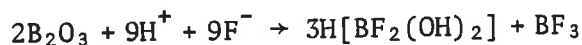
2.  $\text{M} = \text{Re}$ ,  $\text{L}_2 = \text{diphos}, 2\text{PPh}_3$ .

The reaction progress can be followed by monitoring the carbonyl bands and on completion (*ca.* 30 min.) the  $\text{AgClO}_4$  is easily removed by filtration. Failure to use plastic vessels and fluorinated benzene will result in the formation of the by-products  $\text{M}(\text{CO})_3(\text{L}_2)\text{Cl}$  ( $\text{L}_2 = \text{bpy}^{102}$ )

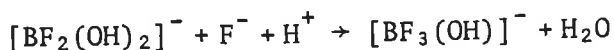
and  $M(\text{CO})_3(\text{L}_2)(\text{HOBF}_3)$  (Chapter 3 and § 4.4). However, by far the most efficient way of preparing the metal fluoride complexes is via the direct halide-abstraction from the metal halides (Chapter 3).

#### 4.5.2 Metal Carbonyl Trifluorohydroxy borates

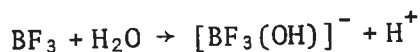
The origin of the  $[\text{HOBF}_3]^-$  anion in the compounds  $[\text{Mn}(\text{CO})_3(\text{diphos})(\text{HOBF}_3)] \cdot \frac{1}{2}(\text{dpeo})$  (§ 4.4) and  $[\text{Re}(\text{CO})_3(\text{tmen})\text{F}]_2\text{H} \cdot \text{HOBF}_3$  (Chapter 3), has been traced to a surface reaction involving fluoride ( $\text{F}^-$ ) ions and glass. In the case of the manganese complex the  $[\text{HOBF}_3]^-$  anion was formed during the preparation of  $\text{Ph}_4\text{AsF}$  in a pyrex glass vessel. While, in the rhenium case the fluoride ion from  $\text{AgF}_2\text{H}$  reacted with the glass during the halide abstraction reaction. Pyrex glass contains 12.6 percent (w/w) boric oxide and it is the fluorination of this oxide that produces the trifluoroborate. Reactions of  $\text{B}_2\text{O}_3$  with fluorine are known<sup>114</sup> to yield the difluorodihydroxy borate anion,  $[\text{BF}_2(\text{OH})_2]^-$ :



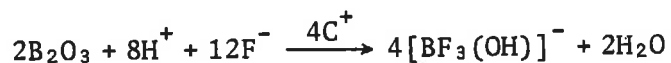
Trifluorohydroxy borate is formed by fluorination of the  $[\text{BF}_2(\text{OH})_2]^-$  anion according to the following reaction scheme:



The trifluoro borate ( $\text{BF}_3$ ) from the former reaction above is readily hydrolysed forming the stable trifluorohydroxy borate species according to:



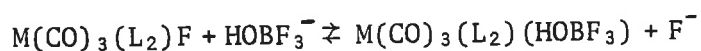
Hence, the following overall equation for the reaction occurring at the glass surface for both the manganese and rhenium systems can be postulated as:



where, the spectator cation ( $\text{C}^+$ ) is  $\text{M}^+$  ( $= \text{Mn}^+$ ),  $[\text{Ph}_4\text{As}]^+$  or  $\text{H}^+$ .

Exchange and equilibrium studies<sup>127, 128</sup> have shown that the fluoroborate species,  $[\text{BF}_n(\text{OH})_{4-n}]^-$  (where,  $n = 1 - 4$ ), are in equilibrium and that  $[\text{BF}_3(\text{OH})]^-$  is formed from solutions containing  $[\text{BF}_n(\text{OH})_{4-n}]^-$  (where,  $n = 1$  and  $2$ ) and  $\text{F}^-$  within minutes. This is well within the reaction times (30-45 mins.) of the halide abstraction reaction. However, under the reaction conditions prevailing (i.e. with  $\text{AgF}_2\text{H}$  or  $\text{Ph}_4\text{AsF}$ ) only the species  $[\text{BF}_3\text{OH}]^-$  was observed in both  $^{19}\text{F}$  n.m.r. (§ 4.2.2) and structural analysis (Chapter 3 and § 4.4) suggesting that this fluoroborate is favoured in our systems.

The coordinating abilities of both  $\text{F}^-$  and  $[\text{HOBf}_3]^-$  in non-aqueous solvents are of the same order, but favouring the former. Thus, one would expect that the reaction product to be predominantly the metal fluoride if excess  $\text{AgF}_2\text{H}$  is used. However, this is not the case as has been seen in this chapter (§ 4.4). An explanation would be the proposal that an equilibrium exists between the metal fluoride and metal trifluoro borate complexes:



The factor that determines which of the complexes is isolated first or predominantly during crystallization is their relative solubility. In the work-up procedures (Chapter 3 and § 4.2) or crystallization, therefore, the more insoluble complex is isolated first and exclusively until the respective anion is depleted. In the case of the complexes,  $[\text{Re}(\text{CO})_3(\text{L}_2)\text{F}]_2\text{H}\cdot\text{HOBf}_3$  (where,  $\text{L}_2 = \text{bpy}$ ,  $\text{tmen}$ ), their relatively greater insolubility than the corresponding  $\text{Re}(\text{CO})_3(\text{L}_2)\text{F}$  and  $\text{Re}(\text{CO})_3(\text{L}_2)(\text{HOBf}_3)$



complexes resulted in their crystallizing first and predominantly until all of the  $[\text{HOBf}_3]^-$  anions were depleted. Subsequently, the crystals formed by concentration of the reaction solutions contained the metal fluoride complexes only because no  $[\text{HOBf}_3]^-$  anions were left for the formation of the next most insoluble complex,  $\text{Re}(\text{CO})_3(\text{L}_2)(\text{HOBf}_3)$ . In the manganese system (§ 4.2),  $[\text{Mn}(\text{CO})_3(\text{diphos})(\text{HOBf}_3)] \cdot \frac{1}{2}(\text{dpeo})$  is found to be less soluble than  $\text{Mn}(\text{CO})_3(\text{diphos})\text{F}$ . Hence, the former is expected to be isolated first. However, when  $\text{F}^-$  and  $[\text{HOBf}_3]^-$  are in relative excess then only the trifluoro borate complex is isolated if manganese is depleted before the anions. Thus, in the examples described above, the product isolated is determined by its solubility and the relative concentration of the anions and metal complexes.

#### 4.5.3 Manganese Carbonyl Fluorides

The preparation of *fac*- $\text{Mn}(\text{CO})_3(\text{L}_2)\text{F}$  complexes was successful for compounds with the bi-dentate ligands *diphos*, *Phen* and *tmen*. However, decomposition occurred in each of the three cases where the ligand (L) of the  $\text{Mn}(\text{CO})_3(\text{L}_2)\text{Br}$  was  $\text{PPh}_3$ ,  $\text{P}(\text{O}Ph)_3$  and  $\text{SbPh}_3$ . In each case halide abstraction resulted in decarboxylation of the precursors forming uncharacterized dark brown to black insoluble products.

As a by-product of the preparation of manganese fluoride complexes it was hoped that structural data on the (Mn-F) bond length could be obtained for comparison with the (Mn-O) bonds (§s 4.3 and 4.4). Unfortunately, no suitable crystals for x-ray analysis could be grown in the available time.

#### 4.6 EXPERIMENTAL

The preparations of the manganese fluoride complexes were carried out in an atmosphere of dry high-purity nitrogen. Only plastic vessels were employed for the reactions. The solvents were dried with Linde 4A molecular sieves before use. The complexes isolated were stored in a desiccator and sent for elemental analysis in sealed sample tubes containing dry nitrogen. The results are given in Table 4.6.1. The solution infrared spectra were recorded with calcium fluoride cells and the complete spectra were recorded as nujol mulls between calcium fluoride plates.

##### Mn(CO)<sub>3</sub>(Phen)Br

To a 30 ml solution of petroleum ether (120-160°C) containing 0.07 gm (0.18 mmol) of Mn(CO)<sub>3</sub>Br a 10% molar excess of Phen was added. The reaction mixture was heated (*ca.* 100°C) and stirred for *ca.* 20 min. On cooling the filtered product (yield, 80%) was washed with diethylether, recrystallized from chloroform-light petroleum (40-60°C) and dried in a vacuum.

##### Mn(CO)<sub>3</sub>(L<sub>2</sub>)F (where, L<sub>2</sub> = diphos, Phen, tmen)

In each case, 0.08 - 0.12 gm of Mn(CO)<sub>3</sub>(L<sub>2</sub>)Br and a 50% molar excess of finely divided AgF<sub>2</sub>H were added to *ca.* 10 ml dichloromethane. The above quantity of Mn(CO)<sub>3</sub>(Phen)Br used will not completely dissolve in 10 ml dichloromethane. However, all the Mn(CO)<sub>3</sub>(Phen)F formed will dissolve due to the increased solubility of the latter. The reaction mixture was shielded from light and stirred at room temperature for *ca.* 30 min. The filtered solution was concentrated to 5 ml and the

yellow product was precipitated and washed with light petroleum spirit. The  $\text{Mn}(\text{CO})_3(\text{L}_2)\text{F}$  complexes were recrystallized (yield, 65-75%) from chloroform-light petroleum (40-60°C) and dried in a vacuum.

TABLE 4.6.1

## Elemental Analysis Results

Compound		C[%]		H[%]		F[%]		N[%]		P[%]	
		Found	Required	Found	Required	Found	Required	Found	Required	Found	Required
<i>fac</i> -Mn(CO) <sub>3</sub> (diphos)F	C <sub>27</sub> H <sub>24</sub> FMNO <sub>3</sub> P <sub>2</sub>	62.71	62.60	4.5	4.35	3.5	3.41			11.2	11.13
<i>fac</i> -Mn(CO) <sub>3</sub> (Phen)F	C <sub>15</sub> H <sub>8</sub> FMnN <sub>2</sub> O <sub>3</sub>	53.22	53.28	2.3	2.38	5.6	5.62	8.32	8.28		
<i>fac</i> -Mn(CO) <sub>3</sub> (tmen)F	C <sub>9</sub> H <sub>16</sub> FMnN <sub>2</sub> O <sub>3</sub>	39.35	39.43	5.9	5.88	7.1	6.93	9.95	10.22		

## CHAPTER 5

### METAL CARBONYL AQUA COMPLEXES

#### 5.1 INTRODUCTION

After the unsuccessful attempts to coordinate hexafluorophosphate to metal carbonyl complexes<sup>14,15</sup> the research was directed towards coordinating hexafluoroarsenate and tetrafluoroborate. Silver hexafluoroarsenate was used as an alternate to the phosphate salt in the halide abstraction reaction with the hope that the former would be stable towards hydrolysis in the presence of a metal centre or at least be a source of fluoride giving rise to the metal fluoride complexes of the type reported in Chapters 2 and 3. As reported in this chapter, the hexafluoroarsenate was found to be stable towards hydrolysis and could in fact be coordinated.

In the last ten years many transition metal compounds containing coordinated tetrafluoroborates have been prepared.<sup>29,32,129,130,131,132</sup> The decomposition reactions of these compounds have been studied with interest in recent years. The decomposition of the tetrafluoroborate anion has resulted in a number of novel compounds. Among these were monomeric and dimeric metal fluorides as well as cubane-type clusters.<sup>133-139</sup>

The attempts to coordinate hexafluoroarsenate and tetrafluoroborate to metal carbonyl centres resulted mainly in the formation of aqua-complexes. This chapter reports their preparation as well as the isolation of the metal complexes containing coordinated hexafluoroarsenate and tetrafluoroborate. The compounds were characterized by elemental analysis, infrared, N.M.R. and crystal structure determinations.

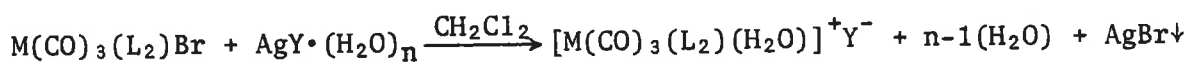
## 5.2 PREPARATIONS AND PROPERTIES

### 5.2.1 $[M(CO)_3(L_2)(H_2O)]^+ \cdot Y^-$

(where, 1.  $M = Mn$ ,  $L_2 = 2P(OPh)_3$ ,  $Y^- = AsF_6^-$ ,  $BF_4^-$ ;

2.  $M = Re$ ,  $L_2 = 2(CO)$ ,  $bpy$ ,  $2(P\{OPh\}_3)$ ,  $tmen$ ,  $Y^- = AsF_6^-$ ,  $BF_4^-$ )

These aquo-complexes were prepared from the respective bromide precursors by halide abstraction using the hexafluoroarsenate and tetrafluoroborate silver salts. In each case the metal carbonyl bromide complex was dissolved in dichloromethane followed by the addition of an excess of finely divided hydrated silver salt as shown by the equation:

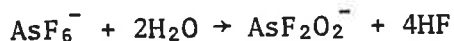


(where,  $n = 1 \rightarrow 2.5$ )

The respective reaction mixture was stirred at room temperature (*ca.* 25°C) under an atmosphere of dry nitrogen for 30 - 40 minutes. Within minutes the solution became cloudy due to the precipitation of silver bromide. The progress of the reaction was monitored in the carbonyl region by infrared spectroscopy using calcium fluoride solution cells. The precipitate and any unreacted silver salt ( $AgY \cdot (H_2O)_n$ ) were removed from the reaction mixture by filtration. The product was isolated as microcrystals or a fine powder by an initial concentration of the reaction mixture followed by its addition to light petroleum. Crystals suitable for x-ray diffraction studies were grown by cooling (*ca.* 0°C) or by slow solvent evaporation of the concentrated solution.

The rhenium pentacarbonyl complexes,  $[Re(CO)_5(H_2O)]^+ \cdot Y^-$ , are hydrascopic and will slowly decompose when dissolved in dichloromethane or fluorobenzene to form  $[Re(CO)_3(OH)]_4$ . In the case of the arsenate compound, decomposition occurs in the solid state resulting in the dimer species  $[Re(CO)_4F]_2$  at reduced pressure and a temperature of about 170°C.

Presumably the source of fluoride ions is the hydrolysis of hexafluoroarsenate:



This type of hydrolysis has also been observed with hexafluorophosphate in the presence of the complexes  $[\text{M}(\text{CO})_3(\text{L}_2)(\text{S})]^+$  (where, 1.  $\text{M} = \text{Mn}$ ,  $\text{L}_2 = 2(\text{CO})$ ,  $\text{bpy}$ ,  $2(\text{PPh}_3)$ ,  $2(\text{P}\{\text{Oph}\}_3)$ ; <sup>14</sup> 2.  $\text{M} = \text{Re}$ ,  $\text{L}_2 = 2(\text{CO})$ ,  $\text{bpy}$ ; <sup>15</sup> and,  $\text{S} = \text{H}_2\text{O}$  or  $\text{CH}_2\text{Cl}_2$ ), where the reaction half-life is of the order of 5 hours at room temperature. However, in sharp contrast, hexafluoroarsenate is more stable and will not undergo any observable hydrolysis even under reflux condition (ca.  $120^\circ\text{C}$ ). The isolated pentacarbonyl complexes are also hygroscopic and should be stored in a desiccator. The metal tricarbonyl complexes,  $[\text{M}(\text{CO})_3(\text{L}_2)(\text{H}_2\text{O})]^+\cdot\text{Y}^-$ , were found to be stable in a mildly humid atmosphere and have shown no decomposition over a period of six months when stored in sealed sample tubes.

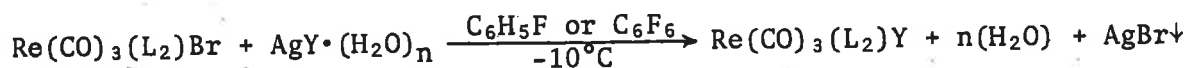
All of the aqua-complexes were characterized by their full nujol infrared spectra (Table 5.2.1 and § 5.2.3) and microanalysis (§ 5.7). The compounds,  $[\text{Re}(\text{CO})_5(\text{H}_2\text{O})]^+\cdot\text{AsF}_6^-$  and  $[\text{Re}(\text{CO})_3(\text{tmen})(\text{H}_2\text{O})]^+\cdot\text{Y}$  (where,  $\text{Y} = \text{AsF}_6^-$ ,  $\text{BF}_4^-$ ) were also characterized by their crystal structures (§ 5.3, 5.4 and 5.5). With the exception of the decomposition products of the rhenium pentacarbonyl complexes, no molecular ions or their fragmentation ions were observed in the mass spectra of any of the aquo-complexes. Hence the absence of mass spectra data.

#### 5.2.2 $\text{Re}(\text{CO})_3(\text{L}_2)\text{Y}\cdot\text{H}_2\text{O}$

- (where, 1.  $\text{L}_2 = \text{bpy}$ ,  $\text{Y} = \text{AsF}_6^-$ ;  
2.  $\text{L}_2 = \text{tmen}$ ,  $\text{Y} = \text{BF}_4^-$ )

The complexes,  $\text{Re}(\text{CO})_3(\text{L}_2)\text{Y}\cdot(\text{H}_2\text{O})$ , were also prepared from the bromide complexes by the abstraction method using the corresponding silver

salts, according to the equation:



The preparative method differs from that used for the synthesis of the aquo-complexes. Instead of isolating the respective compounds after the filtration step, the reaction mixture was cooled to *ca.*  $-10^\circ\text{C}$ , stirred and the solvent ( $\text{C}_6\text{H}_5\text{F}$  or  $\text{C}_6\text{F}_6$ ) allowed to evaporate over a period of 7 days in a desiccator containing an atmosphere of dry nitrogen over phosphorus pentoxide. Fluorinated benzene was used in favour of dichloromethane to reduce the rate of evaporation and to stop the formation of the chloro-complexes (i.e.  $\text{Re}(\text{CO})_3(\text{L}_2)\text{Cl}$ ) during the reaction. The isolated products,  $\text{Re}(\text{CO})_3(\text{L}_2)\text{Y} \cdot (\text{H}_2\text{O})$ , were characterized by their full nujol infrared spectrum (Table 5.2.1 and § 5.2.3). Only powders or microcrystals of the products were formed in the above procedure and crystallization at room temperature ( $18 - 25^\circ\text{C}$ ) resulted in their conversion to the corresponding aquo-complex. For these reasons no x-ray studies could to date be undertaken to verify the coordination of the anions,  $\text{AsF}_6^-$  and  $\text{BF}_4^-$ .

### 5.2.3 Characterization by Infrared Spectroscopy

All complexes presented in this chapter have been characterized by their infrared spectrum and the crystal structures of those analysed by x-ray diffraction (§ 5.3, 5.4 and 5.5) are consistent with the results given in this section. Three types of absorption bands are considered (Table 5.2.1), namely the  $\nu(\text{O-H})$  bands due to water,  $\nu(\text{C=O})$  bands due to carbonyl groups and  $\nu(\text{As, B-F})$  bands resulting from the anions  $\text{Y}^- (\text{AsF}_6^-, \text{BF}_4^-)$ . Metal fluoride absorption bands are expected in the region  $200 - 480 \text{ cm}^{-1}$ . However, the long-wavelength limit of the spectrometer ( $250 \text{ cm}^{-1}$ ) and the use of KBr plates made the observation of  $\nu(\text{M-F})$  bands



difficult. Thus, no  $\nu(\text{M-F})$  band assignments were undertaken.

(a) Water absorption bands

The water molecule exhibits anti-symmetric and symmetric (O-H) stretching in the region  $3100 - 3700 \text{ cm}^{-1}$ , (H-O-H) bending at  $1550 - 1650 \text{ cm}^{-1}$  and librational modes (rocking, wagging and rotational oscillations) in the region  $300 - 600 \text{ cm}^{-1}$ .<sup>57</sup> In the compounds described in this chapter lattice and coordinated water is best distinguished by their respective (O-H) stretching and (H-O-H) bending absorption bands, since these do not overlap with any other bands exhibited by the rest of the complex. As shown in Table 5.2.1 all aquo-complexes,  $[\text{M}(\text{CO})_3(\text{L}_2)(\text{H}_2\text{O})]^+\text{Y}^-$ , have a broad absorption maxima at  $3390 - 3520 \text{ cm}^{-1}$  and a sharp peak at  $1580 - 1610 \text{ cm}^{-1}$ . These bands have been assigned to the stretching and bending modes of coordinated water. The complexes,  $[\text{Re}(\text{CO})_3(\text{L}_2)\text{Y}] \cdot (\text{H}_2\text{O})$ , have the stretching band maxima at the lower region  $3325 - 3330 \text{ cm}^{-1}$ , but lack the bending mode near  $1600 \text{ cm}^{-1}$ . Thus, the absorption maxima in the range  $3200 - 3400 \text{ cm}^{-1}$  which are also observed in the infrared spectra of some of the aquo-complexes are due to the (O-H) stretching modes of lattice water.

(b) Tetrafluoroborate absorption bands

The "free" or uncoordinated  $\text{BF}_4^-$  anion has the tetrahedral symmetry  $T_d$  and exhibits four normal modes of vibration ( $\nu_{1-4}$ ).<sup>57</sup> The vibrations  $\nu_1(A_1)$  and  $\nu_3(F_2)$  are stretching modes while,  $\nu_2(E)$  and  $\nu_4(F_2)$  are deformation modes. Of these modes only  $\nu_3$  and  $\nu_4$  are infrared active.  $\text{AgBF}_4$  has a very strong absorption band at  $1045 \text{ cm}^{-1}$  ( $\nu_3$ , stretching mode) and a weaker band at  $528 \text{ cm}^{-1}$  ( $\nu_4$ , bending mode). The theoretically infrared inactive stretching mode  $\nu_1$  is seen as a weak absorption peak at  $765 \text{ cm}^{-1}$  but,  $\nu_2$  was not observed. The aquo-complexes,

$[M(\text{CO})_3(\text{L}_2)(\text{H}_2\text{O})]^+ \cdot \text{BF}_4^-$ , were characterized by the absorption maxima at  $1040 - 1050 \text{ cm}^{-1}$  which was assigned to the stretching mode ( $\nu_3$ ) of the "free"  $\text{BF}_4^-$  anion.

When the  $\text{BF}_4^-$  anion coordinates to a metal ion via a single fluorine atom its symmetry is lowered to  $\text{C}_{3v}$ . This results in the splitting of each of the triply degenerate asymmetric modes ( $\nu_3$  and  $\nu_4$ ) into two bands ( $\text{F}_2 \rightarrow \text{A}_1 + \text{E}$ ). In addition, the infrared inactive modes  $\nu_1$  and  $\nu_2$  become infrared active. In the region  $1200 - 400 \text{ cm}^{-1}$  of its infrared spectrum the complex  $[\text{Re}(\text{CO})_3(\text{tmen})\text{FBF}_3] \cdot (\text{H}_2\text{O})$  exhibits  $\nu(\text{B-F})$  absorption bands at  $1142, 1054, 995, 960$  and  $760 \text{ cm}^{-1}$ . This is consistent with the monodentate coordination of the  $\text{BF}_4^-$  anion. The bands at  $1140$  and  $1054 \text{ cm}^{-1}$  are assigned to the high energy (E) components of the  $\nu_3$  mode of vibration. While, the bands at  $995$  and  $960 \text{ cm}^{-1}$  are assigned to the low energy ( $\text{A}_1$ ) components of the  $\nu_3$  mode ( $\text{A}_1 + \text{E}$ ). The band at  $760 \text{ cm}^{-1}$  is assigned to the  $\nu_1(\text{A}_1)$  mode of the coordinated  $\text{BF}_4^-$  anion. Absorption maxima in the region  $500 - 550 \text{ cm}^{-1}$  could not be assigned to the  $\nu_4$  mode ( $\text{A}_1 + \text{E}$ ) due to the presence of tmen bands. The further splitting of the  $\nu_3$  mode which can be observed is due to the isotopic effect and the intensities are approximately consistent with the natural abundance of Boron ( $^{10}\text{B}$ , 20% and  $^{11}\text{B}$ , 80%). With both the observation of the splitting of the  $\nu_3$  mode and the absence of the (H-O-H) bending mode of water near  $1600 \text{ cm}^{-1}$ , the complex  $[\text{Re}(\text{CO})_3(\text{tmen})\text{FBF}_3] \cdot (\text{H}_2\text{O})$  is unambiguously characterized as containing a coordinated  $\text{BF}_4^-$  anion.

(c) Hexafluoroarsenate absorption bands

The uncoordinated  $\text{AsF}_6^-$  anion has an octahedral structure ( $\text{O}_h$ ) and six normal modes of vibration ( $\nu_{1-6}$ ).<sup>57</sup> For  $\text{CsAsF}_6$  the two triply degenerate infrared active vibrations  $\nu_3(\text{F}_{1u})$  and  $\nu_4(\text{F}_{1u})$  are observed at  $699$  and  $392 \text{ cm}^{-1}$ , respectively.<sup>53, 57, 58</sup> However, from the infrared

spectra of the aquo-complexes,  $[M(CO)_3(L_2)(H_2O)]^+ \cdot AsF_6^-$ , only the stretching mode ( $\nu_3$ ) in the region  $680 - 730 \text{ cm}^{-1}$  (Table 5.2.1) can be identified. This indicates that the  $AsF_6^-$  anion in these compounds is "free" which is consistent with the presence of the sharp  $\delta(H-O-H)$  bending mode at  $1580 - 1610 \text{ cm}^{-1}$  due to the coordinated water molecule.

The monodentate coordination of  $AsF_6^-$  lowers the local symmetry of the molecule from  $O_h$  to  $C_{4v}$  and as a result four new infrared active  $\nu(As - F)$  vibrations ( $3A_1 + E$ ) are expected. The spectrum (Fig. 5.2.1) of the complex  $[Re(CO)_3(bpy)FAsF_5] \cdot (H_2O)$  shows four absorption maxima at  $765, 705 (F_{1u} \rightarrow A_1 + E), 530 (A_{1g} \rightarrow A_1)$  and  $390 \text{ cm}^{-1} (E_g \rightarrow A_1 + B_1)$  (inactive)). This observation and the lack of a  $\delta(H-O-H)$  bending peak near  $1600 \text{ cm}^{-1}$  is consistent with the  $AsF_6^-$  anion being coordinated to the rhenium metal through a single fluorine atom.

#### (d) Carbonyl absorption bands

The monosubstituted carbonyl complexes,  $[Re(CO)_5(H_2O)]^+ \cdot Y^-$  (where,  $Y^- = AsF_6^-, BF_4^-$ ); each exhibit three carbonyl stretching bands ( $2A_1 + E$ ) in their solution infrared spectrum (Table 5.2.1). The number and relative band intensities are consistent with  $C_{4v}$  symmetry (Chapter 1.2). All the tricarbonyl complexes with bidentate ligands show carbonyl bands in their spectrum consistent with the *fac*-isomeric form (Chapter 1.2). While, the complexes with the ligands  $PPh_3$  and  $P(OPh)_3$  have carbonyl bands consistent with *mer*-isomer. The carbonyl bands (Table 5.2.1) of both pentacarbonyl and tricarbonyl complexes are at higher frequency relative to the respective metal carbonyl bromides. This is presumably because the coordinated water and fluoride ligands ( $AsF_6^-, BF_4^-$ ) are more electron-withdrawing than the bromide ion.

TABLE 5.2.1

Compound	Colour	$\nu(\text{CO})$			Medium
$\text{Re}(\text{CO})_5\text{Br}$	White	2153m	2045s	1990s	$\text{CH}_2\text{Cl}_2$
$[\text{Re}(\text{CO})_5(\text{H}_2\text{O})]^+ \cdot \text{AsF}_6^-$	White	2161vw	2056s 2025s	2008s 1960s	$\text{CH}_2\text{Cl}_2$ nujol
$[\text{Re}(\text{CO})_5(\text{H}_2\text{O})]^+ \cdot \text{BF}_4^-$	White	2160vw	2057s 2028s	2004s 1962s	$\text{CH}_2\text{Cl}_2$ nujol
<i>cis</i> - $\text{Re}(\text{CO})_3(\text{bpy})\text{Br}$	Yellow	2035s	1920	1900s	$\text{CH}_2\text{Cl}_2$
<i>cis</i> - $[\text{Re}(\text{CO})_3(\text{bpy})(\text{H}_2\text{O})]^+ \cdot \text{AsF}_6^-$	Yellow	2035s 2026s	1930s 1939s	1897s	$\text{CH}_2\text{Cl}_2$ nujol
<i>cis</i> - $[\text{Re}(\text{CO})_3(\text{bpy})(\text{H}_2\text{O})]^+ \cdot \text{BF}_4^-$	Yellow	2037s 2025s	1929s 1940s	1895s	$\text{CH}_2\text{Cl}_2$ nujol
<i>cis</i> - $\text{Re}(\text{CO})_3(\text{bpy})\text{FAsF}_5 \cdot \text{H}_2\text{O}$	Yellow	2037s 2028s	1927s 1942s	1910s	$\text{CH}_2\text{Cl}_2$ nujol
<i>cis</i> - $\text{Re}(\text{CO})_3(\text{tmen})\text{Br}$	White	2027s	1922s	1883s	$\text{CH}_2\text{Cl}_2$
<i>cis</i> - $[\text{Re}(\text{CO})_3(\text{tmen})(\text{H}_2\text{O})]^+ \cdot \text{AsF}_6^-$	White	2040s 2029s	1935s 1944s	1908s 1902s	$\text{CH}_2\text{Cl}_2$ nujol
<i>cis</i> - $[\text{Re}(\text{CO})_3(\text{tmen})(\text{H}_2\text{O})]^+ \cdot \text{BF}_4^-$	White	2041s 2028s	1935s 1945s	1907s 1900s	$\text{CH}_2\text{Cl}_2$ nujol
<i>cis</i> - $\text{Re}(\text{CO})_3(\text{tmen})\text{FBF}_3 \cdot \text{H}_2\text{O}$	White	2030s	1940s	1912s	nujol
<i>trans</i> - $\text{Mn}(\text{CO})_3\{\text{P}(\text{OPh})_3\}_2\text{Br}$	Yellow	2067w	1996s	1958s	$\text{CH}_2\text{Cl}_2$
<i>trans</i> - $[\text{Mn}(\text{CO})_3\{\text{P}(\text{OPh})_3\}_2(\text{H}_2\text{O})]^+ \cdot \text{AsF}_6^-$	Yellow	2088w 2078w	2013s 2000s	1972m 1920m	$\text{CH}_2\text{Cl}_2$ nujol
<i>trans</i> - $[\text{Mn}(\text{CO})_3\{\text{P}(\text{OPh})_3\}_2(\text{H}_2\text{O})]^+ \cdot \text{BF}_4^-$	Yellow	2088w 2098m	2013s 2005s	1970s 1955s	$\text{CH}_2\text{Cl}_2$ nujol

TABLE 5.2.1 (Continued)

Compound	$\nu(\text{OH}), \delta(\text{HOH})$	$\nu(\text{Y-F})_{\text{Y=As,B}}$	Medium
$[\text{Re}(\text{CO})_5(\text{H}_2\text{O})]^+ \cdot \text{AsF}_6^-$	3390b 1600s	710s	nujol
$[\text{Re}(\text{CO})_5(\text{H}_2\text{O})]^+ \cdot \text{BF}_4^-$	3400b 1600s	1050s	nujol
<i>cis</i> - $[\text{Re}(\text{CO})_3(\text{bpy})(\text{H}_2\text{O})]^+ \cdot \text{AsF}_6^-$	3410b 1602s	710s	nujol
<i>cis</i> - $[\text{Re}(\text{CO})_3(\text{bpy})(\text{H}_2\text{O})]^+ \cdot \text{BF}_4^-$	3420b 1600s	1040s	nujol
<i>cis</i> - $\text{Re}(\text{CO})_3(\text{bpy})\text{FAsF}_5 \cdot \text{H}_2\text{O}$	3325b -	765s, 700s, 530m, 390s	nujol
<i>cis</i> - $[\text{Re}(\text{CO})_3(\text{tmen})(\text{H}_2\text{O})]^+ \cdot \text{AsF}_6^-$	3410b 1595s	710s	nujol
<i>cis</i> - $[\text{Re}(\text{CO})_3(\text{tmen})(\text{H}_2\text{O})]^+ \cdot \text{BF}_4^-$	3520b 1597s	1050s	nujol
<i>cis</i> - $[\text{Re}(\text{CO})_3(\text{tmen})\text{FBF}_3 \cdot \text{H}_2\text{O}$	3320b -	1140ms, 1054m, 995mw, 960m, 760mw	nujol
<i>trans</i> - $[\text{Mn}(\text{CO})_3\{\text{P}(\text{OPh})_3\}_2(\text{H}_2\text{O})]^+ \cdot \text{AsF}_6^-$	3450b 1582s	760s	nujol
<i>trans</i> - $[\text{Mn}(\text{CO})_3\{\text{P}(\text{OPh})_3\}_2(\text{H}_2\text{O})]^+ \cdot \text{BF}_4^-$	3520wb 1585s	1045s	nujol

#### 5.2.4 Reactions of $[M(CO)_3(L_2)(H_2O)]^+ \cdot Y^-$ and $Re(CO)_3(L_2)Y \cdot (H_2O)$

Both types of complexes undergo rapid (seconds - minutes) substitution reactions in solution with halide ions (i.e.  $Cl^-$ ,  $Br^-$ ,  $I^-$ ) to form the respective metal halide complexes. In polar organic solvents (e.g. acetone, methanol, nitromethane) the corresponding solvento complex,  $[M(CO)_3(L_2)(Solvent)]^+ Y^-$ , is formed. This susceptibility towards substitution is in sharp contrast to general stability of the rhenium fluoride complexes (Chapter 3).

### 5.3 STRUCTURE DETERMINATION OF $[\text{Re}(\text{CO})_5(\text{H}_2\text{O})]^+ \cdot \text{AsF}_6^-$

#### 5.3.1 Crystal Data

Crystals of this compound were grown by slow evaporation of a dichloromethane solution at *ca.* 0°C in a desiccator containing phosphorus pentoxide and dry nitrogen. The colourless crystals formed were needle-like in morphology with the b axis along the needle axis. The space group was C2/c determined from the reflections collected on the CAD4. The cell constants were calculated by a least-square refinement using 25 high angle reflections. A flotation solution of 1,2-dichloroethane containing iodoform indicated a crystal density greater than 2.4 gm/cc. The crystal data is given below:

$\text{C}_5\text{H}_2\text{AsF}_6\text{O}_6\text{Re}$ ; M.W. = 533.2; Monoclinic space group C2/c,  $a = 27.085(5)$ ,  $b = 7.208(1)$ ,  $c = 13.404(3)$  Å,  $\beta = 105.50(1)^\circ$ ;  $U = 2522(2)$  Å<sup>3</sup>;  $Z = 8$ ;  $D_c = 2.808$  g.cm<sup>-1</sup>,  $D_m > 2.4$  g.cm<sup>-1</sup>;  $\lambda\text{MoK}_\alpha = 0.7107$  Å;  $F(000) = 1943$  electrons;  $\mu = 124.3$  cm<sup>-1</sup>.

A crystal of dimensions  $0.05 \times 0.06 \times 0.30$  mm<sup>3</sup> was coated and mounted using epoxy resin. 1514 unique reflections in the range  $1.5 < \theta < 23^\circ$  with intensities  $I > 2.5\sigma(I)$  were collected using a  $\omega$ -n/3 scan mode (where,  $n = 3$ ) (Chapter 7). The intensity of three standard reflections was measured at 50 minute intervals and the orientation matrix (refer to Experimental Chapter) was checked after every 100 reflections during the data collection. A comparison of the standard reflections showed that decomposition had occurred. The intensities were corrected for Lorentz and polarization<sup>98</sup> effects and for crystal absorption.<sup>99</sup> The maximum and minimum transmission factors were estimated to be 0.65 and 0.16, respectively. The crystallographic details are given in Table 5.3.1.

TABLE 5.3.1  
Crystallographic Details

Temperature	290°K	Crystal dimension	0.05 × 0.06 × 0.30 mm <sup>3</sup>
(Sin $\theta_{\max}$ )/ $\lambda$	0.50 Å <sup>-1</sup>	Crystal faces:	[101], [-10-1], [010], [0-10], [823], [-8-2-3]
Radiation	Mo		
Scan Method	$\omega/2\theta$	Aperature width	2.4 + 0.5 * tan $\theta$
Scan ranges (°)		Sig(I)/I(prescan)	0.40
$\theta_{\min} = 1.3$ , $\theta_{\max} = 23$		Sig(I)/I(final scan)	0.08
$\Delta\omega = 1.0 + 0.35 * \tan(\theta)$		Speed (prescan)	6.67 deg/min
Slit width	3 mm	Scan time (max)	250 sec
Total number of unique reflections collected 1514			



TABLE 5.3.2  
Atomic coordinates and thermal parameters for  $[\text{Re}(\text{CO})_5(\text{H}_2\text{O})]^+ \cdot \text{AsF}_6^-$

Atom <sup>a</sup>	x	y	z	U <sub>11</sub> <sup>b</sup>	U <sub>22</sub>	U <sub>33</sub>	U <sub>23</sub>	U <sub>13</sub>	U <sub>12</sub>
Re	12045(2)	29531 (7)	12669 (3)	429 (3)	518 (3)	417 (4)	-17 (2)	120 (2)	-38 (2)
As(1)	50000(0)	35391(25)	25000 (0)	473 (9)	595(10)	501(12)	4140 (0)	131 (8)	4140 (0)
As(2)	25000(0)	25000 (0)	50000 (0)	389 (8)	808(14)	533(12)	-80 (9)	74 (8)	50 (9)
F(1)	500(0)	1363(24)	2500 (0)	521(47)	68(10)	199(24)	414 (0)	-37(25)	414 (0)
F(2)	5140(6)	3621(25)	1398(10)	224(14)	309(18)	110(10)	-20(11)	99(10)	52(14)
F(3)	5607(4)	3660(26)	3134(13)	87 (7)	284(17)	224(16)	-20(15)	-28 (8)	35(10)
F(4)	500(0)	5840(19)	2500 (0)	396(32)	59 (9)	179(19)	414 (0)	92(20)	414 (0)
F(5)	2144(3)	3598(14)	3922 (7)	104 (6)	136 (7)	79 (6)	21 (6)	4 (5)	33 (6)
F(6)	2052(4)	812(16)	4735 (9)	114 (7)	156 (9)	146(10)	19 (8)	-7 (7)	-49 (7)
F(7)	2169(4)	3597(19)	5713 (8)	132 (8)	225(11)	103 (8)	-45 (8)	36 (7)	73 (8)
O(1)	2380(4)	2336(15)	1618(10)	62 (6)	115 (8)	140(11)	-16 (7)	31 (6)	13 (6)
O(2)	1455(4)	6859(13)	2323 (8)	86 (6)	68 (6)	88 (7)	-15 (6)	32 (5)	-5 (5)
O(3)	22(4)	3539(13)	844 (8)	60 (6)	89 (6)	96 (7)	8 (6)	30 (5)	5 (5)
O(4)	975(4)	-921(13)	163 (8)	89 (7)	67 (6)	102 (8)	-21 (6)	27 (6)	-6 (6)
O(5)	1137(3)	4931(14)	-800 (8)	89 (6)	99 (7)	60 (7)	10 (6)	23 (5)	-22 (6)
O(6)	1244(3)	1602(12)	2763 (6)	81 (5)	87 (6)	48 (5)	11 (4)	6 (4)	-12 (5)
C(1)	1964(4)	2558(18)	1505(11)	40 (7)	78 (9)	79(10)	-6 (7)	15 (6)	3 (7)
C(2)	1361(4)	5443(18)	1970 (9)	68 (8)	59 (8)	49 (9)	-3 (6)	29 (6)	-9 (6)
C(3)	452(5)	3348(16)	1038 (9)	50 (7)	66 (9)	52 (8)	5 (6)	16 (6)	-8 (6)
C(4)	1060(4)	460(18)	563(10)	58 (7)	65 (8)	63 (9)	9 (7)	21 (7)	11 (6)
C(5)	1170(4)	4168(18)	-38(11)	55 (7)	74 (9)	65(10)	-7 (7)	21 (7)	-15 (6)

<sup>a</sup> Re and As coordinates  $\times 10^5$ , others  $\times 10^4$ .

<sup>b</sup> Re and As thermal parameters  $\times 10^4$ , others  $\times 10^3$ .

TABLE 5.3.3

Atomic distances (Å) for  $[\text{Re}(\text{CO})_5(\text{H}_2\text{O})]^+\text{AsF}_6^-$ 

Atoms	Distance(Å)	Atoms	Distance(Å)
(a) Bond lengths and their standard deviations			
O(6)-Re	2.206 (8)	C(1)-Re	2.016(12)
C(2)-Re	2.019(14)	C(3)-Re	1.998(12)
C(4)-Re	2.019(14)	C(5)-Re	1.936(15)
F(1)-As(1)	1.569(18)	F(2)-As(1)	1.621(10)
F(3)-As(1)	1.638(10)	F(4)-As(1)	1.658(14)
F(5)-As(2)	1.702 (8)	F(6)-As(2)	1.687(10)
F(7)-As(2)	1.674 (8)	C(1)-O(1)	1.108(14)
C(2)-O(2)	1.125(13)	C(3)-O(3)	1.132(13)
C(4)-O(4)	1.126(14)	C(5)-O(5)	1.143(15)
(b) Hydrogen bonding distance			
F(3)...O(6)	2.860(12)	F(5)...O(6)	2.900(12)
(c) Selected interatomic distances			
O(3)...F(1)	3.02 (2)	O(2)...F(3)	3.08 (2)
O(4)...F(2)	3.15 (2)	O(3)...F(4)	2.96 (2)
		O(4)...F(6)	3.12 (2)

TABLE 5.3.4

Bond angles ( $^{\circ}$ ) for  $[\text{Re}(\text{CO})_5(\text{H}_2\text{O})]^+\text{AsF}_6^-$ 

C(1)-Re(1)-O(6)	89.7 (5)	C(2)-Re(1)-O(6)	90.9 (4)
C(2)-Re(1)-C(1)	88.4 (5)	C(3)-Re(1)-O(6)	90.1 (4)
C(3)-Re(1)-C(1)	179.7 (2)	C(3)-Re(1)-C(2)	91.4 (5)
C(4)-Re(1)-O(6)	89.3 (4)	C(4)-Re(1)-C(1)	90.6 (5)
C(4)-Re(1)-C(2)	179.0 (4)	C(4)-Re(1)-C(3)	89.6 (5)
C(5)-Re(1)-O(6)	179.3 (4)	C(5)-Re(1)-C(1)	90.5 (5)
C(5)-Re(1)-C(2)	88.4 (5)	C(5)-Re(1)-C(3)	89.7 (5)
C(5)-Re(1)-C(4)	91.4 (5)	F(2)-As(1)-F(1)	92.1 (7)
F(3)-As(1)-F(1)	93.1 (6)	F(3)-As(1)-F(2)	91.4 (8)
F(4)-As(1)-F(1)	180.0 (0)	F(4)-As(1)-F(2)	87.9 (7)
F(4)-As(1)-F(3)	86.9 (6)	F(6)-As(2)-F(5)	86.8 (5)
F(7)-As(2)-F(5)	89.8 (5)	F(7)-As(2)-F(6)	89.8 (7)
F(2)-As(1)-F(2)	175.8(13)	F(3)-As(1)-F(3)	173.9(13)
F(6)-As(2)-F(6)	180.0 (0)	F(7)-As(2)-F(7)	180.0 (0)
O(1)-C(1)-Re(1)	178.8(13)	O(2)-C(2)-Re(1)	176.9(11)
O(3)-C(3)-Re(1)	175.6(11)	O(4)-C(4)-Re(1)	179.2(11)
O(5)-C(5)-Re(1)	177.4(11)		

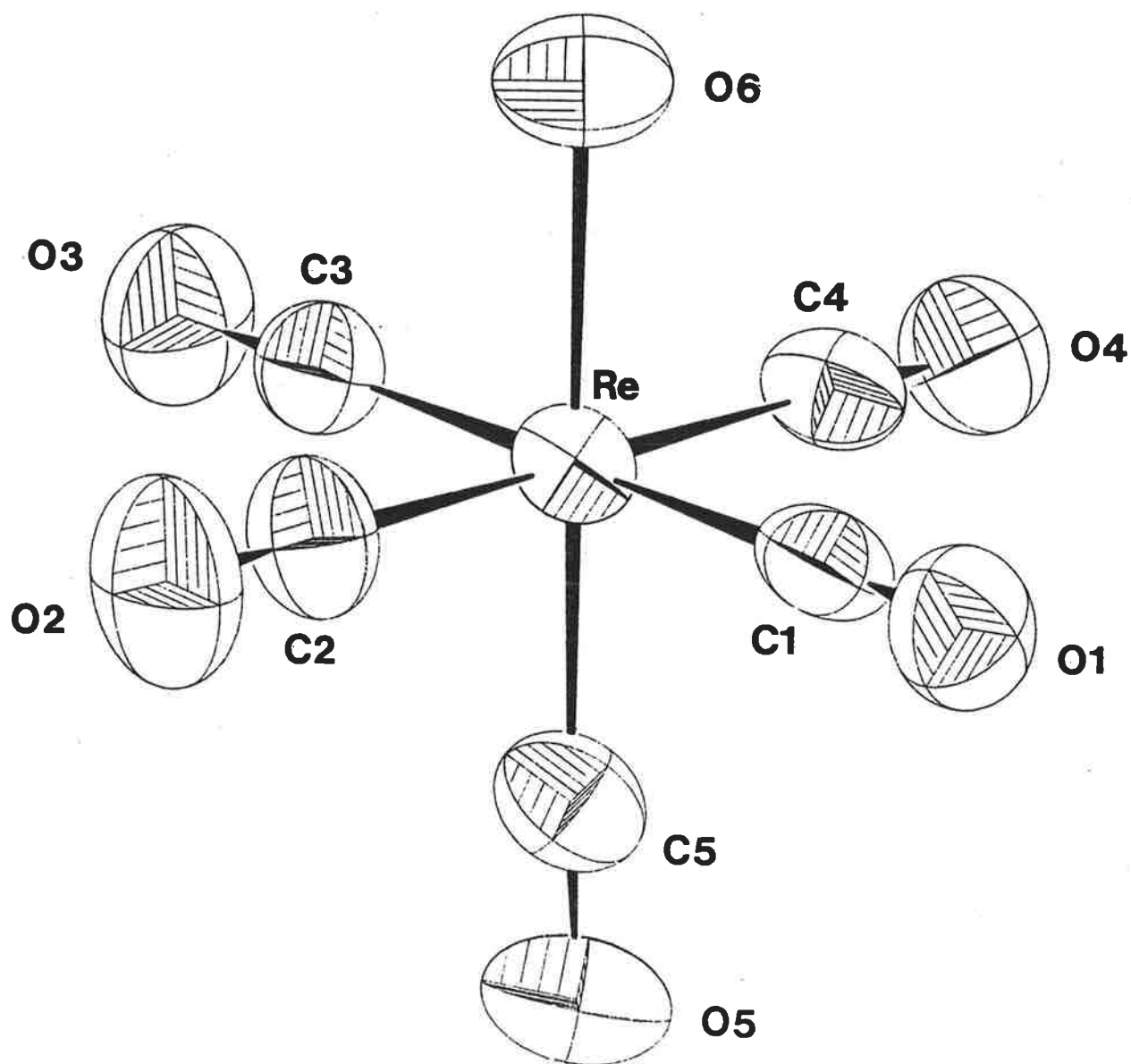


FIGURE 5.3.1. The molecular structure of the  $[\text{Re}(\text{CO})_5(\text{H}_2\text{O})]^+$  cation (50% probability ellipsoids).

### 5.3.2 Structure Solution and Refinement

The structure was solved using the heavy atom technique. The unique rhenium coordinates were determined from the strongest peaks in the Patterson map. A subsequent difference Fourier synthesis based on the rhenium atom gave a difference Fourier map which revealed all the non-hydrogen atoms, with the arsenic atoms located on the symmetry sites  $(0\ y\ \frac{1}{4})$  and  $(\frac{1}{4}\ \frac{1}{4}\ \frac{1}{2})$ . A full matrix least-squares calculation, including all located atoms and modelling the rhenium and arsenic atoms anisotropically, refined giving an R value of 0.045. When applying the weighting scheme (Chapter 7.1) and with all the non-hydrogen atoms modelled anisotropically the refinement converged with  $R = 0.027$ ,  $R_w = 0.028$ ,  $k = 0.99$  and  $g = 5.1 \times 10^{-4}$ . The largest peaks remaining in the final difference map was  $0.5\ e\text{\AA}^{-3}$ . The hydrogen atoms of the water molecule were not located. The non-hydrogen atomic parameters, bond lengths and bond angles are given in Tables 5.3.2, 5.3.3 and 5.3.4 respectively. The hydrogen parameters are given on microfiche.

### 5.3.3 Description of the Structure

Figure 5.3.1 is an ORTEP<sup>78</sup> plot of the  $[\text{Re}(\text{CO})_5(\text{H}_2\text{O})]^+$  cation showing the atom numbering scheme employed. The geometry about the rhenium atom is octahedral with all deviations from  $90^\circ$  and  $180^\circ$  being less than  $3\ \sigma$ . Although the standard deviations in the (Re-C) bond distances are large, the average equatorial distance of  $2.013(8)\text{\AA}$  is significantly larger than the axial distance (i.e. Re-C(5)) of  $1.94(2)\text{\AA}$ . This observation is not unusual and is seen in a number of other metal carbonyl systems.<sup>140, 141, 142, 143</sup> The average (C-O) distance of  $1.12(1)\text{\AA}$  is as expected for rhenium carbonyl systems. The (Re-O) bond length (i.e. Re-O(6)) in  $[\text{Re}(\text{CO})_5(\text{H}_2\text{O})]^+ \cdot \text{AsF}_6^-$  is found to be  $2.206(8)\text{\AA}$  which is

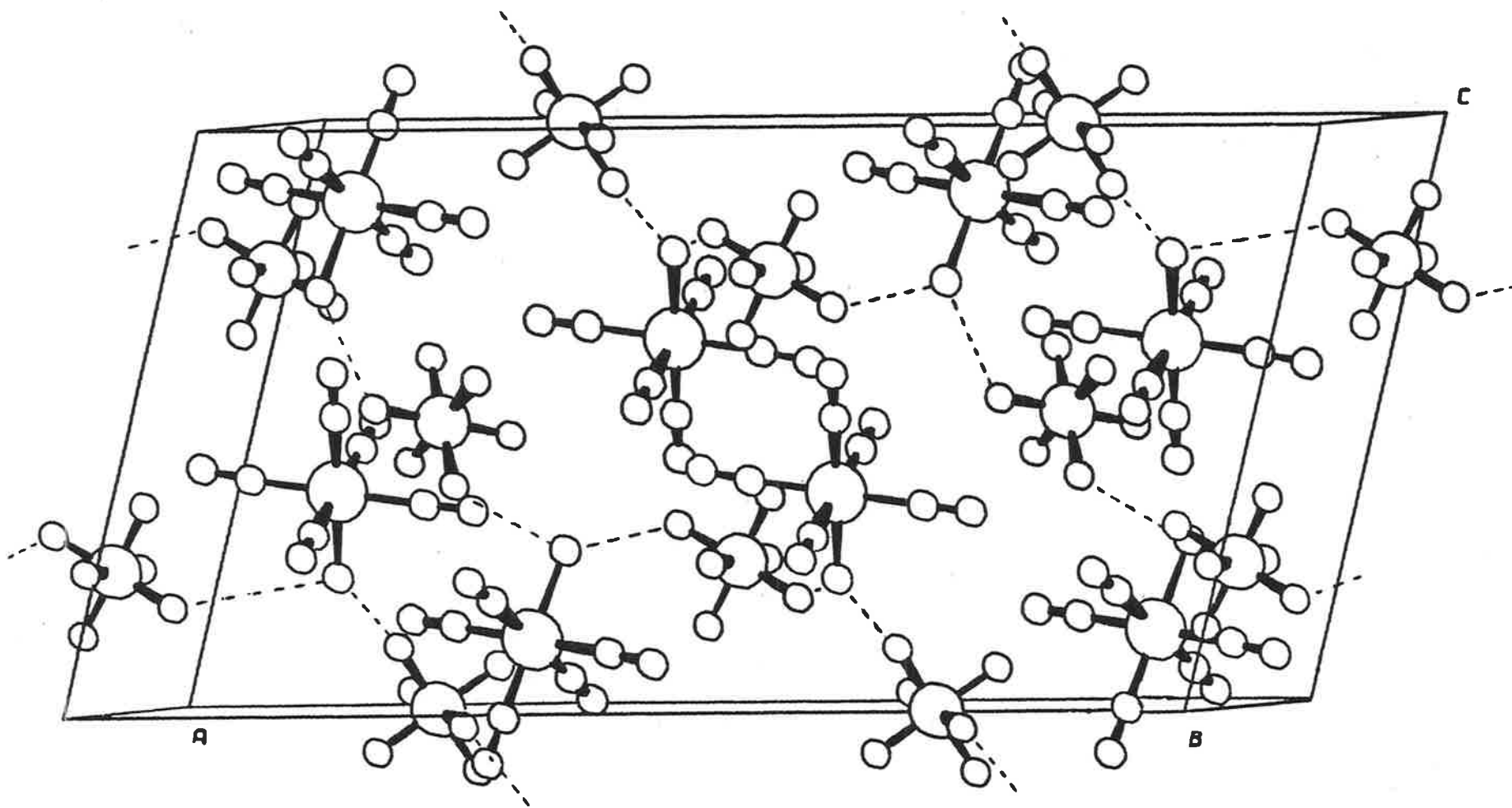


FIGURE 5.3.2. A PLUTO unit cell plot for  $[\text{Re}(\text{CO})_5(\text{H}_2\text{O})]^+ \cdot \text{AsF}_6^-$  showing the hydrogen bonding interactions between the rhenium molecule and the  $\text{AsF}_6^-$  anion.

considerably larger than the (Re-F) bond length of 2.040(4)Å observed in  $\text{Re}(\text{CO})_3(\text{tmen})\text{F}$  (Chapter 3). The  $\text{AsF}_6^-$  anion is disordered and this is reflected in both the large thermal parameters and the slight deviation from an octahedral geometry. The average (As-F) bond length is 1.65(1)Å.

The crystal lattice of  $[\text{Re}(\text{CO})_5(\text{H}_2\text{O})]^+ \cdot \text{AsF}_6^-$  is made up of the ions  $[\text{Re}(\text{CO})_5(\text{H}_2\text{O})]^+$  and  $\text{AsF}_6^-$  held together by hydrogen bonding. Two  $\text{AsF}_6^-$  anions are hydrogen bonded to the coordinated water molecule (i.e. 0(6)) of each  $[\text{Re}(\text{CO})_5(\text{H}_2\text{O})]^+$  cation at the distances 2.86(1) and 2.90(1)Å (Table 5.3.3). This is illustrated in the PLUTO<sup>144</sup> plot of the unit cell (Fig. 5.3.2). Other non-hydrogen bonding intramolecular contacts are listed in Table 5.3.3.

## 5.4 STRUCTURE DETERMINATION OF $[\text{Re}(\text{CO})_3(\text{tmen})(\text{H}_2\text{O})]^+ \cdot \text{AsF}_6^-$

### 5.4.1 Crystal Data

A portion of filtered solution containing the reaction product,  $[\text{Re}(\text{CO})_3(\text{tmen})(\text{H}_2\text{O})]^+ \cdot \text{AsF}_6^-$ , was allowed to crystallize at 0°C in a dessicator containing dry nitrogen. The white crystals formed were prismatic to needle-like, with the elongation extending along the b axis. The reflection data collected on the CAD4 indicated the centered monoclinic system while the mean  $\text{Abs}(E^*E-1)$  (Chapter 7.1) calculation using the SHELX program determined the space group as  $P2_1$ . The cell constants were calculated and refined using 25 high angle reflections. The density was measured by the floatation technique<sup>100</sup> using a 1,2-dibromoethane solution containing iodoform.

Crystal data:  $\text{C}_9\text{H}_{18}\text{AsF}_6\text{N}_2\text{O}_3\text{Re}$ ; M.W. = 577.3; Monoclinic space group  $P2_1$ ,  $a = 7.858(1)$ ,  $b = 15.68(1)$ ,  $c = 7.887(2)$  Å and  $\beta = 117.11(1)^\circ$ ;  $U = 864.8(9)$  Å<sup>3</sup>;  $Z = 2$ ;  $D_c = 2.217$  g.cm<sup>-3</sup>,  $D_m = 2.23(2)$  g.cm<sup>-3</sup>;  $\lambda\text{MoK}\alpha = 0.7107$  Å;  $F(000) = 560$  electrons;  $\mu = 90.87$  cm<sup>-1</sup>.

A crystal of dimension  $0.04 \times 0.06 \times 0.22$  mm<sup>3</sup> was coated with epoxy resin and mounted on a glass fibre in an atmosphere of dry nitrogen. The intensity of three reference reflections were checked at 50 minute intervals and these indicated that no decomposition had occurred during the data collection. 1877 reflections were collected in the theta range  $1.5 < \theta < 25^\circ$  of which 1362 with  $I > 2.5\sigma(I)$  were used in the calculations. Each reflection was measured using a  $\omega$ -n/3 $\theta$  scan mode, where n (=1) was optimized by  $\omega/\theta$  profile analysis (Chapter 7.1). The intensities were corrected for Lorentz,<sup>98</sup> polarization effects<sup>98</sup> and for absorption.<sup>99</sup> The maximum and minimum transmission factors were estimated to be 0.73 and 0.53, respectively. Further experimental details are given in Table 5.4.1.



TABLE 5.4.1

Crystallographic details for  $[\text{Re}(\text{CO})_3(\text{tmen})(\text{H}_2\text{O})]^+ \cdot \text{AsF}_6^-$ 

Temperature	290°K	Crystal dimension	$0.04 \times 0.06 \times 0.26 \text{ mm}^3$
$(\text{Sin } \theta_{\text{max}})/\lambda$	$0.59 \text{ \AA}^{-1}$	Crystal faces	[100], [-100], [010] [0-10], [001], [00-1]
Radiation	MoK $\alpha$	Aperture width	$2.90 + 0.5 * \tan(\theta)$
Scan method	$\omega/2\theta$	Sig(I)/I(prescan)	0.40
Scan range (°)		Sig(I)/I(final scan)	0.50
	$\theta_{\text{min}} = 1.50, \theta_{\text{max}} = 25.0$	Speed(prescan)	6.67 deg/min
	$\Delta\omega = 1.00 + 0.35 * \tan(\theta)$	Scan time (max)	250 sec
Slit width	3 mm		

Total number of unique reflections collected 1466

#### 5.4.2 Structure Solution and Refinement

The structure was solved by the heavy atoms method. The rhenium atom coordinates were determined from a three-dimensional Patterson map. A least-squares calculation with the rhenium atom gave an R value of 0.31 and the associated difference map revealed the arsenic, four fluorides, a carbonyl group and the two nitrogen atoms of the tmen ligand. The difference Fourier synthesis based on the rhenium and arsenic atoms gave an R value of 0.14 and the difference map revealed all the non-hydrogen atom positions. In subsequent calculations the located atoms were systematically refined with anisotropic temperature factors and the position of the hydrogen atoms of the tmen ligand was calculated assuming tetrahedral geometry about the respective carbon atoms at a bond distance of 0.98 Å. The methyl groups were refined as rigid groups and the hydrogen atoms were refined with a unique group temperature factor. A full-matrix least-squares calculation, employing the weighting scheme and modelling all non-hydrogen atoms anisotropically, converged with  $R = 0.021_2$  and  $R_w = 0.022_4$ . However, when the signs of all the atomic coordinates were changed, the above calculation converged with  $R = 0.020_9$  and  $R_w = 0.022_0$ . Hence establishing the absolute configuration (Chapter 7.1). The final least-squares refinement converged with  $R = 0.020_5$ ,  $R_w = 0.021_5$ ,  $k = 0.27$  and  $g = 1.8 \times 10^{-3}$ .

In the final difference map the highest peak remaining was equal to  $0.9 \text{ e}\text{\AA}^{-3}$ , which are spurious peaks about the rhenium atom. The atomic parameters, bond lengths and bond angles of the non-hydrogen atoms are given in Tables 5.4.2, 5.4.3 and 5.4.4. The hydrogen atom parameters are given on microfiche.

TABLE 5.4.2

Atomic coordinates and thermal parameters for  $[\text{Re}(\text{CO})_3(\text{tmen})(\text{H}_2\text{O})]^+\cdot\text{AsF}_6^-$ 

Atom <sup>a</sup>	x	y	z	$U_{11}$ <sup>b</sup>	$U_{22}$	$U_{33}$	$U_{23}$	$U_{13}$	$U_{12}$
Re	-42634 (5)	75000 (0)	-2847 (5)	330 (2)	283 (2)	359 (2)	36(10)	174 (1)	50(10)
As	37(84)	-80(30)	-50060(83)	392 (4)	331 (4)	355 (4)	18 (3)	160 (3)	-5 (3)
F(1)	-1382(44)	-4054(17)	-5923(43)	72(12)	82(16)	85(14)	12(10)	39(11)	34(10)
F(2)	-1502(32)	-5532(15)	-7109(30)	74 (9)	76(12)	46 (7)	-9 (7)	23 (6)	-41 (8)
F(3)	-1487(37)	-5295(18)	-4217(36)	78(13)	91(20)	97(16)	14(13)	58(12)	-4(14)
F(4)	1309(27)	-4549(11)	-2867(31)	45 (7)	31 (6)	52 (8)	-17 (5)	16 (6)	-13 (6)
F(5)	1550(23)	-4665(12)	-5918(21)	43 (8)	83(12)	39 (7)	-24 (8)	18 (6)	-23 (8)
F(6)	1160(38)	-5920(11)	-4226(35)	86(10)	34 (8)	40 (7)	3 (6)	12 (6)	22 (7)
O(1)	-5829(37)	-3776(21)	1536(44)	51(13)	75(23)	124(21)	7(18)	30(13)	-23(13)
O(2)	4140(41)	-1127(17)	1420(30)	132(20)	80(16)	62(10)	-37(11)	62(12)	17(14)
O(3)	1770(12)	-2465(18)	-3650(12)	42 (4)	63 (6)	73 (5)	1(16)	5 (4)	32(11)
O(4)	-1336(10)	-2399(23)	-7731(10)	44 (4)	46(13)	44 (4)	16 (8)	12 (3)	9 (7)
N(1)	-2961(36)	-3384(15)	-1578(36)	77(17)	17 (8)	37(15)	-16 (8)	32(13)	-20 (9)
N(2)	-3043(27)	-1524(16)	-1615(34)	19 (8)	56(16)	41(13)	-1(10)	5 (8)	-19 (8)
C(1)	4779(24)	-3254(19)	807(39)	20 (8)	55(15)	79(19)	-15(11)	22 (9)	-8 (7)
C(2)	-5247(43)	-1591(19)	801(33)	132(25)	23 (8)	36(13)	-17 (8)	52(14)	-5(10)
C(3)	3313(16)	-2528(40)	-2377(17)	40 (5)	36(16)	48 (5)	2(10)	20 (5)	-15(10)
C(4)	-4544(49)	-4004(18)	-2887(48)	101(20)	82(19)	106(21)	-89(18)	64(17)	-54(15)
C(5)	-1830(40)	-4095(17)	-269(39)	87(16)	57(14)	41 (9)	12(10)	26(10)	25(11)
C(6)	-1691(27)	-2961(12)	-2184(31)	62(12)	27 (9)	99(16)	12 (9)	57(11)	14 (8)
C(7)	-2530(29)	-2109(14)	-2923(27)	87(14)	52(10)	78(12)	-25(10)	68(11)	-36(11)
C(8)	-4392(35)	-1082(21)	-3276(44)	36 (9)	82(17)	93(17)	19(13)	26(11)	-2(11)
C(9)	-1253(39)	-1123(17)	-293(38)	94(18)	70(18)	54(11)	-19(12)	48(13)	-53(14)

<sup>a</sup> Re and As coordinates  $\times 10^5$ , others  $\times 10^4$ .<sup>b</sup> Re and As thermal parameters  $\times 10^4$ , others  $10^3$ .

TABLE 5.4.3

Atomic Distances for  $[\text{Re}(\text{CO})_3(\text{tmen})(\text{H}_2\text{O})]^+ \cdot \text{AsF}_6^-$ 

Atoms <sup>a</sup>	Distance(Å)	Atoms	Distance(Å)
(a) Bond lengths (and standard deviations)			
O(4)-Re	2.268 (8)	N(1)-Re	2.225(26)
N(2)-Re	2.294(24)	C(1)-Re	1.813(28)
C(2)-Re	1.988(28)	C(3)-Re	1.866(12)
F(1)-As	1.796(17)	F(2)-As	1.745(16)
F(3)-As	1.611(18)	F(4)-As	1.678(21)
F(5)-As	1.761(16)	F(6)-As	1.652(18)
C(1)-O(1)	1.215(43)	C(2)-O(2)	1.100(39)
C(3)-O(3)	1.173(15)	C(4)-N(1)	1.543(32)
C(5)-N(1)	1.502(37)	C(6)-N(1)	1.447(29)
C(7)-N(2)	1.563(31)	C(8)-N(2)	1.432(35)
C(9)-N(2)	1.456(33)	C(7)-C(6)	1.484(22)
(b) Hydrogen bonds			
O(4)...F(1)	2.96 (3)	O(4)...F(6) <sup>I</sup>	2.75 (3)
(c) Selected non-bonding distances			
C(1)...F(1)	3.19 (3)	O(3)...F(2) <sup>I</sup>	3.11 (3)
H(5)...F(2)	2.43 (3)	C(8)...F(3) <sup>I</sup>	3.18 (3)

<sup>a</sup>Superscript in Roman refers to the following equivalent position, with respect to the unique asymmetric unit at x, y, z:

$$I = -x, 0.5 + y, -z$$

TABLE 5.4.4

Bond angles and standard deviations for  $[\text{Re}(\text{CO})_3(\text{tmen})(\text{H}_2\text{O})]^+ \cdot \text{AsF}_6^-$ 

Atoms	Angle (°)	Atoms	Angle (°)
N(1)-Re-O(4)	87.6 (9)	N(2)-Re-O(4)	83.9 (8)
N(2)-Re-N(1)	80.2 (4)	C(1)-Re-O(4)	95.5 (9)
C(1)-Re-N(1)	100.9(10)	C(1)-Re-N(2)	178.7(11)
C(2)-Re-O(4)	90.2(10)	C(2)-Re-N(1)	172.7(10)
C(2)-Re-N(2)	92.6(11)	C(2)-Re-C(1)	86.2 (6)
C(3)-Re-O(4)	177.3(23)	C(3)-Re-N(1)	94.4(14)
C(3)-Re-N(2)	94.7(14)	C(3)-Re-C(1)	85.9(15)
C(3)-Re-C(2)	87.6(16)	F(1)-As-F(2)	88.9 (7)
F(1)-As-F(3)	89.3 (7)	F(1)-As-F(4)	91.6 (8)
F(1)-As-F(5)	88.6 (6)	F(2)-As-F(3)	87.0 (7)
F(3)-As-F(4)	87.8 (8)	F(4)-As-F(5)	93.1 (6)
F(5)-As-F(2)	92.1 (8)	F(6)-As-F(1)	178.3 (8)
F(6)-As-F(2)	88.4 (7)	F(6)-As-F(3)	90.0 (8)
F(6)-As-F(4)	90.9 (5)	C(4)-N(1)-Re	107.4(18)
F(6)-As-F(5)	92.1 (7)	C(5)-N(1)-C(4)	92.2(23)
C(5)-N(1)-Re	113.4(17)	C(6)-N(1)-C(4)	122.2(23)
C(6)-N(1)-Re	113.4(15)	C(7)-N(2)-Re	101.5(14)
C(6)-N(1)-C(5)	106.5(20)	C(8)-N(2)-C(7)	89.1(20)
C(8)-N(2)-Re	116.8(16)	C(9)-N(2)-C(7)	105.6(17)
C(9)-N(2)-Re	115.3(17)	O(1)-C(1)-Re	178.2(25)
C(9)-N(2)-C(8)	121.1(26)	O(3)-C(3)-Re	173.5(49)
O(2)-C(2)-Re	175.5(28)	C(6)-C(7)-N(2)	118.0(20)
C(7)-C(6)-N(1)	106.9(17)		

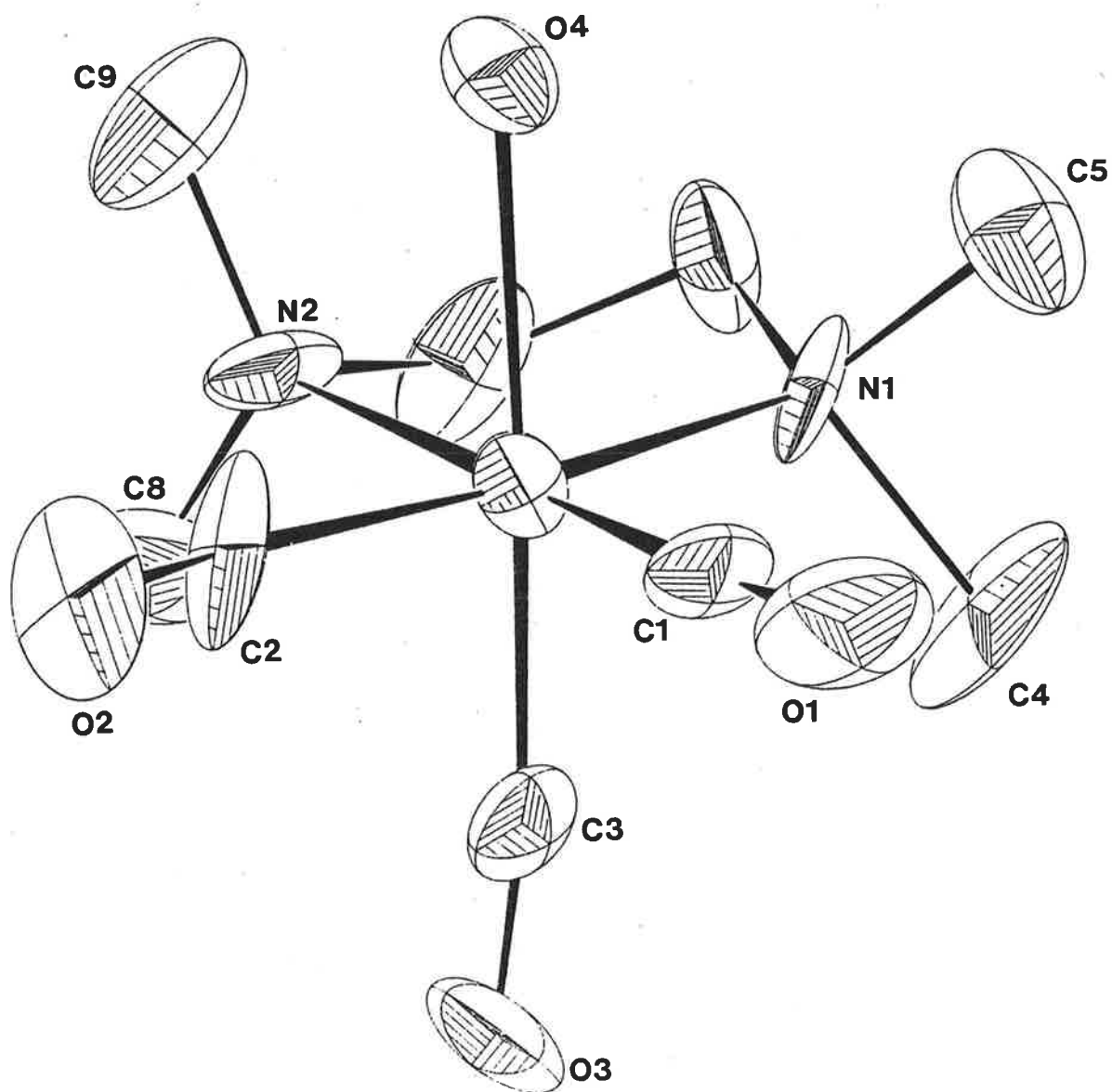


FIGURE 5.4.1. The molecular structure of the *cis*-[Re(CO)<sub>3</sub>(tmen)(H<sub>2</sub>O)]<sup>+</sup> cation (50% probability ellipsoids).

### 5.4.3 Description of the Structure

The ORTEP<sup>78</sup> plot (Fig. 5.4.1) of the  $[\text{Re}(\text{CO})_3(\text{tmen})(\text{H}_2\text{O})]^+$  cation shows the *facial* stereochemistry of the molecule as predicted from the infrared data (§ 5.2).

The geometry about the rhenium atom is that of a distorted octahedron<sup>on</sup> with the carbonyl groups in a mutually *cis* stereochemistry. The distortion results from the restriction of the bite angle of the tmen ligand to  $80.2(4)^\circ$ . Further deviations from the ideal octahedral angles of  $90^\circ$  and  $180^\circ$  are seen in some of the axial and equatorial bond angles. The average (Re-C) and (C-O) bond lengths are usual for rhenium carbonyl systems and are in the ranges  $1.87 - 2.02 \text{ \AA}$  and  $1.07 - 1.61 \text{ \AA}$ ,<sup>84, 145-147</sup> respectively. The (Re-O) bond length in  $[\text{Re}(\text{CO})_3(\text{tmen})(\text{H}_2\text{O})]^+$  is  $2.268(8) \text{ \AA}$  which is slightly larger but comparable to that found in both  $[\text{Re}(\text{CO})_3(\text{H}_2\text{O})]^+ \cdot \text{AsF}_6^-$  (§ 5.3) and  $[\text{Re}(\text{CO})_3(\text{tmen})(\text{H}_2\text{O})]^+ \cdot \text{BF}_4^-$  (§ 5.5).

The  $\text{AsF}_6^-$  anion has an octahedral geometry and no substantial deviation from  $90^\circ$  and  $180^\circ$  bond angles occurs. The anion is disordered about the arsenic position resulting in both the high fluorine thermal parameters and the high standard deviations. The average (As-F) bond length of  $1.71(2) \text{ \AA}$  is unexceptional for an  $\text{AsF}_6^-$  anion and is equal to that found in  $[\text{Re}(\text{CO})_5(\text{H}_2\text{O})]^+ \cdot \text{AsF}_6^-$  (§ 5.3) within experimental error.

The crystal lattice consists of an equal number of  $[\text{Re}(\text{CO})_3(\text{tmen})(\text{H}_2\text{O})]^+$  and  $\text{AsF}_6^-$  ions. The coordinated water molecule of the cation is hydrogen bonded to two  $\text{AsF}_6^-$  anions at the respective distances  $2.96(3)$  and  $2.75(3) \text{ \AA}$  (Table 5.4.3). The closest non-hydrogen bonded intramolecular contacts are also given in Table 5.4.3.

## 5.5 STRUCTURE DETERMINATION OF $[\text{Re}(\text{CO})_3(\text{tmen})(\text{H}_2\text{O})]^+\cdot\text{BF}_4^-$

### 5.5.1 Crystal data

Crystals grown by the diffusion of petroleum spirit (30° - 40°C) into a solution of dichloromethane and  $[\text{Re}(\text{CO})_3(\text{tmen})(\text{H}_2\text{O})]^+\cdot\text{BF}_4^-$  are white prismatic to needle-like in morphology. The initial cell constants were determined from Precession photographs ((0K1), (1K1), (K01), (K11)). The systematic absences in the photographs:

$$hK1: h + K = 2n + 1 \quad h01: (h = 2n + 1) \quad 0K0: (K = 2n + 1)$$

are in accord with the extinctions of the C-centered space groups C2, Cm and C2/m. The statistical test ( $|E^2 - 1|$ , Chapter 7.1) for centric and acentric distribution of intensities performed in SHELX<sup>75</sup> incorrectly determined the space group to be noncentrosymmetric. The refinements in the space group C2 failed to converge and did not allow anisotropic modelling for the carbon and nitrogen atoms. While, refinement with rhenium in the special position (x,0,y) revealed two further rhenium atoms in equivalent positions consistent with the space group C2/m. The refinement in this space group converged smoothly (§ 5.5.2). Hence, correctly determining the space group as C2/m.

The final cell constants were obtained by the least-squares refinement routine on the CAD4 using 25 high angle reflections. The crystal density ( $D_m$ ) was determined by the floatation technique using a solution mixture of carbontetrachloride and 1,2-dibromoethane.

Crystal data:  $\text{C}_9\text{H}_{18}\text{BF}_4\text{N}_2\text{O}_4\text{Re}$ ; M.W. = 491.26; Monoclinic space group, C2/m,  $a = 14.134(4)$ ,  $b = 16.010(4)$ ,  $c = 7.729(1)$  Å,  $\beta = 113.16(2)^\circ$ ;  $U = 1608(1)$  Å<sup>3</sup>;  $Z = 4$ ;  $D_c = 2.029$  g.cm<sup>-3</sup>,  $D_m = 2.04(2)$  g.cm<sup>-3</sup>;  $\lambda_{\text{MoK}\alpha} = 0.7107$  Å;  $F(000) = 830$  electrons;  $\mu = 76.78$  cm<sup>-1</sup>.

A crystal of dimensions  $0.03 \times 0.08 \times 0.11$  mm<sup>3</sup> was mounted about c on the STOE (Chapter 7.1). The intensity of reflections, with the indices from hK0 to hK9 in the theta range of  $1.5 < \theta < 25^\circ$ , were measured using



the  $\omega$  scan technique. A step count time of 0.1 second at each  $0.01^\circ$  of the scan range ( $\Delta\omega$ ) was used for each peak and a total time of 6 seconds was spent on the background. Further experimental details are given in Table 5.5.1. The Lorentz and polarization corrections were applied by the data reduction programme AUPTP.<sup>74</sup> The absorption corrections and symmetry averaging were computed by the programme SHELX<sup>75</sup> for all 1830 reflections (1374) with  $I > 2.5 (I)$ . The maximum and minimum transmission factors were estimated to be 0.78 and 0.69, respectively.

### 5.5.2 Structural Solution and Refinement

The initial rhenium atomic coordinates were determined from a Patterson synthesis ( $x, 0, y$ ). Three cycles of least-square refinement for the rhenium atom gave an R value of 0.48. The difference map based on the rhenium position revealed all non-hydrogen atoms. The positions of the hydrogen atoms were calculated for the respective carbon atoms assuming tetrahedral geometry at a fixed carbon-hydrogen bond length of 0.97 Å. The methyl groups were refined as rigid groups with a unique common hydrogen group temperature factor. The inter-layer scale factors were subsequently refined (with all atoms isotropic) in a full-matrix least-squares calculation, which gave an R value of 0.148. In all additional calculations the inter-layer scale factors were fixed. When applying the weighting scheme (Chapter 7.1) in the SHELX<sup>75</sup> programme to a refinement with only the rhenium and fluoride atoms anisotropic the R value reduced to 0.075 and  $R_w$  to 0.084. In the final full-matrix least-squares calculation all the non-hydrogen atoms were modelled anisotropically and the refinement converged with  $R = 0.064$ ,  $R_w = 0.070$ ,  $k = 1.35$  and  $g = 2.9 \times 10^{-3}$ . The largest peak remaining in the final difference map was  $2 \text{ e}\text{\AA}^{-3}$  and identified as a spurious peak around the rhenium atom. The absolute configuration was determined by changing the sign of all coordinates and performing a least-squares refinement (Chapter 7.1). The R values converged at  $R = 0.061$  and  $R_w = 0.064$ , with  $k = 0.94$  and

TABLE 5.5.1

Experimental details for  $[\text{Re}(\text{CO})_3(\text{tmen})(\text{H}_2\text{O})]^+ \cdot \text{BF}_4^-$ 

Temperature	295°K	Levels	hk0 → hk9
$(\text{Sin } \theta_{\text{max}})/\lambda$	$1.2 \text{ \AA}^{-1}$	Crystal dimensions	$.26 \times .86 \times 1.32 \text{ mm}^3$
Radiation	$\text{MoK}\alpha$	Crystal faces	[100], [-100], [010],
Rotation axis	<u>C</u>		[0-10], [011], [0-11], [0-2-1]
Scan method	$\omega$	Background scan time	6.0 sec
Scan range (°)		Step scan time	0.1 sec
	$2.5 < 2\theta < 55$	Number of unique reflections	
$\Delta\omega^{\#} = 1.2 + 0.7(\sin\mu/\tan(\psi/2))$		collected	2667

<sup>#</sup>  $\mu$  is the equi-inclination angle and  $\psi$  is the detector angle.

$g = 6.2 \times 10^{-3}$ . The atomic parameters, bond lengths and bond angles of the non-hydrogen atoms are given in Tables 5.5.2, 5.5.3 and 5.5.4. The hydrogen atomic parameters and the structure factor tables are given on microfiche.

### 5.5.3 Description of the Structure

The crystal structure of  $[\text{Re}(\text{CO})_3(\text{tmen})(\text{H}_2\text{O})]^+ \cdot \text{BF}_4^-$  confirms the coordination of the water molecule and verifies the facially substituted octahedral stereochemistry. Figure 5.5.1 is an ORTEP plot of the  $[\text{Re}(\text{CO})_3(\text{tmen})(\text{H}_2\text{O})]^+$  cation showing the atom numbering scheme.

The overall coordination about the rhenium atom approximates an octahedral geometry. The (N-Re-N) angle (bite angle of the tmen ligand) of  $81(1)^\circ$  is the only angle which deviates substantially from an octahedral geometry and is comparable with that found in  $\text{Re}(\text{CO})_3(\text{tmen})\text{Br}$  and  $\text{Re}(\text{CO})_3(\text{tmen})\text{F}$  (Chapter 3). The three carbonyl groups are in a *fac* arrangement which is consistent with the  $\nu(\text{CO})$  stretching absorption bands observed in the infrared spectrum (§ 5.2). The water molecule coordinates at a distance of  $2.22(2)\text{\AA}$  from the rhenium atom. The non-planar tmen ligand is disordered as shown in Figure 5.5.1 by the operation of the mirror plane. Separate sites exist for the C5, C5', C6 and C6' atoms, but the methyl substituents generally exhibit high temperature factors. The unusually high standard deviation in the bond lengths and bond angles is due to the disordered  $\text{BF}_4^-$  anion. The anion has the expected average (B-F) bond length of  $1.30(7)\text{\AA}$ . In the crystal lattice each  $\text{BF}_4^-$  anion is hydrogen bonded to the water molecules of two  $[\text{Re}(\text{CO})_3(\text{tmen})(\text{H}_2\text{O})]^+$  cations (Fig. 5.5.2). The hydrogen bonding distances are equal to  $2.62(7)$  and  $2.64(7)\text{\AA}$ , respectively. The closest non-hydrogen bonding intramolecular contacts are listed in Table 5.5.3 and are of the normal van der Waal distances.

TABLE 5.5.2

Atomic positional and thermal parameters for  $[\text{Re}(\text{CO})_3(\text{tmen})(\text{H}_2\text{O})]^+ \cdot \text{BF}_4^-$ 

Atom <sup>a</sup>	x	y	z	U <sub>11</sub> <sup>b</sup>	U <sub>22</sub>	U <sub>33</sub>	U <sub>23</sub>	U <sub>13</sub>	U <sub>12</sub>
Re	21391 (6)	00 (0)	46915(10)	357 (4)	568 (5)	347 (4)	00 (0)	106 (2)	00 (0)
F(1)	-245(20)	2795(15)	1128(32)	145(18)	104(14)	99(13)	18(11)	54(12)	-52(13)
F(2)	44(99)	3212(84)	1562(97)	312(57)					
F(3)	643(31)	3933(31)	733(82)	170(30)	231(43)	387(64)	-215(47)	165(39)	-135(31)
F(4)	1082(34)	3508(28)	1104(58)	108(12)					
O(1)	1588(17)	1354(11)	6928(26)	193(19)	110(12)	120(12)	-10(10)	102(13)	42(12)
O(2)	-132(14)	00 (0)	2078(34)	51(10)	246(33)	94(14)	00 (0)	9(10)	00 (0)
O(3)	3798(12)	00 (0)	6662(19)	64 (9)	90(10)	35 (6)	00 (0)	-17 (6)	00 (0)
C(1)	1787(15)	834(14)	6067(26)	90(12)	110(15)	67(10)	9(10)	37 (9)	9(11)
C(2)	757(16)	00 (0)	3039(28)	47(11)	137(23)	49(11)	00 (0)	13 (9)	00 (0)
C(3)	1756(19)	1446(14)	1784(36)	121(17)	86(14)	121(17)	66(13)	37(14)	19(13)
C(4)	3485(18)	1469(17)	4044(35)	106(16)	125(19)	117(18)	36(14)	27(14)	-47(15)
C(5)	2697(34)	369(23)	1258(47)	120(31)	84(22)	38(15)	10(14)	-5(17)	-5(21)
C(6)	3262(29)	-409(21)	2141(47)	89(22)	76(18)	51(17)	18(15)	37(16)	10(17)
N(1)	2606(11)	909 (9)	2991(19)	80 (8)	73 (8)	72 (8)	3 (7)	38 (7)	5 (7)
B(1)	00 (0)	3313(19)	00 (0)	65(13)	92(19)	37(10)	00 (0)	17 (9)	00 (0)

<sup>a</sup>Re coordinates  $\times 10^5$ , others  $\times 10^4$ <sup>b</sup>Re thermal parameters  $\times 10^4$ , others  $\times 10^3$ .

TABLE 5.5.3

Atomic Distances for  $[\text{Re}(\text{CO})_3(\text{tmen})(\text{H}_2\text{O})]^+ \cdot \text{BF}_4^-$ 

Atoms	Distance(Å)	Atoms	Distance(Å)
(a) Bond lengths (and standard deviations)			
O(3)-Re	2.239(14)	C(1)-Re	1.891(21)
C(2)-Re	1.867(20)	N(1)-Re	2.228(14)
B(1)-F(1)	1.343(26)	B(1)-F(2)	1.20 (12)
B(1)-F(3)	1.315(35)	B(1)-F(4)	1.463(44)
C(2)-O(2)	1.182(26)	C(1)-O(1)	1.167(24)
N(1)-C(4)	1.489(25)	N(1)-C(3)	1.473(24)
N(1)-C(5)	1.641(43)	C(6)-C(5)	1.493(42)
		N(1) <sup>III</sup> -C(6)	1.553(34)
(b) Hydrogen bonds			
O(3)...F(3)	2.52 (7)	O(3)...F(3) <sup>II</sup>	2.52 (7)
(c) Selected non-bonding distances			
O(1)...H(5) <sup>I</sup>	2.70 (8)	H(4)...H <sup>I</sup>	2.64 (9)
F(1)...H(2) <sup>II</sup>	2.78 (8)		

Superscript in Roman refers to the following equivalent positions, with respect to the unique asymmetric unit at x, y, z:

$$\begin{aligned} \text{I} &= -x, -y, -z \\ \text{II} &= -x, y, -z \\ \text{III} &= x, -y, z \end{aligned}$$

TABLE 5.5.4

Bond angles and standard deviations for  $[\text{Re}(\text{CO})_3(\text{tmen})(\text{H}_2\text{O})]^+ \cdot \text{BF}_4^-$ 

Atoms <sup>a</sup>	Angles(°)	Atoms	Angles(°)
C(1)-Re-O(3)	93.1 (7)	C(2)-Re-O(3)	179.8 (3)
C(2)-Re-C(1)	87.0 (8)	N(1)-Re-O(3)	85.8 (5)
N(1)-Re-C(1)	94.3 (7)	N(1)-Re-C(2)	94.0 (6)
F(2)-B(1)-F(2) <sup>I</sup>	164.5(56)	F(1)-B(1)-F(1)	103.8(32)
F(3)-B(1)-F(3) <sup>I</sup>	81.9(57)	O(1)-C(1)-Re	178.7(21)
F(4)-B(1)-F(4) <sup>I</sup>	155.3(41)	O(2)-C(2)-Re	176.3(21)
C(1)-Re-C(1)	89.8(12)	C(3)-N(1)-Re	113.5(12)
N(1)-C(5)-C(6)	105.4(21)	C(4)-N(1)-C(3)	107.0(17)
C(4)-N(1)-Re	116.6(12)	C(5)-N(1)-C(3)	95.6(19)
C(5)-N(1)-Re	105.9(15)	N(1)-Re-N(1)	81.6 (7)
C(5)-N(1)-C(4)	116.5(20)	F(3)-B(1)-F(1)	119.8(29)
F(2)-B(1)-F(1)	35.4(63)	F(4)-B(1)-F(1)	103.3(20)
F(3)-B(1)-F(2)	85.1(66)	F(4)-B(1)-F(3)	36.8(27)
F(4)-B(1)-F(2)	79.2(64)		

<sup>a</sup>Superscripts in Roman refer to the following equivalent positions, with respect to the unique asymmetric unit at x, y, z:

$$I = -x, y, -z$$

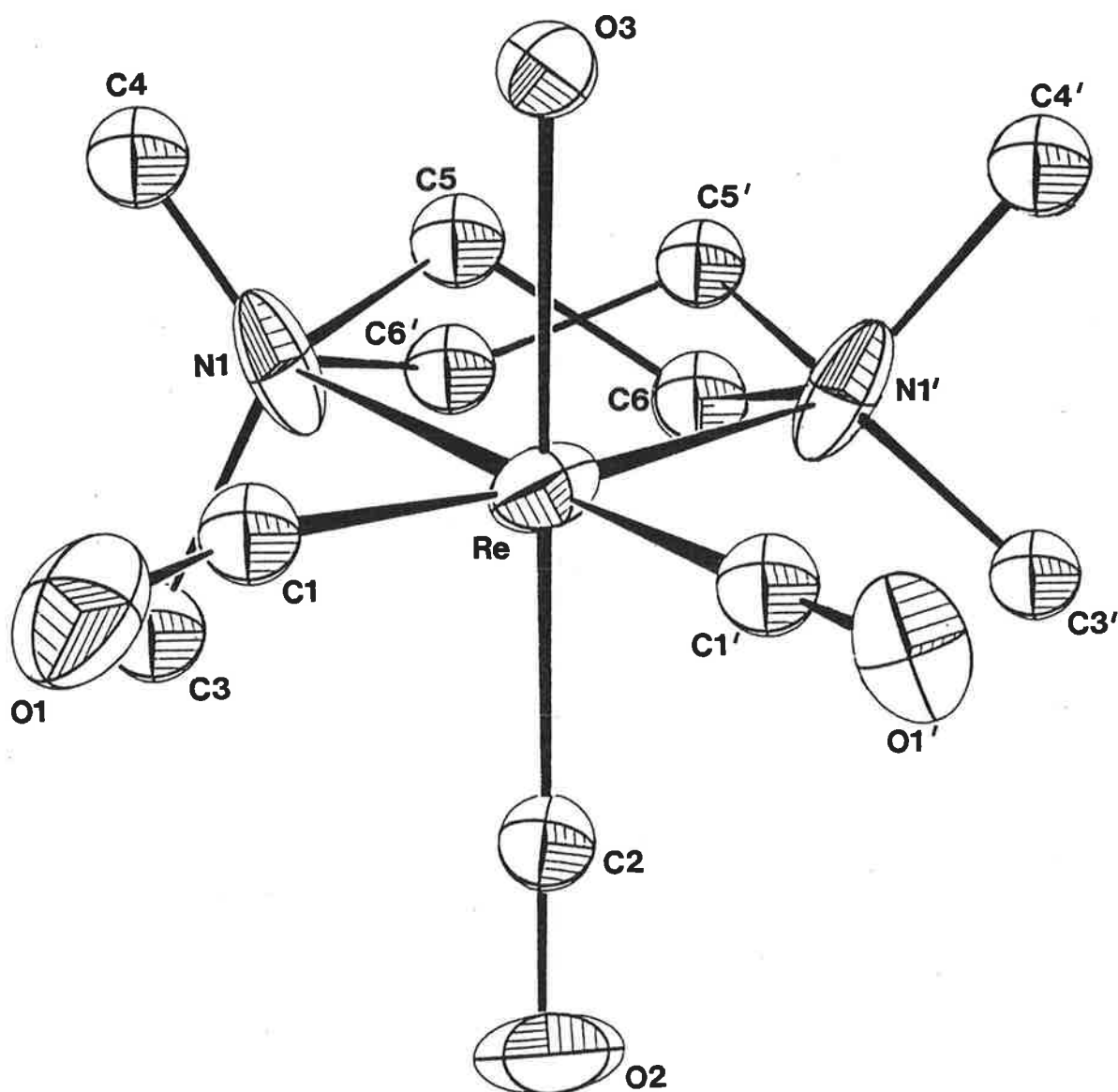
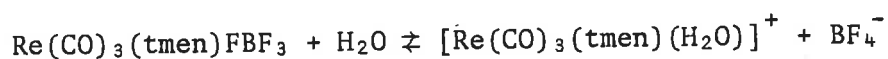


FIGURE 5.5.1. The molecular structure of the cation  $[\text{Re}(\text{CO})_3(\text{tmen})(\text{H}_2\text{O})]^+$  (30% probability ellipsoids). Superscripts in Roman refer to the following equivalent position with respect to the unique asymmetric unit at  $x, y, z$ :

$$I = x, \bar{y}, z$$

## 5.6 A $^{19}\text{F}$ N.M.R. STUDY

Fluorine is found to be an ideal nucleus for N.M.R. investigations since  $^{19}\text{F}$  is the only naturally occurring isotope, has a spin number of one half ( $I = \frac{1}{2}$ ) and hence does not possess a quadrupole moment. However, a number of difficulties can be encountered due to the element's lower sensitivity to N.M.R. detection, the low solubility of most complexes, the signal broadening at room temperature and the large range of  $^{19}\text{F}$  chemical shifts.<sup>148, 149</sup> This section reports a semi-quantitative and by no means an exhaustive  $^{19}\text{F}$  N.M.R. study of the equilibrium between coordinated and uncoordinated  $\text{BF}_4^-$  as represented by the following equation:



### 5.6.1 $^{19}\text{F}$ N.M.R. Spectra

Solutions of the complexes (Table 5.6.1) were prepared by performing the halide abstraction reactions in deuterated dichloromethane. On completion of the reaction the saturated solutions were filtered into 5 mm glass N.M.R. tubes and the proton decoupled spectra recorded within an hour to minimize the formation of the species  $\text{SiO}_n\text{F}_m$  (where,  $n = 3 - 0$ ,  $m = 1 - 6$ ) due to "glass" attack. All spectra were recorded on a Bruker HX90E N.M.R. Spectrometer (Chapter 7.2). The chemical shifts with respect to hexafluorobenzene (external reference) are given in Table 5.6.1.

The  $^{19}\text{F}$  Fourier Transform (FT) N.M.R. (84.67 MHz) spectra were recorded with low resolution (5-10 Hz/pt.), hence all signals due to the  $\text{BF}_4^-$  anion are seen as single peaks and not as the expected quartet or quintet because of the small coupling constant ( $J(^{11}\text{B} - ^{19}\text{F}) = 1 - 6 \text{ Hz}$ ).<sup>150</sup>,

<sup>151</sup> The respective  $^{19}\text{F}$  N.M.R. spectra (Table 5.6.1) of each compound shows two signals due to coordinated and uncoordinated  $\text{BF}_4^-$ . In each



TABLE 5.6.1  
Chemical Shifts of Selected Aquo-complexes

Compound	Concentration (mol dm <sup>-3</sup> )	Temperature (°K)	Chemical Shift*		Peak Ratio (a) : (b)
			(a) Coordinated BF <sup>-</sup>	(b) Free BF <sup>-</sup>	
[Re(CO) <sub>5</sub> (H <sub>2</sub> O)] <sup>+</sup> ·BF <sub>4</sub> <sup>-</sup>	0.018	300	-2846	-3809	1 : 4
[Re(CO) <sub>3</sub> (bpy)(H <sub>2</sub> O)] <sup>+</sup> ·AsF <sub>6</sub> <sup>-</sup>	0.013	300	1172	936	1 : 5
[Re(CO) <sub>3</sub> (bpy)(H <sub>2</sub> O)] <sup>+</sup> ·BF <sub>4</sub> <sup>-</sup>	0.011	300	981	962	1 : 3
[Re(CO) <sub>3</sub> (dppe)(H <sub>2</sub> O)] <sup>+</sup> ·BF <sub>4</sub> <sup>-</sup>	0.016	300	-7108	-7242	1 : 6
[Re(CO) <sub>3</sub> (tmen)(H <sub>2</sub> O)] <sup>+</sup> ·BF <sub>4</sub> <sup>-</sup>	0.024	280	-6900	-7018	4 : 3
[Fe(CO) <sub>2</sub> (Cp)(H <sub>2</sub> O)] <sup>+</sup> ·BF <sub>4</sub> <sup>-</sup>	0.034	300	-2852	-3066	1 : 3

\*The chemical shifts were measured with respect to hexafluorobenzene as the external reference.

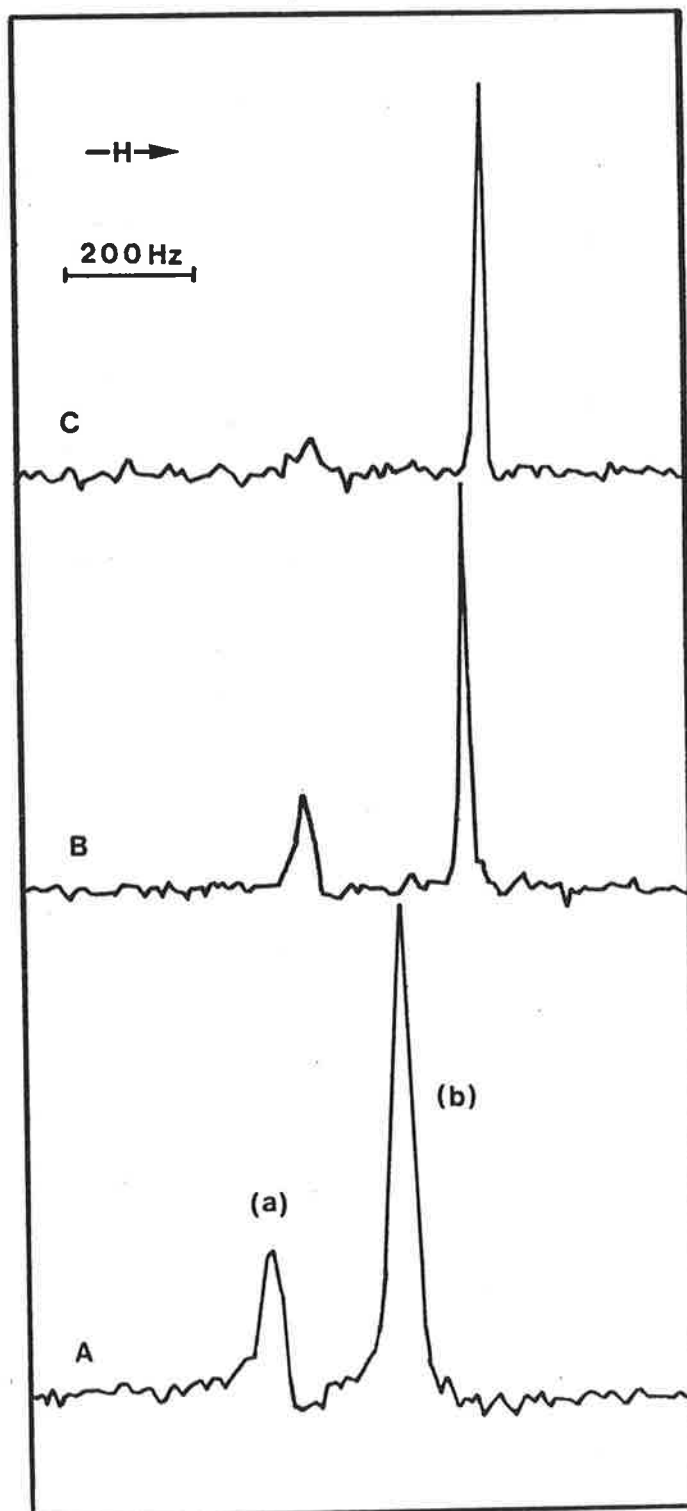


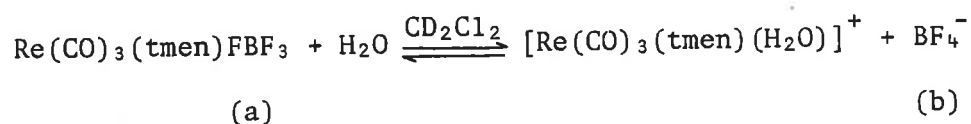
FIGURE 5.6.1.  $^1\text{H}$  decoupled  $^{19}\text{F}$  (84.67 MHz) FT N.M.R. spectra of a  $\text{CD}_2\text{Cl}_2$  solution of  $\text{Fe}(\text{CO})_2(\text{Cp})\text{BF}_4$  ( $0.03 \text{ mol dm}^{-3}$ ) containing varying amounts of  $\text{Cl}^-$ ,  $\text{I}^-$  ions and  $\text{H}_2\text{O}$ . The latter were added in order to displace the coordinated  $\text{BF}_4^-$  anion. Hence, identifying the  $^{19}\text{F}$  signals as being due to the coordinated (a) and "free" (b)  $\text{BF}_4^-$ , respectively. A is the spectrum of the Fe solution with no  $\text{Cl}^-$ ,  $\text{I}^-$  or  $\text{H}_2\text{O}$  present. B represents the solution with  $\text{Cl}^-$ ,  $\text{I}^-$  and  $\text{H}_2\text{O}$  also present. With more  $\text{H}_2\text{O}$  added spectrum C is obtained.

case the signal down field was identified as the coordinated  $\text{BF}_4^-$  anion by its disappearance on addition of traces of halide ions ( $\text{Cl}^-$ ,  $\text{I}^-$  and  $\text{H}_2\text{O}$ ) to the solution. This is illustrated by the  $^{19}\text{F}$  spectra of  $[\text{Fe}(\text{CO})_2(\text{Cp})(\text{H}_2\text{O})]^+ \cdot \text{BF}_4^-$  in  $\text{CD}_2\text{Cl}_2$ . Figure 5.6.1 shows the displacement of the coordinated  $\text{BF}_4^-$  anions by the halide ion and/or water.

### 5.6.2 Variable Temperature $^{19}\text{F}$ N.M.R.

The relatively high solubility of  $[\text{Re}(\text{CO})_3(\text{tmen})(\text{H}_2\text{O})]^+ \cdot \text{BF}_4^-$  in dichloromethane made it a suitable candidate for a variable temperature  $^{19}\text{F}$  N.M.R. study. The complex was prepared in  $d_2$ -dichloromethane and the solution (*ca.*  $0.024 \text{ mol dm}^{-3}$ ) filtered into a 5 mm N.M.R. tube. Figure 5.6.2 shows the resulting  $^1\text{H}$  decoupled  $^{19}\text{F}$  N.M.R. (84.67 MHz) spectra recorded on the Bruker HX90E Spectrometer equipped with a variable temperature unit (Chapter 7.2).

The  $^{19}\text{F}$  FT N.M.R. spectrum of  $[\text{Re}(\text{CO})_3(\text{tmen})(\text{H}_2\text{O})]^+ \cdot \text{BF}_4^-$  at  $240^\circ\text{K}$  exhibits two singlets (a) and (b) which are assigned to coordinated and free  $\text{BF}_4^-$ , respectively (§ 5.6.1). With increasing temperature the equilibrium of the following equation



is shifted to the right. The signal due to the free  $\text{BF}_4^-$  anion increases till the singlets coalesce at  $310^\circ\text{K}$ . The broad signal at coalescence is consistent with rapid exchange between the species ((a), (b)) and their lifetime was approximated at 0.1 sec. Further increase in temperature results in the disappearance of the signal (Fig. 5.6.2). This explains some of the difficulties in detecting or finding the respective  $^{19}\text{F}$  signals for the other aquo-complexes in solution studied at room temperature. The

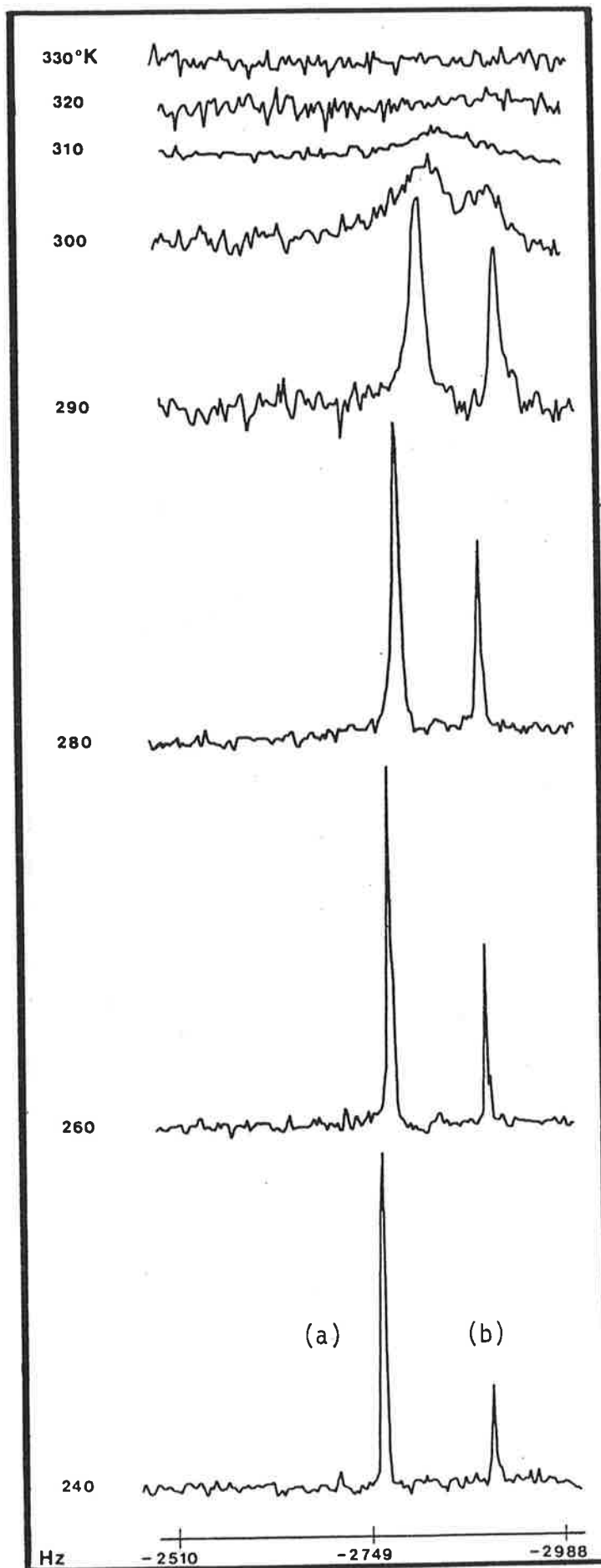
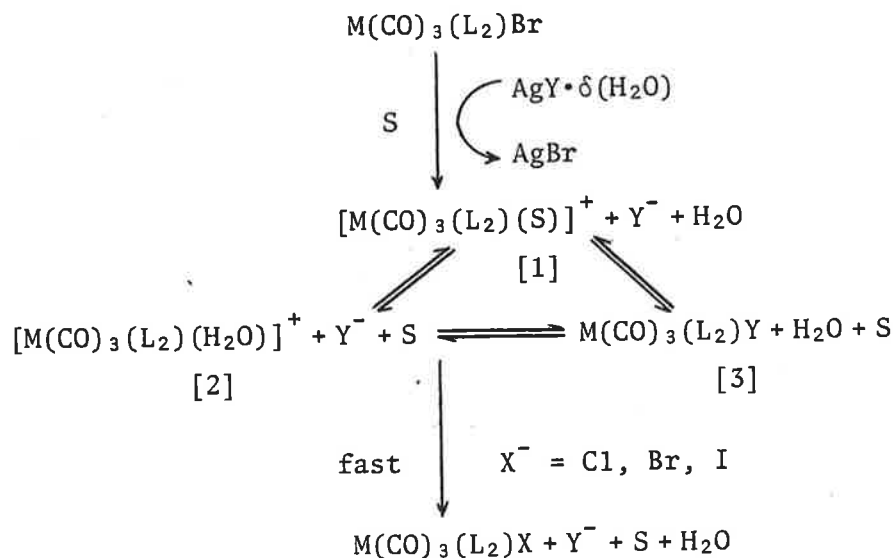


FIGURE 5.6.2.  $^1\text{H}$  decoupled  $^{19}\text{F}$  FT N.M.R. (84.67 MHz) spectra of a solution of  $[\text{Re}(\text{CO})_3(\text{tmen})(\text{H}_2\text{O})]^+\text{BF}_4^-$  ( $0.024 \text{ mol dm}^{-3}$ ) at various temperatures. The singlets (a) and (b) have been assigned to coordinated and uncoordinated  $\text{BF}_4^-$ , respectively,

experiment is reversible and a decrease in temperature resulted in the reappearance of the two singlets. The existence of the described equilibrium is consistent with the infrared data of solids obtained from the above reaction which shows both coordinated and uncoordinated  $\text{BF}_4^-$ .

## 5.7 DISCUSSION

Attempts to remove all the water from the silver salts ( $\text{AgY}$ ,  $\text{Y} = \text{AsF}_6^-, \text{BF}_4^-$ ) by their treatment with high temperatures, molecular sieves and high vacuum have failed. At best at least one half of a molecule of lattice water per silver atom remains behind. It is believed that the remaining water is held in the lattice by strong hydrogen bonding interactions with the fluoride atoms. Water ( $\delta(\text{H}_2\text{O})$ ) was always introduced into the reaction system(s) when these wet silver salts were used and thus inevitably the compounds prepared always contained some water. Infrared and N.M.R. results of the complexes reported in this chapter are consistent with the existence of an equilibrium between the three species, [1], [2] and [3], in the following general scheme.



At room temperature slow (1 - 2 days) evaporation of the solvent ( $\text{S} = \text{CH}_2\text{Cl}_2, \text{C}_6\text{H}_5\text{F}, \text{C}_6\text{F}_6$ ) results in the crystallization of the aquo species [2] exclusively. This is because the aquo complexes are the most insoluble of the three species and thus on evaporation of the solvent the equilibrium is pushed towards [2]. However, if the solvent is removed quickly (mins.) then the product isolated consists of a

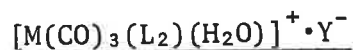
mixture of the species [2] and [3]. On the other hand, slow (*ca.* 7 days) evaporation of the solvent at low temperatures (*ca.*  $-10^{\circ}\text{C}$ ) in the presence of phosphorus pentoxide results in the isolation of only  $\text{M}(\text{CO})_3(\text{L}_2)\text{Y}\cdot\delta(\text{H}_2\text{O})$ . It is believed that the combination of factors such as the change in the solubility properties, the decrease in the amount of water and the increased stability of [3] at low temperature is responsible for the last observation.

Unlike the coordinated fluoride in the metal fluoride complexes (Chapters 2, 3 and 4), the coordinated S,  $\text{H}_2\text{O}$  and  $\text{Y}^-$  molecules in [1], [2] and [3] are very labile. In solution the three species [1], [2] and [3] are susceptible to rapid (secs.) halide ( $\text{X}^- = \text{Cl}^-$ ,  $\text{Br}^-$ ,  $\text{I}^-$ ) substitution. Potentially, therefore, the analogous metal fluoride complexes could be prepared from solutions containing [1], [2] and [3] by adding a soluble fluoride salt such as tetraphenyl ammonium fluoride.

From the crystal structure determinations of three aquo-complexes (§s 5.3, 5.4 and 5.5) the water molecule coordinates to rhenium(I) at an average distance of  $2.246(5) \text{ \AA}$ . This is significantly larger than the rhenium-fluoride bond length of  $2.040(4) \text{ \AA}$  (Chapter 3). Hence, for the rhenium complexes a coordinating atom can be identified as a fluoride or oxygen atom on the basis of the bond length (Chapter 6).

5.8 EXPERIMENTAL

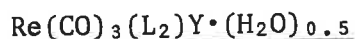
All preparations were carried out under dry conditions to minimize the introduction of any further water to the reaction solutions. However, the aquo complexes can be prepared under normal atmospheric conditions without influencing the reaction yields. The elemental analysis results are given in Table 5.8.1.



(where, 1. M = Mn, L<sub>2</sub> = 2P(OPh)<sub>3</sub>, Y<sup>-</sup> = AsF<sub>6</sub><sup>-</sup>, BF<sub>4</sub><sup>-</sup>;

2. M = Re, L<sub>2</sub> = 2(CO), bpy, 2P(OPh)<sub>3</sub>, tmen, Y<sup>-</sup> = AsF<sub>6</sub><sup>-</sup>, BF<sub>4</sub><sup>-</sup>)

To a 10 - 15 ml dichloromethane solution containing *ca.* 0.15 mmol of the respective M(CO)<sub>3</sub>(L<sub>2</sub>)Br a 50% molar excess of finely divided AgY (where, Y = AsF<sub>6</sub><sup>-</sup>, BF<sub>4</sub><sup>-</sup>) was added. The solution was subsequently stirred for 30 - 40 min., filtered and concentrated to 5 - 10 ml. Microcrystals of the products (yields, 60 - 80%) formed on addition of petroleum spirit (100 - 120°C) and cooling (*ca.* 0°C). Recrystallization was carried out from chloroform-light petroleum spirit (40 - 60°C).



(where, 1. L<sub>2</sub> = bpy, Y = AsF<sub>6</sub><sup>-</sup>;

2. L<sub>2</sub> = tmen, Y = BF<sub>4</sub><sup>-</sup>.)

These complexes were prepared in a similar way to the aqua-complexes. After the filtration step, however, the "plastic" reaction vessels were transferred to a dry nitrogen filled desiccator. The solution was stirred and allowed to evaporate over a period of 7 days at *ca.* -10°C in the presence of phosphorus pentoxide. The products were isolated in good yields (70 - 80%) and not further purified.



TABLE 5.8.1  
Elemental Analysis Results

Compound		C[%]		H[%]		F[%]		N[%]		P[%]		As[%]	
		Found	Required	Found	Required	Found	Required	Found	Required	Found	Required	Found	Required
$[\text{Re}(\text{CO})_5(\text{H}_2\text{O})]^+ \cdot \text{AsF}_6^-$	$\text{C}_5\text{H}_2\text{AsF}_6\text{O}_6\text{Re}$	11.15	11.26	0.42	0.38	21.2	21.37					14.2	14.05
$[\text{Re}(\text{CO})_5(\text{H}_2\text{O})]^+ \cdot \text{BF}_4^- \cdot (\text{H}_2\text{O})_{0.5}$	$\text{C}_5\text{H}_3\text{BF}_4\text{O}_6.5\text{Re}$	13.62	13.65	0.75	0.69	17.2	17.26						
$[\text{Mn}(\text{CO})_3\{\text{P}(\text{OPh})_3\}_2(\text{H}_2\text{O})]^+ \cdot \text{AsF}_6^- \cdot (\text{H}_2\text{O})_{0.5}$	$\text{C}_{21}\text{H}_{18}\text{AsF}_6\text{MnO}_{10.5}\text{P}_2$	33.91	33.90	2.51	2.43	15.3	15.31			8.40	8.33		
$[\text{Mn}(\text{CO})_3\{\text{P}(\text{OPh})_3\}_2(\text{H}_2\text{O})]^+ \cdot \text{BF}_4^- \cdot (\text{H}_2\text{O})_{0.5}$	$\text{C}_{21}\text{H}_{18}\text{BF}_4\text{MnO}_{10.5}\text{P}_2$	39.75	39.29	2.80	2.83	11.9	11.83			9.79	9.65		
$[\text{Re}(\text{CO})_3(\text{bpy})(\text{H}_2\text{O})]^+ \cdot \text{AsF}_6^- \cdot (\text{H}_2\text{O})$	$\text{C}_{13}\text{H}_{11}\text{AsF}_6\text{N}_2\text{O}_4.5\text{Re}$	24.49	23.96	1.66	1.86	17.2	17.48	4.15	4.30			11.6	11.50
$[\text{Re}(\text{CO})_3(\text{bpy})(\text{H}_2\text{O})]^+ \cdot \text{BF}_4^-$	$\text{C}_{13}\text{H}_{10}\text{BF}_4\text{N}_2\text{O}_4\text{Re}$	29.50	29.39	1.99	1.90	14.1	14.30	5.02	5.27				
$[\text{Re}(\text{CO})_3(\text{tmen})(\text{H}_2\text{O})]^+ \cdot \text{AsF}_6^- \cdot (\text{H}_2\text{O})$	$\text{C}_9\text{H}_{19}\text{AsF}_6\text{N}_2\text{O}_4.5\text{Re}$	18.05	17.95	3.20	3.18	19.1	18.92	4.68	4.65				
$[\text{Re}(\text{CO})_3(\text{tmen})(\text{H}_2\text{O})]^+ \cdot \text{BF}_4^- \cdot (\text{H}_2\text{O})_{0.5}$	$\text{C}_9\text{H}_{19}\text{BF}_4\text{N}_2\text{O}_4\text{Re}$	21.65	21.60	3.84	3.83	15.3	15.18	5.54	5.60				
$\text{Re}(\text{CO})_3(\text{bpy})\text{FAsF}_5 \cdot (\text{H}_2\text{O})_{0.5}$	$\text{C}_{13}\text{H}_{11}\text{AsF}_6\text{N}_2\text{O}_4.5\text{Re}$	24.89	25.01	1.50	1.78	18.3	18.25	4.52	4.49			11.87	12.00
$\text{Re}(\text{CO})_3(\text{tmen})\text{FBF}_3 \cdot (\text{H}_2\text{O})_{0.5}$	$\text{C}_9\text{H}_{19}\text{BF}_4\text{N}_2\text{O}_4.5\text{Re}$	22.57	22.42	3.50	3.97	15.6	15.75						

## CHAPTER 6

### CONCLUSION

The main objectives of this work have been achieved. Namely, to establish a facile pathway for the synthesis of metal carbonyl fluoride complexes and their characterization. Most of the success has been due to the use of anhydrous silver bifluoride. The other silver salts ( $\text{AgF} \cdot \delta(\text{H}_2\text{O})$ ,  $\text{AgAsF}_6 \cdot \delta(\text{H}_2\text{O})$  and  $\text{AgBF}_4 \cdot \delta(\text{H}_2\text{O})$ ) used always retained some lattice water ( $\delta = 0.5 - 2.5$  mole) despite heating in a high vacuum and extensive drying over phosphorus pentoxide. At best only a mixture of metal carbonyl aquo- and fluoro-complexes were obtained at room temperature when the hydrated salts were used. The role of hydrogen fluoride in silver bifluoride is therefore important in solvating the silver fluoride. Thus, preventing water solvation and the subsequent formation of aquo complexes. Furthermore, the lability of the carbonyl and triphenylphosphate ligands of the reaction intermediates,  $\text{Mn}(\text{CO})_5\text{F}$ ,  $\text{Re}(\text{CO})_5\text{F}$  and  $\text{Rh}(\text{CO})(\text{PPh}_3)_2\text{F}$  (Chapter 2) has resulted in the formation of the interesting metal fluoride cluster complexes, in which the fluorine atom is involved in  $\mu_3$ -bridging. The crystallographic data obtained from the rhenium system has allowed a comparison of the (Re-F) and (Re-O) bond lengths (§ 6.1).

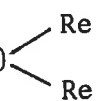
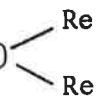
#### 6.1 RHENIUM-FLUORIDE AND -OXYGEN BOND LENGTHS

On an electronic count the fluorine and oxygen atoms differ by one electron. This small difference usually does not enable X-ray crystal structure analysis to distinguish between the atoms on the basis of their scattering powers. Hence, a combination of analysis results (i.e.

infrared absorption, mass spectroscopy, microanalysis) were required to characterize the coordination of the fluoride ion, fluoro- and oxy-anion ligands. However, with the data present in Table 6.1.1 the coordinated fluorine and oxygen atoms can be distinguished by the bonding distances to the rhenium atom. The Pauling covalent radii of the fluorine and oxygen atoms are 0.71 and 0.74 Å, respectively. While, the rhenium radius is of the order of 1.52 Å as calculated by halving the (Re-Re) bond lengths observed in polynuclear rhenium carbonyl compounds.<sup>25, 152-154</sup>

Thus, based on these values one would predict the (Re-F) and (Re-O) bonds to be equal to 2.23 and 2.26 Å, respectively. While this prediction is approximately of the correct order where the (Re-O) bond is concerned, the value for the (Re-F) bond is too large (Table 6.1.1). The average (Re-F) bond length found in the fluorine complexes,  $\text{Re}(\text{CO})_3(\text{tmen})\text{F}$  and  $[\text{Re}(\text{CO})_3(\text{tmen})\text{F}]_2\text{H}\cdot\text{HOBf}_3$  is 2.058(7) Å. While, the average (Re-O) length in the aquo complexes,  $[\text{Re}(\text{CO})_5(\text{H}_2\text{O})]^+\cdot\text{AsF}_6^-$ ,  $[\text{Re}(\text{CO})_3(\text{tmen})(\text{H}_2\text{O})]^+\cdot\text{AsF}_6^-$  and  $[\text{Re}(\text{CO})_3(\text{tmen})(\text{H}_2\text{O})]^+\cdot\text{BF}_4^-$  is 2.238(10) Å, which is significantly larger than the (Re-F) bond. However, when the coordinated fluoride is involved in other bonding (e.g. hydrogen bonding and  $\mu_2$ - or  $\mu_3$ -type bridging) the (Re-F) bond increases towards the (Re-O) distance, as is seen by comparing the respective bond lengths of the rhenium clusters,  $[\text{Re}(\text{CO})_3\text{F}]_4$  and  $[\text{Re}(\text{CO})_3(\text{OH})]_4$ .

TABLE 6.1.1  
Rhenium-fluoride and -oxygen Bond Lengths

Compounds	(Re-F,O) Bond type	Length(Å)
$\text{Re}(\text{CO})_3(\text{tmen})\text{F}^a$	<u>Re-F</u>	2.039 (4)
$[\text{Re}(\text{CO})_3(\text{tmen})\text{F}]_2\text{H}\cdot\text{HOBF}_4^a$	(i) <u>Re-F</u> ···H	2.076 (9)
	(ii) <u>Re-F</u> ··· <sup>H</sup> ···HOBF <sub>3</sub>	2.236(10)
$\text{Re}(\text{CO})_5\text{F}\cdot\text{ReF}_5^b$	(CO) <sub>5</sub> <u>Re-F</u> (μ <sub>2</sub> )-Re	2.17 (3)
$[\text{Re}(\text{CO})_3\text{F}]_4^c$	<u>Re-F</u> (μ <sub>3</sub> ) 	2.200 (5)
$[\text{Re}(\text{CO})_3(\text{OH})]_4^d$	<u>Re-O</u> (μ <sub>3</sub> ) 	2.207 (8)
$[\text{Re}(\text{CO})_5(\text{H}_2\text{O})]^+\cdot\text{AsF}_6^-^e$	<u>Re-OH</u> <sub>2</sub>	2.206 (8)
$[\text{Re}(\text{CO})_3(\text{tmen})(\text{H}_2\text{O})]^+\cdot\text{AsF}_6^-^e$	<u>Re-OH</u> <sub>2</sub>	2.268 (8)
$[\text{Re}(\text{CO})_3(\text{tmen})(\text{H}_2\text{O})]^+\cdot\text{BF}_4^-^e$	<u>Re-OH</u> <sub>2</sub>	2.239(14)

<sup>a</sup>Chapter 3, <sup>b</sup>Reference 24, <sup>c</sup>Chapter 2, <sup>d</sup>Reference 49, <sup>e</sup>Chapter 6.

## 6.2 SUGGESTIONS FOR FURTHER RESEARCH

The use of fluorinated solvents, inert reaction vessels and silver bifluoride enables pure metal (Mn, Re, Rh) fluoride complexes to be readily prepared by the halide abstraction method. However, to prove the generality of the method other metal carbonyl fluorides need to be prepared and fully characterized (Appendix 2). When applying the method to non-carbonyl metal complexes the initial characterization of the metal fluorides may be made by metal-fluoride absorption bands in their infrared spectra in the region  $200 - 600 \text{ cm}^{-1}$ . However, this will prove to be more difficult than the characterization using the  $\nu(\text{CO})$  bands. Since, absorption due to ligand bending and "rocking" modes<sup>52, 57, 58</sup> also occur in this region. Low temperature  $^{19}\text{F}$  N.M.R. spectroscopy could be a possible alternative.

Due to the limited crystallographic data available for the manganese system no (Mn-F,O) bond length comparison could be made. Thus, the crystal structure determination of a number of manganese carbonyl fluoride complexes would be useful in determining whether the trend in the bond lengths exists as is observed for the rhenium system.

## CHAPTER 7

### CRYSTALLOGRAPHY AND EXPERIMENTAL

#### 7.1 CRYSTALLOGRAPHY

##### 7.1.1 Instrumental

This chapter includes descriptions of the equations, instruments, methods and preparations used during the course of the work presented in this thesis. The descriptions in some cases are summaries only since detailed reports are available from instrumental manuals and in the literature.

##### X-ray Photography

Precession photographs were recorded with zirconium filtered molybdenum  $k_{\alpha}$  radiation ( $\lambda = 0.7107 \text{ \AA}$ ) using a Supper Buerger precession camera. While, Weissenberg films were recorded using a Nonius Weissenberg equi-inclination camera. The space group and unit cell parameters were determined from zero and upper level precession and/or Weissenberg films.<sup>77, 100, 155</sup>

##### The STOE

A STOE automated Weissenberg diffractometer equipped with a graphite monochromator was one of the diffractometers used to collect intensity data. The preliminary preparations involved the approximate alignment of a suitable crystal using the photographic technique. The crystal was then accurately centered such that a real crystal axis was aligned with the  $\omega$ - $2\theta$  rotation axis. The cell constants were refined using axial

reflections. For the data collected with the STOE diffractometer only  $\text{MoK}_\alpha$  radiation was used.

Integrative reflection intensity measurements were carried out by the  $\omega$  scan technique according to the equation:

$$\Delta\omega = A + B \left( \frac{\sin \mu}{\tan \psi/2} \right)$$

where, (1) A and B are constants chosen depending on the reflection half-widths,

(2)  $\mu$  is the equi-inclination angle, and

(3)  $\psi$  is the detector angle.

In addition, background measurements before and after each reflection were recorded. Attenuators were inserted for all reflections with intensities greater than 4000 counts per second. The count time for the final scans for reflections with lower intensities was either adjusted by factors of two to eight or the final scan omitted and the reflection assigned as weak for a prescan count rate less than 8 counts per second. A standard reflection was measured at regular intervals to monitor the instrumental stability and any crystal decomposition.

#### The CAD4

A fully automated Enraf-Nonius four-circle diffractometer (CAD4) also equipped with a graphite monochromator was the second machine used to collect crystal data. As indicated in the text both copper and molybdenum radiation was used. No preliminary photographic crystal alignment procedure was required for the CAD4. The crystals were simply centred in the X-ray beam and then the systematic search routine collected up to 25 reflections, which were used to determine the initial lattice

parameters. These were later refined by a least-squares calculation using the setting angles of 25 independent high angle reflections ( $5 < \theta < 20^\circ$ ) chosen from the data collections.

The data collection was carried out by a  $\omega - \frac{n}{3}(\theta)$  scan technique. The value of  $n$  was determined by a  $\omega/\theta$  profile and scan angle analysis which maximized the reflection to background intensity ratio for 10 reflections in the theta range  $1.2 < \theta < 20^\circ$ . The  $\omega$  scan angle and horizontal counter aperture were varied according to equations

$$\Delta\omega = (A + B \tan \theta)^\circ$$

$$\Delta A = (C + D \tan \theta) \text{ mm}$$

where, the values of  $A$ ,  $B$ ,  $C$  and  $D$  depend on the half-width of the individual reflections and the wavelength of the radiation used.

As with the data collections recorded using the STOE, the count times for the final scan measurements were determined by a prescan. Reflections with intensities  $I < 2.5\sigma(I)$  were assigned as weak and no final scan was performed. The count time for the final scan for the stronger reflections ( $I > 2.5\sigma(I)$ ) was determined by the minimum required accuracy. When the ratio  $\sigma(I)/I$  was less than a preset value then the measurement made during the prescan was accepted and no final scan was executed. At constant intervals of x-ray exposure (ca. 1 hr) the intensity of three standards were measured to check for instrumental stability and crystal decomposition.



### 7.1.2 Computing

All calculations described in this section were executed on the University of Adelaide's CYBER 173 computer.

#### Data Reduction

Lorentz and polarization corrections were applied to the STOE data collections by the reduction program AUPTP.<sup>74</sup> This program calculates the corrected reflection intensities (I) using the relation:

$$I = \frac{(P - \{t_p/t_B\} \cdot \{B_1 + B_2\}) \cdot S}{L_p \cdot A}$$

where, (1) P is the uncorrected reflection intensity;

(2)  $t_p$  and  $t_B$  are the peak scan and total background count times, respectively;

(3)  $B_1$  and  $B_2$  are the background counts on either side of the reflection;

(4)  $L_p$  is the Lorentz and polarization correction; and

(5) A and S are the attenuation factor and the scan speed, respectively.

The standard deviation ( $\sigma(I)$ ) of the reflection intensity was estimated by the equation:

$$\sigma(I) = \frac{1}{L_p} \cdot \left[ \frac{(P + \{t_p/t_B\}^2 \{B_1 + B_2\}) \cdot S^2 I^2}{A^2} \right]^{\frac{1}{2}}$$

For data collected on the CAD4 the program SUSCAD<sup>98</sup> was used to perform the data reduction. The program produces a list of structure factors (F) using the relation:

$$F = \left[ \frac{(P - 2\{B_1 + B_2\}) \cdot S}{L_p \cdot A} \right]^{\frac{1}{2}}$$

and estimates the respective standard deviations ( $\sigma(F)$ ) as:

$$\sigma(F) = \frac{1}{F} \cdot \left[ \frac{0.5[(P + 4\{B_1 + B_2\}) \cdot S]}{A} \right]^{\frac{1}{2}}$$

In addition, SUSCAD corrects for any crystal decomposition and/or any long term intensity variations resulting from instrumental instabilities.

Absorption corrections for the STOE were applied with the program SHELX.<sup>75</sup> While, for the CAD4 data the corrections were performed with the program ABSORB.<sup>99</sup> In both cases the dimensions of the crystals used in the calculations were measured with microscopes equipped with calibrated scales.

#### Solution and Refinement

The systematically absent reflections were rejected and the equivalent reflections averaged for both types of data sets (STOE, CAD4) using the program SHELX.<sup>75</sup> Reflections for which the intensity was  $I < 2.5\sigma(I)$  were also omitted.

SHELX<sup>75</sup> has allowed for both a least-square full-matrix or blocked-matrix refinement of the atomic parameters by minimizing the function:

$$\sum w(|F_O| - |F_C|)^2$$

where,  $F_O$  and  $F_C$  are the observed and calculated structure factors. The anisotropic motion of atoms were modelled as ellipsoids of the form  $\exp[-2\pi^2(U_{11}h^2a^{*2} + U_{22}k^2b^{*2} + U_{33}l^2c^{*2} + 2U_{12}hka^*b^* + 2U_{13}hla^*c^* + 2U_{23}klb^*c^*)]$

In final refinement calculations the following weighting scheme was employed

$$w = \frac{k}{(\sigma^2\{F_O\} + |g|F_C^2)}$$

and the values  $k$  and  $g$  were refined. The residual indices ( $R$ ,  $R_w$ ) or

discrepancy factors were determined as

$$R = \frac{\sum (|F_o| - |F_c|)}{\sum |F_o|}$$

$$R_w = \frac{\sum (|F_o| - |F_c|) \cdot \sqrt{w}}{\sum (|F_o| \sqrt{w})}$$

The absolute configuration of a molecule (Chapter 5) determined by re-calculating the final refinement with the signs of all the atomic coordinates changed.<sup>156</sup> The correct configuration was chosen on the basis of the lower R value using Hamilton's significance test.<sup>157</sup>

The centricity of the distribution of reflection intensities was determined from the E-statistics (where, E is the normalized structure factor<sup>158</sup>). The SHELX<sup>75</sup> program was employed to calculate the value of  $|E^2 - 1|$  as a function of  $\sin\theta$ . A structure was considered centrosymmetric and non-centrosymmetric if the average  $|E^2 - 1|$  was approximately equal to 0.968 and 0.736, respectively.<sup>159</sup>

In the final calculation SHELX<sup>75</sup> was also used to determine the bond lengths, bond angles, the respective standard deviations and the non-bonded distances. The observed and calculated structure factors for each structure as tabulated by the program are given on microfiche in the back of this thesis. The molecular structures were plotted by the programs ORTEP<sup>78</sup> and PLUTO.<sup>144</sup>

## 7.2 EXPERIMENTAL

### 7.2.1 General

The preparations and reactions described in this work were carried out in a nitrogen atmosphere, dried using phosphorus pentoxide. A dry box equipped with a connection to a vacuum line was used for all reaction transfers and for the isolation of the products. All non-volumetric glassware was dried in an oven at *ca.* 120°C for a minimum of four hours before use. For short term storage (2 - 3 weeks) the compounds were kept in a desiccator in the dark at room temperature. For longer periods the compounds were stored at *ca.* 0°C over phosphorus pentoxide. Crystallizations were carried out in either the dry box environment at room temperature or in a desiccator placed in a refrigerator at 0°C. Precautions should be taken when undertaking large scale preparations involving the potentially hazardous silver bifluoride to ensure that the laboratory is sufficiently ventilated to remove any hydrogen fluoride gas given off during the reactions.

### 7.2.2 Physical Measurements and Instrumentation

#### Balances

A Mettler H16 balance was used to measure the weights of the precursors and reagents for the preparation of the fluoro-complexes. While, for the routine preparations of the precursors a Sartorius 1202 MP balance with a precision of  $\pm 0.005$  g was used.

#### Elemental Analyses

The elemental microanalyses (C, H, B, F, N, P) were executed by the Australian Microanalytical Service, Melbourne. The samples were sealed

in tubes filled with dry nitrogen and protected from light before they were sent to Melbourne.

### Infrared Spectra

All infrared spectra were recorded using a Perkin Elmer 457 double beam grating spectrometer calibrated with carbon monoxide gas and polystyrene. Solution spectra were recorded in the range 2500 - 1500  $\text{cm}^{-1}$  using calcium fluoride cells. Complete spectra (4000 - 400  $\text{cm}^{-1}$ ) were recorded as nujol mulls between NaCl or KBr plates. The nujol and solvents ( $\text{CH}_2\text{Cl}_2$ ,  $\text{C}_6\text{H}_5\text{F}$ ,  $\text{C}_6\text{F}_6$ ) were dried over Linde 4A molecular sieves before use.

### Mass Spectra

Mass spectra were recorded on an AEI MS 30 spectrometer with a 70 eV beam. No satisfactory spectra were obtained for the aquo-complexes. Their spectra showed no signals corresponding to the molecular ions or the fragmentation species.

### N.M.R. Spectra

$^{19}\text{F}$  broad band proton decoupled Fourier transform N.M.R. spectra were recorded at 84.67 MHz on a Bruker HX-90-E spectrometer. Spectra of the compounds dissolved in dry deuteriochloroform or deuterodichloromethane were recorded on the spectrometer (with  $^2\text{H}$  lock) using 5 mm tubes. For the variable temperature work a copper-constantan thermocouple<sup>160</sup> was employed to maintain a stable temperature ( $\pm 0.3^\circ \text{K}$ ).

### 7.2.3 Gas, Ligands, Reagents and Solvents

#### Gas

The high purity nitrogen supplied by Commonwealth Industrial Gases (CIG) was dried using phosphorus pentoxide and concentrated sulphuric acid.

#### Ligands and Reagents

The ligands listed below were stored in the dark and used without further purification.

Ligand	Origin	Purity
bpy	BDH	LR
DIPHOS	Stream Chemicals	AR
PPh <sub>3</sub>	BDH	LR
P{OPh} <sub>3</sub>	BDH	LR
SbPh <sub>3</sub>	Stream Chemicals	AR
tmen	Fluka	AR

#### Reagents

Manganese and rhenium carbonyl (Stream Chemicals) were stored at -15°C and used as supplied by the manufacturer. Silver bifluoride (Ozark-Mahoning), silver hexafluoroarsenate (Ozark-Mahoning) and silver perchlorate (Pfaltz-Bauer) were stored in a desiccator protected from direct light and used in a dry box environment.

#### Silver Fluoride

Brauer's method<sup>166</sup> was used to prepare silver fluoride from silver carbonate and hydrofluoric acid. The reaction was carried out in a plastic vessel, the solution was then filtered, dried *in vacuo* and the

yellow product was subsequently stored in a desiccator in the dark. However, despite extensive pumping on the vacuum line (6 - 8 hrs) and heating to *ca.* 60°C, some lattice water ( $\delta(\text{H}_2\text{O})$ ) always remained.

#### Silver Tetrafluoroborate

Silver tetrafluoroborate was prepared from silver carbonate by adding aqueous fluoroboric acid (40%) until the evolution of carbon dioxide had stopped. The solution was then filtered and dried on a vacuum line to give the white product.<sup>114</sup> As in the case of silver fluoride, warming (50 - 60°C) the product under high vacuum for a period of six to eight hours failed to remove the lattice water. The reagent was stored in a desiccator over phosphorus pentoxide and manipulated in an atmosphere of dry nitrogen.

#### Solvents

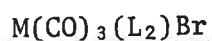
All the solvents (AR grade) used were dried over Linde 4A molecular sieves for a minimum of three days before use.

#### 7.2.4 Preparation of the Precursors



Manganese and rhenium pentacarbonyl bromide were prepared by the method described by Abel and Wilkinson.<sup>7,162</sup> Bromine (1.48 g, 9.26 mmol) was added to the respective metal carbonyl precursor (6.41 mmol) dissolved in carbon tetrachloride (*ca.* 30 ml) and the mixture was then stirred for one hour at *ca.* 40°C. The product was removed from solution by filtration, dried *in vacuo* and finally sublimed (50°C, 0.1 mm) giving yields of the order of 85%.

- (1.  $\text{Mn}(\text{CO})_5\text{Br}$ :  $\nu(\text{CO})$  2145w, 2060vs, 2017s  $\text{cm}^{-1}$ ;
2.  $\text{Re}(\text{CO})_5\text{Br}$ :  $\nu(\text{CO})$  ; ( $\text{CH}_2\text{Cl}_2$  solution))



- (where, 1.  $M = \text{Mn}$ ,  $\text{L}_2 = \text{bpy, DIPHOS, 2(PPh}_3), 2(\text{P}\{\text{OPh}\}_3), \text{tmen}$ ;  
 2.  $M = \text{Re}$ ,  $\text{L}_2 = \text{bpy, dpe, 2(P}\{\text{OPh}\}_3), 2(\text{SbPh}_3), \text{tmen}$ )

These compounds were prepared by the general method developed in the literature<sup>69,163,164</sup> for the preparation of substituted carbonyl halides of manganese and rhenium. In each case a molar excess (15-20%) of the respective ligand was added to the pentacarbonyl bromide complex (0.2 - 0.5 g) dissolved in petroleum ether (25 - 50 ml) and then the reaction mixture was stirred for *ca.* 30 min. at 110-120°C. After cooling the tricarbonyl bromides<sup>were</sup> filtered and washed with diethylether to remove the excess ligand. Recrystallization was carried out from chloroform - light petroleum (40-60°C) to give the product with yields ranging from 60 to 80%. The compounds were subsequently dried *in vacuo*, stored in a desiccator over phosphorus pentoxide and shielded from light. All complexes were characterized by their infrared absorption spectra in the carbonyl region.



Rh(CO)(PPh<sub>3</sub>)<sub>2</sub>Cl

The title compound was prepared from RhCl<sub>3</sub>·(H<sub>2</sub>O)<sub>3</sub> using the method reported by Evans, Osborn and Wilkinson.<sup>164</sup> A hot ethanol solution (ca. 8 ml) containing RhCl<sub>3</sub>·(H<sub>2</sub>O)<sub>3</sub> (ca. 0.20 g) was added to a boiling ethanol solution (ca. 30 ml) containing triphenyl phosphine (ca. 0.72 g). Formaldehyde (38%, 1.5 ml) was added causing the red solution to turn yellow. On cooling the yellow product was isolated and recrystallized from benzene (yield, ca. 45%).

( $\nu(\text{CO})$  1972 cm<sup>-1</sup> (CH<sub>2</sub>Cl<sub>2</sub> solution))

Os(CO)(Cp)(PPh<sub>3</sub>)Br

This complex was kindly prepared by A.G. Swincer from CpOs(PPh<sub>3</sub>)<sub>2</sub>Br using the literature method.<sup>165</sup> The precursor was carbonylated (70°/150 atm) in benzene for ca. 48 hr. Filtration and evaporation of the solution preceded the crystallization of a mixture of orange and yellow crystals (CpOs(PPh<sub>3</sub>)(CO)Br) from acetate-methanol. The yellow product was separated from the starting material by recrystallization from CH<sub>2</sub>Cl<sub>2</sub>/n-hexane.

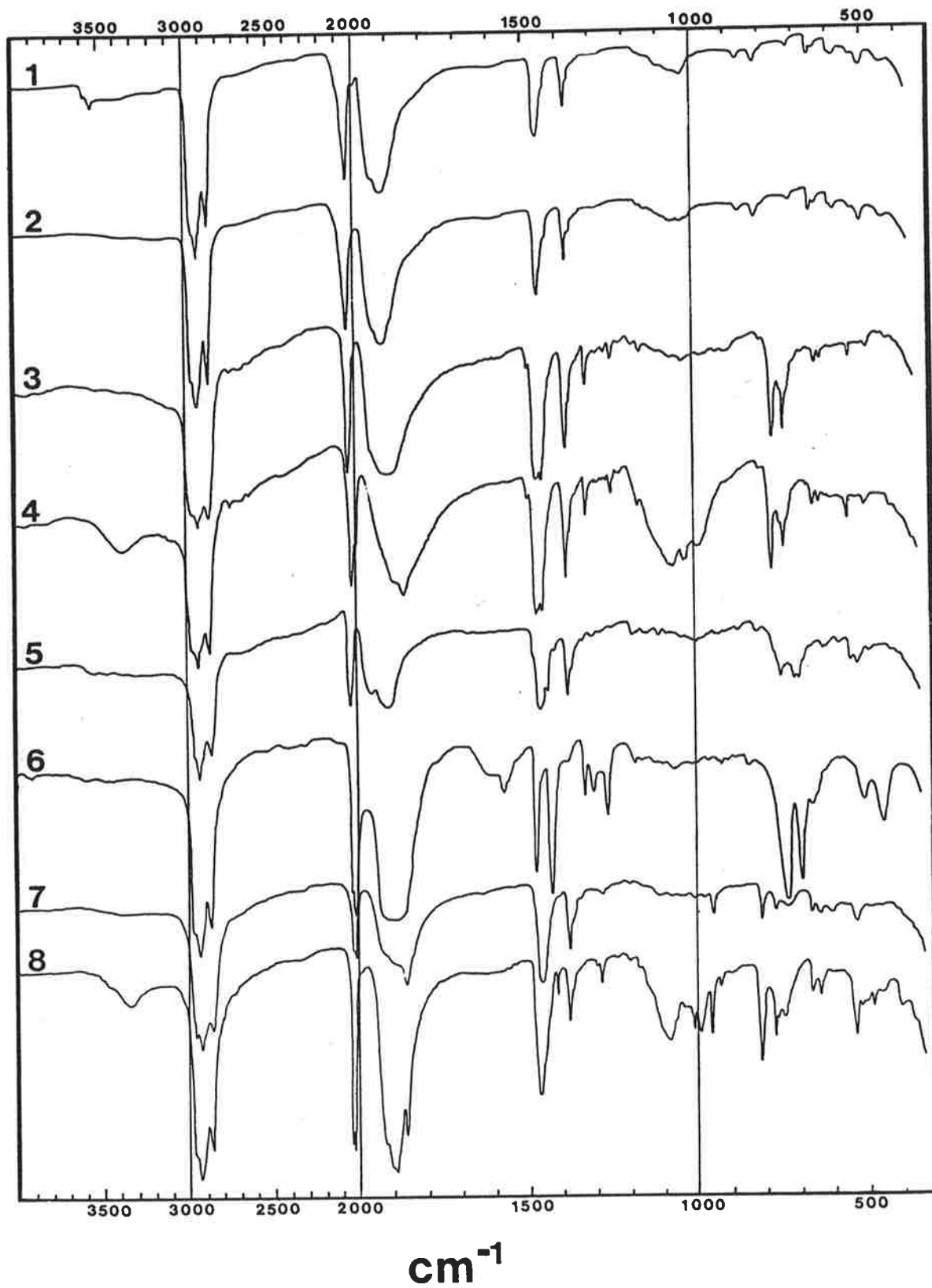
( $\nu(\text{CO})$  1940 s, CH<sub>2</sub>Cl<sub>2</sub>)

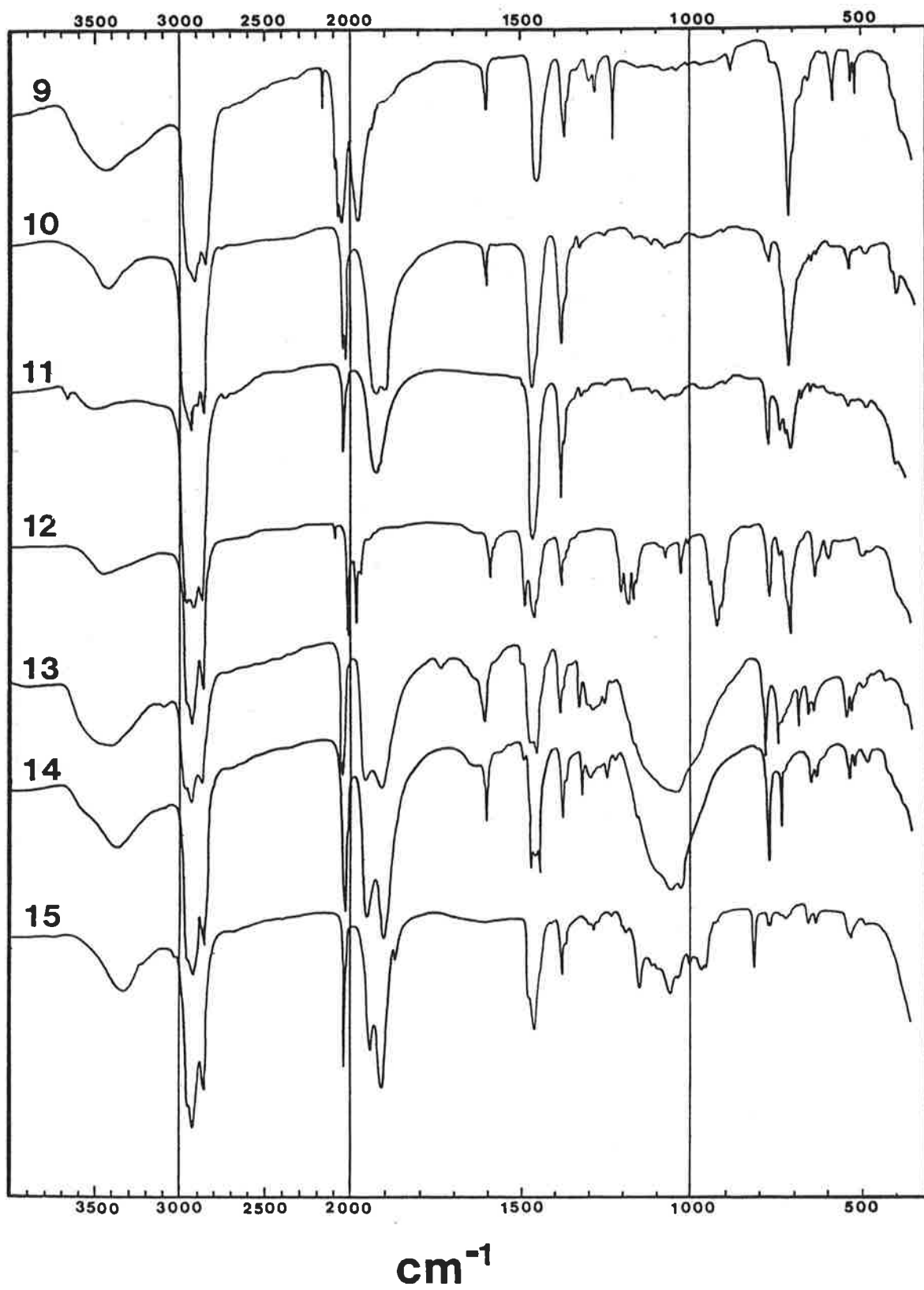
## APPENDIX 1

### SELECTED SOLID STATE INFRARED SPECTRA

The complete nujol spectra ( $4000 - 400 \text{ cm}^{-1}$ ) of a selected number of previously unreported complexes are presented in this Appendix. The number to the left of the spectra correspond to the complexes given below:

1.  $[fac-Re(CO)_3F]_4 \cdot (H_2O)_4$
2.  $[fac-Re(CO)_3F]_4$
3.  $fac-Re(CO)_3(bpy)F$
4.  $[fac-Re(CO)_3(bpy)F]_2H \cdot HOBF_3$
5.  $fac-Re(CO)_3(dpe)F$
6.  $mer-Re(CO)_3(SbPh_3)_2F$
7.  $fac-Re(CO)_3(tmen)F$
8.  $[fac-Re(CO)_3(tmen)F]_2H \cdot HOBF_3$
9.  $[Re(CO)_5(H_2O)]^+ \cdot AsF_6^-$
10.  $[fac-Re(CO)_3(bpy)(H_2O)]^+ \cdot AsF_6^- \cdot \delta(H_2O)$
11.  $fac-Re(CO)_3(bpy)FAsF_5 \cdot \delta(H_2O)$
12.  $[mer-Mn(CO)_3(P\{OPh\}_3)_2(H_2O)]^+ \cdot AsF_6^-$
13.  $[fac-Re(CO)_3(bpy)(H_2O)]^+ \cdot BF_4^- \cdot \delta(H_2O)$
14.  $[fac-Re(CO)_3(tmen)(H_2O)]^+ \cdot BF_4^- \cdot \delta(H_2O)$
15.  $fac-Re(CO)_3(tmen)FBF_3 \cdot \delta(H_2O)$





## APPENDIX 2

### OTHER POSSIBLE METAL CARBONYL FLUORIDE COMPLEXES

The halogen abstraction technique described in this thesis was used with a few other transition metal carbonyls to test its generality for coordinating fluoride. The products of the reactions given in this Appendix have only been characterized by infrared spectroscopy and/or are un-identified decarbonylation by-products. In both cases further analysis or experimentation is required.

#### PREPARATION OF $M(\text{CO})(\text{Cp})(\text{PPh}_3)\text{F}$

(where, M = Os and Ru)

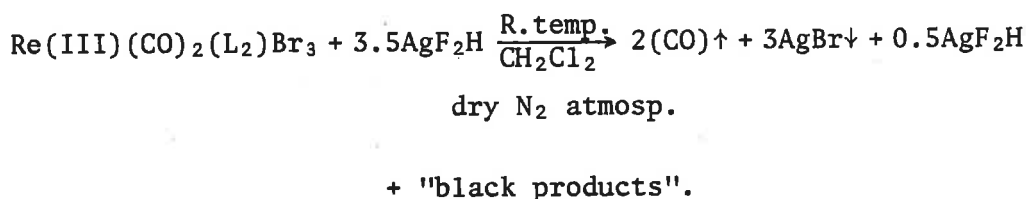
To dichloromethane solutions (*ca.* 5 ml) containing 0.05 - 0.10 mmol of the dissolved  $\text{Os}(\text{CO})(\text{Cp})(\text{PPh}_3)\text{Br}$  and  $\text{Ru}(\text{CO})(\text{Cp})(\text{PPh}_3)\text{Cl}$  complexes<sup>165</sup> finely divided silver bifluoride (0.1 - 0.2 mmol) was added. The reaction mixtures were stirred in polyethylene vessels for *ca.* 30 minutes under the dry nitrogen atmosphere of a dry box. The silver halides (F(excess), Cl and Br) were moved by filtration and the solutions dried *in vacuo*. In each case the  $\nu(\text{CO})$  stretching band of the osmium and ruthenium "fluorides" was observed at a higher frequency than the respective bromide and chloride complexes, as expected (Chapter 1.3). This change in the  $\nu(\text{CO})$  stretching frequency was also accompanied by a colour change (see below). The full nujol spectra of the "fluoride" complexes showed no absorption due to either coordinated or lattice water (Chapter 5.2.3(a))

		$\nu(\text{CO}) (\text{cm}^{-1})$	medium
$\text{Os}(\text{CO})(\text{Cp})(\text{PPh}_3)\text{Br}$	(yellow)	1940s	$\text{CH}_2\text{Cl}_2$
" $\text{Os}(\text{CO})(\text{Cp})(\text{PPh}_3)\text{F}$ "	(yellow/orange)	1957s 1946s	$\text{CH}_2\text{Cl}_2$ nujol
$\text{Ru}(\text{CO})(\text{Cp})(\text{PPh}_3)\text{Cl}$	(brown/red)	1963s	$\text{CH}_2\text{Cl}_2$
" $\text{Ru}(\text{CO})(\text{Cp})(\text{PPh}_3)\text{F}$ "	(yellow/brown)	1976s 1976s	$\text{CH}_2\text{Cl}_2$ nujol

REACTION OF  $\text{Re(III)(CO)}_2(\text{L}_2)\text{Br}_3$  WITH  $\text{AgF}_2\text{H}$

(where,  $\text{L}_2 = \text{bpy, diphos and phen}$ )

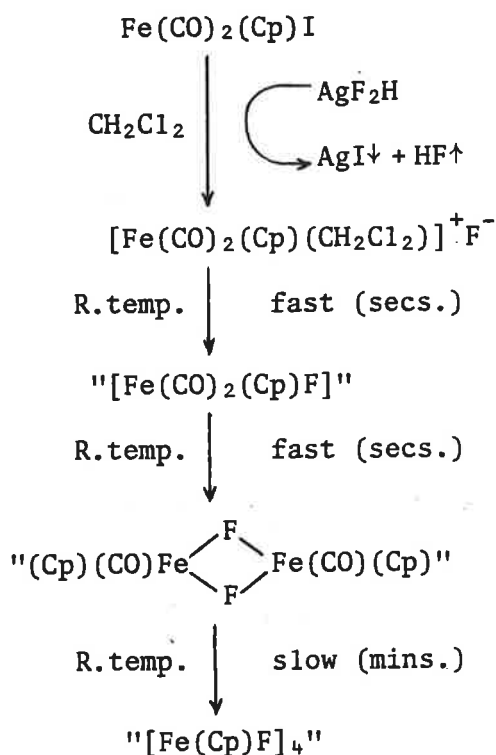
All reactions of the seven coordinated rhenium (III) carbonyl bromide complexes<sup>166</sup> with silver bifluoride resulted in decarbonylation and the formation of unidentified insoluble black products:



Hence, no further work was carried out.

REACTION OF  $\text{Fe(CO)}_2(\text{Cp})\text{I}$  WITH  $\text{AgF}_2\text{H}$

When  $\text{Fe(CO)}_2(\text{Cp})\text{I}$  (ca. 0.10 mmol) was reacted with silver bifluoride (ca. 0.15 mmol) in dichloromethane at room temperature the solution changed from a dark brown to a red colour. The initial precipitation of silver iodide was followed by the rapid formation of an insoluble brown product, which exhibited no  $\nu(\text{CO})$  or  $\nu(\text{OH})$  stretching bands in the infrared spectrum. The infrared spectrum of the reaction mixture in the carbonyl region indicate the presence of two soluble species. The two  $\nu(\text{CO})$  absorption bands at high frequency are consistent with the presence of the iron fluoride complex, " $\text{Fe(CO)}_2(\text{Cp})\text{F}$ ". While, the absorption band at  $1960 \text{ cm}^{-1}$  is most likely due to an iron-carbonyl-fluoride dimeric species. With time the filtered reaction mixture became lighter in colour (brown-red) and the  $\nu(\text{CO})$  bands disappeared. Presumably, the species in solution were the intermediates in the formation of the brown-red product, which is postulated to be the iron fluoride cluster complex, " $[\text{Fe(Cp)F}]_4$ ". The proposed reaction scheme leading to the formation of the cluster is given below:



Further work is required in this system. Firstly, to attempt to isolate the intermediate species by performing the above reaction at lower temperature (*ca.* 0°C). Secondly, to fully characterize the iron "cluster" by a crystal structure determination and microanalysis.

		$\nu(\text{CO}), (\text{cm}^{-1})$	medium
$\text{Fe(CO)}_2(\text{Cp})\text{I}$	brown	2035s, 1999s	$\text{CH}_2\text{Cl}_2$
" $\text{Fe(CO)}_2(\text{Cp})\text{F}$ "	red	2054s, 2016s	$\text{CH}_2\text{Cl}_2$
" $[\text{Fe(CO)(CpF)}_2]$ "	red	1960m	$\text{CH}_2\text{Cl}_2$

## LIST OF PUBLICATIONS

The publications containing some of the material reported in this thesis are given below:

1. "Tetranuclear Carbonylfluorohydroxymanganese(I) Clusters,  $[\text{Mn}_4(\text{CO})_{12}\text{F}_x(\text{OH})_{4-x}]$ ", Horn, E., Snow, M.R. and Zeleny, P.C., *Aust. J. Chem.*, 1980, 33, 1659.
2. "Perchlorate and Difluorophosphate Coordination Derivatives of Rhenium Carbonyl", Horn, E. and Snow, M.R., *Aust. J. Chem.*, 1980, 33, 2369.
3. "A Tetranuclear Carbonyl Fluoro Rhenium(I) Cluster,  $[\text{Re}(\text{CO})_3\text{F}]_4 \cdot (\text{H}_2\text{O})_4$ ", Horn, E. and Snow, M.R., *Aust. J. Chem.*, 1981, 34, 737.
4. "Coordinated Fluoride in Rhenium(I) Carbonyl Complexes", Horn, E. and Snow, M.R., *Aust. J. Chem.*, 1983, (in print).
5. "Manganese(I) and Rhenium(I) Carbonyl Aquo Complexes", Horn, E. and Snow, M.R., 1983, (manuscript in progress).



## REFERENCES

1. Mond, L., Langer, C. and Quinke, F., *J. Chem. Soc.*, 1890, 57, 749.
2. Mond, L., *J. Soc. Chem. Ind.*, 1895, 14, 945.
3. Abel, E.W., *Quart. Rev.*, 1963, 17, 133.
4. Abel, E.W. and Stone, F.G.A., *Quart. Rev.*, 1969, 23, 325.
5. Abel, E.W. and Stone, F.G.A., *Quart. Rev.*, 1970, 24, 498.
6. Calderazzo, F., "Halogen Chemistry" Vol. 3, Gutmann, V., Ed., Academic Press, London, 1967, p. 383.
7. Abel, E.W. and Wilkinson, *J. Chem. Soc.*, 1959, 1501.
8. Chatt, J., Pauson, P.L. and Venanzi, L.M. in H.H. Zeiss, (Ed.), *Organometallic Chemistry*, ACS Monograph No. 147, Reinhold, New York, N.Y., 1960, 509.
9. Brimm, E.O., Lynch, Jr., M.A. and Sesney, W.J., *J. Amer. Chem. Soc.*, 1954, 76, 3831.
10. Chaudhuri, M.K., Kaschani, M.M. and Winkler, D., *J. Organomet. Chem.*, 1976, 113, 387.
11. Horn, E., Snow, M.R. and Zeleny, P.C., *Aust. J. Chem.*, 1980, 33, 1659.
12. Snow, M.R. and Wimmer, F.L., *Aust. J. Chem.*, 1976, 29, 2349.
13. Marks, T.J. and Seyam, A.M., *Inorg. Chem.*, 1974, 13, 1624.
14. Wimmer, F.L. and Snow, M.R., *Aust. J. Chem.*, 1978, 31, 267.
15. Horn, E. and Snow, M.R., *Aust. J. Chem.*, 1980, 33, 2369.
16. Mews, R., *Angew. Chem. internat. Edit.*, 1975, 14, 640.
17. Cihonski, J.L. and Levenson, R.A., *Inorganica Chimica Acta*, 1976, 18, 215.
18. Abel, E.W. and Towle, D.H., *J. Chem. Soc. (Dalton Trans.)*, 1979, 1943.

19. Lewis, H.C. and Storhoff, B.N., *J. Organomet. Chem.*, 1972, 43, 1.
20. Colton, R. and Garrard, J.E., *Aust. J. Chem.*, 1973, 26, 1781.
21. Hargreaves, G.B. and Peacock, R.D., *J. Chem. Soc.*, 1960, 1099.
22. O'Donnell, T.A., Phillips, K.A. and Waugh, A.B., *Inorg. Chem.*, 1973 12, No. 6, 1435.
23. O'Donnell, T.A. and Phillips, K.A., *Inorg. Chem.*, 1972, 11, No. 10, 2563.
24. Bruce, D.M., Holloway, J.H. and Russell, D.R., *J. Chem. Soc. Chem. Comm.*, 1973, 321.
25. Bruce, D.M., Holloway, J.H. and Russell, D.R., *J. Chem. Soc. Dalton Trans.*, 1978, 64.
26. Bruce, D.M., Hewitt, A.J., Holloway, J.H., Peacock, R.D. and Wilson, I.L., *J. Chem. Soc. Dalton Trans.*, 1976, 2230.
27. Bruce, D.M. and Holloway, J.H., *Transition Met. Chem.*, 1978, 3, 217.
28. Isobe, K., Nanjo, K., Nakamura, Y. and Kawaguchi, S., *Chem. Letters*, 1979, 1193.
29. Mattson, B.M. and Graham, W.A.G., *Inorg. Chem.*, 1981, 20, 3186.
30. Horn, E. and Snow, M.R., *Aust. J. Chem.*, 1980, 33, 2369.
31. Peone, J. Jr. and Vaska, L., *Angew. Chem. Internat. Edit.*, 1971, 10, No. 7, 511.
32. Beck, W. and Schlöter, K., *Z. Naturforsch.*, 1978, 33b, 1214.
33. Wada, M. and Oguro, K., *Inorg. Chem.*, 1976, 15, 2346.
34. Uson, R., Royo, P. and Gimeno, J., *J. Organomet. Chem.*, 1974, 72, 299.
35. Johnson, M.D. and Winterton, N., *J. Chem. Soc. (A)*, 1970, 511.

36. Colton, R. and Knapp, J.E., *Aust. J. Chem.*, 1972, 25, 9.
37. Cihonski, J.L. and Levenson, R.A., *Inorg. Chem.*, 14, 1975, 1717.
38. White, J.F. and Farona, M.F., *J. Organomet. Chem.*, 1972, 37, 119.
39. Vaska, L. and Peone, Jr., J., *Inorg. Syn.*, 1974, 15, 64.
40. Gregorio, G., Pregaglia, G. and Ugo, R., *Inorg. Chim. Acta.*, 1969, 3, 89.
41. Reed, C.A. and Roper, W.R., *J. Chem. Soc. (Dalton Trans.)*, 1973, 1370.
42. Hieber, W. and Rieger, K., *Z. anorg. allg. Chem.*, 1959, 300, 288.
43. Hieber, W., Englert, K. and Rieger, K., *Z. anorg. allg. Chem.*, 1959, 300, 295 and 304.
44. Hieber, W. and Englert, K., *Z. anorg. allg. Chem.*, 1959, 300, 311.
45. Herberhold, M., Wehrmann, F., Neugebauer, D. and Huttner, G., *J. Organomet. Chem.*, 1978, 152, 329.
46. Reimann, R.H. and Singleton, E., *J. Chem. Soc. Dalton*, 1974, 808.
47. Herberhold, M., Süß, G., Ellermann, J. and Gäbelein, *Chem. Ber.*, 1978, 111, 2931.
48. Herberhold, M. and Süß, G., *Angew. Chem. Internat. Edit.*, 1975, 14, 700.
49. Nuber, B., Oberdorfer, F. and Ziegler, M.L., *Acta Cryst.*, 1981, B37, 2062.
50. Cotton, F.A. and Kraihanzel, C.S., *J. Amer. Chem. Soc.*, 1962, 84, 4432.
51. Cotton, F.A. and Wilkinson, G., in "Advanced Inorganic Chemistry", 1980, 4th edit., John Wiley and Sons, p. 82 and p. 1049.

52. Coulson, C.A. in "*Valency*", 1961, 2nd edit., Oxford University Press, p. 222.
53. Braterman, P.S. in "*Metal Carbonyl Spectra*", 1975, Acad. Press.
54. Dobson, G.R., Stolz, I.W. and Shelton, R.K., *Adv. Inorg. Chem. Radiochem.*, 1965, 8, 1.
55. Hamilton, W.C., *Acta Cryst.*, 1965, 18, 502.
56. Haines, L.M. and Stiddard, M.H.B., *Adv. Inorg. Chem. Radiochem.*, 1969, 12, 53.
57. Nakamoto, K. in "*Infrared and Raman Spectra of Inorganic and Coordination Compounds*", 1978, 3rd edit., John Wiley and Sons, p. 279.
58. Adams, D.M. in "*Metal-Ligand and Related Vibrations*", 1967, Edward Arnold Ltd., p. 146 and p. 149.
59. Orgel, L.E., *Inorg. Chem.*, 1962, 1, No. 1, 25.
60. Angelici, R.J., Basolo, F. and Poë, A., *J. Amer. Chem. Soc.*, 1963, 85, 2215.
61. Wilson, Z., *Naturforsch.*, 1958, 13b, 349.
62. Hieber, W. and Wagner, G., *Z. Naturforsch.*, 1958, 13b, 339.
63. Coffield, Kozikowski and Closson, *J. Org. Chem.*, 1957, 22, 598.
64. Dahl, L.R. and Morton, S., *Acta Crystallogr.*, 1963, 16, 611.
65. Green, P.T. and Bryan, R.F., *J. Chem. Soc. A*, 1971, 1559.
66. Clegg, W. and Morton, S., *Acta Crystallogr., Sect. B*, 1978, 34(5), 178, 1707.
67. Cihonski, J.L. and Levensen, R.A., *Inorg. Chim. Acta*, 1976, 18, 215.
68. Hieber, W. and Schulten, H., *Z. Anorg. Allgem.*, 1939, 243, 164.

69. Hieber, W., Schuh, R. and Fuchs, *J. Inorg. Chem.*, 1911, 248, 213.
70. Abel, E.W., Butler, L.S., Ganorkar, M.C., Jenkins, C.R. and Maid, H.B., *Inorg. Chem.*, 1966, 5, 25.
71. Beck, W. and Schloter, K., *Z. Naturforsch.*, 1978, 33b, 1214.
72. Nyholm, R.S., Truter, M.R. and Bradford, C.W., *Nature*, 1970, 228, 648.
73. LSUCRE, Program for "Least-Squares Unit Cell Refinements", Institute of Crystallography, Freiburg i. Br., 1972.
74. AUPTP, Program for "Reading and processing the STOE diffractometer paper tape output", Hill, R.J., University of Adelaide, 1973.
75. SHELX, "Program for crystal structure determination", Sheldrick, G.M., Cambridge University, 1976.
76. Busing, W.L. and Levy, H.A., FUORFLS, "Least-Squares Refinement Program", modified by Taylor, M.R., Flinders University, 1973.
77. "International Tables for X-ray Crystallography", Vol. 4, Kynoch Press, Birmingham, 1974, pp. 77, 99, 149.
78. Johnson, C.K., ORTEP, "A program used to produce computer drawn structure diagrams, 1965, ORNL-3794, Oak Ridge Nat. Lab., Oak Ridge, Tennessee.
79. Bright, D., *Chem. Commun.*, 1970, 1169.
80. Albano, U.G., Bellon, P.L., Ciani, R. and Manassero, M., *J. Chem. Soc. D.*, 1969, 1242.
81. Albano, U.G., Ciani, G., Manassero, M. and Sansoni, M., *J. Organomet. Chem.*, 1972, 34, 353.
82. Spiro, T.G., Templeton, D.H. and Taekin, H., *Inorg. Chem.*, 1968, 7, 2165.

83. Abel, E.W., Harrison, W., McLean, R.A.N., March, W.C. and Trotter, J., *Chem. Soc. D.*, 1970, 1531.
84. Horn, E. and Snow, M.R., *Aust. J. Chem.*, 1981, 34, 737.
85. Penfold, B., private communication.
86. Jansen, J.C., Koningsveld, H. van and Reedijk, J., *Nature* (London), 1977, 269, 318.
87. O'Donnell, T.A., in "Comprehensive Inorganic Chemistry", p. 1009 (Pergamon: Oxford, 1973).
88. Snow, M.R., *J. Am. Chem. Soc.*, 1970, 92, 3610.
89. Obi, M. and Iwamura, H., *J. Am. Chem. Soc.*, 1967, 89, 576.
90. Basila, M.R., Saier, E.L. and Cousins, L.R., *J. Am. Chem. Soc.*, 1965, 87, 1665.
91. Nakatsu, K., Yoshioka, H., Kunimoto, K., Kinugusa, T. and Ueji, S., *Acta Crystallogr.*, Sect. B, 1978, 34, 2357.
92. Aubry, A., Protas, J., Moreno-Gonzalez, E. and Marrand, M., *Acta Crystallogr.*, Sect. B, 1977, 33, 2572.
93. Foust, A.S., Dahl, L.F., *J. Am. Chem. Soc.*, 1970, 92, 7337.
94. Harrison, W., Marsh, W.C. and Trotter, J., *J. Chem. Soc. (Dalton)*, 1972, 1009.
95. Astakhova, I.S., Seminon, V.A. and Struchkov, Y.T., *J. Struct. Chem.*, 1969, 10, 419.
96. Foust, A.S., Graham, W.A.G. and Stewart, R.P., *J. Organomet. Chem.*, 1973, 54, C22.
97. Churchill, M.R. and Bau, R., *Inorg. Chem.*, 1969, 6, 2086.
98. SUSCAD, "Data reduction program for the CAD4 diffractometer", University of Sydney, 1976.

99. ABSORB, "Program for applying crystal absorption corrections".
100. Stout, G.H. and Jensen, L.H. in "X-ray Structure Determination", 1968, Macmillan Pub. Co., Inc., p. 270 and pp. 98-147.
101. Sherwood, D. in "Crystals, X-rays and Proteins", 1976, Longman Group Ltd., p. 428.
102. Abel, E.W., Hargreaves, G.B. and Wilkinson, G., *J. Chem. Soc.*, 1958, 3149.
103. Snow, M.R. and Zeleny, P.C., private communication.
104. Zingales, F., Sartorelli, U., Canziani, F. and Raveglia, M., *Inorg. Chem.*, 1967, 6, 154.
105. Freni, M., Valenti, V. and Giusto, D., *J. Inorg. Nucl. Chem.*, 1965, 27, 2635.
106. Moelwyn-Hughes, J.T., Garner, A.W.B. and Gordon, N., *J. Organomet. Chem.*, 1971, 26, 373.
107. Freni, M. and Valenti, V., *J. Inorg. Nucl. Chem.*, 1961, 16, 240.
108. Colton, R. and Garrard, J.E., *Aust. J. Chem.*, 1973, 26, 529-39.
109. Chatt, J., Duncanson, L.A. and Venanzi, L.M., *J. Chem. Soc.*, 1955, 4456.
110. Jolly, P.W. and Stone, F.G.A., *J. Chem. Soc.*, 1965, 5259.
111. Nyholm, R.S., Snow, M.R., Stiddard, M.H.B., *J. Chem. Soc.*, 1965, 6564.
112. Reger, D.L., Coleman, C.J. and McElligott, P.J., *J. Organomet. Chem.*, 1979, 171, 73.
113. Horn, E. and Snow, M.R., private communication (1980-81).
114. Gmelin, L., Meyer, R.J., Pietsch, E.H.E. and Kotowski, A., in "Gmelin Handbuch der Anorganischen Chemie", Boron Compounds, Springer-Verlag Berlin, 1st Suppl., 2, pp. 276-281.

115. Bruce, D.M., Holloway, J.H. and Russell, D.R., *J. Chem. Soc. Dalton*, 1978, 64.
116. Santoro, A. and Mighell, A.D., *Cell reduction programme*.
117. Bull, W.E. and Moore, L.E., *J. Inorg. Nucl. Chem.*, 1965, 27, 1341.
118. Pavkovic, S.F. and Meek, D.W., *Inorg. Chem.*, 1965, 4, 1090.
119. Wickenden, A.E. and Krause, R.A., *Inorg. Chem.*, 1965, 4, 404.
120. Davis, A.R., Murphy, C.J. and Plane, R.A., *Inorg. Chem.*, 1970, 9, 423.
121. Kuhlmann, K. and Grant, D.M., *J. Phys. Chem.*, 1964, 68, 3208.
122. Hathway, B.J. and Underhill, A.E., *J. Chem. Soc.*, 1961, 3091.
123. Cohn, H., *J. Chem. Soc.*, 1952, 4282.
124. Greenwood, N.N., (Ed.), "Spectroscopic Properties of Inorganic and Organometallic Compounds" Vol. 1, The Chemical Society, London, 1968, p. 204.
125. Allen, F.H. and Sze, S.N., *J. Chem. Soc. (A)*, 1971, 2054.
126. Wuyts, L.F. and van der Kelen, G.P., *Inorg. Chim. Acta.*, 1977, 23, 19.
127. Mesmer, R.E. and Rutenberg, A.C., *Inorganic Chemistry*, 1973, Vol. 12, No. 3, 699.
128. Chernyshov, B.N., Shcherbakov, V.A. and Davidovich, R.L., *Spectroscopy Letters*, 1972, Vol. 5, No. 2, 421.
129. Tomlinson, A.A.G., Bonamico, M., Dessy, G., Fares, V. and Scaramuzza, L., *J. Chem. Soc. Dalton*, 1972, 1671.
130. Gaughan, A.P., Dori, Z. and Ibers, J.A., *Inorganic Chemistry*, 1974, Vol. 13, No. 7, 1657.
131. Isobe, K., Nanjo, K., Nakamura, Y. and Kawaguchi, S., *Chem. Letters*, 1979, 1193.



132. Gelfand, L.S., Schwartz, E.S.C., Pytlewski, L.L. and Karayannis, N.M., *Inorganica Chimica Acta*, 1980, 39, 143.
133. Musgrave, T.G. and Lin, T.S., *J. Coord. Chem.*, 1973, 2, 323.
134. Guichelaar, M.A., Van Hest, J.A.M. and Reedijk, J., *Inorg. Nucl. Chem. Lett.*, 1974, 10, 999.
135. Smit, S. and Groeneveld, W.L., *Inorg. Nucl. Chem. Lett.*, 1975, 11, 277.
136. Hidai, M., Kodama, T., Sato, M., Harakawa, M. and Uchida, Y., *Inorg. Chem.*, 1976, 15, 2694.
137. Reedijk, J., Jansen, J.C., Van Koningsveld, H. and Van Kralingen, C.G., *Inorg. Chem.*, 1978, 17, 1990.
138. Jansen, J.C., Van Koningsveld, H. and Reedijk, J., *Nature*, 1977, 269, 318. ≡ 86
139. Mikulski, C.M., Gelfand, L.S., Schwartz, E.S.C., Pytlewski, L.L. and Karayannis, N.M., *Inorg. Chim. Acta*, 1977, 24, LI.
140. Bau, R., Kirtley, S.W., Sorrell, T.N. and Winarko, S., *J. Amer. Chem. Soc.*, 1974, 96, 988.
141. Coyle, B.A. and Ibers, J.A., *Inorg. Chem.*, 1972, 11, 1105.
142. Simon, G.L., Adamson, A.W. and Dahl, L.F., *J. Amer. Chem. Soc.*, 1972, 94, 7654.
143. Brown, L.D., Raymond, K.N. and Goldberg, S.Z., *J. Amer. Chem. Soc.*, 1972, 94, 7664.
144. PLUTO, "Program for crystal and molecular plotting", Motherwell, W.D.S., University of Cambridge, 1977.
145. Couldwell, M.C., Robinson, W.T. and Simpson, J., *J. Organometal. Chem.*, 1976, 107, 323.

146. Anglin, J.R., Calhoun, H.P. and Graham, W.A.G., *Inorg. Chem.*, 1977, 16, 2281.
147. Couldwell, M.C. and Simpson, J., *J. Chem. Soc. Dalton Trans.*, 1978, 1101.
148. Einsley, J.W., Feeney, J. and Sutcliffe, L.H. in "High Resolution Nuclear Magnetic Resonance Spectroscopy", 1966, Pergamon Press, Vol. 2, p. 871.
149. Lynden, B. and Harris, R.K. in "Nuclear Magnetic Resonance Spectroscopy", 1975, Academic Press.
150. Chambers, R.D., Clark, H.C., Reeves, L.W. and Willis, C.J., *Can. J. Chem.*, 1961, 39, 258.
151. Kuhlmann, K. and Grant, D.M., *J. Phys. Chem.*, 1964, 68, 3208.
152. Dahl, L.F., Ishishi, E. and Rundle, R.E., *J. Chem. Phys.*, 1957, 26, 1750.
153. Kaesz, H.D., Bau, R. and Churchill, M.R., *J. Amer. Chem. Soc.*, 1967, 89, 2775.
154. Elder, M., *Inorg. Chem.*, 1970, 9, 762.
155. Buerger, M.J., *The Precession Method*, Wiley, New York, 1964.
156. Bijvoet, J.M., Peerdeman, A.F. and Van Bommel, A.J., *Nature*, 1951, 168, 271.
157. Karle, J. and Hauptmann, H., *Acta Cryst.*, 1956, 9, 635.
158. Karle, I.L., Dragonette, K.S. and Brenner, S.A., *Acta Cryst.*, 1965, 19, 713.
159. Van Geet, A.L., *Analytical Chem.*, 1968, 40, 2227.
160. Brauer, G., "Handbook of Preparative Inorganic Chemistry", Vol. 1, 2nd Edition, Academic Press, New York, 1963, p. 240.

161. Abel, E.W. and Tyfield, S.P., *Canad. J. Chem.*, 1969, 47, 4627.
162. Abel, E.W., Hargreaves, G.B. and Wilkinson, G., *J. Chem. Soc.*, 1958, 3149.
163. Evans, D., Osborn, J.A. and Wilkinson, G., *Inorg. Synthesis*, 11, 99.
164. Blackmore, T., Bruce, M.I. and Stone, F.G.A., *J. Chem. Soc. (A)*, 1971, 2376.
165. Drew, M.G., Davis, K.M., Edwards, D.A. and Marshalsea, J., *J. Chem. Soc. (Dalton)*, 1978, 1098.
166. Bamford, C.H. and Coldbeck, M., *J. Chem. Soc. (Dalton)*, 1977, 4.